THE UNIVERSITY
of EDINBURGH

This thesis has been submitted in fulfilment of the requirements for a postgraduate degree (e.g. PhD, MPhil, DClinPsychol) at the University of Edinburgh. Please note the following terms and conditions of use:

This work is protected by copyright and other intellectual property rights, which are retained by the thesis author, unless otherwise stated.
A copy can be downloaded for personal non-commercial research or study, without prior permission or charge.
This thesis cannot be reproduced or quoted extensively from without first obtaining permission in writing from the author.
The content must not be changed in any way or sold commercially in any format or medium without the formal permission of the author.
When referring to this work, full bibliographic details including the author, title, awarding institution and date of the thesis must be given.

Structural behaviour of cross-laminated timber elements in fires

Felix Wiesner

THE UNIVERSITY
of EDINBURGH

A thesis submitted in fulfilment of the requirements
for the degree of
Doctor of Philosophy
to
The University of Edinburgh
2019

This page is intentionally left blank.

Structural behaviour of cross-laminated timber elements in fires

by

Felix Wiesner

This thesis has been supervised by

Prof. L.A. Bisby

Dr R.M. Hadden

The examining committee consisted of

Dr D. Hopkin

Dr A. Law

This page is intentionally left blank.

DECLARATION

This thesis and the work reported within has been composed by Felix Wiesner at the University of Edinburgh under the supervision of Prof. Luke Bisby. The thesis has not been submitted in any previous application for a degree of any kind. References are provided for sources, and where others have contributed.

Felix Wiesner

November 2019

This page is intentionally left blank.

ABSTRACT

Cross-laminated timber (CLT) is a comparatively novel engineered material consisting of timber boards that are arranged in layers of alternating directions and bonded with adhesives. It is increasingly the material of choice to realise mid height to tall timber buildings; however, because timber is a combustible material there are concerns with respect to its fire safety when used for tall buildings. As an engineered material the configuration of CLT can be varied in multiple ways, with currently unknown implications for its fire performance. While a vast body of knowledge exists for the structural behaviour of sawn timber, it is unknown whether this knowledge can directly be applied to CLT, which is utilised in the form of factory produced large floor slabs and wall panels. Structural fire resistance for CLT panels has so far mostly been assessed in furnace testing following standard temperature time curves, and there remains a paucity of data on the structural fire performance of CLT walls. The understanding of how specified adhesive types and board configurations influence the fire performance of CLT elements is lacking. The research presented in this thesis studies how two adhesive types and two ply configurations may influence the response and load bearing capacity of CLT walls (and other elements) through all stages of a fire.

Three experimental series have been completed, all investigating different loading and heating conditions at different scales for CLT that was sourced from one producer but with two variants in adhesive type and ply lay-up. This results in four different CLT configurations being considered. The first series assessed the axial compressive strength of CLT at small scale when heated to non-charring temperatures of up to 220 °C. The median strength retention upon heating in small scale compression experiments was observed to be 9 % less for CLT specimens bonded with the polyurethane (PU) adhesive type than for those bonded with melamine formaldehyde (MF) when only transient experiments or those with remaining moisture in the timber were considered. The influence of migrating moisture was observed to be the driving mechanism weakening

timber in compression, and ultimately inducing failure.

The second experimental series investigated the flexural behaviour of CLT beams under slow transient heating to non-charring temperatures of up to 150 °C at two applied load ratios, and illuminated the significance that shear stresses and the resulting shear strains at the adhesive bonds exert on the deflections of the different CLT configurations. Mean heat induced deflections were observed to be 40 % higher for specimens which utilised a polyurethane adhesive type compared to those using melamine formaldehyde; this effect was amplified for CLT made up of three plies compared to five plies. Through heating and subsequent cooling these experiments also demonstrated that heat induced deflections in bending for CLT are dominated by creep, and are irrecoverable.

A third experimental series subjected CLT wall strip elements to a radiative heat flux, representative of conditions that might occur in a real fire, under equal constant load ratios. Walls that were bonded with the PU adhesive type failed significantly earlier (20 percentage points) than the mean failure time for all specimens. Samples consisting of three plies exhibited shorter (17 percentage points) failure times than the overall mean failure time. These occurred at similar char depths and with good repeatability, and were attributed to accelerated deflections due to increasing shear deflections in these samples causing exponentially increasing bending moments from P-Delta effects and subsequent buckling failure. In addition, heating and additional cooling of samples highlighted the propensity of CLT walls to fail in the decay phase of a fire, due to the tendency of heat to transfer deeper into the timber even after the primary heat source is removed. Numerical simulations of the wall strips with a wide range of mechanical input parameters highlighted the importance of accounting for weakening glue lines at elevated temperatures to predict failure in fire numerically. The simulations also showed that the failures in the fire decay phase could not be explained solely by redistribution of elevated temperatures through the cross-section; instead they were likely caused by creep due to changes in moisture content.

The findings in this thesis are novel and have significant potential to aid manufacturers and designers to assess and improve their products' response to fire in the production stages. The results and their analysis presented herein raise questions regarding the applicability of standardised fire resistance furnace tests in qualifying CLT for use in tall timber buildings; instead more holistic approaches are advocated.

Overall this thesis describes novel experimental set-ups that have been used to assess the response of CLT in previously unknown detail with a unique materials stock that

allowed variation of two experimental variables whilst keeping the underlying timber quality and manufacturing constant. The results consistently demonstrated that adhesive type had no discernible influence on the load bearing capacity at ambient reference temperatures, but the PU adhesive type was found to significantly reduce the structural performance of CLT exposed to heat or fire. This was especially evident for CLT walls, where additional deflections caused by weakening of the bond lines led to earlier global buckling failures. Failure of CLT walls in the fire decay phase, as presented and investigated in this thesis, should be a concern for all engineers that work on tall timber buildings. The potential for structural collapse after burnout of the fuel load is shown as a real possibility and engineers and architects working with and advocating for tall timber buildings should be aware of the limits of their own knowledge and the limits of the state of the art on these issues.

This page is intentionally left blank.

LAY SUMMARY

This research project investigates the ongoing capacity of engineered timber elements to carry load when exposed to fires in buildings. Modern timber building use engineered timber to carry loads comparable to steel or concrete buildings. Engineered timber is made up of individual pieces of timber that are pieced together using glue or fasteners. For cross-laminated timber (CLT), boards of lumber are stacked crosswise to each other resulting in a large piece of wood with alternating strong and weak layers which are held together by glue, which can be selected from a variety of different types of glues. In its essence this work investigates whether the load bearing performance of CLT in fire is simply the sum of its parts, or if the effect of heat and fire will result in different outcomes depending on the thickness of the layers and the glues that are used to bond them together.

Three different experimental series with different loading and heating conditions were completed for different sizes of CLT that varied in its configuration of layers, and were bonded together with one of two possible types of glue. For the layers, CLT consisting of three and five plies was tested, and for the glue, a polyurethane and melamine urea formaldehyde adhesive type were used.

The results from the different test series show very clearly that the chosen adhesive has a significant effect on the overall structural capacity of CLT in fire. CLT that was bonded with the polyurethane glue, consistently experienced larger deflections when it was heated and these deflections ultimately led to earlier structural failure and therefore an earlier failure of the fire safety strategy. In addition, it was found that CLT elements with three layers and thicker layers on their outside were more affected, structurally, by the effects of fire than the those consisting of five layers.

The experimental results also show that structural failure of CLT walls can occur after a fire is extinguished due to accumulated and delayed effects of heating in the timber as

a zone of elevated temperatures continued to heat up previously cold timber even after any external heat sources were removed. Calculations showed that the failure after a fire could not be explained by a redistribution of heat alone, and it is suggested that the effects of changing moisture content of the timber will also weaken it further. Once a sufficient amount of energy had been supplied the timber was observed to continue to generate its own heat, even where no flames were visible; this will further weaken timber structures after an initial fire. This creates a potential for timber structures to collapse after a building is perceived to have survived a fire and could have grave consequences for occupants and fire and rescue services.

These findings are not currently accounted for in the design of timber buildings, which are being proposed and built to ever greater heights. They highlight that the current state of the art with respect to fire safety in timber buildings is not developed sufficiently. There is a tendency within the construction industry to simplify the risks from fires in buildings made from engineered timber products; this introduces the possibility that unknown risks are placed into the emerging building stock, and this could compromise the sustainable development that timber buildings are supposed to represent.

ACKNOWLEDGMENTS

Time sure flies when you are having fun. There are a considerable number of people who have enabled me to enjoy the last four years, to grow both academically and as a person, and who aided me in one way or another to complete this thesis with the majority of my sanity intact.

First and foremost I would like to thank Prof. Luke Bisby, my primary supervisor, who has shown remarkable patience and remains a constant source of wisdom and inspiration to me. Likewise, Dr Rory Hadden performed his pastoral tasks as second supervisor with bravura. I could not have hoped for a better supervisory team. Special thanks are also due to Dr Susan Deeny of Arup, who acted as an industrial supervisor, and whose advice often helped me to look beyond the hallways of the proverbial ivory tower.

I am grateful for the technical support I have received from Michal Krajovic and Mark Partington. Their dedication has helped me to perform all experimental work safely and their insightful technical advice improved my experiments in all aspects. I would also like to express my gratitude to Sebastian Knoflach and Mayr-Melnhof Holz, for their generous supply of material that enabled these studies. I would like to thank Arup for their financial and intellectual support of my studies, and for their vision of design informed by novel research.

I consider myself lucky to have been given the opportunity to teach and supervise tremendously gifted students during my PhD, and I hope they learned as much from me as I did from them. Special mentions are due here for Louis, Fred, Wing, Balsa and Darren.

Like most things in life, this work had its highs and its lows, and I consider myself lucky to have had an amazing bunch people around to share these with me. I am grateful to the academic community within the Edinburgh Fire Group who have made

sure that the time for my doctoral studies was not only an academic exercise but rather an unique part of my life that will remain a positive memory for the rest of my life. There are too many people to name them all, but I would like to especially, and in no particular order, thank the following for their friendship and support: Dr Juan Hidalgo, Dr Jamie Maclean, Dr Ieuan Rickard, Dr Emma McIntyre, Nikolai Gerasimov, Simon Santamaria, Zak Campbell-Lochrie, Dr Chris Thomas, Ulises Rojas, Dr Daryan Othman, Dr Mohamad El Houssami, Dr Martyn McLaggan, Dr Eric Mueller, Dr Simone Zen, Dr Benjamin Ralph, Dr Sorcha Daly, and Dr Zafiris Triantafyllidis.

I would also like to thank all of my friends who have welcomed me into this country many years ago and who keep putting up with me. Louise, Andrew, Grant, Olga, Sean, Freddy, and especially my best bud, Daniel, I am very grateful for our ongoing friendship and all of your support and kindness.

Special thanks are due to my parents, Klaus and Elke Wiesner, who have supported me throughout my education, and without whom I would not be where I am today; it was their loving upbringing that enabled my curiosity for science and engineering. I would also like to acknowledge my paternal grandfather, Peter Wiesner, whose life, work and attitude I greatly admire. I could not have finished this PhD without the loving care and support from Delia Murguia, who was always there for me, and whom I owe tremendous gratitude for her love.

LIST OF PUBLICATIONS

The following publications either resulted directly from the work in this thesis or were published during the doctoral studies associated with it.

Journal papers

- **F. Wiesner** and L. Bisby. "The structural capacity of laminated timber compression elements in fire: A meta-analysis". In: *Fire Safety Journal* 107 (2019), pp. 114-125.
- **F. Wiesner**, L. A. Bisby, A. I. Bartlett, J. P. Hidalgo, S. Santamaria, S. Deeny, and R. M. Hadden. "Structural capacity in fire of laminated timber elements in compartments with exposed timber surfaces". In: *Engineering Structures* 179 (2019), pp. 284-295.
- **F. Wiesner**, F. Randmael, W. Wan, L. Bisby, and R. M. Hadden. "Structural response of cross-laminated timber compression elements exposed to fire" In: *Fire Safety Journal* 91.Supplement C (2017), pp. 56-67.
- R. M. Hadden, A. I. Bartlett, J. P. Hidalgo, S. Santamaria, **F. Wiesner**, L. A. Bisby, S. Deeny, and B. Lane. "Effects of exposed cross laminated timber on compartment fire dynamics". In: Fire Safety Journal 91 (2017), pp. 480-489
- A. I. Bartlett, R. M. Hadden, J. P. Hidalgo, S. Santamaria, **F. Wiesner**, , L. A. Bisby, S. Deeny, and B. Lane. "Auto-extinction of engineered timber: Application to compartment fires with exposed timber surfaces". In: Fire Safety Journal 91 (2017), pp 407-413

Conference papers

- **F. Wiesner**, M. Klippel, C. Dagenais, A. Dunn, B. Östman, M. L. Janssens, and K. Kagiya. "Requirements For Engineered Wood Products And Their Influence On The Structural Fire Performance". In: *World Conference on Timber Engineering*. Seoul, Republic of Korea, 2018.
- **F. Wiesner**, D. Bell, L. Chaumont, L. Bisby and S. Deeny. "Rolling Shear Capacity of CLT at Elevated Temperature". In: *World Conference on Timber Engineering*. Seoul, Republic of Korea, 2018.
- A. I. Bartlett, A. Chapman, C. Roberts, **F. Wiesner**, R. M. Hadden and L. A. Bisby. "Thermal and flexural behaviour of laminated bamboo exposed to severe radiant heating". In: *World Conference on Timber Engineering*. Seoul, Republic of Korea, 2018.
- A. Bartlett, **F. Wiesner**, R. Hadden, L. Bisby, B. Lane, A. Lawrence, P. Pedro, and F. Andrea. "State-Of-The-Art And Research Needs For Total Fire Engineering Of Mass Timber Buildings". In: *World Conference on Timber Engineering*. Ed. by J. Eberhardsteiner, W. Winter, A. Fadai, and M. Pöll. Vienna, Austria, 2016.

CONTENTS

This page is intentionally left blank.

LIST OF FIGURES

This page is intentionally left blank.

LIST OF TABLES

CHAPTER 1

Introduction

This page is intentionally left blank.

1.1 Motivation

The population on earth has increased exponentially over the last decade and is projected to grow further throughout this century [1]. At the same time, the proportion of people living within urban agglomerations has increased to over 50 % [2, 3]. This has created shortages of housing in economic centres and the requirement to construct affordable housing in a short time frame. With limited resources and an increased consideration of global warming, sustainability has become an important aspect for urban building designs to be considered by architects and engineers alike. Engineered timber has emerged as a credible addition and alternative to traditionally utilised construction materials like steel and concrete.

Engineered timber is produced by connecting multiple machined pieces of timber into a custom section. Most commonly the connection is achieved through adhesives, as is the case for what are probably the most widely utilised structural engineered timber products: Cross-laminated timber (CLT) and glue laminated timber (glulam). For cross-laminated timber boards are aligned into layers of alternating direction which are bonded to form slabs and panels and can therefore be used as floor and wall elements. The prefabrication process allows for accelerated and off-site construction in dense urban areas and as a renewable material timber is generally considered to have a better carbon balance than steel or concrete.

By 2015 the global production volume of CLT was estimated as 700,000 m^3 [5]. Research suggests that there is further future growth potential for the use of CLT as a construction material in the American market [6]. Similarly, in Japan, the government is actively pushing for increased uptake of CLT in construction through subsidies, in order to reduce costs and fully utilise the potential of the national timber industry [7]. The height of timber buildings has traditionally, in many jurisdictions, been restricted by fire safety concerns and limitations in size of sawn timber, however, the raised confidence in engineered mass timber products has recently led to proposals of increasingly higher multi-storey buildings utilising engineered timber for their primary structural members [8]. The term 'timber-skyscrapers' has been used to describe this development. One example of a recently constructed high rise timber building is the 14-storey 'Treet' building in Bergen, Norway [9]. It utilises a glulam truss system for the majority of load transfer and CLT for the elevator shaft. CLT is also increasingly used for high-level architecture on prestigious projects in a variety of countries. Several proposed sites for the 2020 Olympic and Paralympic Games in Tokyo are proposed to utilise elements of CLT [7]. Architects have shown increasing interest in utilising CLT

Figure 1.1. Factory production of CLT [4].

for more complex forms, which has included form finding of origami like folded shell structures of CLT plates as building envelopes, leading to more robust and aesthetically pleasing structural forms [10, 11]. Despite this recent rapid growth in the mass timber industry, concerns over the fire safety of tall timber developments remain.

1.2 General problem statement

1.2.1 Combustibility of timber

Because of its combustibility, and historical precedence of large fires in cities which were predominately made up of timber buildings [12, 13] (e.g. see Figure 1.2), timber has a problematic reputation with regards to its fire performance when compared to non-combustible building materials like steel, brick or concrete. The divergence between a rising population and falling occurrences of mass conflagrations for cities in developed countries from 1850s onwards, denominated as 'fire gap' by Frost and Jones [14], is in large parts attributed to the more widespread use of non-combustible building materials. Therefore there are concerns that a 'timber renaissance' will close that fire gap and lead to more and more destructive fires.

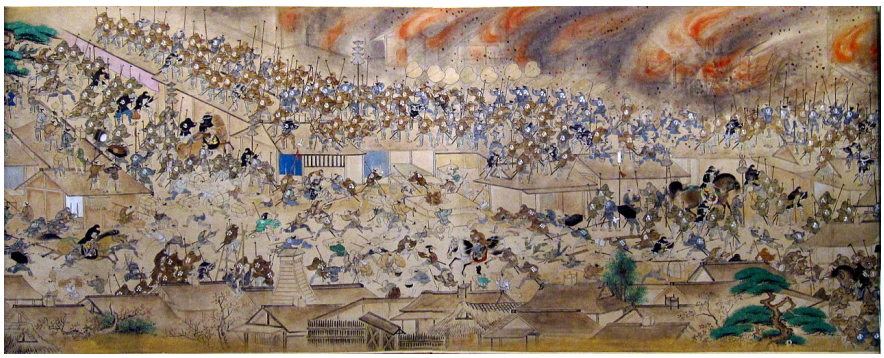

Figure 1.2. Depiction of the Meireki fire in 1657 in Edo (modern day Tokyo), one of many mass conflagrations in timber cities that occurred internationally before the widespread use of non-combustible building materials [15].

The fire performance of building products is an important criterion for many architects [16] and a lack of knowledge and confidence in its fire behaviour is seen as a limiting factor for the full implementation of timber, especially for high rise buildings, where fire protection regulations are more stringent [17]. This means that more guidance and knowledge about the fire resistance of CLT is required to ensure it can be utilised to its full potential [6]. Fire safety has been identified as a key obstacle to the development of multi-storey timber buildings [18] and a key research area for tall timber building design [19]. In most countries the use of timber and exposed timber as a structural material is restrained by building regulations by limits on the number of storeys or the overall height [20–22].

As stated above, the reputation of timber in fire is poorly perceived due to its combustibility. Yet, for large mass timber sections, the structural capacity can be maintained in a fire for an extended period of time [23] and in series of tests timber columns have been observed to perform better in fire than their steel counterparts, with comparable working loads applied [24]. Similar sentiments have been reported by firemen in Victorian Britain, who felt that the fire resistance of iron columns was too short and unpredictable, [25]

> "whereas good solid timber posts endured for a long time and the men being able to reckon their term of duration, felt more confidence"
> *James Braidwood* 1853 [25]

Fleischer [26] related the fate of two similar warehouses, one made of timber and one of non-combustible construction. Both buildings experienced large fires and while the

timber one was operational after minor repairs, the non-combustible one suffered complete collapse and required complete demolition and a clean-up operation over multiple months. Similarly, Walford [27] relates a discussion on the difference between the combustibility of a material and its ability to withstand fire, with cast iron columns in warehouses as an example. Of course the instances described above are anecdotes and not science. Nevertheless, they highlight that it is the construction detail and not the necessarily the combustibility of the material that determines the structural performance in case of fire. Overall a discrepancy of opinion on the fire performance of timber exists. Its combustibility is seen in opposition to its relatively predictable structural resistance in fire. In a real fire these two aspects are linked, although their assessment is currently mostly done separately.

The current structural fire safety engineering approach for building approval and codified guidance relies on a fire resistance duration which elements of construction have to achieve in a standard fire test [28]. The origin of fire resistance time as measured in a standard fire is based on equivalence of severity compared to complete burnout of compartment fires with varying fuel loads (as expected for different occupancies) [29]. This initial definition of fire resistance time equivalence did not account for contribution of the structure to the fire. In the construction industry the prevalent approach to the fire resistance of timber seems to be the encapsulation of exposed timber surfaces in non-combustible construction, such as gypsum plasterboard. The total fire resistance is then sometimes taken as the summation of the fire resistance of the encapsulation and the fire resistance of timber, based on a defined charring rate [30]. The problem with this approach is that it takes the initial assumption of burn-out, implicit in the fire resistance, but also accounts for the encapsulation to fail, thereby involving the combustible surfaces and adding to the fuel load, increasing the required time to burnout, potentially until the affected compartment structure or the building itself is completely consumed. Alternatively encapsulation can be provided to ensure that timber will not contribute to the fuel load during a fire; in this case the fire resistance rating will mainly be provided by the encapsulation system, as long as the timber substrate maintains its structural capacity. This research need is also driven in part by the desire of architects and developers to leave some timber in compartments exposed, driven by both aesthetic and financial considerations. In a building with exposed timber the structure interacts with the fire dynamics [31] and in order to achieve an equivalent level of safety to non-combustible construction, an appropriate design solution will have to achieve self-extinction after the burn out of moveable combustible material [18]. Therefore there is an urgent need to better understand the load bearing

capacity of mass engineered timber elements both when timber is exposed to a fire, and during the cooling phase after a fire extinguishes.

The structural durability of heavy timber in fire, mentioned above, can be attributed to the formation of a char layer, which causes a steep temperature gradient underneath the wood-char interface and thereby protects the uncharred timber underneath. Below this interface the wood temperatures will be elevated, causing a partial loss of strength and stiffness but interior timber will remain at low temperatures for considerable durations. Most modern design recommendations for heavy timber in fire only address the temperature behind the char through simplified assumptions, like a zone of zero strength, or an accelerated charring rate. The proposed values for this, were often derived from limited standard fire tests on glulam beams in bending. As engineered timber products become more complex and designers aim for more holistic approaches these simplifications of the zone affected by elevated temperature may no longer be appropriate. The effect and extent of the heated depth below the char layer must be better understood and quantified in order to promote safe and efficient design of tall timber buildings. The work herein explores the effect of varying heating conditions in order to further the understanding of the potential consequences of fire or high temperature exposure on the load bearing capacity of engineered timber.

1.2.2 Structural behaviour of compression elements

In theory the structural behaviour of elements in pure compression is rather simple, as the stress can be derived from the applied force and the cross sectional area. In addition a majority of traditional materials behave favourably in compression compared to tension or bending. Most readers will be intimately familiar with this structural engineering concept when considering ancient buildings (or their remains), which are mostly made of masonry or concrete (two materials that should primarily be used in compression) as this constituted a simple workable solution to available construction methods.

More slender (i.e. longer and/or thinner) compression elements tend to require far more complex analysis than tension or bending elements for one reason: Instability. This is manifested in lateral deflections, which will cause large bending stresses, that eventually exceed the material strength. Since fire exposed timber elements will reduce in cross-section, their slenderness ratio will increase as a fire progresses, reducing the resistance against buckling. In addition one sided fire exposure will cause eccentricities and $P - \Delta$ effects which will exasperate the probability of buckling failure. A '*known*

unknown' in this case is the contribution of additional deflections in engineered timber members, due to their specific make, that are not easily detected in a pass or fail scenario like fire resistance testing. The heightened complexity of failure of timber members due to instability is manifested in the difficulty to develop a reliable model to predict the fire resistance of CLT compression members [32], whilst the focus of recent simplified modelling efforts was limited to bending elements [33]. Part of this project will therefore investigate the propensity of timber columns and walls to buckle and aim to provide improved models describing the physics of instability failure and its conditions.

1.3 Optimisation considerations

Modern buildings have to fulfil a number of criteria concerning feasibility, safety and sustainability and engineered timber products can be fathomed to a multitude of configurations. It is therefore logical to vary the latter in order to achieve optimal improvements for the former and thereby maximise the potential of engineered timber. For the case of CLT and Glulam this means for designers and producers to be able to optimise the properties of the finished material for the needs of the construction industry, from timber as simply a raw material input. For CLT, optimisation can be applied to the overall geometry, the lay-up configuration of the lamellae, the quality of timber used, and the adhesive holding the plies together. For example, the performance of adhesives is driven by environmental considerations and the release of formaldehyde but an optimised adhesive should equally yield fast production times whilst maintaining the required load bearing capacity for all likely scenarios. In a fire scenario the adhesive will have to continue to perform its function in order to maintain the composite action between the layers. While research is and has been undertaken to understand the influence of these parameters on the structural performance for normal use [5, 34, 35], there is a paucity of data available on the influence of the layers and the adhesives on the structural fire performance of CLT (not to be confused with the influence of the layers and adhesives on the fire dynamics). This work will investigate the influence of adhesives and layer thickness on the load-bearing capacity in fires and for CLT subjected to high temperatures and aims to advance the fundamental understanding behind the contribution of bonding to the structural fire performance. This will help to drive optimisation considerations in design as early as the specification of materials.

1.4 Specific project objectives

The aim of this work is to provide a new insight into the effects of production parameters on the load bearing capacity of engineered timber products, specifically for CLT, to assess the suitability of available design tools in relation to CLT, and to equip engineers with the required knowledge and tools to design cross-laminated timber structures to acceptable levels of safety in case of fires.

- Collate and disseminate existing knowledge on laminated timber compression elements in fire and assess its suitability for the determination of the load bearing capacity of CLT wall elements in fire and the influence of high temperatures on the strength and effective stiffness of engineered timber products.
- Supply data on compression strength and stiffness reduction of CLT with increasing temperatures with consideration of the influence of lamellae configuration and adhesives. So far all studies on the strength and stiffness of structural timber with increasing temperatures have focused on sawn timber but have not considered how commonly accepted reduction models might vary for cross-laminated timber (or other engineered timber products). This work incorporates the first series of compression experiments on CLT exposed to varying heating conditions through control of the gas phase temperatures.
- Assess suitability of existing mechanical models for heated timber with respect to engineered timber, with a focus on CLT.
- Experimentally assess the load bearing capacity of of slender CLT compression elements subjected to fire, with a special focus on stability and the effect of shear and increasing P-Delta effects thereupon. This will also include novel experiments on the load bearing capacity during the decay phase of a fire.
- Assess influence of the adhesive line through different loading and heating conditions, thereby illuminating the influence of shear stresses on the bond line for different scales, loading conditions and thermal penetration depths through multiple series of novel experiments and the application of novel analytical tools.
- Develop a thermomechanical model for CLT compression design with a special focus on the effect of P-Delta deflections in context of loss of composite action between CLT plies due to the progression of heat. This model will be assessed against the generated experimental data and recommendations made to move to close emerging knowledge gaps for the buckling behaviour of CLT systems.

1.5 Thesis outline

Chapter 2 provides a literature review to critically highlight the current state of the art for structural fire safety engineering of engineered timber. An overview of wood as a raw material is given and its use in the building sector as timber is described. The concept of engineered timber is illuminated, as is the assessment of its structural load bearing capacity at ambient temperatures. The background of fire dynamics in timber lined compartment and the burning behaviour of timber is described. Finally, the engineering background is given for the load bearing capacity of engineered timber when it is exposed to fire or high temperatures. The most common concepts and codified methods are explained and reviewed. A meta-analysis is performed to assess common methodologies against available fire test results.

Chapter 3 describes measurements to characterise, at ambient temperatures, the cross-laminated timber for fire safety related experiments in this thesis in order to establish a baseline of physical and mechanical characteristics and to introduce the main parameters that are investigated in this thesis: adhesive type and ply configuration. Experimental determinations of both density and moisture content are provided, and the results are assessed statistically in the context of the changing scales of the following experimental chapters, and the different CLT configurations (i.e. adhesive and number of plies).

In Chapter 4 the experiments and results from heated compression experiments on CLT on a small scale are described and analysed. The reduction of strength and elastic modulus is assessed against temperature and the different CLT configuration, yielding reduction factors that are compared against the commonly used factors for timber that is not cross-laminated. Both transient and steady state heating are considered for this chapter when the ultimate load bearing capacity is assessed in compression, thus providing an insight into the effect of moisture movements.

Chapter 5 describes experiments on full scale CLT beam elements under four point bending when slow, controlled heating is applied. In this heating scenario no charring is observed and the bending and glue line behaviour of CLT at low temperatures with a low temperature gradient are investigated. Both heating until failure as well as time-limited heating with a subsequent measurement of the recovery of strength and stiffness are performed in a bespoke combined heating and loading set-up.

Chapter 6 describes the assessment of the structural endurance of loaded CLT wall strips of varying ply number and with different adhesives when exposed to a number

of differing heat flux scenarios from one side. The bespoke experimental set-up is described as is the deflection behaviour for high heat, time-limited and low heat flux exposure. The findings from this chapter will enable engineers to make more informed decisions for CLT wall elements in buildings with regards to their fire safety and how different fire scenarios need to be considered.

The findings from the experimental results in previous chapters are used in Chapter 7 to describe how the structural load bearing capacity and deflection of cross-laminated timber walls can be assessed with engineering methodology through incorporation of the temperature profile and the consideration of increasing eccentricity and P-Delta effects with advancing fire duration. This chapter also includes an identification of knowledge gaps that hinder accurate numerical simulations of CLT wall systems in fire.

This page is intentionally left blank.

CHAPTER 2

Literature Review

This page is intentionally left blank.

This chapter provides an overview of previous work on the structural fire engineering performance of engineered timber. It summarises the most important basic characteristic properties and peculiarities of timber, before giving a more in-depth review of current design practices in timber and how these are applied to fire design of timber elements and structures. As part of a meta-analysis of available design guidance methodologies for the determination of the fire resistance of cross-laminated timber walls this chapter assesses these methods against available experimental results within the literature. As the structural fire and burning behaviour of timber are intertwined, the review also highlights the most important concepts and research for the fire dynamics in compartments with exposed timber surfaces. The purpose of this literature review is threefold: (1) to equip the reader with the required knowledge to place the following chapters into the appropriate context, (2) to appropriately recognise the previous work undertaken in this field and (3) to demonstrate a sufficient level of understanding by the author of the subject matter.

2.1 Timber

Timber describes a range of products which are sourced and produced from the wood of trees. Wood itself is a composite, made up of a multitude of materials that form cells and sections that fulfil specific natural functions. As a building material, timber is mostly sourced from the stems of trees, which function as the main load bearing structure of trees. The three major constituents of timber are cellulose, hemi-cellulose and lignin. The compressive strength of timber is mainly provided by lignin, which acts as a binding agent for the cellulose and hemi-cellulose portions of timber [36, 37]. An increase in lignin correlates with an increase in the crushing strength of timber [38]. On a material scale, timber can be seen as a composite of the natural materials it is made of, each providing a different mechanical function. In compression, the failure mode is manifested as buckling of the wood cells [39, 40], which propagates and causes plastic failure [41]. This is most influenced by the lignin in the timber [36, 42], which acts as a bonding material between the cellulose fibres. Breaking of these bonds is assumed to lead to failure by buckling of the fibres [39]. The mechanical properties of timber are closely related to its density, and density is therefore often treated as an indicator to estimate the mechanical properties of timber [38].

Due to its natural origin and the functionality of its various cells, timber is orthotropic and shows great variability in physical properties in different directions. The recognised orientations of timber are (1) parallel to the grain in a longitudinal axis along the stem,

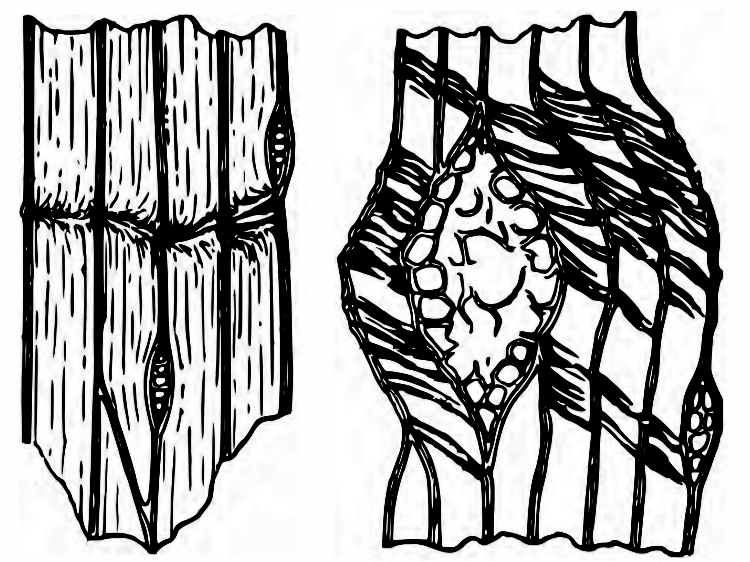

Figure 2.1. Buckling of timber fibres and cell walls in compression, adapted from Tiemann [40].

(2) orthogonal to the growth rings on a radial axis from the stem centre to the bark and (3) tangential to the growth rings [36, 38]. For mechanical considerations in practice, the two latter orientations are generally treated synonymously so that only parallel and orthogonal to the grain axes are considered as relevant orientations for design [34]. Similar to mechanical properties, the thermal properties of timber also vary with the principal directions. The thermal conductivity of timber in the grain direction falls in a range between 0.38 and 0.88 W/mK (depending on moisture content) [43] and is estimated to be between 2.25 to 2.75 times higher as compared to across the grain, and the conductivity in the radial direction is up to 10 % higher than in the tangential direction [38].

2.1.1 Moisture content and movement in timber

The cells and fibres of timber can absorb moisture from the surrounding environment and chemically bind them. The rate and limit of the moisture exchange will depend on the temperature and moisture content of the surrounding medium. For most timbers, a moisture content of around 27 to 30 % [43] will constitute a limit of the amount of chemical bound (i.e. not free) water in timber. This point is often referred to as fibre saturation point and any additional water will exist as free water in the cavities

between cells causing a seemingly higher bulk moisture content [40]. From the technical definition of moisture content as evaporated water mass divided by dry mass, timber can theoretically have a moisture content above 100 %, as many timber species are less dense than water, so the mass of timber can be less than the mass of water in the timber [43]. The proportional moisture content of lignin is lower, relative to cellulose and hemi-cellulose [43]. With decreasing moisture content the failures in timber become increasingly brittle, with splitting along fibres as an additional potential failure mode [40].

The change in moisture content in timber leads to swelling with increasing moisture content and shrinkage for decreasing moisture content. It is therefore recommended that, before it is installed, timber should be seasoned, meaning the moisture content should be altered to a range that can be expected in the built environment. Large changes in size due to shrinkage can induce cracking or warping of the timber [44], as well as damages to building components attached to the timber [25]. As with mechanical and thermal properties, the dimensional changes in timber due to changes in moisture content vary with direction, it is larger (by a factor of 40) perpendicular to the grain, compared to parallel to the grain [38, 43, 45, 46]. In their natural state (i.e. in a tree) the fibres of timber allow for water to be transported from the roots to any other part of the tree. As a consequence, the permeability (i.e. the flow of fluids through the timber) is about four orders of magnitude faster along the fibre orientation, compared to crosswise [36, 43]. In thick timber sections, the outside will dry faster than the inside and in some drying conditions this can cause *casehardening*, where a hard shell of outer dried timber essentially locks moisture into the centre of the timber [40], thereby causing gradients in moisture content through a cross-section, which will also change the strength and stiffness through the cross-section and make surface moisture content readings unreliable indicators for the overall moisture content.

2.1.2 Timber construction types

There are two types of timber construction that can be differentiated. Light timber frame construction and heavy timber construction.

2.1.2.1 Light timber frame

Light timber framing refers to construction of walls and floor systems from individual studs of timber which form the framework for planar elements to be attached. This

method leaves large cavities in the wall system which are often filled with insulation materials. Light timber frame is suitable for manual construction, where only few or no machinery is available to aid the construction process. The comparatively large number of light timber parts requires more work input (i.e. more hands) than work with larger prefabricated elements. Its ease of use and cheap cost has made light timber a dominant form of construction for housing since the 18th century [23].

2.1.2.2 Heavy timber

Heavy timber (also referred to as mass timber) describes larger sections of timber, either cut directly from a tree or engineered timber, which is created by connecting multiple boards or parts of timber to form customised sections (refer to Subsection 2.1.6). Connectors can be adhesives, dowels, nails or screws. The research and analysis presented herein will exclusively cover engineered mass timber, and any reference to timber will refer to engineered timber. Contrary to light timber, heavy timber usually requires some form of heavy machinery to assist with the construction process. The reduced availability of mechanised construction aides in the 19th century, made the construction of heavy timber a complex and laborious process, thereby driving up its costs [23]. Nowadays, the widespread availability of cranes enables heavy timber buildings to be erected with a small amount of labour [47]. Engineered timber, such as CLT and Glulam is less prone to cracking, compared to sawn lumber, when stored in conditions that cause shrinkage and swelling [44]. A common hazard for light timber framing projects are fires during the construction phase. Unlike light timber, heavy timber construction does not necessarily rely on encapsulation for its "fire resistance", and the fire risk during construction is therefore widely considered to be reduced [48].

2.1.3 Recent timber construction development

The height of structural timber buildings has traditionally been restricted by fire safety concerns and limitations to its load bearing capacity, however, increasing confidence in engineered mass timber products and improved active and passive fire safety measures [49] have recently led to proposals of increasingly higher multi-storey buildings utilising timber for their primary structural members [17, 18, 21, 49–52]. The term 'timber-skyscrapers' has been used to describe this development and a global overview of what can be considered tall timber construction is shown in Figure 2.3. One example of a recently constructed high rise timber building is the 14-storey 'Treet' building in

Bergen, Norway [9]. It utilises a glulam truss for the main structural frame and CLT for the elevator shaft in combination with concrete floors. Timber has also been suggested as the main structural material for super tall buildings with a height of 300 m [8], however, these super tall timber proposals are admittedly provocative and should be seen as thought exercises rather than actual building proposals. Smith and Frangi [49] proposed that maximum heights between 60 and 80 m will be feasible where seismic and wind loads will be the limiting structural factors. The following subsections highlight the advantages of building with timber and therefore in part explain the recent eagerness of architects and developers to promote mass timber concept buildings.

Figure 2.2. Construction site of a mass timber building in London, UK [50].

2.1.4 Advantages of timber construction

This section describes some of the advantages that arise for constructors, owners and residents from building with timber and in part explains the drive by architects and developers for more and taller timber buildings.

2.1.4.1 Strength to weight ratio

Timber has an excellent strength to weight ratio, compared to steel and concrete, which enables ease of construction as well as savings on foundation costs [5, 8, 53, 54]. This

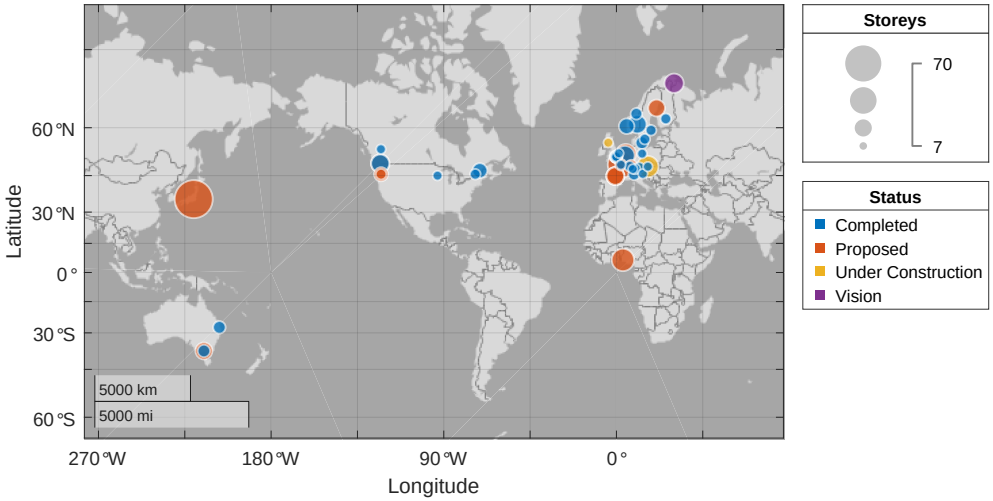

Figure 2.3. Tall timber projects across the world by status and number of storeys.

high strength to weight ratio of timber makes it especially suitable for structures where the construction material itself constitutes a significant portion of the overall mass, e.g. high rise buildings or bridges [37].

2.1.4.2 Ease of use

Due to the precise prefabrication, the construction with engineered timber products, like CLT, allows quick erection [16, 17, 47, 52, 54, 55] through the use of simple fast connections, resulting in buildings with good air tightness [55, 56]. Being a relatively novel material for high rise buildings, contractors tend to trial new construction methods to enable fast and safe assembly of CLT buildings [47, 54], and it can therefore be assumed that the currently observed construction speed will increase as best practice solutions emerge from increased experience and familiarity with the material. As an engineered material, CLT and glulam can be modified during the production processes to meet the needs of design, for example steel bars can be embedded within CLT [52], thereby offering increased strength and higher flexibility for specialised applications.

2.1.4.3 Cost

Laguarda Mallo & Espinoza [16] presented a case study showing that CLT can be cost competitive with traditional steel/concrete construction systems when labour, material and connection costs are considered. Similar findings are presented by Green [17], for comparison of a benchmark multi-storey concrete and timber buildings. He notes that the detailing level and the fire safety requirements will push the price of the timber building up, if encapsulation is required. From comparable case studies between traditional construction materials and mass timber construction, Smith et al. [54] determined that mass timber projects are likely to cost more (up to 43 % additional cost per m^2) than traditional construction if the project is a pilot project, i.e. if the associated design and the construction team have not worked with mass timber on a similar scale before, yet, on average, their study found that mass timber construction can lead to cost savings of 4.2 % compared traditional construction. For large timber projects, incorporating engineered mass timber, a lack of experience can drive up projects costs [17] and this lack of intimate knowledge causes architects to be reluctant to utilise mass timber, and this has been observed especially with regards to unfamiliarity of the fire safety requirements and code intent for tall timber [6].

2.1.4.4 Sustainability

Plants sequester carbon dioxide from the atmosphere and carbon is stored in the wood as trees grow, which means carbon is 'locked' into the timber during its life time. Generally more carbon is stored in growing young trees that replace the trees which were taken to be used for construction [37, 57, 58]. In addition, the harvest of timber products is described as using only a fraction (as low as 10%) of the energy required to produce other building materials and results in less residual waste products compared to mining operations (which are required to source raw materials for steel and concrete) [18, 46]. This means that timber buildings, from properly managed forests, can achieve carbon savings, by locking carbon into the structure. This is only sustainable if the building has a sufficiently long lifespan and experiments on disused timber columns have shown that they can retain a majority of their strength after a service life of over 50 years [59]. At the end of its lifespan, CLT panels can be recycled into other timber products or used as fuel to be converted into energy [55].

Van de Kuilen et al. [52] estimate that a 40 storey building incorporating CLT walls and floors can reduce CO_2 emissions by 50,000 tons, compared to a concrete building.

A report by Skidmore, Owens & Merill [18] estimates that the use of a mass timber structure in high rise buildings can save between 60 and 75 % of embodied carbon emissions compared to concrete or steel construction. It is important to consider that active measures need to be taken to ensure that timber is sourced responsibly, otherwise illegal logging can have devastating effects on forests and the communities within [60].

Due to the selective grading of the individual boards for the composition of CLT, the timber can be sourced from low quality forests, which might not otherwise be suitable for timber production [6]. There are increasing efforts on research to validate the strength and stiffness of local timbers for CLT production [61], which will open up more species for the use in timber construction and therefore increase the available supply as well as reducing transportation costs. Additionally, more variety of timber species uses, will offer more opportunities for bespoke timber products to be used in construction [37].

2.1.5 Drawbacks of timber construction

Like all materials, timber exhibits certain drawbacks for its use as a building material, most of which originate from wood as an organic living material. Since timber is made up mostly of polymers, it is combustible, meaning it will burn when supplied with sufficient heat and oxygen, and thereby contribute heat and flames, as well as emit toxic gases. The combustibility of timber and its burning behaviour is discussed in more detail in Section 2.3. From a structural perspective, the high variability of timber is a major drawback. Because it is a naturally grown material, timber exhibits a large spread of strengths [36, 41]. Knots, which originate from junctions between branches in the tree, cause a reduction in strength as they constitute a localised area of cross-grain and an accumulation of knots will therefore reduce the load bearing capacity of structural timber members [38, 43, 62]. In steel and concrete, designers and producers have significant influence over the material properties through the fabrication or mixing process. This enables engineers to obtain the distributed material properties of a population through tests on a sample. Since timber is a bio-based material, less control is attainable and significant variation within populations occur. These variations include tree genetics, applied forest management and environmental conditions during the growth period. This means that variations in strength and stiffness vary between scales, from regions of timber growth down to variations within the same tree [36, 63]. This variability of timber is addressed through grading of each board into strength classes based on either visual or machine grading.

Because of its anisotropy, failure in timber is best described by a weakest link theory, where a weaker area of material in a cross section will cause failure of the member. Therefore, it is more likely for a weak spot to reach its ultimate capacity if the whole cross-section is exposed to pure tension stress, compared to bending where the tension and compression stress within a member varies. Therefore, for timber, the stress distribution within a member will also influence its ultimate stress capacity [64, 65], and the modulus of rupture (MoR), which is also referred to as 'bending strength', is used to assess its structural load bearing capacity. These bending strengths are derived from bending tests, and are therefore empirical, rather than pure material properties. In design, the use of the bending strength prohibits the utilisation of the plasticity of timber in compression. This means that in complex engineered timber products, which are strengthened in the tension zone, the full stress distribution and moment resistance cannot be exploited [66]. In bending, the dominant failure mode will be due to brittle tension failure, and the size effect factors used for visually graded softwood lumber have therefore been shown to be consistent between tension and bending [41]. Additionally, in design, reduction factors can be utilised to account for the variation in strength as the length or cross section size of lumber is increased. These reduction factors are usually based on strength Weibull distributions and theoretically allow scaling of experimental data to widen its applicability [41, 64, 65].

For CLT, as an engineered product, additional levels of variability can occur (1) between producers, (2) between different batches by the same producer, and (3) within any batch by the same producer [67]. Damage from insects, like termites or beetles, must be considered for timber buildings in some parts of the world, meaning its use is restricted or additional measures (e.g. chemical treatment) must be taken to ensure longevity [38, 51, 53, 68].

2.1.6 Engineered timber

Engineered timber describes timber for which sawn lumber boards are combined either with other boards or incorporating supplementary materials to form composite sections with favourable mechanical properties. Some engineered timber products don't rely on boards but chips of timber (e.g chipboard). Currently the two most prominently used engineered timber products are glue-laminated timber (glulam) and cross-laminated timber (CLT). For the former, solid timber boards are stacked on top of each other and adhesively bonded to form engineered and custom sized structural members, which can be utilised as beams, columns or tension members. For CLT, timber boards are aligned

in horizontal layers, which alternate in the direction of their fibres as they are placed on top of each other. This forms large plates of timber comprised of layers (between 3 and 7) of alternating orientation that can be utilised as load bearing floor or wall elements. While glulam has been produced and used in buildings for a relatively long time, CLT only emerged in the 1990s as a building material in its own right [5]. As a consequence, many certification and calculation procedures that are well defined for sawn lumber and glulam are not yet fully developed and investigated for CLT and values for glulam are often substituted where specific data on CLT is lacking and work on this area is ongoing. For example, Fink et al. [67] recently performed a simplified reliability analysis to demonstrate that the currently recommended partial safety factor of 1.25 that is applied to glulam can be applied to CLT as well to achieve a target reliability index β of 4.2, especially if further harmonisation of production requirements is considered. Until further and similar studies such as these are completed, there remains uncertainty in the use of CLT with regards to defined target reliabilities.

Additional engineered timber products include laminated veneer lumber (LVL), parallel laminated timber, nail laminated timber, dowel laminated timber, chipboard and many more [36, 43]. This thesis will focus on CLT as it requires the most research attention due to its rapid rise in prominence, with occasional comparisons to glulam, due to its similarity as a composite of boards bonded with polymeric adhesives.

2.1.6.1 Adhesives and bonding

The bonding strength between timber laminates is an important construction parameter and will influence the loading response of CLT, along with the appropriate methods of analysis. Most prevailing structural calculations of bending are based on the assumption of 'plane sections remaining plane'. However for reduced bond strengths, shear deformations between the layers will render this assumption invalid and will influence results from structural calculations.

Different adhesive formulations offer different advantages and disadvantages for manufacturers. Costs and effects on construction and service life performance will have to be considered when adhesives are chosen for the manufacture of laminated timber products. Timber itself is a variable material while adhesives have been devised and manufactured under tight production requirements and can therefore be assumed to have lower variability. On the other hand, research into timber has been more extensive historically and for adhesives uncertainties are introduced due to the wide range of possible formulations, even within one adhesive type, and the constant development

of novel, application specific adhesive types. This means that while the mechanical characteristics of timber and its constituent are well investigated, there is a lack of data on some adhesives in that regard [69]. The ability to develop and vary adhesives also presents opportunities to engineer adhesives for specific uses [70, 71]. For the production of cross-laminated timber two adhesives types are favoured by most major manufacturers: (1) polyurethane (PUR) and (2) melamine urea formaldehyde (MUF). Similar to MUF, some manufacturers use MF, which is melamine formaldehyde, i.e. MUF without added urea.

Polyurethane (PUR) glues, are attributed advantages such as short hardening times, easy application without heat, a colourless glue line and utilisation of moisture from the timber for its activation [71–74]. PUR is favoured for its lack of formaldehyde emissions, since there are requirements to limit its emission concentrations in many jurisdictions [71, 75, 76]. PUR adhesives are also considered highly versatile with scope to change the behaviour based on changes in the formulation [71, 76]. Note that all reference to PUR in this work will imply one component PUR, as these are mostly used for the manufacture of engineered timber. MUF and MF adhesives are highly cross linked polymer chains and therefore exhibit a high elastic modulus and rigidity, as well as a low creep factor [69, 74] and, like PUR, are also favoured due to its invisible bond line [74]. While thermoplastic PURs exhibit elastic-plastic stress strain behaviour, thermosetting MUF adhesives are elastic with brittle failure mode [76].

PUR forms CO_2 as it reacts and therefore foams and can display a high porosity [69]. The formation of bubbles in the bond line will weaken the bond and therefore sufficient pressure is required in the production to suppress foamed bond lines [74]. Failure to apply sufficient pressure during production will lessen the bond quality and structural calculations will be non-conservative if they do not account for reduced bond strengths, as experienced in experiments by Vilguts et al. [77]. In addition to the pressure, the moisture level must be controlled during production as they will influence the bond strength and sub optimal manufacture conditions can increase the probability of lamellae separating from each other, which is referred to as delamination. This has been reported for CLT panels, bonded at uncontrolled moisture levels and without the required pressure by Hindman and Bouldin [61]. Moisture will generally influence both the timber as well as the adhesive present in a bond line and lead to softening of both [70, 76]. No relevant difference between PUR and MUF glues has been identified with respect to the influence of moisture during the manufacturing process [70].

The production of engineered timber also provides the opportunity to utilise multi-material composites. While MUF and PUR are most widespread to bond wood on

wood, epoxies (EP) have been proposed for the use of bonding between wood and non-wood materials, e.g. carbon fibre reinforced polymers (CFRP) [73].

The actual bond between two adjacent pieces of timber is reliant on the interface between adhesive and timber, where the adhesive seeps into cavities and cell walls of the timber. This means that it is difficult to test the actual performance of specific adhesives in absence of the timber. Nano-indentation has shown good correlation between microfilm of adhesive polymers and timber adhesive bond lines [69].

Debonding or peeling of plies can occur when interfacial shear and normal (peeling) stresses exceed the shear and normal strength of adhesive. Smith & Teng [78] have described the governing equations as well as general solutions, which can be adapted for various boundary conditions, to calculate the interfacial shear and normal stresses in the adhesive layer, subject to the following assumptions: linear elastic behaviour, stresses do not vary throughout adhesive layer thickness, curvatures are assumed to be the same. Plastic yield deformation in the substrate (i.e. timber) will cause excessive deformation in the bond line and lead to a break of the bond [71].

The shear stress within an adhesive layer can also be determined from simple beam theory, assuming full composite action, although this approach tends to underestimate stresses near the edges of the bonded layers [78].

2.2 Cross-laminated timber at ambient temperatures

This section describes a series of methodologies and techniques that can be used to analyse the structural behaviour of CLT at ambient temperatures and how these account for the variation in strength and stiffness between the layers in CLT panels or slabs. Special focus is also given to rolling shear, as it is a peculiar failure mode for CLT subjected to out of plane loads.

2.2.1 Effective Cross-section method

For bending, compression and tension, or a combination thereof, the possibly simplest method of analysis is to use a transformed (also often referred to as *effective*) cross-section [79, 80]. In this method an equivalent cross section with a uniform Young's modulus is created by expanding or reducing the width of different layers of the cross section based on the ratio of the stiffness of the layers involved. This is based on

the assumption that strain throughout a cross section varies linearly and that resulting stresses in the different layers vary according to the layer's stiffness. In its simplest form, this cross-sectional transformation can be used for Euler-Bernoulli bending, compression and tension of beams, however, it does not account for shear deformations or variable bonding strengths.

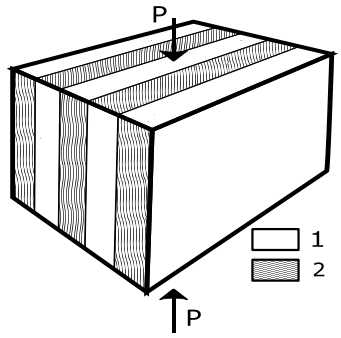

Figure 2.4. Schematic CLT sample in compression.

The ratio of elastic modulus between parallel and cross-wise oriented layers in CLT is often assumed to be around 30, for calculation and grading purposes [81, 82]. The transformed section can also be used to account for variability in elastic modulus between parallel layers only [83], if the strength and stiffness contribution of crosswise layers is ignored.

The principle of the transformed section concept can be derived by considering a piece of cross-laminated timber (or any other other composite material with layers of varying stiffness) in uniform compression or tension, as schematically shown in Figure 2.4. Assuming no shear deformation and perfect bonding, all layers must deform by the same amount, therefore the strain ϵ in all layers will be equal, but the load share of the layers, and therefore the stress σ will vary according to Equation 2.1, which, when inserted into Equation 2.2 can be formulated to yield an expression for the effective stress of one orientation through transformation into an effective area.

$$\sigma_1 = E_1 \cdot \epsilon \qquad \sigma_2 = E_2 \cdot \epsilon \qquad \frac{\sigma_1}{\sigma_2} = \frac{E_1}{E_2} \tag{2.1}$$

$$P = \sigma_1 \cdot A_1 + \sigma_2 \cdot A_2 \tag{2.2}$$

$$\sigma_2 = \frac{P}{A_1 \cdot \frac{E_1}{E_2} + A_2} \tag{2.3}$$

It can therefore be assumed that the normal stress, σ in each layer will vary, depending on the elastic modulus and that an effective cross section can be achieved by scaling the cross section areas by the ratio between the elastic moduli.

A drawback of the effective cross-section method is that it is based on an assumption of the ratio of the elastic moduli between the crosswise and parallel boards. In an experimental setting, in order to measure the elastic modulus, this assumption will influence the final determined elastic moduli. This can only be avoided if the moduli of the individual boards are known, however, this information is unlikely to be available.

2.2.2 Composition method

The Composite theory takes its name from a range of composition factors, which are used to obtain effective strength and stiffness values, depending on loading situation, the relationship of stiffness between parallel and crosswise layers and the depth of the layers [84, 85]. These composition factors (as shown in Figure 2.5) can then be used to calculate the effective bending and axial stiffness of the CLT element and stresses in the different layers. The composite theory does not take shear deformations into account and should therefore not be used for short beams with a span to depth ratio below 30, which is often used (along with 20) as a cut-off value, above which shear deflections are assumed to become negligible [36, 86]

2.2.3 Gamma method

The theory of mechanically jointed beams and columns is given in EN-1995-1-1 (EC5) [87] and recommended by Wallner-Novak et al. [83] to analyse and design CLT members. This method is also often referred to as 'Gamma method' [83, 85, 88, 89], based on a factor γ, which describes the efficiency of the shear transfer between the CLT layers. γ is taken as unity for rigidly connected or glued layers [85]. The use of a factor γ enables the calculation of an effective stiffness (see Eq. 2.4) for the whole cross-section, whilst implicitly accounting for shear deformations, which can arise between the parallel layers, due to the low shear resistance of the crosswise layers [83]. Equation 2.4 can be used for the common, symmetrical three and five layer CLT build ups, whereas for any higher number of laminations a matrix approach, as outlined by Wallner-Novak et al. [83], should be used to account for the influence of shear deformations between

	k_i
	$k_1 = 1 - \left(1 - \frac{E_{90}}{E_0}\right) \cdot \frac{a_{m-2}^3 - a_{m-4}^3 + \ldots \pm a_1^3}{a_m^3}$
	$k_2 = \frac{E_{90}}{E_0} + \left(1 - \frac{E_{90}}{E_0}\right) \cdot \frac{a_{m-2}^3 - a_{m-4}^3 + \ldots \pm a_1^3}{a_m^3}$
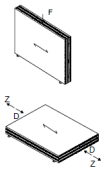	$k_3 = 1 - \left(1 - \frac{E_{90}}{E_0}\right) \cdot \frac{a_{m-2} - a_{m-4} + \ldots \pm a_1}{a_m}$
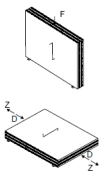	$k_4 = \frac{E_{90}}{E_0} + \left(1 - \frac{E_{90}}{E_0}\right) \cdot \frac{a_{m-2} - a_{m-4} + \ldots \pm a_1}{a_m}$

Figure 2.5. Composition factors for CLT panels [84].

layers.

$$EI_{eff} = \sum_{i=1}^{n_{pa}} (E_i A_i + \gamma E_i A_i a_i) \tag{2.4}$$

In the Gamma method in EC5 [87], only the strength and stiffness of the layers with the grain running parallel to the loading direction is utilised for the determination of load bearing capacities. It should be noted that the Gamma method was originally derived for sinusoidal distributed loads on slabs in bending [90], and therefore has to be treated with caution when it is applied to other loading scenarios, as it has not been assessed whether the reduction in second moment of area is directly transferable to different shear or moment distributions.

In CLT of more than three layers, some manufacturers will place longitudinal layers with higher material stiffness in the outer layers compared to longitudinal layers closer to the centre of the CLT element. This will cause the stress to consist of a local and global component [85]. The assumption for these is that the CLT element bends as a whole, causing global stress and that the individual layer bends itself. The stresses can be calculated as shown in Eqs 2.5 and 2.6 The maximum bending stress σ_m will occur

in an extreme fiber of an outer layer as the summation of σ_{local} and σ_{global}.

$$\sigma_{local} = \frac{0.5 E_i h_i M}{EI_{eff}} \tag{2.5}$$

$$\sigma_{global} = \frac{\gamma_i E_i a_i M}{EI_{eff}} \tag{2.6}$$

2.2.4 Shear Analogy

This method, developed by Kreuzinger [90], is considered to be more accurate in predicting deformation and stresses in beams compared to the other methods outlined above [84, 85]. It is based on creating two virtual beams, A and B, which are connected by perfectly rigid rods to ensure that they have the same deformation. Beam A is utilised to calculate any stresses and deformations that arise from bending, and Beam B is used to calculate stresses and deformations arising from shear flow. The bending stiffness of Beam A can be calculated as the sum of the individual bending stiffnesses of each layer:

$$[EI]_A = \sum_{i=1}^{n} E_i b_i \frac{h_i^3}{12} \tag{2.7}$$

The bending stiffness of Beam B is calculated as the sum of tension and compression stiffness and the neutral axis distance of each layer:

$$[EI]_B = \sum_{i=1}^{n} E_i A_i z_i^2 \tag{2.8}$$

Additionally Beam B is assigned a virtual shear stiffness, calculated from the outer and inner layers, which accounts for connection slips via a factor c_i, as shown in Equation 2.9. For a completely bonded glued connection c_i is taken as unity and reduced for flexible or slipping connections.

$$\frac{1}{S} = \frac{1}{a^2}\{\sum_{i=1}^{n-1}[\frac{1}{c_i} + \frac{h_1}{2G_1 b_1}] + \sum_{i=2}^{n-1}[\frac{h_i}{G_i b_i} + \frac{h_n}{2G_n b_n}]\} \tag{2.9}$$

The bending stresses in the layers can then be calculated individually for both virtual beams A and B and the summation of these bending stresses then gives the overall bending stress in each layer.

According to Kreuzinger [90] this approach can be used in hand or spreadsheet calculations and is therefore less computationally intensive than a finite element model yet at the same time it is supposed to be more accurate than the γ-method or k-method described above. Outside of work by Kreuzinger, or mentions of this method in summaries on CLT [85], it does not actually seem to experience a lot of use. This could be due to the fact that many of the original articles on shear analogy were published in German and other methods have seen wider distribution internationally.

O'Ceallaigh et al. [91] compared results from the composition method, γ method and the shear analogy and found that the resulting differences for the modulus of rupture and the rolling shear strength were between 1 and 1.4 %, even where shear deflections are expected to occur, and can therefore be considered negligible.

2.2.5 Rolling shear

Rolling shear has been observed as a failure mode in CLT and other laminated products. Rolling shear can be described as crack formations normal to the tangential and in direction of the radial direction and vice versa respectively [92], and therefore it is generally observed to initiate in layers with fibres orientated crosswise to the direction of the load [93]. In rolling shear the sheared fibres of a crosswise orientated layer start rolling across each other, causing material failure and an analogy of a row of toothpicks, being rolled by adjacent stiff plates can be made for visualisation of this failure mode. Rolling shear strains contribute to deflections in beams and plates loaded out of plane [36, 86, 94, 95]. There are multiple factors influencing the occurrence of rolling shear failure and deflections. Finite element simulation results from Aicher & Dill-Langer [94] as well as tests from Erhart et al. [95] have shown that the rolling shear modulus is not purely a material property, but dependent on a cross section's size, geometry and the sawing pattern with respect to the pith. The apparent rolling shear modulus and strength are increased with the ratio of board width to thickness [95]. It varies between species and it is estimated that most data from manufactures is overly conservative [95]. Kreuzinger [90] indicated that the propensity for a CLT plate to fail in rolling shear increases with increasing usage due to fatigue. Multiscale finite element modelling by Flores et al. [92] demonstrated that edge gluing can increase the rolling shear resistance of CLT slabs, as debonding cracks in the lamellae interface are prevented. Additionally they found that an increasing span to depth ratio will reduce the rolling shear resistance and change the nature of the crack formation. This finding is in contrast to the shear deflection, which increases with a reducing l/d ratio. The

authors do not offer an explanation for this, however, the reduced failure load could be explained by the fact that as the span is increased, the bending moment and therefore the rolling shear in the slab will increase.

Due to the multitude of determining factors on rolling shear strength and stiffness, there is uncertainty regarding the data available. The rolling shear modulus for spruce was measured to lie between 40 and 80 MPa and was determined to positively correlate with the density of the timber [86]. The Eurocodes [87], recommend a rolling shear strength as twice the tensile strength, perpendicular to the grain, which results in 0.8 MPa for all strength classes [96]. Within batches from various producers, rolling shear strength was found to vary less than bending strength by Fink et al. [67], who also found a positive correlation between the elastic modulus and the occurrence of rolling shear in bending tests on CLT slabs (i.e. for a higher quality raw material, there is a higher probability of rolling shear occurring before tensile failure of outer lamellae).

2.2.6 2D plate behaviour of CLT

The purpose of CLT structural elements, as opposed to glulam members, is to use it as floor slabs and wall panels. The correct assessment of the two dimensional load carrying behaviour is complex and is therefore seldom utilised in design [34, 82] as a simple one-directional load carrying design approach is simpler and is generally assumed to yield conservative results [85]. In practice, the use of 2-way acting CLT slabs is currently restricted by the requirements for moment transferring connections between adjacent panels [18, 82, 97].

To investigate the load response of timber plate elements, Stürzenbecher et al. [34] compared several theories for varying loading conditions, lamination configurations and thickness to assess their predictive capability with their respective increasing complexity. They found that shear stresses and shear deflections become less important for increasing slenderness ratios. A zig-zag pattern in stress and deflection between the different lamellae of the investigated plates was observed to reduce for an increased number of lamellae. Additionally a comparison with experimental results demonstrated that, for vertical out of plane deflections, errors between different plate theories and experimental results are small and do not differ much between the applied models. For the normal stresses in the layers the errors between the theories amongst themselves and the experimental results were found to be considerable. Doyle et al. [82] used simple analytical models and experimental results to demonstrate that significant (over 50 %) additional load bearing capacities and effective stiffness can be achieved when

two-way action is utilised in CLT. Especially in fire, when charring renders CLT layers ineffective, the two-way action and the associated load redistribution can provide significant additional load carrying capacity in the ultimate limit state. This can be assessed in terms of the stiffness ratio between the two load directions. From their experiments they also specified that, because the two way action in fire arises from the loss of exposed lamellae, slabs should be made of at least five plies in order to achieve reliable two-way action in fire, since the stiffness ratio between two remaining plies from an original three ply slab is too high to redistribute load into two way action [82].

2.2.7 Influence of layup

CLT can be manufactured with varying layer numbers (at least three) of varying thickness. The variation of the thickness of the parallel and crosswise lamellae and their configuration within CLT walls and slabs gives manufacturers an opportunity to, in theory, design their product to the requirements of the market, engineers or even a specific building. An increase in timber orientated parallel to the main direction of loading can increase the overall structural performance, especially if it is located at a distance to the neutral axis. On the other hand, thick outer layers will make it harder to achieve an aesthetically satisfying finish as the cost of a high surface quality reduces with increasing board thickness. Research by O'Ceallaigh et al. [91] on the influence of the layup configuration showed that the rolling shear strength reduced as the overall panel thickness was increased. They also found that the variance of both the modulus of rupture and the rolling shear strength was reduced for five ply CLT, compared to three ply panels.

For pure compression the strength of the connection between the layers should not vary much, however for bending problems, like buckling of slender compression elements, the second moment of area I of a section will vary by n_l^3 between a perfect and no connection for elements made of n_l equal layers [98].

2.3 Fire safety

2.3.1 Regulatory guidance

The regulation of fire safety for buildings and infrastructure has evolved over thousands of years, often reacting to changes in construction techniques and material or

after catastrophic fire events [27]. Legislation today is anchored in building regulations, setting out broad performance criteria, which mostly focus on the safety of inhabitants and fire fighters. Within the European Union the distribution of construction products is harmonised and regulated through Regulation No 305/2011 [99]. The safety in case of fire for construction works legislates that in the outbreak of fire (1) the load bearing capacity must be maintained for a specific period of time, (2) the spread and generation of fire and smoke is limited, (3) the spread of fire to neighbouring construction is limited, (4) the safe escape and/or rescue of occupants is enabled and (5) the safety of rescue teams is guaranteed. The requirements of this directive are then enacted through legislation in the individual member states. In England and Wales the Building Regulations [100] are orientated on the five requirements above, although phrased in more detail and in slightly different order. One difference is that the Building Regulations require buildings to maintain stability for a *reasonable* period of time, while the EU directive [99] requires load bearing maintenance for a *specific* period of time. This distinction is interesting, as it implies that for the directive collapse of buildings is acceptable after a fixed amount of time, while the building regulations leave more room for interpretation and *reasonable* could be interpreted as minimising the failure probability to values approaching *never* (although zero failure probabilities would be prohibitively expensive to achieve) for important buildings with reasonably worst case envisaged fires, which aligns more closely to the original intent of fire resistance for buildings to survive a burnout of the fuel load. These legislative requirements can be achieved in any manner as people undertaking construction see fit, although guidance documents are provided which provide means presumed to adhere to the requirements for buildings that are assumed to be *common*. For elements of construction these guidance documents will generally aim to ensure that the fire growth and spread is limited through adequate compartmentation.

2.3.2 Timber decomposition and charring

Wood is mostly made up of polymers and, like most other bio-based materials, it decomposes when exposed to heat by releasing volatile pyrolysis gases and leaving behind a char residue [101]. When mixed with oxygen in the right proportions the pyrolysis gases can ignite and thereby provide heat feedback to the pyrolising surface, causing sustained burning.

The decomposition process can be subdivided into multiple phases and while there is broad agreement on the phases and their wider working, there is disagreement on

the temperature ranges in which each phase occurs, most likely resulting from the variability of timber and its species.

Jönsson and Pettersson [46] have translated and transcribed the charring of timber from Fredlund [102] as a process in multiple zones of differing temperatures with charring occurring at temperatures as low as 95 °C while flaming ignition, due to a limitation of release of sufficient pyrolysis gases, does not occur below 280 °C. The formation and growth of a char layer in timber at around 300 °C will limit the flow of heat to underlying timber. Above 500 °C the char begins to oxidise on its surface and therefore regresses. The ranges above are corroborated by results reported by Emberley et al. [103], showing that pyrolysis of wood occurs between 280 and 380 °C and that oxidation occurs between 400 and 600 °C whereby all solid char is oxidised above 600 °C.

Figure 2.6. Compartment fire experiment on a CLT compartment.

There are varying values for the decomposition temperature ranges for cellulose, lignin and hemi-cellulose (the three main components of wood). Mikkola [104] states, that lignin, cellulose and hemicellulose all begin to decompose between 160 and 180 °C, while Browne [105] summarises ranges of 240-350 °C, 280 to 500 °C and 200 to 260 °C for the decomposition of cellulose, lignin and hemi-cellulose respectively.

Char generally has negligible mechanical strength or stiffness. It is highly porous and experiences high radiative heat losses on its surface. Through this it acts as an insulator and reduces the heat exposure of underlying timber as well as reducing the flow of pyrolysis gases to the surface. It is therefore often said to act as a sacrificial protection layer for timber in fire and thereby reduces the thermal penetration depth and burning rate [104–106]. For test and analysis purposes it is often assumed that the 300 °C isotherm is a reasonable indicator for the position of a char line and there is a wide ranging consensus for this assumption [46, 56, 107–109]. However, other values, like 280 [110], 288 [111, 112], 260 [113], 265 [114] or 360 °C [104], have been utilised or calculated as the char layer isotherm and some researchers have identified temperatures of 200 °C and above to mark zones of complete charring with zero strength [115].

Since char has negligible mechanical properties, the progression of the char layer into the timber is of paramount importance to quantifying the structural behaviour in fire.

This is expressed as a charring rate, the progression of char per unit time. The char formation of timber and therefore the charring rate varies with a variety of factors. However, in Europe it is often assumed that a single averaged char rate can be applied to all timber species, while in North America, charring rates are taken as species and/or density dependant [107]. Research by Fahrni et al. [116] showed that the charring rate of timber is negatively correlated to its density and this was also shown in a review of available literature by Bartlett et al. [117, 118].

Lie [119] proposes a rate of 0.6 mm/min and Stanke et al. [120] calculated an average charring rate of 0.695 mm/min for their experiments on glulam columns following a standardised cellulosic time temperature curve within a range between 0.6 and 0.8 mm/min [44]. Haksever's [121] test results on glulam columns also confirmed an average charring rate of 0.7 mm/min in standard fire exposure. Peter and Göckel [114] also obtained charring rates in a range between 0.6 and 0.77 mm/min. Technical Report 10 (TR 10) [111, 112] assumes a base charring rate of 0.635 mm/min, which can be adjusted to account for longer burning durations where the average charring rate is reduced. In Australia and New Zealand, for the purpose of verification of fire resistance through calculation, the nominal charring rate is dependent on the density of the timber, as shown in Equation 2.10 [122]. For timber with a density of 550 kg/m^3 this results in a charring rate of 0.65 mm/min. These provisions do not account for CLT and thereby ignore potential char rate increases due to the potential for char to fall off at the glue lines, which is explained in more detail in Subsection 2.3.4.

$$\beta_n = 0.4 + (\frac{280}{\rho})^2 \tag{2.10}$$

For full scale furnace tests of loaded CLT panels, Goina [123] reported varying charring rates for different tests, between 0.37 mm/min and 0.79 mm/min. These rates were inferred from the remaining cross section depths and the charring rate increased as the remaining cross section depth reduced, i.e with the exposure duration. From compartment fire experiments with exposed cross-laminated timber surfaces Li et al. [124] found an average charring rate of 1.22 mm/min. Johansson and Svenningsson [125] describe varying charring rates throughout the duration of their furnace experiments (set to simulate various fire curves) on CLT, with an accelerated rate of charring of up to 1.5 mm/min at the start of experiments, which reduces towards 0.65 as the duration of burning continues and a char layer has formed. The rate of char oxidation influences char regression and therefore the depth of char above timber undergoing pyrolysis, thereby influencing the overall rate of charring. It can therefore be assumed that the

charring behaviour will differ between different ventilation conditions.

Both Bartlett et al. [117] and Hasburgh et al. [75] describe the acceleration of char along grooves and gaps in the timber due to increased permeability for pyrolysis gases. This introduces local variability of the charring behaviour, which can make the determination of the load bearing capacity in fire more uncertain and also negatively affects the integrity fire resistance criterion. These accelerated charring rates can also be observed in timber where the grain is orientated perpendicular to the main exposure plane [117]. This can occur where the sawing patterns of lumber boards result in 'open' tangential patterns. Hasburgh et al. [75] found that, as a consequence, the ply configuration (independent of the thickness of the individual boards) influences the overall charring pattern and rate.

2.3.3 Burnout and self-extinction

For situations where fire fighting interventions are difficult or not possible (e.g. high rise buildings), a defend in place fire strategy is often needed in which the fire is contained in its compartment of origin for a 'reasonable period of time'. The development of fire resistance times was based on this concept and requires that the combustible contents of a compartment will eventually all be consumed, causing the fire to extinguish without intervention as it is starved of fuel. For compartments with significant surface areas of exposed timber this condition may never be met, as the timber (and therefore the compartment boundary itself) supplies additional fuel to fire. If this extends the fire to the point of a structural or integrity failure of the compartment boundaries, then the defend in place strategy has failed and the damage and loss from the fire will increase significantly and the building itself may be lost.

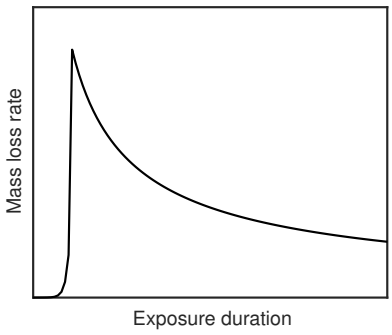

Figure 2.7. Schematic mass loss rate of timber exposed to a constant heat flux

The mass loss rate of burning timber, and therefore its heat release rate and charring rate, generally experience a peak shortly after ignition before reducing to a quasi-constant value as the char layer reaches a steady state thickness [105, 126]. The schematic mass loss rate, with an early peak and subsequent reduction during heat exposure is shown in Figure 2.7. At low external heat fluxes the mass loss rate will

reduce until it reaches a critical value and self-extinction will subsequently occur as not enough pyrolysis gases are produced to sustain flaming. A useful analogy for this is the burning of logs in a fire place. A single log will eventually extinguish, while multiple logs can provide each other with sufficient heat feedback to continue burning [105]. The critical heat flux for ignition of timber has been reported to be between 10 and 13 kW/m^2 [105, 109]. For non piloted experiments in the cone calorimeter, Quiquero et al. [127] reported a critical heat flux for autoignition above 30 kW/m^2. Crieelard et al. [126] reported extinction as the cessation of smouldering and found, from cone calorimeter experiments, that this will occur for heat fluxes below 6 kW/m^2. They also observed an influence of airflow on extinction, with flow speeds of 0.5 m/s aiding extinction through cooling and flow speeds of 1 m/s accelerating smouldering through the additional supply of oxygen.

Compartment fire research investigates the burning behaviour in built compartments with predetermined fuel loads and varying ventilation parameters. Frangi and Fontana [128] performed a series of post-flashover compartment fire experiments on wooden hotel modules. They found that, for exposed timber surfaces, the external flaming was more severe compared to non-combustible interior surfaces, due to the contribution of the timber as additional fuel, however, the authors did not quantify this increased severity of external flaming. Since most of this additional fuel burned outside the compartment opening, the authors concluded that the interior temperatures did not vary significantly (without quantification of this significance) between exposed and non-exposed timber construction. Li et al. [124] performed multiple experiments on timber compartments with exposed and unexposed timber surfaces. They found an increase in total heat release rate of up to 80 % for an exposed CLT compartment fire, where they observed that a majority of the additional heat was released from pyrolysis gases burning outside the compartment opening and that therefore the gas phase temperatures inside the compartment for fully developed fires did not vary by more than 100 °C between exposed and non-exposed experimental cases. They concluded that the fire performance of elements of construction will differ between compartment fire experiments, for which the temperature development is a function of the available fuel and the ventilation conditions, and standard fire tests, for which temperatures are forced to follow a standardised temperature time curve, and are explained in more detail in Section 2.4 in the context of fire resistance ratings.

Hadden et al. [129] performed a set of CLT compartment fire experiments with different numbers and types (wall or ceiling) of timber surfaces exposed, specifically to look at the necessary conditions to achieve auto extinction in timber lined compartments. The

results from these experiments showed that extinction is possible for an exposed timber ceiling and wall, as long as char-fall off (see Subsection 2.3.4) can be avoided. This was confirmed by an experiment by Emberly et al. [130], who also achieved burn out and auto extinction in a CLT compartment fire. In addition, multiple large scale experiments on the fire dynamics in full scale timber compartments were performed at the National Institute of Standards and Technology (NIST) and described by Su et al. [131] and during the same time (highlighting a rising interest in the fire safety of CLT in North America) multiple CLT burnout experiments were reported by Zelinka et al. [132]. Both of these experimental series concluded that auto extinction can be achieved under the right conditions, depending on the amount of exposed wood, the ventilation, and the integrity of the glue lines bonding the timber lamellae of the CLT when heated. Medium scale work on CLT compartment fire dynamics has been undertaken by Bateman et al. [133], which showed that the moveable fuel load has a critical influence on self-extinction of timber compartments, as has the configuration, with two walls exposed posing a more adverse scenario for auto-extinction than a wall and a ceiling. Gorska et al. [134] describe laboratory scale experiments on scaled down CLT compartments and found that the critical incident heat flux on timber surfaces for auto-extinction is much lower than in large scale testing. They postulated that this was caused by a change in the temperature gradient through the CLT, which could be attributed to the change in scale and the change in heat losses through the compartment boundaries as the surface to volume area changes.

2.3.4 Delamination/Fall off of char

Because CLT is made up of multiple lamellae, which adhere to each other through the use of adhesives, it is susceptible to delamination in fire. This process, which is also denoted as a 'loss of stickability' by some authors [135], describes the fall off of charred lamellae as the char front reaches or passes the glue lines (shown in Figure 2.8). The char, by virtue of its high insulation capacity, performs a protective function for the underlying timber and its loss therefore has consequences for the fire dynamics and the subsequent rate of charring and the temperature development in the timber. Experiments on CLT floor slabs by Frangi et al. [56] showed that the falling off of charred layers will temporarily increase the charring rate of the underlying timber layers, resulting in higher average charring rates over the duration of a furnace test. It was also highlighted that for horizontal slabs, made of fewer thicker boards, the average charring rate will be reduced, as it takes longer for the heat to penetrate to the first adhesive line and therefore for the boards to fall off, as compared to thinner lamellae.

This was confirmed by Osborne et al. [136], who performed tests on CLT walls made of varying ply thickness and found an increased charring rate for thinner plies. A similar behaviour was found by Suzuki et al. [113], and from their experiments they postulated that the effect of thicker lamellae ceases to be significant above a layer depth of 27 mm. Considering these findings, a three-layer CLT panel can show improved fire behaviour than a five-layer panel of the same overall thickness, but only if the rate of charring is considered as the main performance indicator.

The orientation of CLT is also considered to influence the potential of delamination, with vertically orientated panels, as would be used in walls, experiencing less pronounced delamination than horizontal ones [136, 137]. This results in an overall reduced charring rate, compared to horizontal CLT slabs [135]. Still, Emberley et al. [138] reported the occurrence of delamination of vertically orientated samples at bench scale in mass loss cone testing, which was deemed to cause a subsequent increase in mass loss rate and flaming. Crieelard et al. [126] also observed delamination of CLT in vertical wall elements in small scale compartment fire experiments.

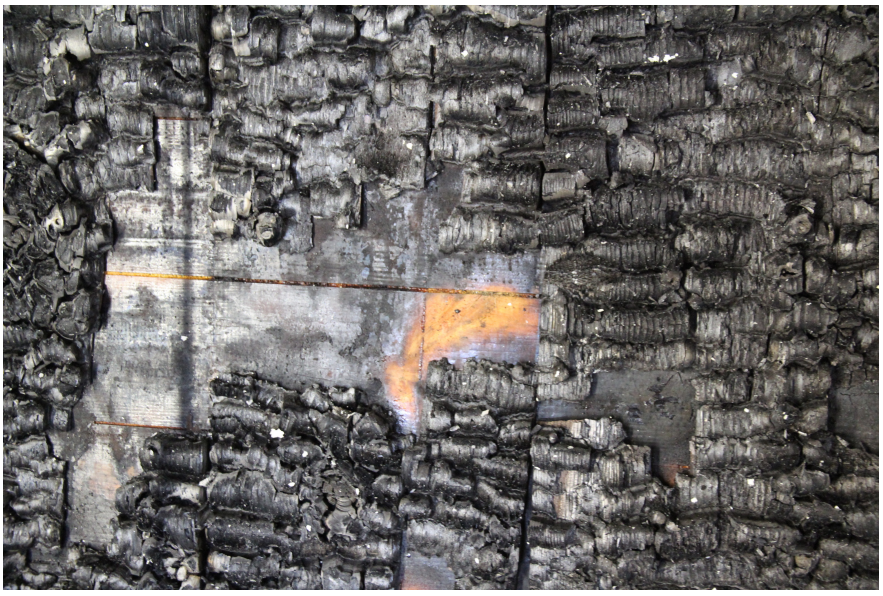

Figure 2.8. Char fall-off (delamination) as observed after a fire in a compartment with polyurethane bonded CLT, from experiments by [129].

The choice of adhesives in CLT production will affect the potential for delamination, which complicates comparisons between different tests. It has been reported that CLT panels bonded with Polyurethane reactive (PUR) adhesives will experience delamination [126], while those with Melamine-Urea-Formaldehyde (MUF, or the related MF)

will show reduced or no delamination at all [88, 139]. Similarly, Klippel and Schmid [135], for their assessment of a proposed charring model, assumed that MUF and phenol resorcinol formaldehyde (PRF) adhesives do not experience char fall off, however, they note that this assumption is not strictly valid for all MUF or PRF tests. Hasburgh et al. [75] performed standard furnace tests on CLT slabs with different adhesives and found that the fall off of charred timber was significantly lower in MF and PRF bonded slabs, compared to slabs manufactured with PUR and emulsion polymer isocyanate (EPI) adhesives. Fackler [140] reported delamination on a glulam column using melamine based adhesive. Test on vertical CLT elements in Japan [113] demonstrated that API glues will lead to approximately 10 % higher charring rate than the use of PRF adhesives. Johansson and Svenningsson [125] performed a study of the delamiantion potential of different adhesives where they attempted to replicate the conditions in a CLT compartment fire described by Su et al. [131] in a furnace. They observed delamination of the CLT bonded with regular one component PUR but did not observe delamination with any of the other adhesives, one of which was an one component PUR adhesive that had been formualted specifically to avoid delamination. The other assessed adhesives were MF, PRF and EPI.

Delamination in CLT will also heavily influence the compartment fire dynamics as it exposes 'fresh' timber below char layers and adds to the overall fuel load in a compartment. This can delay the onset of self-extinction of the timber after all the moveable combustible load within the compartment has burnt out [103]. Su et al. [131] reported secondary flashover due to delamination of the PUR adhesive used in their timber compartment experiments. Product requirements for certified CLT in the USA and Canada requires adhesives to be assessed to maintain their adhesion up to 220 °C as well as not show char fall off in a compartment fire test to a specified burnout heat release rate induced by a gas burner, in order to minimise delamination of the end product [81].

2.3.5 Temperature Distribution

To analyse the thermomechanical response of structurally loaded timber elements, the temperature distribution underneath the surface must be known. It is generally assumed that the char layer, through high insulation properties and a reduced flow of pyrolising gases, protects the virgin timber underneath and reduces the so called "thermal penetration depth" [104, 106]. Östman et al. [137], as well as Klippel and Schmid [135], state that the temperature affected properties in CLT exposed to cellulosic standard time temperature curves will be located along a depth of 35 to 40 mm below

the char layer, which is confirmed by findings of experimental studies [141]. Similarly, Frangi and Montana [106] measured mean thermal penetrations depth between 25 and 35 mm below the char layer, for various engineered timber products (solid, glue laminated and nail laminated timber) exposed to cellulosic standard time temperature exposure. In initially protected timber slabs, the temperature gradient has been found to be lower, causing a deeper temperature penetration from a lower heating rate [142]. At 100 °C an arrest in the development of temperatures is usually observed due to latent heat required to evaporate moisture in this temperature range [75, 143].

The determination of timber temperatures below the char is an ongoing field of research and is complicated by the pyrolysis of timber when heated. Reszka and Torero [144] employed a semi-infinite solid model and determined that at exposure heat fluxes of 10 kW/m^2 or lower timber can be treated like an inert material. Above this heat flux, self-heating from exothermic reactions has to be accounted for. Poncsak et al. [143] reported exothermic heat generation in timber at temperatures as low as 150 °C. The internal conduction heat flux in timber samples has been determined to peak at 6 kW/m^2 and to reach 3 kW/m^2 as the timber reaches a steady state phase of burning [103]. EC5 [145] provides material properties to calculate the temperature evolution within timber elements from advanced calculation methods, however, these values are effective values that have been determined through calibration of standard furnace tests and therefore should not be applied to natural fires [107]. Scheer et al. [146] presented an empirical model for the temperature at the centre of the cross section of a structural timber member from which they calculate the strength and stiffness reduction of the remaining cross section, however, due to the temperature gradient, the temperature at the centre is often not of high relevance compared to temperatures closer to the char timber interface. In addition it is unlikely that such an empirical model is applicable to a wide range of timber sizes and heating scenarios.

White and Woeste [147] commented that the temperature profile during the cooling phase in real fires is likely to be flatter and of longer duration than for standard fires and this must be taken into account to assess the post-fire damage from thermal degradation of timber. In a similar note, Hopkin et al. [148] have identified that current considerations of temperatures and their distribution are only accounting for the duration of burning, but do not consider the contribution of heated or smouldering timber after burn out of a compartment.

2.3.6 Fire retardant treatments

There is a widespread perception that the addition of certain surface covers and impregnations can reduce the flammability of timber and therefore increase the fire resistance [7], however, these treatments often only delay ignition of timber; it remains combustible and the fire resistance is usually not improved through these measures [26, 105, 122, 149, 150]. The effect of chemical treatment, which encourages early onset of charring, has been found to have no influence for large cross-sections of timber members [151]. Chemically treated timber might not be converted to energy at its end of life, due to an increased toxicity of released pyrolysis gases, thereby reducing the sustainability of a building project [37, 58].

2.3.7 Encapsulation

A commonly used method to deal with the combustible nature of timber is to cover it in non-combustible insulation, thereby preventing or delaying its involvement in the fire. This approach has a long history and especially after large timber conflagrations the idea of completely fire proof buildings often advocated either a complete replacement of timber with non-combustible material or to cover timber with plaster [152]. Su et al. [131] reported complete encapsulation of timber, using three layers of plasterboard, as an effective means to prevent structural timber elements to become involved in the fire and to ensure burnout of the moveable fuel load. This will of course vary for different fuel loads, and three layers of plasterboard should therefore not be seen as a panacea for the fire safety of CLT for situations other than the ones bounded by the described experiments. The application of three layers of plasterboard is also unlikely to be cost effective as it adds material and labour costs to timber projects, in addition to additional weight, and a reduction of the effective internal floorspace.

Hasburgh et al. [153] found that an air gap between gypsum boards and the encapsulated CLT will increase the time to fall off of the encapsulation but will subsequently lead to a higher rate of charring of the first CLT layer. Similarly, their study found that for two or more gypsum boards the onset of charring was delayed compared to one layer of gypsum board (as would be expected) but the resulting charring rate was higher, which the authors attribute to the higher gas temperatures in the furnace when the encapsulation fails. The increase in charring rate of the first timber ply between an unprotected panel and a panel with three layers for gypsum board was reported as 18.7 %. The best encapsulation performance was reportedly achieved by spray on

non combustible materials [153], although these are not commonly used in practice for timber. On the contrary to the findings by Hasburgh et al. [153], Li et al. [124] found that a tight fit of encapsulation with no air gap, where encapsulation was attached to CLT, produced a better protective performance than plasterboard on a timber frame with air gaps between the timber studs. This highlights that there are still knowledge gaps regarding the quantification of the protection provided to timber by plasterboard or simialr noncombustible covers.

Many standards and guidance documents for the calculation of fire resistance treat the contribution of encapsulation as additive to the fire resistance [122, 137] and this approach is therefore utilised by developers to meet a required fire resistance ratings [55]. The inclusion of encapsulation in the calculation of fire resistance is often accompanied by a recommended increase in the charring rate of the encapsulated timber for the determination of its fire resistance. In Australia and New Zealand the nominal charring rate (refer to Eq. 2.10) should be increased by 10 % to account for the accelerated charring after the failure of encapsulation. The involvement and contribution of initially protected timber in the fire after encapsulation has fallen off is self explanatory and has been well documented in literature [128, 129]. With the considerations of burn out in mind, it should be obvious that relying on additive fire resistance and incorporating the fall off of encapsulation into the fire design of timber compartments is potentially a recipe for disaster and should be avoided in most cases.

2.4 Structural fire safety

This section describes the current state of the art of determining and designing for structural fire resistance. The fire resistance approach is generally described within the standardised fire resistance framework. The meaning of fire resistance for timber elements is discussed and past tests on glulam columns and CLT walls are presented alongside codified guidance approaches to demonstrate fire resistance through calculations.

As the concerns regarding structural collapse of buildings affected by fire rose in the 19th century [25], building systems began to compete with each other in their capacity to withstand building fires. Comparative tests were required in order to rely on quantitative rather than anecdotal evidence on the relative fire performance of different systems. Reports on non-quantified comparative fire testing can be traced back as

early as the 1790s, but it was not until the 1880s that fire resistance tests became increasingly utilised in various countries [154]. The thermal exposure utilised by various test stations varied but were all based on either a limiting maximum gas temperature or an initial rise followed by a maximum gas temperature that tested structures had to withstand. The required temperature increase was formalised into a standard time temperature curve in 1917, which has remained almost unchanged since then in most national and international standards assessing fire resistance. This temperature curve was not based on actual building fires, but rather the capacities available at that time to generate the temperature curves that building elements were thought to be required to withstand [155]. The exact provisions for the determination of fire resistance by means of standard testing vary between jurisdiction. For example there are differences in the specific set-up and the pass-fail requirements between the ISO 834 [28] and the ASTM E119 [156] fire resistance time temperature curve. However, for timber in practice, as Janssens and White [157] have pointed out, these differences do not cause any significant variation in the thermal response (i.e. charring depth and thermal penetration) of timber members. The advantage of determining fire resistance based on a standard temperature curve in a furnace is that it allows a direct comparison between building elements without having to consider the complex fire dynamics that influence the severity of a real building fire.

In contrast to a standard fire curve stands the burnout fire, which incorporates a cooling phase as the fuel load in compartment is consumed by a fire. Experiments on burnout fires led Ingberg [29] to propose the original intent of fire resistance ratings as a measure for equivalence of fire severity on the exposed elements of construction. The idea was to relate the complete burnout (including the cooling phase) of the fuel load in a compartment to an equivalent fire duration in a standard fire furnace. This was proposed to be achieved through an equivalence in area under the curve between a base line temperature of 150 or 300 °C and the two temperature curves considered. From a series of compartment fire tests with varying fuel loads the required equivalent fire resistance was determined for a range of fuel loads (representing different occupancies, e.g. office or record room). Ingberg himself recognised that the proposed methodology of a temperature time area could not satisfy the underlying physics of the heat transfer between the compartment and the elements of construction. In addition, there were large margins of error for the required fire resistances based on the choice of a baseline temperature. The approach was acknowledged as deficient, yet the author had '*so far found no better measure of comparison that can be conveniently applied*' [29], indicating

that a better approach might arise in future. With further development of the knowledge of fire dynamics it was recognised that ventilation is another critical parameter that determines the temperatures inside a fire compartment. Thomas [158] describes that the requirement for construction elements to withstand the effects of fire until burnout is dependent on the fuel load, as well as the available ventilation openings. He points out that most codified guidance documents do not account for this properly, but rather assign required fire resistance based on building category and that this should not be seen as an adequate approach for engineers. Similarly, Harmathy and Mehaffey [159] stated that fire resistance requirements have generally been inflated (without providing quantification thereof) in order to account for the known shortcomings of the original fire resistance concept based on fire loads.

From the reviewed sources above it can be summarised that fire resistance ratings arose from a necessity for a comparative analysis of building elements in fires[25, 154], and were initially defined by technical limitations in generating sufficiently hot temperatures [155] before the concept was codified with respect to different fuel loads and a required fire resistances to reach burn out of the initial fuel loads [29]. The underlying principle of fire resistance ratings have not changed in the last 100 years, which has, at times, attracted criticisms from the fire science community [158, 159]. In lieu of testing, the comparative structural fire performance can also be obtained through calculation of the expected reduction in load bearing capacity in fire; this requires detailed knowledge of the effects of fire and elevated temperatures on the mechanical material properties of timber, which are reviewed in the following chapter.

2.4.1 Structural properties of heated timber

The effect of heating on the mechanical properties of timber must be considered to assess the load bearing capacity of timber elements and systems in case of fire. For compression elements the most important mechanical properties to consider are the compressive strength and the elastic modulus. The elastic modulus at ambient temperatures is generally assumed to be the same for tension and compression (parallel to the grain), however, upon heating the elastic modulus in tension and compression shows a different reduction with increasing temperature and moisture. Any advanced constitutive models must account for this by consideration of their strain distribution [160, 161]. The changes in the mechanical properties can be attributed to chemical and physical changes in the timber. Schaffer [162] postulated that at least three reaction processes are responsible for the deterioration of compressive strength in timber

and that, while thermal and mechanical (stress induced) degradation of timber are linked, both processes can reduce the chemical bonds of various timber components independently of each other.

Multiple authors have published detailed experimental work on the compressive strength of heated timber. A non exhaustive overview is shown in Table 2.1 to highlight the varying experimental conditions that past experimental series have applied to investigate the compression strength and stiffness of timber when heated. It can be seen that the employed heating methods have varied between samples, including oven heating, heating in hot water baths and conductive heating with hot plates. This will change the temperature and moisture content distribution in the samples. This explains the variable outcome that can be seen for the normalised reduction with increasing temperature in strength and elastic modulus in figures 2.9 a) and b) respectively. The following paragraphs give a more detailed overview of the influence of experimental variables on the strength and elastic modulus in heated timber. To the knowledge of the author no targeted studies currently exist on the effect of heat and moisture on cross-laminated (or similarly engineered) timber.

Table 2.1. Overview of selected experiments for heated timber in compression

Source	**Timber Species**	**MC** (%)	**Experimental method**
Van Zeeland et al. [163]	Pinus Contarta	10	Aluminium heating platens for conductive heating during load.
Young and Clancy [62]	Pinus Radiata	12	Steel plate heating of samples to target temperature followed by loading.
Glos and Henrici [164]	Spruce	8 & 12	Oven heating to target temperature followed by loading with infra-red heating.
Figueroa et al. [165]	Pinus taeda	12	Oven heating 180 minutes followed by loading in environmental chamber.
Kundson and Schniewind [166]	Douglas Fir	12	Oven heating between 15 and 60 minutes, followed by loading. Elastic excitation experiments with simulteanous heating.
Sano [167]	Ash, Spruce	13 - 15	Heating and loading in hot water bath.

2.4.1.1 Species

Different researchers have focused their research on different timber species, however, it has been proposed that, as the proportion of lignin and cellulose is comparatively similar for most timber species, the reduction in strength and elastic modulus when heated

can be determined from select species and then applied to a wider range [62]. This is confirmed by results from Sano [167], who found the slope of the reduction curves of samples for both ash and spruce to be similar upon heating, thereby deducing that that the relative loss of mechanical properties can be treated independent of species. In contrast to this, Gerhards [170] remarked that a multitude of studies he reviewed had found variations between species when it came to changes in strength or stiffness, and has called for more fundamental research on the physical changes in the material rather than the changes itself. His views are supported by Figueroa et al. [165], who performed heated strength reduction experiments on three timber species under constant uniform temperatures in an environmental chamber. The three species exhibited different reduction factors for strength and it was also observed that the modes of failure for all species changed with increasing temperatures through a variation in the observed angle of the shear failure plane that arose on failure of the wood fibres.

2.4.1.2 Moisture content

Gerhards [170] published an in-depth literature review on the effect of mechanical properties when the moisture content and the temperature are changed. He reported that a correct assessment of the strength reduction is made difficult experimentally, as heating and heating times will affect the moisture content and an increased moisture

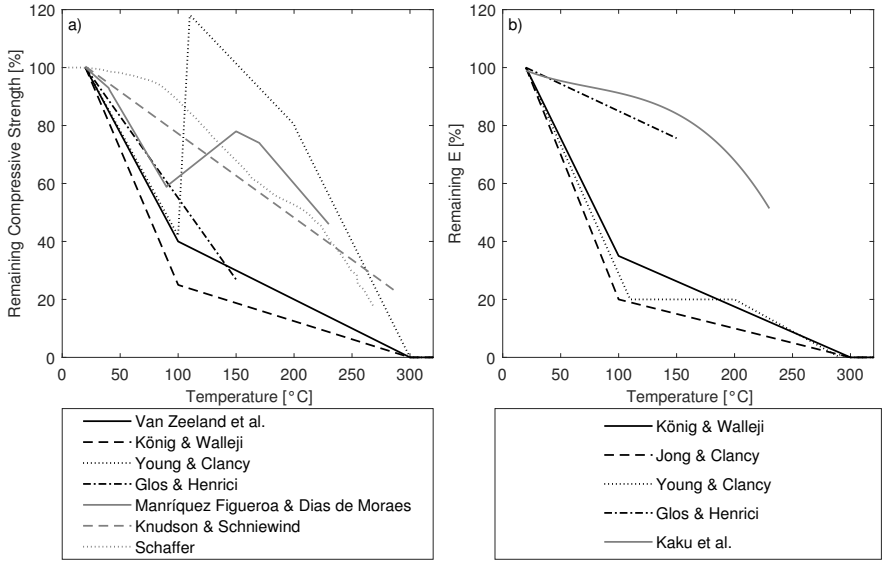

Figure 2.9. Reduction in a) strength [62, 108, 163–166] and b) elastic modulus [62, 108, 164, 168, 169] with increasing temperatures from various authors.

content was deemed to amplify the effects of heat for most of the assessed properties. As a counterpoint, Tiemann [40] stated, that rather than an increase in temperature, it is an increase in moisture content of the cellulose fibres that is the primary driver in weakening and softening timber and that temperature will exasperate this effect through its lowering of the fibre saturation point. In his experiments he found that an increase in moisture from ambient levels (12 %) to saturated timber will reduce the strength by a factor of up to 2.4 and the elastic modulus by a factor of up to 1.6.

> "Moisture has more effect on the strength of wood than any other extrinsic condition."
> *Harry Donald Tiemann* 1906 [40]

Van Zeeland et al. [163] conducted their own strength reduction tests for timber and found that a majority of models they reviewed against their experimental data, did not accurately account for the strength reduction they observed. They highlight the fact that, due to the complex interaction of moisture, heat and strength for timber, the experimental conditions will heavily influence any empirical findings on strength reduction. The elastic modulus in compression has been found to reduce drastically in moist timber samples, compared to dried ones, upon heating [62]. There is much debate about the correct reduction in elastic modulus with temperature and it is likely to be influenced by the method of measurement employed. While an increase in temperature will reduce the elastic modulus, a reduction in moisture will increase it according to Stanke et al. [120]. The difference in moisture content and movement can be seen in the curves in Figure 2.9 a). Reduction factors by Young and Clancy [62] and Figueroa et al. [165] show an increase in strength around 100 °C, which can be attributed to their use of steady state heating, which causes the samples to dry before loading is applied and therefore increases the ultimate strength. Other researchers like Van Zeeland et al. [163], who utilised transient heating on samples subjected to a constant load, found more severe reduction factors, especially above 100 °C. The most severe reduction curve for timber compression strength by König and Walleji [108] originates from inverse modelling on timber studs in fire resistance experiments and considers moisture implicitly. This reduction curve is widely used through its association with Eurocode 5 [145] which is thought to be based on this work.

2.4.1.3 Duration of combined heating and loading

Creep has been implicated to cause additional deflections in compression experiments, requiring an assessment of deflections of heated timber elements over time [62]. Schaffer

[162] found that the remaining compressive strength at elevated temperatures increased after two hours of heated creep loading compared to immediate heated loading. A similar development was found for the failure strain. He attributed this to the production of phenol resin in the timber, causing new bond formations and an increase in lignin. Knudson and Schniewind [166] found that the time used for heating small scale compression test samples had only a minimal effect on the resulting strength reduction. They also found that the residual compressive strength after heating, cooling and reconditioning to the original moisture content will be higher than the original strength for temperatures up to 150 °C, after which the residual strength was reduced. As for Schaffer's [162] research, the increase in strength is attributed to changes in lignin content. Jong and Clancy [168] found in experiments that creep constitutes a significant proportion (up to 75 %) of deflections for heated timber samples in compression. The measurement of mechano-sorptive creep has been attempted previously, however, the results have been found to be inconsistent as the internal moisture distribution within samples is difficult to control [168]. For constant temperatures, Armstrong and Kingston [171] found a twofold increase in relative creep under constant bending loads with decreasing moisture content, and further experiments by Armstrong and Christensen [172] showed that increase in moisture content from a dry state to saturation increased the measured deflections of constantly loaded beams by a factor of about 2, and that subsequent reduction of the vapour pressure to dry conditions further increased the deflections by an additional factor of 0.5 of the initial elastic deflections. Additional cyclic changes between dry and saturated vapour pressure increased the creep ratio to 11, which maintained a ratio of 9 upon unloading and only recovered upon recondition to initial moisture contents.

The heating and loading history is also relevant when considering the residual strength and elastic modulus after heating has occurred. This is relevant not only to assess the remaining strength of members *after* a fire but also to assess the remaining load bearing capacity *during* a fire event, due to the progression of heat into deep timber sections in the burnout stages of a fire [173]. Heated, non-charred sections of timber will continue to lose strength, but this strength may be partially restored upon cooling [36, 149]. Any continued smouldering or transfer of heat will continue to increase the temperature and thereby reduce the capacity to resist loads [148]. Irreversible changes to the strength of timber have been reported at temperatures as low as 65 °C [109, 174]. This is also dependent on the exposure duration, and for exposure of hours (as would be expected in most fires) White and Woeste [147] assume that irreversible damage occurs at temperatures above 100 °C. Thermal treatment (to enhance the aesthetics

and durability of timber) studies [143] on birch timber have shown that the residual modulus of rupture (MoR) after heating and reconditioning to ambient moisture levels will experience a slight decrease around 120 °C before recovering beyond ambient values and experiencing a sharp drop above 200 °C. This effect is exacerbated by a low heating rate and increased holding time, indicating a negative effect of the duration of heating and exothermic chemical reactions within the timber. For the elastic modulus the reductions above 200 °C were found to be less pronounced and there was no effect of heating rate. Tiemann [40] found that timber that is dried and then reconditioned will reduce in strength and stiffness compared to their original values before drying.

2.4.1.4 Comparison of influence on tension and compression

One peculiarity of timber compared with steel or concrete is that both the retained fraction of strength and the elastic modulus are affected differently from the effect of heating in tension and compression [118, 160, 170, 175, 176]. This is illustrated in Figure 2.10 for the recommended reduction curves from EN-1995-1-2 (EC5) [145]. This adds additional complexity to the structural analysis of timber elements in fire (or heat) subject to bending forces as the temperature profile within the member will influence the location of the neutral axis and therefore the internal stress distributions.

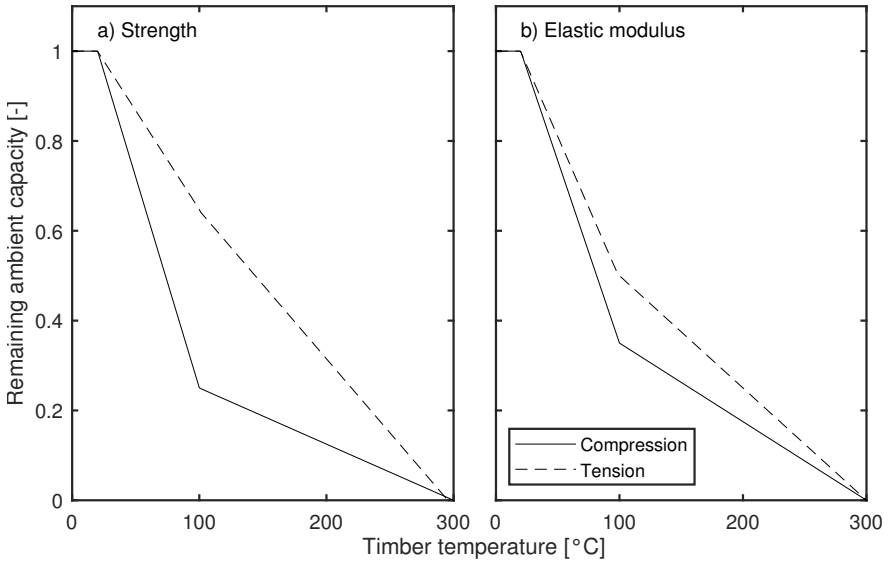

Figure 2.10. Reduction in tension and compression according to EN 1995-1-2 [145] in a) strength and b) elastic modulus with increasing temperatures.

2.4.2 Structural influence of adhesives under heating

Engineered timber relies on adhesion of adjacent lamellae to create composite action. This is achieved through the use of adhesives (although there are options for non-adhesive engineered timber, for example dowel laminated timber, which are not discussed in this work). The adhesive performance is already reviewed in Subsection 2.3.4 with respect to delamination of char. This section deals with debonding, which should not be confused with delamination, although the terms are sometimes used interchangeably. Debonding describes loss of composite mechanical action between lamellae, with both plies still theoretically capable of performing a significant load bearing function, while for delamination the char only retains and insulating function and its consequences therefore primarily affect the fire dynamics and only affect the load bearing capacity through secondary effects like the extension of the burning duration. Building timber elements bonded with adhesives are considered to experience no interlayer slip at normal use conditions [98].

It has been proposed by Emberley and Torero [177] that a reduction of strength of the glue lines for CLT below the charring temperature of 300 °C will lead to slip between the layers, reducing the composite action of the CLT, leading to increasing deflections and eventually failure of the whole system. A change in failure mode from failure of the timber to failure to the glue line in single-lap heated shear tests has been described by Emberley et al. [93] for temperatures between 80 and 100 °C [178] for PUR bonded timber. They also performed a structural bending test on CLT beam elements, heated with a low heat flux of 6 kW/m^2 to temperatures below the charring temperature for timber. The heated beams experienced debonding failures and the recorded mid span deflection at failure increased more than threefold compared to ambient tests. Rolling shear failures were observed in regions where discontinuities began to form in the bond line, propagating to full timber failures. This can can be attributed to the occurrence of elevated shear and normal stresses at the edges of bonded plates [78]. Increased deflection due to a reduced effective stiffness could be critical in combined bending and compression as it magnifies P-Delta effects and will propagate to local or global instability of a member. Another experiment by Emberley et al. [138] showed debonding along the glue line and subsequent fall off of timber lamellas for vertically orientated samples subjected to a constant heat flux, which is shown in Figure 2.11.

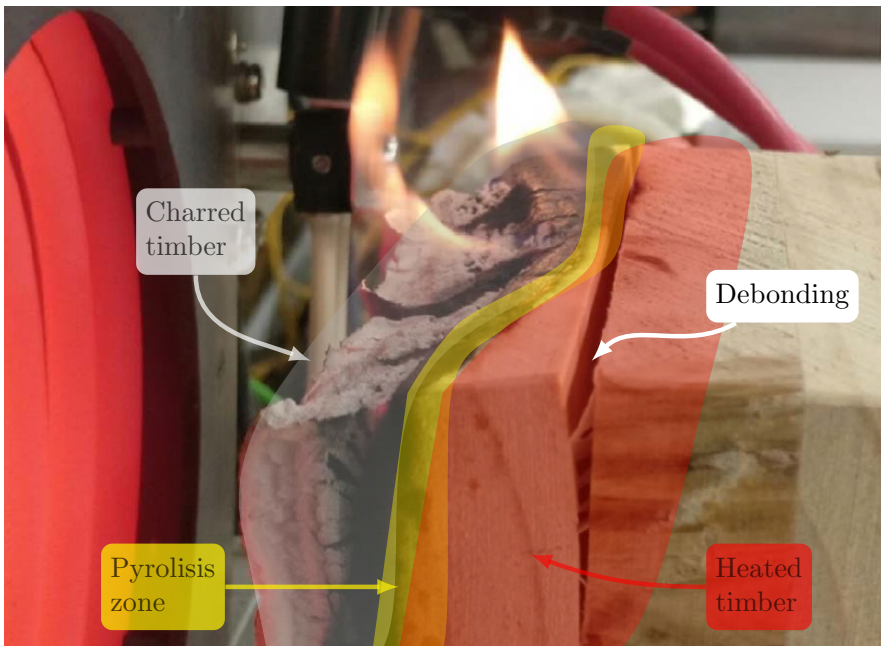

Figure 2.11. Debonding, charring and pyrolysis shown on a CLT sample in vertical orientation exposed to a constant heat flux. Adapted from [138].

2.4.2.1 Adhesives in heat

Differences exist in the performance of different adhesives at elevated temperatures [72, 83]. This is to be expected as adhesives are organic polymers and will therefore exhibit a change in strength and stiffness over a range of temperatures [71]. The following section provides an overview of available findings on the strength stiffness of adhesive glue lines for elevated temperatures. The focus is on studies involving PUR, MUF or MF adhesives, as these are preferentially used in the CLT manufacturing process. Shear tests on PUR glued timber pieces by Frangi et al. [72] have shown that even within a narrowly defined group as one component PUR, the reduction in cohesive strength of the glue will vary significantly between different products. Care should therefore be taken not to generalise experimental observations on glue line behaviour from one formulation to all related adhesive products. Serrano and Källander [74] describe variation between PUR compositions but also variation in failure time for different samples with the same PUR formulation. Richter and Steiger [73] found an accelerated reduction in shear modulus (also called G-modulus) of PUR bonded beech surfaces in Dynamic Thermomechanical Analysis (DTMA) compared to solid wood samples. This effect was especially pronounced as the thickness of the bond lines was

increased.

For the heat induced weakening of glues a distinction can be made between cohesive failure and adhesive failure of the glue. It has been found that for PUR adhesives, the shear resistance of bonded connections experiences a steep strength loss up to temperatures of 70 °C and that cohesive failures become more likely at increasing temperatures [72]. Similarly, from a review of multiple studies, Stoeckel et al. [70] identified PUR to be subjected to relatively large losses in stiffness at elevated temperatures, while MUF was found to only suffer minor performance losses in this regard, most likely due to its high cross-linking. Clauß et al. [174] performed lap shear tests on beech samples bonded with different adhesives at temperatures between 20 and 220 °C. The adhesives used were MF, UF, MUF, PRF, EPI as well as three different formulations of PUR. The results showed that for MUF, UF and MF adhesives the percentage of timber failure remained close to 100 % up to the highest applied temperatures, indicating a good thermal stability of these adhesives. For the PUR samples, one PUR adhesive performed equivalent to the melamine and urea adhesives while the others experienced a high degree of adhesive failure even at moderate (between 50 and 150 °C) temperatures, highlighting variability in the thermomechanical performance of different PUR formulations. The PUR that performed well had a longer curing time and slower reactivity. Niemz and Allenspach [179] found from lap shear tests that for increasing temperature both a PUR and an urea formaldehyde based adhesive showed a reduced wood failure percentage in the cross-sections, although this effect was more pronounced for PUR. No tangible difference was found for the shear strength of the specimen at elevated temperatures. Quiquero et al. [127] assessed the residual strength and stiffness of glulam samples bonded with PRF and PUR at small and large scale. From shear experiments on samples heated in the cone (and subsequently reconstituted) they found that the strength and stiffness of the adhesive line reduced by more than would be expected if only the effect of the char depth was considered. This was also confirmed from experiments on glulam beams that were either charred by fire, or had material carved out manually. In the shear region the charred elements performed worse, suggesting underlying permanent heat induced damage to the adhesive line. They could not identify a significant difference between PUR and PRF samples. Richter and Steiger [73] found that the effect of temperatures should also be considered where timber is bonded to other materials. For the bonding of CFRP to wooden surfaces, using EP adhesives, temperatures of the bond line up to 50 °C were considered non-problematic, while temperatures above this value can significantly reduce the bond strength.

When assessing the performance of adhesives at elevated temperatures, the glass transition temperature (T_g) would come to mind as a critical parameter. Detailed information on glass transition temperatures on individual adhesives is not widely published and therefore not readily available for most cases. Verdet et al. [180] found a T_g of 86 °C from DMA tests for a PUR adhesive that conforms to Type 1 in EN 301 [181], which is also the requirement that is met by both adhesives that were used to bond the CLT for the experiments described in this thesis. Verdet et al. [180] also found that there was no correlation between the glass transitions temperature and the performance of glued in rods in pull-out tests. They attributed this to the fact that both strength and stiffness of the adhesive deteriorated before the glass transition temperature (from separate DMA tests) was reached. Multiple authors working with PUR adhesives have cautioned not to attribute too much importance to the glass transition temperature with respect to performance; Kläusler et al. [76] stated that the glass transition temperature T_g for most PURs used in timber construction are below room temperature and that this does not inhibit their use. Similarly, Burchhardt [71] gives the example of a PUR that has a glass transition temperature of -53 °C but provides continuous long lasting performance in wind shields at temperatures far above this T_g. At the same time he describes a PUR adhesive with a T_g of 57 °C, thereby highlighting the wide range this value can take within the same adhesive group.

A lot of research into the elevated temperature behaviour of adhesives is not explicitly carried out in the context of structural fire safety bur rather with durability concerns or the use in special environmental conditions. In a fire, rapid temperature changes will not only increase the temperature but also cause changes in the moisture content within an engineered timber product and its glue lines. Therefore, the influence of elevated relative humidity or wet conditions should also be considered for the fire performance of adhesives.

2.4.2.2 Moisture content

In addition to elevated temperatures, moisture is another environmental variable that can negatively influence the material properties of adhesives. Kläusler et al. [76] assessed the tensile strength and elastic modulus for PUR, MUF and PRF adhesives when conditioned to varying levels of relative humidity, ranging from 5 to 95 % as well as immersion in water, and found that both PUR and MUF experience a linear reduction for both assessed parameters. MUF adhesives experienced the largest reduction (up to 75 % of elastic modulus) but its absolute strength and elastic modulus remained

higher than for PUR, which experienced a more moderate decrease for both. A high relative humidity was observed to have more severe effects than water immersion, which indicates that water vapour can be more critical to the performance of adhesives than liquid water. All these reductions were found to be reversible upon reconditioning of the sample pieces. Similarly Kläusler [182] reported that timber bonded with a PUR adhesive, of a similar formulation to the one investigated in this thesis, exhibited wood failure percentages that were about three times lower than samples bonded with a MUF adhesive in lap shear tests; he also found that inclusion of additives in the PUR adhesive can improve its moisture performance. Niemz and Allenspach [179] performed lap shear experiments on common beech samples bonded with PUR (which was reinforced with chalk) or a urea formaldehyde (UF). The investigated influencing variables were temperature and relative humidity (at ambient temperature). They found that the percentage of wood failure increased for UF with increasing moisture content, while a drastic reduction was observed for the PUR adhesive, indicating a plastification of the glue at elevated moisture levels. The effect of moisture on adhesives and their bond strength is of potential importance for adhesive bonded engineered timber in fire and for the cross-laminated timber samples studied in this thesis, because water in fire exposed timber will move away from the heating front and deeper into the timber, where elevated moisture concentrations can occur. Konnerth et al. [183] tested the tensile shear strength and wood failure percentage under increasing moisture contents for three adhesive types on nine different timber species, thereby varying both the adhesive and the adherent. They found that, for a combination of spruce and a PUR adhesive that corresponds to the timber and adhesive used for experiments described in this thesis, the shear strength and wood failure percentage reduced by 22 and 20 % more in wet conditions, respectively, than for a combination of spruce and MUF adhesive.

2.4.2.3 Consequences of debonding

From full scale fire resistance tests Malhotra and Rogowski [149] found a mean reduction of 10 minutes in fire resistance duration with 90 % confidence for casein compared to phenolic glues; this was attributed to the lower (unquantified by the authors) decomposition temperature for casein compared to phenolic adhesives. Other large scale test series on glulam columns found that the glue has no statistically significant influence on the fire resistance [120]. Fackler [140] did not observe differences in the fire resistance between two glulam columns, where one used a melamine based glue and the other was bonded using a urea formaldehyde based adhesive. From numerical simulations of standard fire exposure, Klippel and Klippel and Frangi [184, 185] have concluded that

bending stresses rather than shear along the glue line, will be the governing failure mechanism for glulam beams in bending, thereby indicating that weakening of the glue line is less influential on the structural capacity than the deterioration of the strength of timber. From experimental results of fire resistance tests and small scale elevated temperature tests Klippel [184] concluded that a significant adhesive strength loss in elevated temperature tests is not an indicator for a reduced fire resistance performance due to the steep temperature gradients in standard fire tests and a similar stance has been expressed by Serrano and Källander [74].

2.5 Meta-Analysis of available codified guidance methodologies

This section presents available data from fire resistance experiments on cross-laminated timber walls and reviews available methods for the determination of fire resistance through calculations. For a meta analysis, the input values are sourced from available research and fire testing papers on CLT walls and then used as input values in the reviewed calculations models to allow a comparative assessment between the calculated and achieved fire resistance. Note that some of the methodology and results presented in the following sections have already been published by Wiesner and Bisby [32], which also contains an extended look at laminated timber compression elements and non-codified methodologies.

2.5.1 Fire test and experimental data on CLT walls

Multiple authors have previously investigated the load bearing capacity of timber compression elements in fire, in most cases subjected to standardised temperature-time curves. However, due to the relative novelty of CLT as a construction material (compared to steel, concrete, masonry, or sawn timber) the publicly available experimental data on the structural behaviour of CLT walls in fire is limited. In addition, due to the low number of completed large CLT projects there are no observations and reports from real fires in buildings utilising cross-laminated timber. The following paragraph describes the results from reviewed experiments and fire resistance tests on CLT wall elements.

2.5.1.1 Fire resistance tests

Osborne et al. [136] tested three loaded CLT walls in furnaces to determine their fire resistance. From deflection measurements they observed a continuous increase in midspan out of plane displacement, which ultimately led to a global buckling failure of the walls. The three wall panels consisted of one three and two five ply configurations bonded with a PUR adhesive (Purbond). Schmid et al. [186] describe a series consisting of seven furnace tests of constantly loaded cross-laminated timber wall elements at multiple scales which were exposed to a standard cellulosic temperature time curve [28]. For these tests fire resistance durations between 48 minutes, for a proportionate design load of 34 % and 140 minutes for a load ratio of 7 % were reported. The results showed that, due to the potential for instability failures, the authors' own models for the load bearing capacity of CLT walls were sensitive to small changes in the size of the residual cross section of only a few millimetres, especially where the residual cross section was close to a boundary between parallel and crosswise orientated plies. Klippel et al. [187] report on six wall tests on CLT with ply configurations of three (2) and five plies (4) with varying structural boundary conditions. The deflection measurements in these tests vary between positive and negative deflection measurements (i.e. walls bending away and towards the fire respectively). Since all tests were stopped before structural failure occurred and because no pattern could be recognised in the deflection response, no clear conclusions can be drawn for the structural capacity in fire for these tests. Suzuki et al. [113] describe eight tests with four different load levels of CLT walls made up of five and seven plies (four each) of Japanese cedar and bonded with an API adhesive. They found that, as the char and heated front moves through the crosswise orientated plies, the rate of deflection decreases significantly (effectively to zero) until the strength and stiffness of the next parallel ply is compromised by the heat travelling through the timber. However, this plateauing of the deflection was not observed for higher load levels, highlighting the complex interplay between mechanical and thermal response of CLT.

In addition to peer reviewed published research projects outlined above there are also data available from commercial fire resistance tests on CLT wall elements. The Canadian Wood Council [188] commissioned a standard fire test on a Type X gypsum board protected three-layer CLT panel, which, with 200 kN/m axial load applied, experienced gypsum board failure after 45 minutes, and achieved a standard fire resistance rating of 66 minutes, with structural global buckling failure as the structural failure mode. A 175 mm thick, five-layer CLT wall panel with Type X gypsum board protection was tested

with 127 kN/m axial load applied by the American Wood Council: the gypsum board was reported to have failed after 28 minutes, and the wall achieved a fire resistance rating of 186 minutes, after which the wall panel failed structurally [189]. Since fire resistance testing is a requirement to approve a building product it is likely that manufacturers of CLT have more data on fire test results available, however, these are often subject to non-disclosure agreements and therefore constitute non-accessible data. The fire resistance durations for the experimental and commercial testing reviewed in the paragraphs above are shown in Figure 2.14.

2.5.1.2 Experimental work

Wiesner et al. [190] performed experiments on CLT wall strips exposed to a constant radiative heat flux at their centre for three and five ply CLT bonded with MUF adhesive and loaded to two different equivalent load levels of 10 % and 20 % of their ambient nominal loading capacity. They found that all samples failed in buckling due to progressive increase in lateral deflection caused by the eccentricity induced by one dimensional heating as well as secondary moments from a P-Delta effect. They observed that three ply samples performed worse (i.e. failed earlier) than five ply samples, which is attributed to the fact that in a three ply configuration more parallel orientated timber is placed on the outside and therefore the overall load bearing capacity is reduced faster. Similar to Suzuki et al. [113], Wiesner et al. also observed an arrest in the deflection for the five ply samples as the heat moved through the cross-wise samples, however, this arrest was less pronounced, which can be explained by the thinner plies used for Wiesner et al.'s experiments (20 mm compared to 30 mm for Suzuki et al.).

2.5.2 Guidance methods for fire resistance of CLT walls

Multiple calculation methodologies are presented in the literature to enable designers to predict the structural fire resistance of mass timber compression elements (i.e. columns and walls) for standard fire exposures in furnace tests. The available methods are reviewed and described in this section. For the calculation of CLT, all of the methodologies are underpinned at least partly by engineering mechanics; some of these were explicitly developed as prescriptive design guidance, and are therefore inherently conservative, whilst others were developed to predict fire resistance rather than yielding inherently conservative outputs. The predictive performance of the respective models is compared in Section 2.5.3 against the available test data found in the literature.

2.5.2.1 Method requirements

The available methodologies need to address multiple aspects of structural timber in fire in order to predict the load bearing capacity in fire or the fire resistance duration. The two most critical aspects concern the reduction in the mechanical properties of the timber. As timber chars (as described in Subsection 2.3.2) any timber that completes pyrolysis and is turned into char and should be considered to have zero strength and stiffness (readers who ever squeezed a piece of char from the remains of a camp fire will be familiar with this). This is generally addressed through a prescribed charring rate that calculates the char depth at a required time. In addition to the mechanical losses in the char layer, a gradual loss of strength and stiffness must be accounted for in the heated timber below the char layer (see Subsection 2.4.1).

In addition to the effect of heat and fire on the timber, most guidance methods should also incorporate a structural model to assess the load bearing capacity of mass timber elements after the effects of fire have been accounted for. For CLT these calculation methods must be able to account for the reduced strength and stiffness in the crosswise layers relative to the lamellae orientated parallel to the main loading direction.

2.5.2.2 Reduced cross-section method

The reduced cross-section method (RCSM) is one of the most widely recommended approaches to assess the fire resistance of structural timber elements. In its essence, it relies on the removal of heated timber cross-section below the char layer by a finite amount(lumped into an assumed depth of zero strength) and the remaining (reduced) cross-section is then generally treated in calculations as virgin unaffected timber and ambient temperature calculation procedures are applied. This is schematically shown in Figure 2.12. The details of the exact amount of cross-section to remove from calculations as zero strength vary between codes and jurisdictions but can generally be summarised as all the char plus either a distance proportionate to the char depth or a fixed distance below the char layer to account for heated timber.

The original zero strength layer of 0.3 in (which today is most commonly translated as 7 mm) was developed for solid wood or glulam beams in bending in the 1980s from simulated results and only validated against one beam in a fire resistance test [191]. Since then this value has been implemented in multiple codified guidance documents globally [122, 145, 192, 193]. Its use has recently been challenged with the advent of CLT (and other engineered timber products) and a realisation that a ZSL of 7 mm

does not suffice to represent the strength losses in CLT under standard [194, 195] or non-standard [141, 190] fire conditions. Schmid et al. [194] studied existing literature results of CLT and proposed that the cross-wise nature of CLT requires an increased zero strength layer to account for the fact that the timber with loading crosswise to the fibres has much lower strength than when parallel orientated. They suggested that varying zero strength layer values are required for different loading situations and since then a multitude of values have been proposed for the depth of the ZSL [137], however, none have been formally accepted by the scientific community as a whole and some authors have suggested that the ZSL might be an overly simplified concept to be used for a complex material like CLT in fire [190]. In addition to CLT, and as a consequence of the renewed interest in engineered timber products, the zero strength layer concept associated values have also been critically questioned for structural glulam members. Hopkin et al. [196] proposed that the ZSL of 7 mm, which was originally conceived for bending members, should not be applied to uni axially loaded members, especially in compression. A recent investigation of the zero strength layer for glulam beams,for which the mechanical properties were very well characterised at ambient temperature conditions, in four point bending yielded a wide scatter of possible zero strength layer depths ranging between 1.5 mm to 11.8 mm with a coefficient of variation of 67 % [116], thereby highlighting significant uncertainty in the accurate determination of the ZSL even for the relatively simple timber products and load cases it was originally determined for.

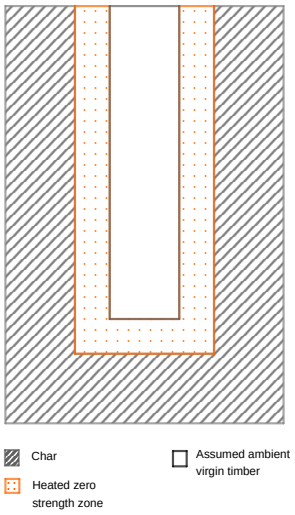

Figure 2.12. Reduced cross-section concept schematic drawing

2.5.2.3 EC5 method

The procedures outlined in the harmonised guidance in EN 1995-1-2 (EC5) [145] are not strictly applicable to CLT elements in fire, yet it is likely that practising engineers may apply them to these cases regardless. EC5 [145] advises designers to use the RSCM to determine the remaining effective cross-section of wood based structural products (e.g. glulam or LVL) during standard fire exposures. A ZSL depth of 7 mm is currently suggested in EC5 [145] for use with the RCSM. The remaining residual cross section is, for calculation purposes, assumed to be at ambient temperature, and the ambient temperature design guidance for timber structural elements from EN-1995-1-1 [87] is used to determine its capacity. In addition, EC5 also contains a reduced properties method, which reduces the strength and stiffness of heated timber based on a section factor. This method is due to be removed from future editions of EC5 and is not permitted in some jurisdictions. In addition, it is considered less accurate and cannot be applied to walls or slabs [107]. Because of these limitations it is therefore not considered in the meta analysis presented herein.

EC5 [145] assumes an average one dimensional charring rate of 0.65 mm/min for solid or glued-laminated timber. If corner rounding is to be expected (i.e. for glued-laminated timber columns exposed from more than one side) the charring rate is increased to a notional charring rate of 0.7 mm/min. An extended charring model for CLT has been proposed by Klippel et al. [161] and this model is intended to be implemented in the upcoming revision of EC5. This model is therefore used for the meta analysis herein to calculate charring rates for CLT walls. The charring rates are calculated from the multiplication of numerous k factors, which take into account the gap width, orientation, and expected falling off of charred layers [135, 161]. It is assumed that all considered CLT panels in this study have a gap width of 2 mm or less. Therefore the charring rate for CLT walls constitutes 0.65 mm/min where only the outermost layer is charred and 0.8 mm/min where charring progresses past the first layer.

If protective gypsum board claddings are used, additional calculations in EC5 can be added which assume that the applied protection delays charring until a calculated fall-off time of the gypsum board, and the charring rate is increased thereafter. For gypsum board of types A and H the fall off time is assumed to be equal to the time to onset of charring of the timber behind it, which (for one layer of type A, F, or H gypsum board with thickness h_p) can be calculated using Eq. 2.11.

$$t_{ch} = 2.8h_p - 14 \tag{2.11}$$

To account for buckling in the structural capacity evaluation, EN-1995-1-1 [87] imposes a reduction factor, k_c, which is applied to the ambient temperature compressive strength of the timber. This factor is dependent on the element's slenderness and the relationship between its strength and its flexural rigidity. Additionally, the reduction factor is influenced by a variable, herein denoted c, to implicitly account for inherent (accidental) load eccentricities depending on the type of timber used. For glued-laminated timber c is 0.1 in EC5 and is multiplied with the difference between the relative slenderness and 0.3, to determine the k_c; the higher c is the lower k_c will be. It is assumed that the value of 0.1 for c for glulam can also be applied to CLT (in the absence of specific guidance stating otherwise). This is derived from a constitutive relationship proposed by Ylinen [197] that accounts for deviation from Hooke's Law in the relationship between stress and strain in the inelastic range. To achieve this, the 'straightness factor', c, is taken as a function of the proportional limit, the elastic modulus, and the yield strength of the material. EC5 does not currently address CLT explicitly and therefore does not provide details on how the reduced strength and stiffness should be accounted for. Secondary literature [83] implies that the gamma method (refer to Equation 2.4) should be used for ambient temperature calculations to obtain a reduced 'effective' stiffness to account for the effect of the reduced stiffness of the crosswise layers. Wallner-Novak et al. [83] state that the consideration of shear deformations is only applicable to serviceability criteria and that the calculation of γ scaling factors can therefore be omitted for the calculation of fire resistances.

2.5.2.4 The Fire Safety in Timber Buildings (FSTB) method

The *Fire Safety in Timber Buildings (FSTB)* report [137] was produced as an unofficial technical guideline for Europe that provides amended guidance to EC5 for the determination of fire resistance for various timber products. The additional guidance relates to protective encapsulation, as well as weakening through a compensation layer (analogous to the zero strength layer described for the RCSM) of CLT in standard fire exposures. For the progression of the char front FSTB [137] states that char ablation (i.e. falling off) is less pronounced for vertical elements as compared with horizontal elements, and can therefore be ignored for walls or columns, although the experimental evidence for this design approach appears to be somewhat limited [137]. The ZSL (called a 'compensation' layer) for CLT in the FSTB report is assumed to depend on the element type (floor or wall), the loading condition (tension or compression side), and the overall thickness and number of lamellae. For example, for an unprotected

five-layer wall, the depth of the ZSL is determined using Eq. 2.12:

$$ZSL = \frac{h}{15} + 10.5 \tag{2.12}$$

where h is the overall thickness of the slab. For a fixed value of h, the ZSL increases as the number of layers increases and with the addition of protective claddings (as the heating through protective claddings can occur before the onset of charring, thereby leading to deeper thermal penetration).

In addition to the guidance on protective claddings in EC5 [145], FSTB [137] alternatively offers the calculation of fall-off and start of charring times based on a database of gypsum board test results from across Europe. Since FSTB is considered as a companion document to EC5 [145], all other required calculation aspects (e.g. structural assessment) are assumed from EC5 [87, 145] in the meta analysis presented herein. As for the EC5 method the extended charring model by Klippel et al. [161] is considered for the FSTB method.

2.5.2.5 NDS method

The *National Design Specifications (NDS)* [111] for wood construction in the USA recommends a mechanics-based calculation model in which the remaining load bearing capacity in fire is assessed against the applied load for CLT and glulam amongst other wood products. The NDS method [111, 112] assumes that the average charring rate is dependent on the total burning duration (i.e. the fire resistance duration in this case), with a baseline one-hour charring rate of 0.635 mm/min. This approach attempts to implicitly account for the charring rate peak experienced during the early stages of a fire, however it fails to account for the initial accelerated loss of cross section. This would only affect outcomes for smaller structural elements or fire resistance ratings of less than one hour, which are unlikely to apply for tall timber construction. Additionally, the NDS [111] provides empirically derived equations that can be used to adjust the charring depth, a_c, to account for the influence of falling off of charred of CLT lamellae during heating; this (Eq. 2.13) depends on the number and thickness of lamellae as follows:

$$a_c = 1.2\big[\sum_{i=1}^{n_l} h_{l,i} + \beta_n(t - \sum_{i=1}^{n_l} t_{gl,i})^{0.813}\big] \tag{2.13}$$

where n_l is the number of lamellae, h_l is the depth of each lamella, and $t_{gl,i}$ is the time taken to char through a lamella to the glueline. To account for the strength loss of heated timber, the NDS approach [111] artificially increases the charring rate 20 % above the applicable nominal charring rate, to implicitly account for the loss of strength of heated timber; this 20 % increase is also assumed to implicitly account for corner rounding [112].

Similarly to EC5 [87], the NDS method reduces the strength of the remaining cross section (assumed to be at ambient temperature since heating is accounted for implicitly through an increased charring rate) by multiplication by a factor, k_c, to account for the effects of instability. This factor depends on the slenderness, the ratio of strength to stiffness of the assessed wall or column and a straightness factor c, which is given as 0.9 for both glued-laminated timber and CLT. Due the manner in which the equations are formulated the influence of c of 0.9 on the buckling capacity in NDS is the same as for of a value of c of 0.1 in EC5 [87] , i.e. 10 %, for both methods. If all partial safety and adjustment factors are stripped out of these equations, k_c, is equal for the NDS and EC5 methods, as shown in Figure 2.13, which also shows that the reduction is more severe for higher strength-to-stiffness ratios. The NDS [111] only provides a method for predicting the fire resistance of exposed (i.e. unprotected) timber members. This is a form of the RCSM for which the ZSL is varied proportionally to the char depth.

2.5.2.6 CSA method

The *Engineering Design in Wood* guidance of the Canadian Standards Association (CSA) [193] employs a mechanics-based approach to verify the structural fire resistance of glulam columns and CLT slabs and panels at a specified time of fire exposure. The calculations relating to fire exposure of timber structural members given in CSA [193] are part of an informative annex. The charring rate for glued-laminated timber is given as 0.65 mm/min for one-dimensional charring. For CLT, it is suggested that the one-dimensional charring rate should be applied if the char front remains in the first lamella during the fire. If charring progresses into any subsequent layers, an average charring rate of 0.8 mm/min is recommended for the full fire resistance duration, which is a very similar approach to the charring model proposed for CLT for future EC5 editions. For heated timber below the char, CSA recommends use of the RCSM with a ZSL of 7 mm. To account for instability, a buckling reduction factor, k_c, is multiplied by the compressive strength, which as for EC5 [87] and NDS [111], depends on the element's

slenderness ratio and strength-to-stiffness ratio.

Structural failure is then determined using a linear interaction equation between the compressive load capacity ratio and bending capacity moment ratio. For CLT protected with gypsum board, the CSA guidance suggests that the fire resistance rating can be increased by a nominal fixed value, depending on the thickness of encapsulation applied. For example, 12.7 mm of Type X gypsum board is assumed to increase the calculated fire resistance by 15 min; the interaction between encapsulation fall off and delayed and/or accelerated charring is not explicitly considered.

2.5.2.7 Instability parameter

For timber, due to varying inherent eccentricities the buckling behaviour can either approach the idealised Euler buckling load closely or can show significant deformation as the load is increased and $P - \Delta$ effects increase [98]. All of the methods that are reviewed for this analysis address instability implicitly through a factor that reduces the compressive strength. Figure 2.13 shows the buckling reduction factor, k_c, for the different methods as described above. Shown are the factors that designers should apply to the compressive strength to account for the fact that structural elements that experience instability cannot reach their theoretical compressive strength. It is clear that more reduction is applied for all methods as slenderness increases. Additionally, the EC5, NDS and CSA methods increase the reduction for increasing strength-to-stiffness ratios, since buckling depends on the stiffness of a member rather than its material strength, and a strong column with a low elastic modulus is more likely to experience instability. At low slenderness, failure by crushing is expected and k_c tends to 1.0.

2.5.2.8 Advanced methods

This paragraph introduces additional analytical and numerical methods that have been introduced in literature. Due to either a reliance on data that is not generally available from fire resistance testing, or their numerical complexity, these methods cannot easily reproduced and are therefore not included in the meta analysis in Subsection 2.5.3. Tavakkol-Khah and Klingsch [198] proposed an advanced calculation model to determine the ultimate load bearing capacity of structural timber elements in fire. This included the calculation of the charring depth and temperature distribution for timber members exposed to a standard fire through an numerical model, although the given

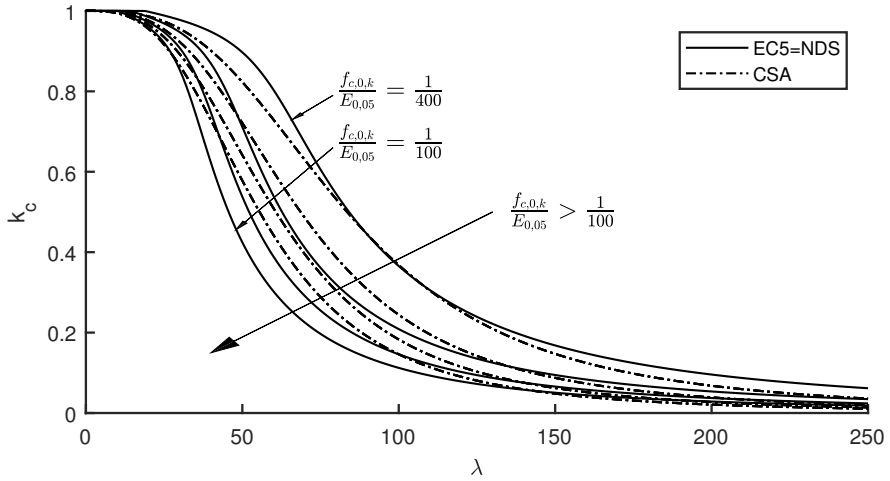

Figure 2.13. Normalised strength reduction curves with slenderness and strength-to-stiffness ratios for laminated timber compression elements in fire for EC5, NDS and CSA. The CSA lines correspond to the same strength-to-stiffness ratios as the EC=NDS lines [32].

details of this procedure were not provided by the authors. The proposed model then calculates the equilibrium between applied load and load carried for each time step until failure is computed from divergence of deformations. The proposed calculation iteratively accounts for the changing location of the neutral axis (due to plastification and a differing reduction in stiffness for tension and compression). This method cannot be assessed in the meta analysis due to a lack of details on the numerical heat transfer model to calculate the temperature profile.

Suzuki et al. [113] suggest to calculate the critical buckling load for a fire-exposed CLT wall using a secant formula (Eq. 2.14), which is derived from the Euler buckling equation, with the additional consideration of load eccentricity caused by the loss of effective cross-section (refer to Subsection 2.2.1) due to charring and in-depth thermal gradients. To model the reduction of strength in heated timber specifically for CLT walls, Suzuki et al. [113] propose a simple effective cross-section analysis (not to be confused with the RCSM), wherein the widths of small horizontal slices of a CLT wall panel are reduced according to their current temperature and resulting local reduction in elastic modulus. In this approach, layers with different elastic moduli are scaled in width according to the ratio of elastic moduli, which are determined from linearly interpolated experimental in-depth temperature data, in conjunction with the reduction curve proposed by Kaku et al. [169] (refer to Figure 2.9 b)). The critical buckling load and deflection of the wall can then be calculated using an analytically derived secant

formula, shown in Eq. 2.14.

$$P_{cr} = \frac{\sigma_y A}{1 + e_c/r^2 \sec\left(\frac{\pi}{2}\sqrt{P_{cr}/P_e(T)}\right)} \tag{2.14}$$

where P_{cr} is the critical buckling load, σ_y is the compressive strength of timber, e and c are the eccentricity and location of the neutral axis from the edge of the remaining cross section respectively, r is the radius of gyration, and P_e is the Euler buckling load of the transformed (based on the temperature profile) section. Since the reviewed datasets for tests on CLT walls do not give information about the temperature profiles in the walls, this method cannot be included in the meta-analysis that follows.

Many more methodologies have been proposed for timber columns although the majority of those cannot easily be translated into meaningful application to CLT walls and are therefore omitted here. Interested readers are referred to Wiesner and Bisby [32] for further information on calculation procedures for timber columns.

2.5.3 Meta analysis

Where tests were performed with exposure to a standardised time temperature curve, these can be used to assess the accuracy of guidance documents to calculate the fire resistance of load bearing CLT elements. While there are minor differences between standardised temperature time curves and their applications, they are similar enough that they are treated as equal in this assessment.

Calculations for CLT walls require consideration of axial load and moment interaction, and the assessment criterion for failure therefore require bending strength or bending moment resistance to be weighed against bending stresses or moments. In timber, bending strengths (also often called moduli of rupture (MOR)) are nominal values determined from failure at the tensile fibre in beam bending tests [41, 42]. For CLT in fire, the theoretical bending resistance in fire varies between the compressive and tensile faces of walls in fire due to movements of the neutral axis and the changing elastic moduli of the various lamellae. Because bending strength values originate from tensile ruptures in beam tests, any bending resistance in the analysis presented herein is derived at the outermost tension fibre, which is assumed to lie on the unexposed side of walls (i.e. it is assumed that CLT walls under initially concentric loading can be expected to buckle away from their fire-exposed face [190]).

2.5.3.1 Meta input values

One issue with historical datasets is that it is often difficult to obtain and verify essential mechanical input parameters that are required to perform structural fire calculations. Both Simpson [199] and Schmid et al. [195] have previously highlighted the significant challenges in obtaining and assessing historical data from standard fire tests (or any other fire or heated tests) on timber structural elements. The importance of imperfections is relevant to the load bearing capacity in fire. Structural fire resistance tests on sawn timber columns experienced failures near imperfections in four out of five tested cases in a study by Neale [200]. This adds additional difficulty to experimental determination of the load response in fire for structural timber. Since fire resistance ratings obtained through furnace testing are random variables (due to variability in the test specimen, as well as the furnace) [159], it is not unexpected to see some variability in the results. In an ideal case input values are given by the authors from reference tests at ambient temperatures (as done by Schmid et al [186] and Suszuki et al. [113] in Table 2.2). Where this is not possible, the mechanical properties can be back calculated from the strength class and the associated characteristic values. To obtain mean from characteristic values a log-normal distribution of values is assumed in combination with a CoV of 15% for the strength and 13% for the elastic modulus, as recommended by the Probabilistic Model Code [201] for timber.

Where no information is given in the source publications regarding the strength or elastic modulus of the timber used, these are inferred from the permissible stresses of the strength classes used in the country of origin at the time that the testing was undertaken, as outlined by EN 1912 [202] and taken from EN 338 [96].

Input parameters from structural fire resistance tests, which are described in more detail in section 2.5.1 are shown in Table 2.2. These input parameters constitute the main parameters that are required to implement the methods described in Subsection 2.5.2. The ratio of applied load to Euler buckling load is given, since the buckling load is a commonly well defined theoretical upper limit for the structural capacity of compression elements of differing effective length and therefore provides a common comparative variable across different CLT configurations.

The value of a meta analysis comes from comparing outcomes of calculations results without safety factors and based on mean values. While design methods should generally return ‘safe’ design solutions, they should also not be overly conservative (i.e. inefficient), and should therefore be able to reasonably predict test results. When no

Table 2.2. Key input parameters from datasets for furnace tests on CLT walls.

Authors	**# of Tests**	**Initial Slenderness Ratio λ[a]**	**Effective Length [mm]**	**Mean Elastic Modulus [MPa]**	**Mean Compressive Strength [MPa]**	**# of Lamellae**	P/P_u **[%][b,c]**
Schmid et al. [186]	7	49-78	2040-2470	9070-12320	43-46	3-5	7-22
Suzuki et al. [113]	8	43-49	2150-3300	4200-4670	25-31	5-7	14-48
Osborne et al. [136][a]	3	53-88	3048	10190-12450	16-28	3-5	7-24
CWC [188][a]	1	88	3048	9520	17	3	25
AWC [189][a]	1	53	3048	12340	28	5	3

[a] mean mechanical property values back calculated from reference data

[b] based on parallel layers only

[c] P_u taken as Euler buckling load, P as applied load

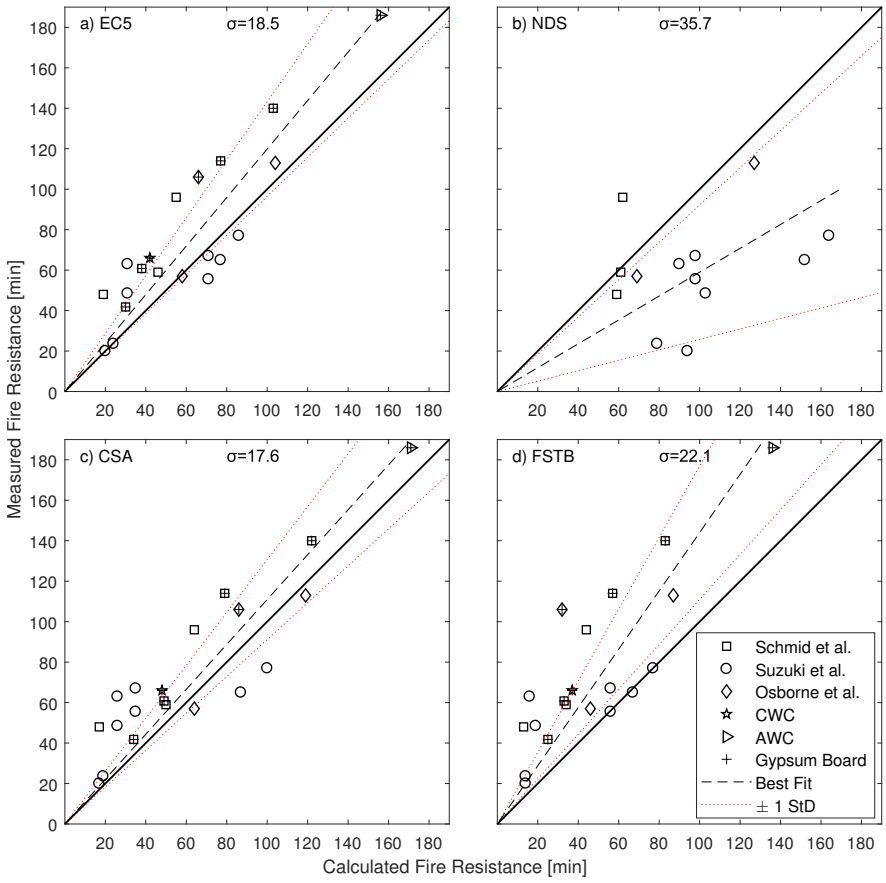

Figure 2.14. Meta-analysis plots comparing measured and predicted fire resistances for CLT compression elements for: a) the EC5 method [145], b) the NDS method [111], c) the CSA method [193], and d) the charring and ZSL model as outlined in the FSTB [137] method (in combination with structural considerations in EC5). Fitted means are forced through the origin.

safety factors (i.e. material or member reduction factors) are included in the calculations, the methods should ideally provide an accurate prediction of the unity line in Figure 2.14, with as small a mean percentage error (MPE) and mean absolute percentage error (MAPE) as possible. MPE and MAPE were chosen as a relative measure of forecast accuracy between the assessed methods since the measured fire resistance data naturally does not contain zero or negative values and MAPE offers a simple, easy to read comparison for these cases [203]. One potential pitfall of MPE and MAPE as measures of forecast accuracy is that negative errors can be weighted heavier than positive errors, however, this should not constitute a significant shortcoming for the comparison presented herein as all the *measured* fire resistance values are fixed and do not change between the assessed methods. Assuming that the residual data points are normally distributed about the mean, the meta-analysis comparisons can be used to statistically quantify the performance and level of conservativeness of each of the assessed models in light of the available test data. Normality of the residuals is demonstrated across methods in Figure 2.15, with only few minor outliers near the extreme quantiles. Since all material input parameters used in the calculations were, to the extent possible, adjusted to reflect mean values, a 'perfect' model would have a mean slope of one and an MAPE of zero. This assumes that the assessed models aim to provide accurate prediction of the unity line.

Table 2.3. Summary of meta-analysis comparisons for CLT walls

Method	**Best Fit Slope**	**MAPE [%]**	**MPE [%]**	**# of Conservative Results [%]**	**R^2 of Fit**	**Mean β_f at Failure[a] [mm/min]**
EC5 [87, 145]	1.2	25.1	18.4	79	0.76	0.92
NDS [111, 112]	0.59	94.2	-88.8	12	-0.18	0.86
CSA [193]	1.11	27.7	19.6	73	0.74	0.82
FSTB [137]	1.44	37.8	37.4	90	0.58	1.24

[a] Taken as the rate of loss of cross section (including heated timber at failure), for exposed timber tests only

For CLT walls the EC5 and CSA methods result in similar MAPE values, as well as similar levels of conservativeness. While the accuracy of the EC5 method returns the lowest MAPE value (25 %), the majority of the individual data points lie out with of one standard deviation from the mean, highlighting a level of inconsistency for this method (or, perhaps, for the test results themselves). A similar observation can be made for the CSA method, where most of the results from protected CLT walls lie within one standard deviation from the mean yet the majority of data points for unprotected specimen fall outwith one standard deviation.

The alternative zero strength layer model proposed in the FSTB method yields more

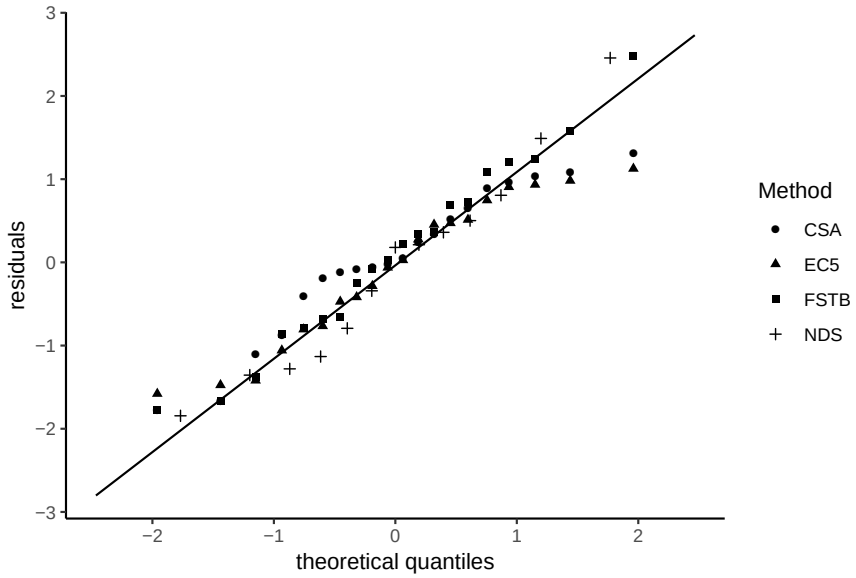

Figure 2.15. Quantile-quantile plot of the residuals for the reviewed methods.

conservative results than the EC5 method; this is expected since the FSTB approach essentially increases the effective loss of cross section compared to the EC5 method. The NDS methodology yields non-conservative results 88 % of the time. The NDS methodology considers an increased charring rate for the fall off of lamellae, yet its assumed effective charring rate at calculated failure times β_{ef} are only slightly lower than for EC5. The reason for the limited predictive capability is therefore thought to be due to the mechanical aspects of the model. For instance, the nonlinear design interaction equation that is used to assess failure may not be appropriate. Indeed, Wang et al. [204] performed experiments on eccentrically loaded CLT walls and concluded that nonlinear interaction equations are non-conservative for some load cases for CLT, and should be replaced with a linear interaction equation (as is now used by the CSA guidance [193]). Additionally, the NDS uses a slenderness factor, c, of 0.9; however, Zahn and Rammer [205] state that this value was never validated and should probably be reduced (i.e. the influence of slenderness increased). However, changing the slenderness factor in the NDS analysis does not significantly change the results, since its influence on the compressive strength of a column or a wall is limited to ∼10 % (for a generic assumed relative slenderness).

Considering the results in Figure 2.14 b), it is evident that the NDS methodology makes reasonable predictions for the results from Schmid et al. [186] and Osborne et al. [136], but is badly non-conservative for the tests by Suzuki et al. [113]. For the

data from the latter, two differences can be identified as compared to the tests by the former. First, half of the experiments were performed on seven layer CLT (rather than five layer CLT). Second, the elastic modulus from reference tests in Suzuki et al. [113] is, on average, 37 % less than what standards would recommend for the lowest strength grade in Europe [96]. With up to 48 % (as a proportion of the theoretical ultimate buckling load) these tests imposed a higher load level than most tests from the other test series considered. This suggests that the loading interaction equation in NDS should perhaps be revisited for 'high' loads at larger eccentricities, and for CLT with five or more lamellae. The high MAPE for the NDS method should also be taken as a cautionary tale of validating a model against a limited dataset (in this case the results by Osborne et al. [136].

The average MAPE for all methods applied to CLT walls is 46.2 % (30.2 % if NDS is excluded as an outlier) with a minimum MAPE of 25 % and a maximum of 94 %. The forecast accuracy is therefore less than for a similar analysis of glued-laminated columns presented by Wiesner and Bisby [32]. This is not surprising since the structural and thermal boundary conditions for CLT walls are less well defined (e.g. fall off of layers) than for glue-laminated columns. In addition there are significantly fewer test results available for CLT walls compared to glulam columns. It is noteworthy that the calculations performed herein are based on mean input parameters, and while design methods should give safe results, they will lead to uneconomical designs if their predictive capability errs too far on the conservative side as a consequence of failing to capture the relevant physical realities. Structural engineering methods for CLT wall elements in fire at high loads (as could be expected as timber buildings increase in height) will need to be improved, and more reliable tools to produce economical and safe designs will need to be developed.

For the EC5 method [145], a reasonable correlation is observed for protected CLT walls in Figure 2.14 a), suggesting that the current model for the delay of charring by gypsum board protection, and the subsequent increased charring rate once gypsum board falls off, may be adequate for the range of test results considered to date (although only seven data points are available). A similar observation can be made for protected tests assessed using the CSA [193] method. However, while the agreement of these results may be interpreted as beneficial with regards to the power of the these methodologies, there is an obvious and dangerous flaw in the philosophy of relying on additive fire resistance of non-combustible encapsulation. As explained in Subsection 2.3.7 a fall-off of plasterboard during a fire will involve newly exposed timber as additional fuel load and potentially extend the burning duration to infinity.

From the method requirements and the scatter in the results of this meta analysis it becomes obvious that there is a concerning level of variability in the calculation of fire resistance of CLT walls. For the European market alone engineers have a choice between two different guidance documents and multiple different charring models and applications of the zero strength layer, which will likely be further revised for the next version of the Eurocodes. This means that clear guidelines for practising engineers are currently missing to design cross-laminated timber to a quantified level of risk in standard fire exposures. No codified approaches were found for CLT wall elements exposed to non-standard fires, highlighting a serious barrier for the use of performance based design with regards to the fire safety of a material that does not fit very well into established norms and procedures.

2.6 Literature review conclusions

This review gives an overview of timber as a construction material and its engineering use at ambient temperatures before explaining the basic concepts of fire safety and highlighting the peculiarities arising from having combustible timber in compartments. Special focus was given to the requirements and existing research on the structural performance of cross-laminated timber in fire and a meta analysis was performed to assess commonly used calculation methodologies against available test data.

While much of the early fire resistance work focussed on non-combustible construction, there have been recent increased efforts to better understand the fire dynamics inside compartments with exposed timber surfaces from engineered mass timber elements. However, many of these did not focus (or even consider) the structural fire endurance requirements. This means that, while there is a greater understanding in the need and the means to achieve burn out, the structural capacity is often still assessed within the fire resistance framework through furnace tests, which was developed without the consideration of significant additional fuel contribution from combustible exposed surfaces. Especially for wall elements of CLT a paucity of data was found in the literature review, leaving a significant knowledge gap. The limited available data resulted in one methodology in a meta analysis being assessed as non-conservative in a majority of cases, which could in part be attributed to a limited dataset that was originally used to calibrate and assess said methodology. It was also identified that many widely used codified guidance documents either do not address the particularities of CLT explicitly or users are expected to patch knowledge gaps through the use of secondary publications and literature. This can in part be explained by the fast uptake of CLT by the

construction industry and the fire engineering community having to play catch up with a fast developing market. Instead of empirical solutions, like the zero strength layer, the focus of the research presented in the following chapters is therefore on an understanding of the underlying mechanical issues of CLT walls when subjected to heat and fire.

The reduction in compressive strength and stiffness of timber when heated was reviewed and a wide range of potential reduction curves was found, with differences identified to be most likely caused by the heating method and the accompanying movement of moisture through the sample. All reviewed reduction curves were derived from timber boards and no studies were performed on CLT to assess the applicability of these reduction curves to a composite material like CLT. This applicability of known reduction factors for the strength and elastic modulus is therefore investigated in this thesis in Chapter 4 for both steady state, as well as transient heating conditions for small scale cross-laminated timber samples.

Only few studies investigated the structural influence of the laminations and previous studies on the effect of different adhesives were limited to connection details for glulam products. Studies on the bonding performance at elevated temperatures and moisture contents generally showed a reduced performance of PUR adhesives compared to MUF formulations, however, the large variability within PUR adhesives makes a definite comparison difficult. Two studies described the performance of the same PUR adhesive type that is used for experiments in chapters 4, 5, and 6 and in each of these studies, this adhesive showed a lower wood failure percentage (i.e. a reduced adhesion) than reference MUF bonds. No targeted studies into the effect of adhesives on the overall load bearing performance of cross-laminated timber in fire exist. The research presented in the following chapters of this thesis thus sets out to close this significant knowledge gap with a series of unique experiments across scales and with varying heating conditions.

This page is intentionally left blank.

CHAPTER 3

Material characterisation

This page is intentionally left blank.

3.1 Motivation

The intent of this chapter is to introduce the reader to the CLT material that is used for all experiments in the following chapters, and to characterise basic ambient temperature properties which are of potential relevance to the thermal and mechanical assessments in subsequent chapters.

3.2 Sample description

The cross-laminated timber samples in this study were all manufactured by the same company [88], with four different configurations arising from variation of two production parameters, (1) the adhesive type and (2) the number of plies. Hence, it can reasonably be expected that a comparative analysis of the effect of heat and fire on the load bearing capacity of these samples can be performed with respect to the four configurations. The timber of the samples was spruce (picea albies) and at least 90 % of the boards will conform to a C24 grading with an admissible share of 10 % C16/L17.

The adhesives used to bond the samples were a one-component polyurethane (PU) and a melamine urea formaldehyde (MF) formulation which was applied in combination with a hardener. The applied pressure for the CLT bonding process was 0.6 to 1 MPa for both adhesive types. The recommended press duration for the MF adhesive can take up to 5.4 time the recommended time for the PU adhesive, however, this is strongly dependent on the ratio of hardener and MF adhesive, as well as moisture content of the timber and ambient relative humidity. The PU and MF adhesive conform to the requirements of EN 14080 [206] and EN 301 [181], respectively.

The ply configurations are 20-20-20-20-20 and 40-20-40 mm of timber boards in the typical orthogonal CLT configuration, with boards on the outside arranged so that the grain direction runs parallel to the main longitudinal (loading) direction. The ply configuration for the three ply samples represented a case where a majority (80 %) of the timber is placed in the parallel outside plies. This was chosen deliberately to further investigate the effects of thick outer plies based on research by Wiesner et al. [190] which had shown that this constitutes a detrimental factor for the load bearing capacity in fire, as early loss of a majority of parallel orientated timber shortened the time to failure.

3.3 Scales

Three different scales (sizes) were used in the experimental series described in the following chapters. These consisted of small, medium, and large scale samples. For the small scale the dimensions are 200, 100, and 100 to 150 mm for height, width, and depth, respectively. The depth for these was varied to accommodate the strength limits of the testing apparatus used. The medium scale samples were wall strips with a height, width and depth of 1700, 300 and 100 mm respectively. The large scale samples were CLT beams with length, width, and depth of 3000, 300, and 100 mm, respectively. The three scales are shown in comparison to each other in Figure 3.1.

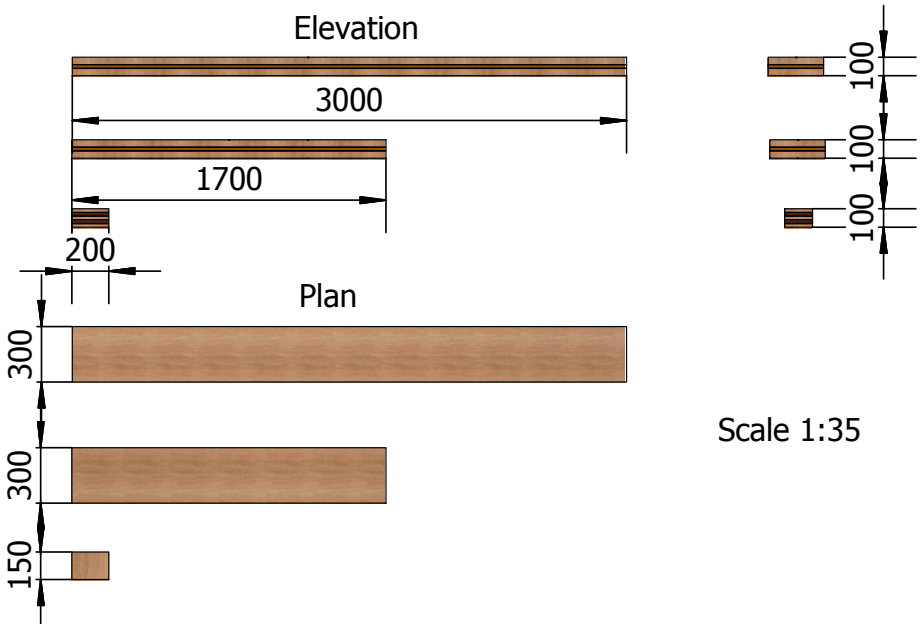

Figure 3.1. Comparative drawing of the different sizes of elements investigated for this study. Note that the medium and large scales are shown for three ply CLT and the small scale sample for five ply.

Figure 3.2. Side-by-side comparison of experimental specimen scales in climate controlled storage room.

3.4 Density

The probability density distribution of the bulk density of all specimens in this study for the various scales is shown in Figure 3.3. In addition, the distribution of the density values for the different lamellae configurations and adhesives is shown in Figure 3.4. From these visualisations it can be seen that the distributions across all scales approximate normal distributions (with some extreme outliers), and it appears that the median density across scales, adhesives and layers does not vary with statistical significance; this is confirmed by p-values of 0.7, 0.2 and 0.08 from analysis of variance (ANOVA) for scales, adhesive type, and number of plies, respectively. This is an important consideration for the comparative experimental analysis that is presented in the following chapters because density is considered an indicator for mechanical properties [43] and influences the propagation of heat into a sample (charring rates have been observed to correlate negatively with density [116–118]). Significant variation in density across adhesives and lamellae would constitute a compounding factor for the assessment of the influence of these variables on the load bearing capacity in fire and when subjected to heating. One noticeable aspect of Figure 3.4 is that the density of five ply samples exhibits less deviation from the mean than the three ply samples, with a coefficient of variation (CoV) of 3, and 6 % for five and three plies, respectively. This is likely due to the fact that for five plies, any boards with an extreme density will not influence the bulk density as much as for the three ply samples. The overall mean density is 460.6 kg/m^3 with a standard deviation of 22 kg/m^3, resulting in a CoV of 4.8 %.

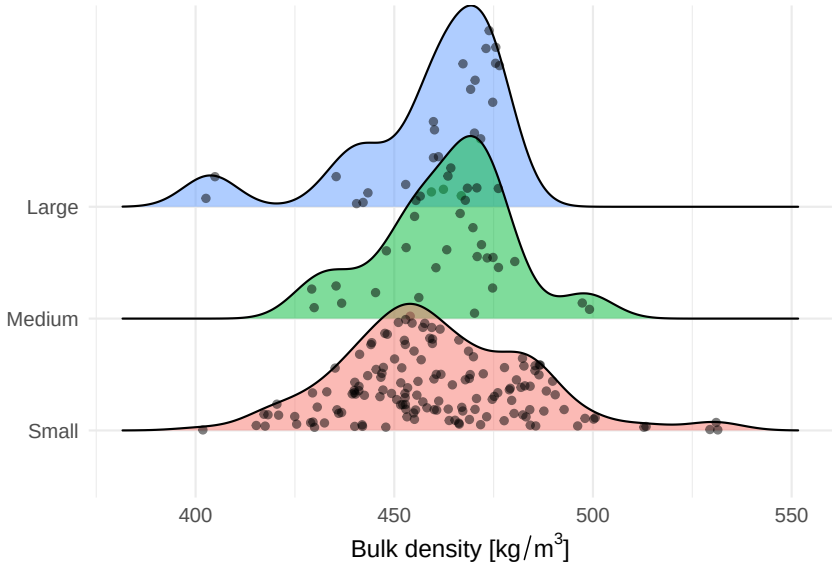

Figure 3.3. Probability density plot of bulk density with randomly jittered (i.e. shifted by a random amount vertically) data points for three scales of CLT. Bandwidth 6.75.

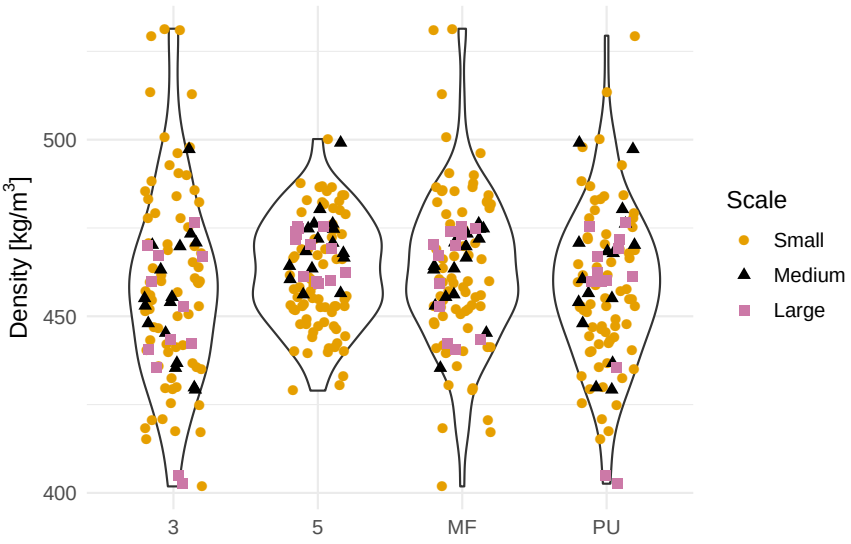

Figure 3.4. Violin plots of bulk density for the two main variables in this study. Individual measurements are shown by scale and jittered (i.e shifted randomly) horizontally.

3.5 Moisture content

As highlighted in Subsection 2.4.1, the moisture content of timber has a non negligible effect on the mechanical properties of timber, especially when paired with heating, with reducing compressive strength and stiffness as moisture content increases. The timber samples for all test series presented herein were stored in a designated conditioning room with temperature between 18 and 22 °C and fitted with a dehumidifier to maintain a quasi-steady state relative humidity, which was observed to vary between 40 and 65 %. Hand-held moisture meters (which infer moisture content from resistivity) are not considered reliable [43, 45] for the determination of moisture content of thick timber as they only provide spot moisture content measurements at the surface. The moisture content of the samples was instead determined by proxy from destructive tests on sacrificial samples that were stored in the same environmental conditions as the samples that were used in the experiments described in the following chapters.

The moisture content was determined for timber from various offcuts or spare samples for all four assessed variables (two adhesive types and two ply configurations) in accordance with EN 322 [207] for which wood samples, which do not contain any adhesive, are dried in an oven at 103 °C and repeated mass measurements were taken until the change in mass within six hours was recorded as less than 0.1 % of the mass of the sample. The moisture content (mc) was then calculated in accordance with Equation 3.1, where m_0 is the final, dried, and m_H the initial mass.

$$mc = 100 \cdot \frac{m_H - m_0}{m_0} \tag{3.1}$$

The moisture content in Figure 3.5 can be seen to vary for different dates of testing, which can be attributed to seasonal changes that cannot be fully compensated through the dehumidifier. In addition the controlled storage space is used by a multitude of users and it has been observed at times that some users will switch off the humidity control, which could explain some of the observed variation between dates. No significant variation in moisture content can be observed between the samples for different layers or adhesives, as would be expected. Overall the variation across dates is not considered sufficient to cause concerns regarding its influence on the parametric studies in this study, especially since experimental series on each of the three scales were performed within limited time frames and the seasonal variation in moisture content between repeats and paired samples can therefore be considered negligible. The mean moisture content from all samples was 9.04 %, with a standard error of the mean of 0.08 %, so

moisture content can be expected to fall between 8.88 and 9.20 % with 95 % confidence. Within buildings the moisture content is generally expected to not exceed 12 %.

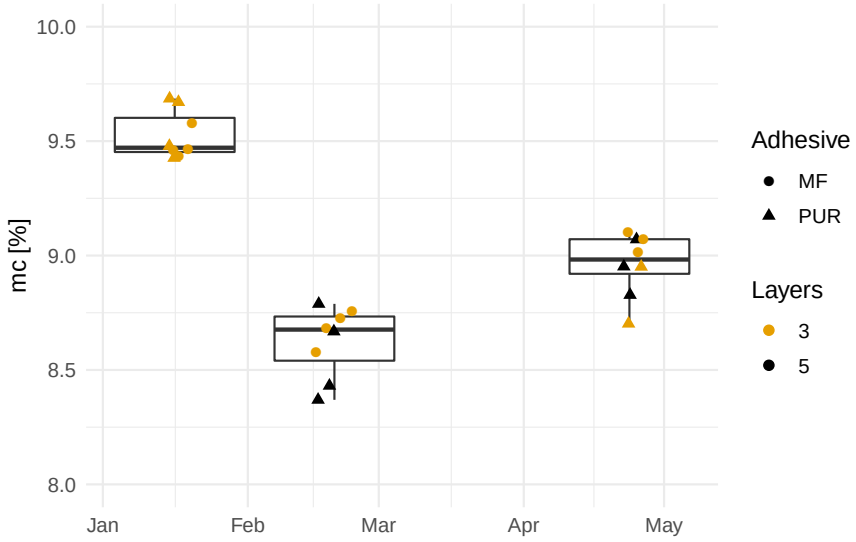

Figure 3.5. Sample moisture content measurements from oven drying to constant mass at different dates. Individual measurements shown by adhesive type and number of plies. Individual markers are jittered horizontally for improved clarity.

3.6 Conclusions

In this chapter the CLT materials for subsequent studies are described and characterised in terms of relevant common parameters. Four configurations of CLT were used, varied by adhesive and number of plies. The adhesives used are a one component polyurethane (PU) and a melamine urea formaldehyde (MF). The density across scales was not found to vary significantly between either adhesive or ply number, with an overall mean density and standard deviation of 460.6 and 22.0 kg/m^3 respectively. Since density is considered to be positively correlated with mechanical properties of timber this should give increased confidence that the timber forming the CLT can be expected to have similarly distributed mechanical properties across the investigated variables. While some variation in sample moisture content was observed with time of testing, the overall variation in moisture content can be bound into a 95 % confidence band between 9.0 ± 0.2 %. The available CLT therefore presents an unique opportunity to study the effects of adhesive and ply number on the structural performance under exposure to fire and/or heating.

CHAPTER 4

Uniformly heated material scale tests

This page is intentionally left blank.

4.1 Motivation

This chapter describes the observations and measurements taken on small scale stocky CLT samples in axial compression at ambient and elevated temperatures.

The motivation for the research presented in this chapter is the lack of available experimental data for cross-laminated timber products and the unknown influence of the glue and lamination configuration on the mechanical properties of heated laminated timber in compression. Compression failures in wood loaded in parallel to the fibre direction propagate as buckled fibres due to breaking of bonding material between the longitudinal cells [39]. For laminated timber products, and CLT in particular, discontinuities arising between lamellae could alter this behaviour and thereby the compressive failure mode and load. In addition the results from the experiments described in this chapter will help to complement the available recommended reduction curves of timber strength and stiffness when heated (refer to Subsection 2.4.1). Currently it is not known with certainty whether codified strength and stiffness retention curves for elevated temperatures, or those arising from past experimental work on sawn timber apply to the strength and elastic modulus of cross-laminated timber (or other engineered timber products that consists of lamellae bonded with adhesives). Furthermore the investigation of the compressive loading behaviour at the material scale will aid the interpretation of results for the larger scale experimental series described in chapters 5 and 6 for which CLT is subjected to more complex loading and heating scenarios.

4.1.1 Experimental overview

This chapter first describes and analyses reference experiments at ambient temperature, and subsequently conveys the details of experiments on specimens loaded in axial compression at elevated temperatures. From both ambient and elevated temperature experimental series, the effects of heating in conjunction with effects of adhesive type and number of lamellae are analysed and discussed. For all four cross-laminated timber configurations considered (described in Chapter 3) the strength and stiffness of samples is assessed for steady state and for transient heating. In steady state heating the samples were heated to a uniform temperature before loading was applied, and for transient heating the samples were loaded to a proportion of their ambient capacity before heating was applied. The experimental matrix for this chapter is shown in Table 4.1 and encompasses a total of 143 experiments. At ambient temperatures the

samples consisted of ten and twelve specimens for three and five lamellae configurations, respectively. For heated samples three repeats were tested for each configuration at each distinct sample group and for some samples an additional specimen was tested where the initial three specimens were inconclusive. The increased number of specimens for ambient compared to heated experiments arose from (1) the desire to obtain reasonable confidence in the ambient temperature reference capacities and (2) the relative speed of experiments at ambient temperatures where multiple experiments can be performed in the same day compared to heated experiments which generally took one whole (working) day to conclude. The upper load ratio of 50 % for experiments with transient heating conditions was chosen to lie sufficiently below the mean ambient temperature capacity (in order to avoid picking heated samples that fail as load was applied and before any heating was applied) yet large was large enough to ensure that failure would occur before drying of the specimens occurred. The lower load ratio of 25 % was chosen as half the upper load ratio.

4.1.2 Significance

The performed experiments described herein are unique in their experimental set-up and in their scope as no previous studies have assessed the axial compressive strength of cross-laminated timber when exposed to either steady state or transient heating conditions below 300 °C. While studies on elevated temperature performance for both adhesives and sawn timber exist no detailed studies have been published assessing the influence of the number of lamellae, the different adhesives types, and heating scenarios for cross-laminated timber as a combined building product of timber bonded with different adhesives types. This study therefore constitutes a novel and significant research insight into the importance of cross-laminated timber configurations on the mechanical performance at elevated temperatures.

Table 4.1. Experimental matrix for small scale ambient and heated CLT samples.

Group Name	**Adhesive** -	**Layers** -	**Steady heating** -	**Transient heating** -	**Target temperature** $[^oC]$	**Heating rate** $[\frac{^oC}{min}]$	**Load ratio**[a] [%]	**Number of specimens** -
S3MF020	MF	3	X	-	20	0	0-100	10
S3PU020	PU	3	X	-	20	0	0-100	10
S5MF020	MF	5	X	-	20	0	0-100	12
S5PU020	PU	5	X	-	20	0	0-100	12
S3MF050	MF	3	X	-	50	5	0-100	4
S3PU050	PU	3	X	-	50	5	0-100	4
S5MF050	MF	5	X	-	50	5	0-100	3
S5PU050	PU	5	X	-	50	5	0-100	4
S3MF100	MF	3	X	-	100	5	0-100	3
S3PU100	PU	3	X	-	100	5	0-100	3
S5MF100	MF	5	X	-	100	5	0-100	3
S5PU100	PU	5	X	-	100	5	0-100	3
S3MF150	MF	3	X	-	150	5	0-100	3
S3PU150	PU	3	X	-	150	5	0-100	3
S5MF150	MF	5	X	-	150	5	0-100	3
S5PU150	PU	5	X	-	150	5	0-100	3
S3MF200	MF	3	X	-	200	5	0-100	3
S3PU200	PU	3	X	-	200	5	0-100	3
S5MF200	MF	5	X	-	200	5	0-100	3
S5PU200	PU	5	X	-	200	5	0-100	3
TX3MF	MF	3	-	X	-	5	50	3
TX3PU	PU	3	-	X	-	5	50	3
TX5MF	MF	5	-	X	-	5	50	3
TX5PU	PU	5	-	X	-	5	50	3
TX3MF	MF	3	-	X	-	0.5	50	3
TX3PU	PU	3	-	X	-	0.5	50	3
TX5MF	MF	5	-	X	-	0.5	50	3
TX5PU	PU	5	-	X	-	0.5	50	3
TX3MF	MF	3	-	X	-	5	25	3
TX3PU	PU	3	-	X	-	5	25	3
TX5MF	MF	5	-	X	-	5	25	3
TX5PU	PU	5	-	X	-	5	25	3
TX3MF	MF	3	-	X	-	0.5	25	3
TX3PU	PU	3	-	X	-	0.5	25	3
TX5MF	MF	5	-	X	-	0.5	25	3
TX5PU	PU	5	-	X	-	0.5	25	3

[a]Samples at ambient and steady state temperature are exposed to load increases until failure is observed.
For transiently heated samples a proportion of the mean failure load at ambient temperatures is applied.

4.2 Ambient reference experiments

4.2.1 Experimental set-up

To assess the axial compressive strength of the samples, they were placed between two rectangular loading platens which are part of an Instron 600LX loading machine, which was used to apply loading for the experiments described in this chapter. This apparatus is a reaction frame with a hydraulic piston at its base and a load cell at a cross head above, as shown in Figure 4.1, allowing for compression and tension of samples via movement of the piston. It was chosen as it allows accurate displacement control and is also fitted with a bespoke environmental chamber which was used for the heated experiments described in this chapter in Section 4.3. The two custom made rectangular loading platens were screwed onto push rods which are connected to a load cell and a hydraulic actuator. The samples were then placed between the platens and loaded to failure in axial compression using displacement controlled loading with a deflection ramp of 0.5 mm/min. The stroke movement of the piston was continued after peak load was reached in order to collect data on the post failure response of the samples.

4.2.2 Sample sizes

The cross-laminated timber samples for this study were sawn to a depth of 150 mm, a height of 200 mm, and (from manufacturing) had a thickness of 100 mm. After all of the three ply samples and two five ply specimens were tested it was determined that high peak loads and out of plane movements of the push rods caused damage to the threads of the platens and the loading frame. All subsequent specimens were therefore sawn to a reduced depth of 100 mm before they were tested, thereby reducing the peak loads.

4.2.3 Instrumentation

The stroke of the Instron and the corresponding loads were recorded throughout each experiment. In addition, a camera was used to record images at an interval of 5 seconds (i.e. a crosshead stroke interval of 0.042 mm) of the front face of the samples (i.e. showing the gluelines) in order to obtain digital image correlation data from which displacements (and subsequently strain) of the front face could then be computed.

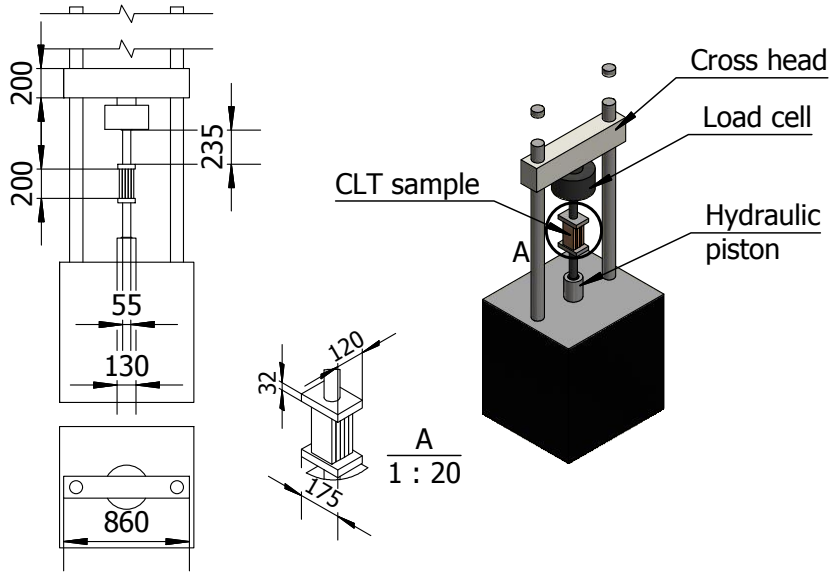

Figure 4.1. Elevation, plan and isometric view of the experimental set-up for material scale cross-laminated timber samples in compression.

4.2.4 Experimental results

4.2.4.1 Displacement stress response

The available area of timber with fibres orientated approximately parallel to main direction of loading varies between the two types of lamealle configuration that are investigated in this thesis. Hence, to obtain a comparable normalised parameter of the stress in the material as the load increased with increasing cross-head stroke, the effective compressive stress is calculated according to Equation 4.1, where P is the measured load, th is the thickness, d is the depth of the sample and subscripts $_{all}$, $_{pa}$ and $_{cs}$ denote overall, parallel and crosswise layers, respectively. This equation accounts for the varying dimensions of parallel and crosswise layers through an effective section theory (as outlined in Subsection 2.2.1) by reducing the contribution of crosswise layers based on an assumed ratio of 30 [201, 208] between the parallel and crosswise elastic modulus. This enables a comparison of the stress response between sample sets made of three and five ply CLT as this effectively determines the stress in the strong layers. Any reference to the stress or strength (i.e. the peak stress) in this chapter refers to the effective stress or strength determined from the effective section theory. The load responses versus increasing crosshead stroke for ambient temperature experiments are shown as supplementary information in Figure A.1.

$$\sigma_{eff} = \frac{P}{\frac{th_{all}}{100} \cdot d \cdot (th_{pa} + \frac{th_{cs}}{30})} \tag{4.1}$$

It can be seen that the three ply samples experienced larger compressive deflections, as it was decided to reduce the ultimate imposed crosshead stroke for the five ply samples. This was motivated by the fact that no valuable additional information was gained at extreme crosshead stroke values for the three ply samples. In addition, at high deflections the out of plane movements of the loading rods contributed to damage to the threads of the machine and the loading platens. Overall it can be observed that the stress for each sample configuration increases with little deviation with increasing imposed stroke until the peak load is reached and strain softening occurs. A slight decrease in the slope of the loading curve, highlighting plastification, can also be observed before the peak stress (i.e. ultimate strength) is reached.

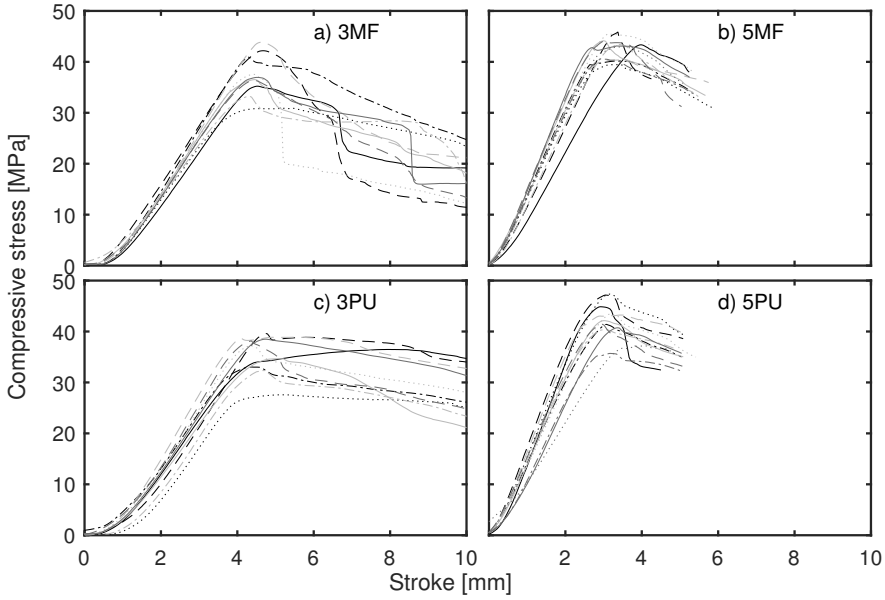

Figure 4.2. Stress response against imposed deflections for small scale CLT samples at ambient temperatures for the four configurations assessed.

4.2.4.2 Ultimate compressive strength

The ambient compressive strength (i.e. the ultimate compressive stress) of the transformed section is plotted against each specimen's bulk density in Figure 4.3. A Pearson

correlation coefficient between density and effective compressive strength can be determined, and this is shown in Table 4.2, along with the mean and standard deviation of the compressive strength of the samples for all four experimental configurations. A Pearson correlation coefficient of 1 indicates perfect correlation, meaning the ranked density values correspond to the ranked strength values, i.e. the highest strength is measured for the specimen with the highest density.

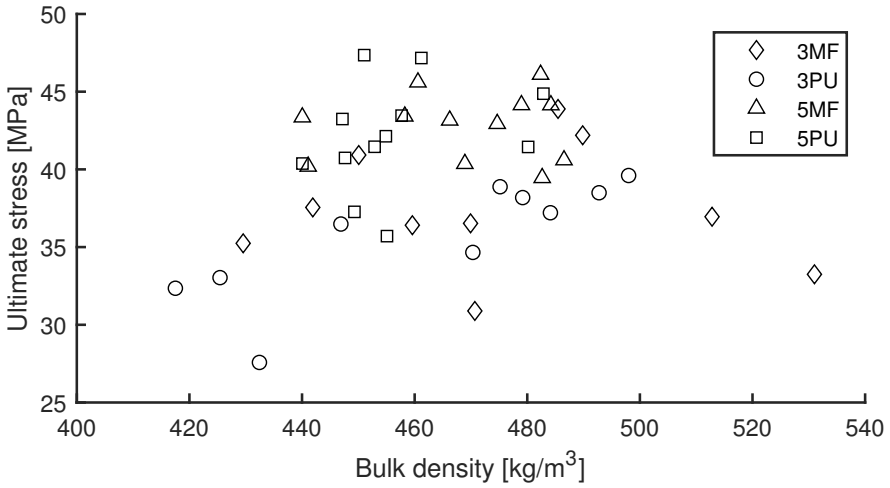

Figure 4.3. Ultimate ambient compressive stress of transformed sections against density for all experimental configurations.

It can be seen that the mean ultimate strength of the 3MF series is slightly higher than the 3PU series and that both the five ply sample groups exhibit higher ultimate strength values than the three ply series. The statistical significance of these differences in ultimate strength is discussed further below. It can be seen that a possible correlation that might be seen in Figure 4.3 is driven only by the 3PU sample and the correlation coefficients for all other samples and the overall correlation are found not to be statistically significant.

4.2.4.3 Elastic moduli

Determining the elastic modulus for timber samples in compression is more challenging than determination of strength values, as has been noted by previous researchers [40]. Strain gauges cannot be used in this setting since any adhesive they rely on would be softened in the heated experiments and thereby invalidate the results. In addition, a material like CLT is made up from different boards, and a spot measurement (as

Table 4.2. Compressive strength, standard deviation and correlation with bulk density at ambient temperature.

Exp. series	$\overline{\sigma}_{eff}$ [MPa]	sd(σ_{eff}) [MPa]	COV(σ_{eff}) [%]	corr(ρ,σ_{eff}) [ ]
3MF	37.7	4.1	10.9	-0.05
3PU	35.6	3.8	10.7	0.82
5MF	43.5	2.2	5.1	0.05
5PU	42.6	3.4	8.0	0.26
All	**39.7**	**4.5**	**11.3**	**0.17**

provided by strain gauges) would therefore only provide a sample of the overall global stiffness response of the specimens as the load is increased.

For the specimens described herein two methods are available to determine the elastic moduli: (1) The measured crosshead stroke of the displacement controlled piston in combination with the recorded load response, and (2) the displacement values of the surface of the samples as determined from digital image correlation (DIC) [209]. For the former, a major obstacle is that the stroke does not only incorporate the deformation of the specimen but also any deflections of the loading frame itself. Large frame deformations were observed visually, which is also shown in Figure 4.5, where the top load platen can be observed to visibly move between zero and the ultimate load. This causes movements of the frame to be included in the strain calculations and therefore reduces the calculated elastic modulus accordingly. As a consequence, mean elastic moduli values determined from the stroke only are lower by a factor of about 3.8 than the expected value, which is 11,000 MPa for timber boards of grade C24 [96].

The second option, DIC, can give more realistic values of the elastic modulus since it allows an insight into the actual strain state on the specimens' surface, independently of in plane movements of the loading frame. Like the stroke method the use of DIC also has some disadvantages that must be considered. Its results can be corrupted by out of plane movements of the sample and it can be difficult to interpret results due to a potential to offer too much data, since a high number of possible locations are available for the determination of strain (and therefore elastic modulus). A description of the use of DIC for the determination of the elastic modulus is provided in the appendix in Section A.2; this also includes a description of possible sources of errors for the DIC analysis. The review of the DIC data concludes that, while DIC can give good and insightful results in some instances, it cannot be relied upon to yield consistent results

for *all* specimens that were tested.

In light of the arguments presented above, it was decided, for the sake of consistency, to use the stroke data for the determination of the elastic modulus. In addition to the stroke data, the movement of the frame was mitigated to some extent by subtraction of movement of the top of the sample, which was obtained from DIC results (note that displacement of DIC points are less susceptible to error than the strains resulting from them).

The ambient elastic moduli, obtained from the stroke data, are plotted against density in Figure 4.4 and summary statistics are given in Table 4.3. As for the ultimate strength, no significant correlation can be identified between the elastic modulus and the bulk density of the sample.

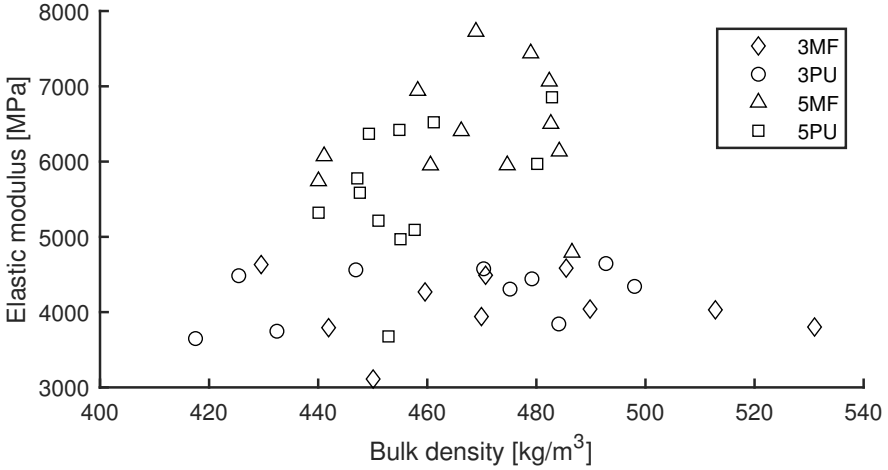

Figure 4.4. Elastic modulus at ambient temperatures of transformed sections against density for all experimental configurations.

4.2.4.4 Failure modes

At ambient temperature the first failure mode for this experimental series was consistently observed as a buckling of the timber fibres in one of the plies. Subsequently failure was observed to propagate to the next adjacent parallel lamella visually (skipping the crosswise oriented ply in between) with a continuous angle of the failure plane visually obvious, as shown in Figure 4.5.

Table 4.3. Elastic modulus, standard deviation and correlation with bulk density at ambient temperature.

	E	sd(E)	COV(E)	corr(ρ,E)
Exp. series	[GPa]	[GPA]	[%]	[ ]
3MF	4.07	0.46	11.3	-0.06
3PU	4.26	0.37	8.7	0.43
5MF	6.40	0.80	12.5	0.08
5PU	5.65	0.87	15.4	0.42
All	**5.09**	**0.63**	**12.4**	**0.22**

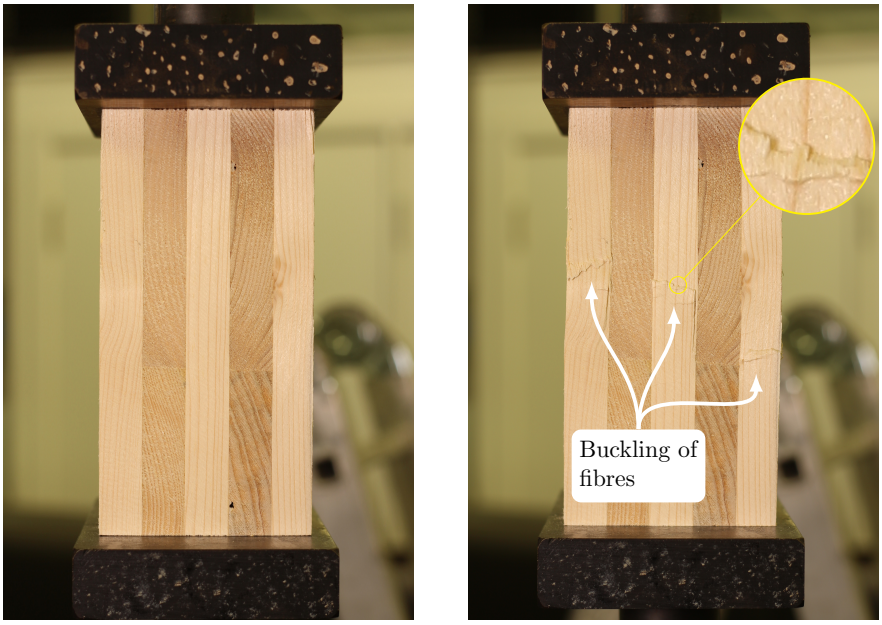

Figure 4.5. Failure mode of a 5-ply polyurethane specimen, as a representative failure mode, in comparison to intact sample before loading commences.

4.2.5 Discussion and analysis of ambient reference experiments

The ultimate compressive strength and the elastic moduli for the four investigated variables are shown as box plots in Figure 4.6. p-values from analysis of variance (ANOVA) are summarised in Table 4.4. It can be seen that for the strength there appears to be a difference between the three and the five ply experiments; This is confirmed by a p-value of $7.2 \cdot 10^{-7}$ between these sample groups. While PU samples on average have a lower ultimate compressive strength, this difference is not judged as

being statistically significant, with a p-value of 0.26 between PU and MF sample groups. For the elastic modulus three ply samples also have lower median values than five ply samples, and with a p-value of $1.2 \cdot 10^{-10}$ the difference is statistically significant well below a 5 % threshold. Between the adhesives no significant difference can be observed for the elastic moduli and the corresponding p-value is 0.15.

Table 4.4. ANOVA p-values summary for investigated variables at ambient temperature.

	Adhesives	Layers
Compressive strength	2.56E-01	7.21E-07
Elastic modulus	1.46E-01	1.20E-10

In addition the statistical inference for the influence at ambient temperature of both the adhesives used and the ply numbers can be investigated between the individual *test series* themselves. The p-values for unpaired two sample t-test with assumed unequal variance between the series are shown in Table 4.5, from which it can be seen that, if a 5 % significance threshold is applied, the null hypothesis of equal means of ultimate transformed stress between the populations of the configurations is upheld when comparing between adhesives but is rejected between the number of lamellae for strength. For the elastic moduli the null hypothesis is not confirmed between the two adhesive types, indicating that both adhesives can not be assumed to be sampled from the same elastic modulus population; with a p-value of 0.04 the statistical significance is very close to the 5 % threshold and the significance is therefore debatable, especially when the p-value is compared against those between layers of different test series, which is much smaller. As for strength, the elastic modulus between layers does vary significantly between the sample groups, if a 5 % threshold is used.

There are two concerns that need to be addressed for this statistical analysis: (1) the relatively small sample size and (2) the assumed distribution of populations of the configurations. The small sample size should not be a major issue, considering that Student's t-test and distribution were developed specifically for small sample sizes [210, 211]. A normal distribution of the population is assumed for applying the t-test to sample data, however, for the strength of CLT, the population is (in general) assumed to be distributed log-normally [201], yet this can still be assumed to fall within the required 'cooked hat' density plot type as assumed by Student [210]. It should also be noted that p-values cannot be treated as a panacea and their use (and abuse) has in recent years revived discussion about the meaning of statistical significance [212]. In this instance what is prominent is the difference in p-values when comparing the effect

of layers and adhesives on the strength and, to a lesser extent, the elastic modulus. This indicates that variation in the effective strength of the underlying population is more likely to occur for a change in the numbers of lamellae but more likely caused by chance for adhesives.

The elastic modulus values, from crosshead stroke data, at ambient temperatures were determined to lie significantly below an expected mean value of 11,000 MPa [96]. However, mean values of elastic moduli are obtained from flexural tests, and some standards [213] specify lower values of elastic modulus in plane of 6,100 MPa. Like the results in this chapter, this indicates that the elastic modulus in compression is lower than what is determined from flexural tests; this is also supported by results published by Suzuki et al. [113], who measured values of compressive elastic modulus in CLT in a range between 4,200 and 6,600 MPa, but did not provide details on the procedure. On the other hand, Goina [123] reported elastic modulus values between 12,200 and 13,400 MPa from linear displacement transducers in direct compression tests on CLT. For the investigations in this chapter the actual absolute values at ambient temperatures are not critical since the main interest is in the reduction with elevated temperatures and therefore consistency is more important than adherence to expected values.

The coefficients of variation (CoV) in tables 4.2 and 4.3 can be compared to those given by the JCSS Probabilistic Model Code [201]. For the ultimate strength the CoV values are significantly less than the 20 % recommended by JCSS, especially for five ply samples. The lamination effect can therefore increase the confidence of engineers in their material. For the elastic modulus no significant difference to the JCSS recommended value of 13 % can be identified.

From the analysis presented it can be concluded that, at ambient temperatures, there is no significant difference in strength between samples using different adhesives, i.e. it can be assumed with reasonable confidence that any samples used for heated tests in this chapter are drawn from a population with the same mean strength value if the only variation is the adhesive type. For a change in ply numbers a different mean strength can be anticipated. This can be explained by a lamination effect, where deficiencies in individual boards of timber are compensated by the presence of other boards, which has previously been postulated from Monte Carlo simulations at ambient temperatures [35]. For the elastic modulus of the samples no significant variation in mean population values was found between adhesives, and, as for the strength, a statistically significant difference was found for a variations in the number of plies used.

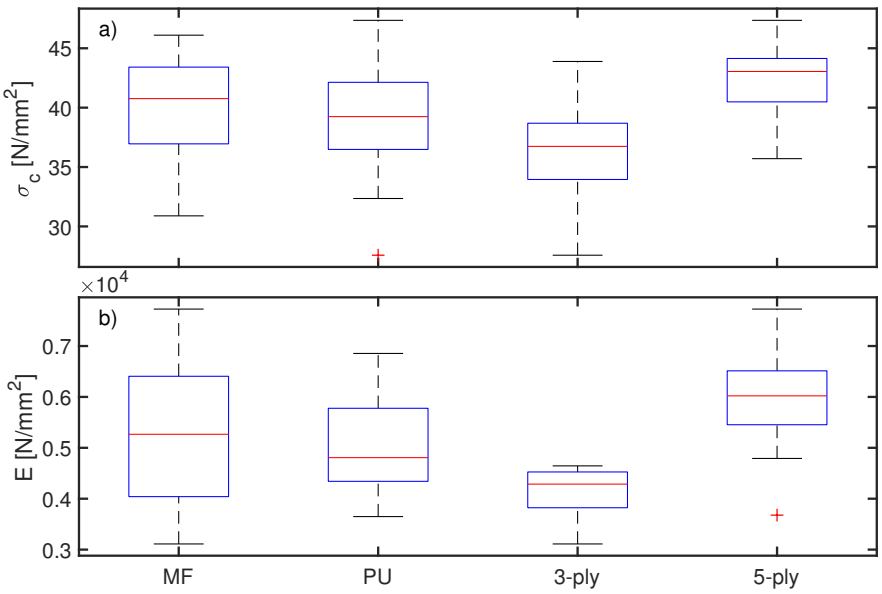

Figure 4.6. Box plot comparison of a) ultimate compression strength and b) elastic moduli for adhesives and number of lamellae.

Table 4.5. *p*-values between test series for unpaired two sample t-test with assumed unequal variances.

(a) Compression strength

	3MF	3PU	5MF	5PU
3MF	1	0.331	0.002	0.009
3PU	0.331	1	$1 \cdot 10^{-4}$	$6 \cdot 10^{-4}$
5MF	0.002	$1 \cdot 10^{-4}$	1	0.570
5PU	0.009	$6 \cdot 10^{-4}$	0.570	1

(b) Elastic modulus

	3MF	3PU	5MF	5PU
3MF	1	0.322	$1 \cdot 10^{-7}$	$4 \cdot 10^{-5}$
3PU	0.322	1	$4 \cdot 10^{-7}$	0.0002
5MF	$1 \cdot 10^{-7}$	$4 \cdot 10^{-7}$	1	0.041
5PU	$4 \cdot 10^{-5}$	0.0002	0.041	1

4.3 Heated small scale compression experiments

4.3.1 Experimental set-up

4.3.1.1 Heating conditions

The cross-laminated timber samples in this study were tested in both steady state and transient heating conditions. For steady state heating conditions the samples were heated until the temperature gradient through their cross-section was deemed

sufficiently small to assume uniform temperatures throughout and the samples were subsequently loaded to failure. For transient heating, the samples were subjected to a fraction of the their ultimate capacity and then heated until failure occurred.

Heating of the samples was achieved in a heating chamber that was attached to the Instron test machine and incorporates the support platens and rods. The heating chamber enclosed the ambient set-up (refer to Figure 4.1) to enable heating and loading to occur simultaneously and is shown in Figure 4.7. The chamber encompassed electrical heating elements at front and centre, an interlock and a fan which was separated from the heating chamber via a mesh and a steel sheet with a circular cut-out to circulate hot air uniformly through the chamber. For samples heated above 150 °C an external extraction system was installed to remove potentially harmful gases into a fume extract system. An annotated image of a heated experiment is shown in Figure 4.8.

Four target steady state timber temperatures were chosen to assess the effect of elevated temperatures on the compressive response of CLT: 50, 100, 150 and 200 °C. The heating was imposed through an increase of the chamber gas temperature, which is controlled by a gas phase thermocouple within the oven and switches the heating elements on and off as required. Due to the comparatively low thermal conductivity of timber, the gas temperature was set as 110 % of the target solid phase timber temperature, i.e. 55, 110, 165 and 220 °C. The gas phase temperatures for the heating regimes are displayed in Figure 4.9. For all steady state experiments the gas phase heating rate was set to 5 °C/min until the required gas temperature was reached. For transient heating the 200 °C heating regime was used. Additional slow heating rate experiments were performed with a reduced gas temperature heating rate of 0.5 °C/min. This slower heating rate was chosen to investigate a possible effect of the heating rate on the loaded response of transiently heated timber as the temperature increase in timber in fires can vary through the fire duration as well as throughout the depth of an heated timber element.

4.3.2 Thermocouple placements

The placement of thermocouples is shown for a five ply sample in Figure 4.10. The location of the thermocouples with respect to the surface of the timber were the same for three ply samples, as this ensures that the temperature gradients at the point of testing can be evaluated consistently.

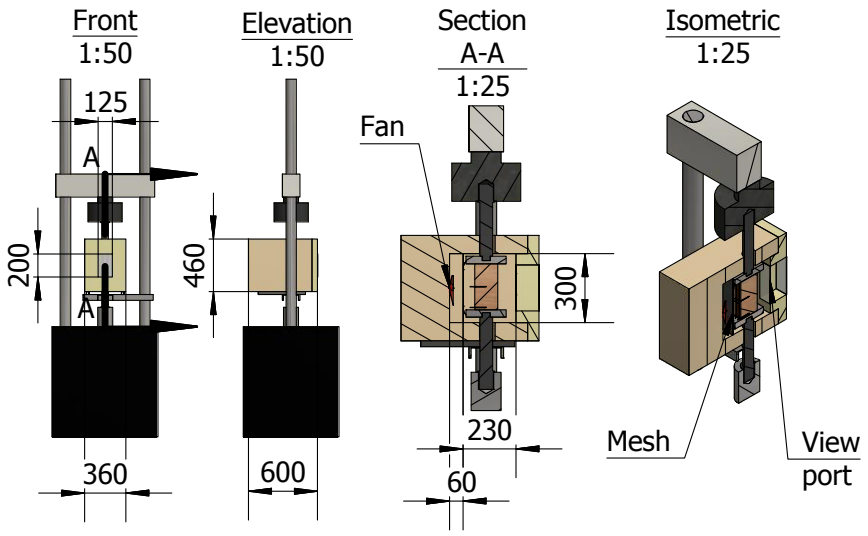

Figure 4.7. Drawing detailing front, elevation, section and isometric views for the experimental set-up for heated compression experiments on CLT samples.

4.3.2.1 Steady state heating

For steady state heating the samples were fitted with three evenly spaced thermocouples located between the surface and the centre of the sample at mid-height. In addition, a thermocouple was placed to measure the gas phase temperature in front of the surface of the section of the specimens that contained the thermocouples of the sample at mid height and one thermocouple was placed to measure the surface temperature of the timber at mid height. The sample was placed between the two loading platens and the piston was adjusted to secure the sample between the platens without applying any significant load. The mean initial load for all test series was 0.9 % of the respective ultimate load at ambient temperatures. The gas temperature of the oven was increased at a heating rate of 5 °C/min using a Eurotherm temperature control system. The temperatures in the sample were monitored during the test and calculations of the temperature gradient and the rate of change of the temperature at the centre of the sample were continuously performed at each time step. Once a steady state temperature distribution through the sample was observed, a displacement stroke ramp of 0.5 mm/min was applied to the sample until a displacement of 15 mm was achieved, i.e. resulting in an experimental loading duration of 30 mins. The final stroke displacement during testing was reduced to a maximum of 8 mm for five ply samples since no significant insights were observed for very large deflections but these were

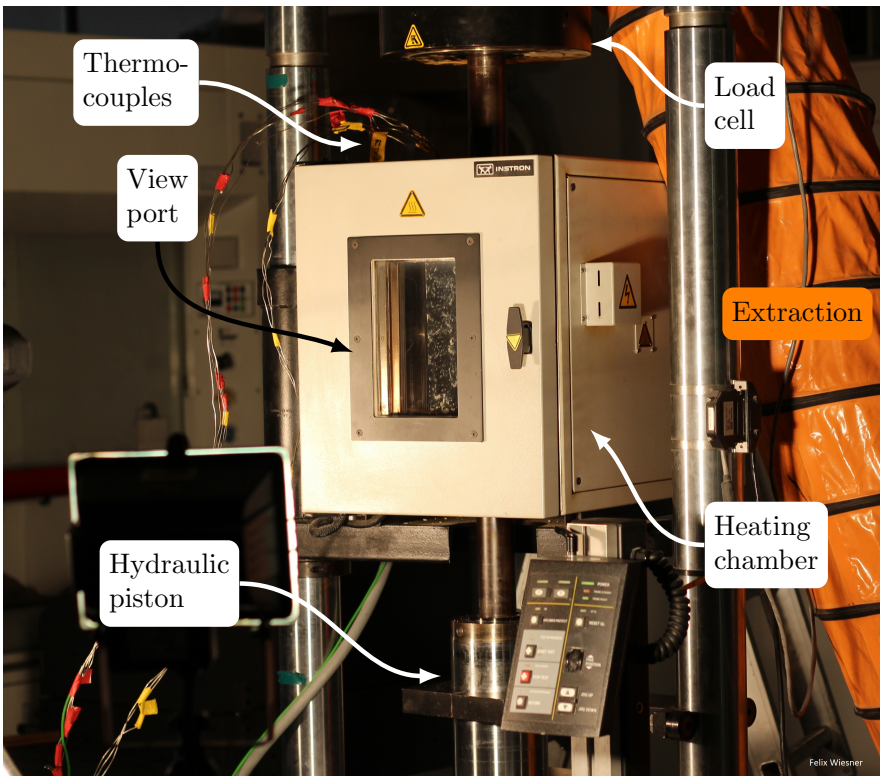

Figure 4.8. Annotated image of configuration for heated compression experiments.

deemed detrimental for the durability of the experimental set up.

Due to the relatively low thermal conductivity of timber (compared to steel) and the relatively large specimen size of the CLT samples (compared to smaller timber specimens tested in compression or tension) the time taken to achieve true steady state temperatures throughout the cross-section of the samples varied for different target timber temperatures. True steady state thermal conditions can take a long time to achieve, or might never truly be achieved since internal exothermic heating can cause the internal temperatures to rise above the external ones. Therefore, instead of waiting for a specific temperature target, steady state was assumed to have been achieved in a sample when the normalised linear slope of the temperature in the sample achieved a predetermined value of -0.003, meaning steady state was assumed to occur when the linear temperature slope through the sample was 0.3 % or less. An example of the evolution of this value throughout the heating phase is shown in Figure 4.11. This method, and the value of 0.3 %, were chosen essentially arbitrarily but provide a consistent means to ensure equivalent heating conditions independent of target temperature

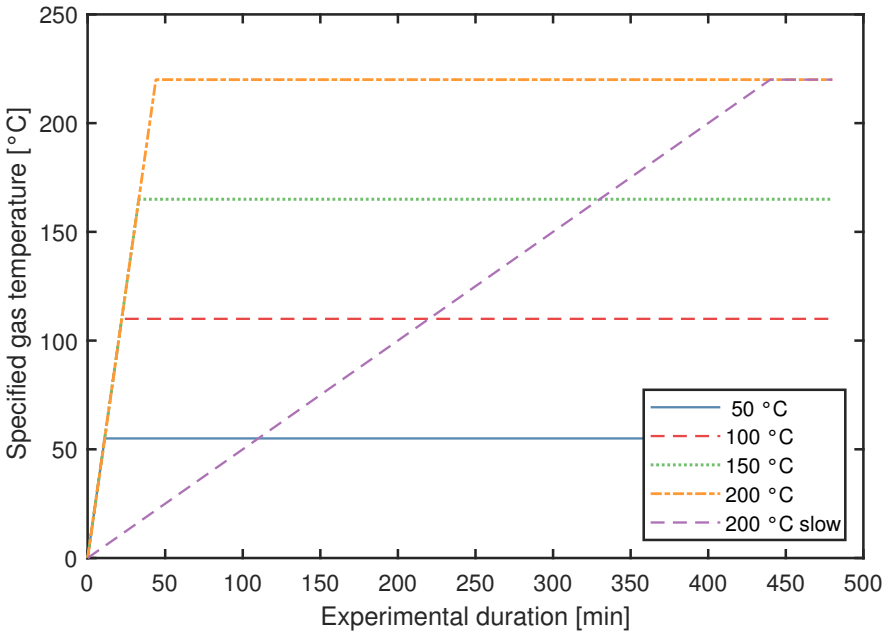

Figure 4.9. Gas temperatures for different heating regimes for small scale experiments.

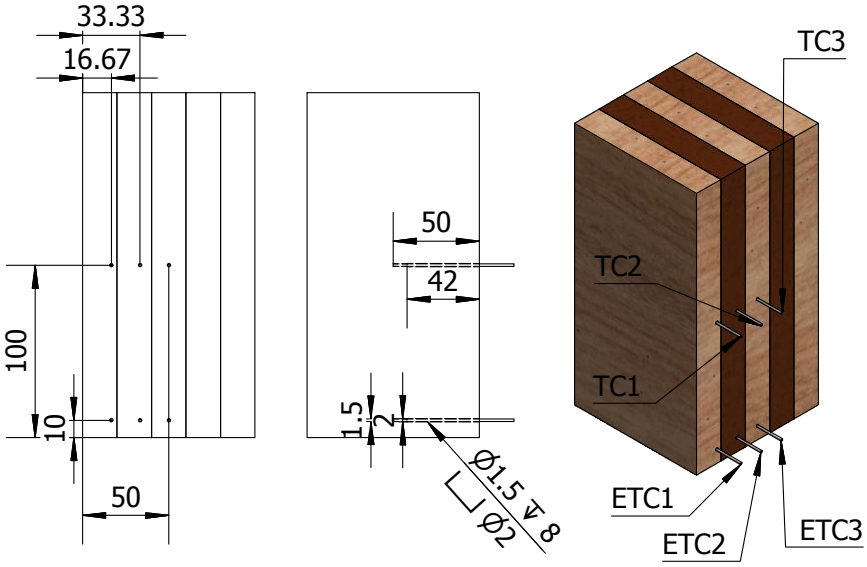

Figure 4.10. Thermocouple positioning and depths for a five ply sample. ETC1 to ETC3 were only used for experiments with transient heating conditions.

between experiments. A linear slope is a poor representation of the temperature gradient at the start of heating, yet as the internal temperatures approach the desired steady state temperature their distribution with depth can be treated as essentially

linear. One shortcoming of this chosen method is that specimens with a different target temperature and to a lesser extent specimens with the same target temperature were subjected to different heating durations and this would have changed the amount of moisture and its distribution within the specimens. While this is likely to have had an effect on the results, the main purpose of steady state heating experiments was to investigate the effect of elevated temperature and additional transient heating experiments, which are described below, were performed to illuminate the effect of transient moisture states of the samples further.

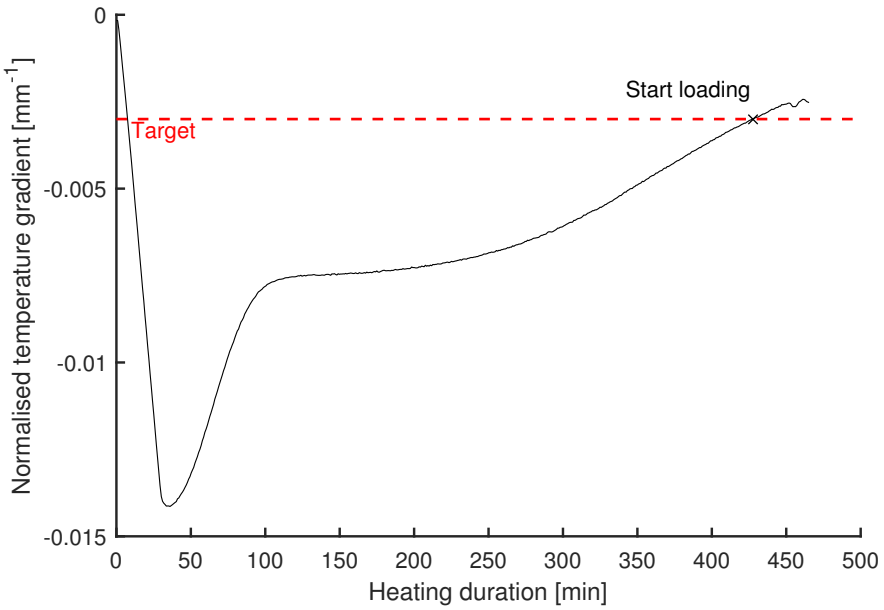

Figure 4.11. Exemplary temperature gradient through CLT depth normalised against target heating temperature to determine steady state heating conditions.

4.3.2.2 Transient heating

For transient heating the specimens were fitted with three internal thermocouples as well as a surface and a gas thermocouple at the same locations as described for the steady state heating. Three additional thermocouples (labelled ETC in Figure 4.10) were placed at 10 mm from the bottom of the specimen at the same depths as the three mid-height thermocouples. These additional TCs were placed since multiple failures near the bottom loading platen were observed for the first set of transient heated specimens.

For transient tests the specimen was placed between the loading platens and loaded

to 50 % and 25 % of the mean ultimate compressive load at ambient. The load was applied via a loading ramp so that the targeted load was reached in 10 and 5 minutes for 50 % and 25 % respectively. The applied load was then held at a constant value and the specimen was heated until failure occurred. Two different heating rates of the gas phase were used for the transient heating experiments: 5 °C/min and 0.5 °C/min, as shown in Figure 4.9. For both heating rates, 220 °C was chosen as the limiting gas phase temperature to try to avoid charring or ignition of the specimens' surface.

4.3.3 Experimental results

4.3.3.1 Steady state heating

The temperature development of the heating phase (including loading until failure) is shown in figures 4.12, 4.13, 4.14 and 4.15 for the different target temperatures. In addition, the temperature histories are split between number of lamellae. The arithmetic temperature mean for each thermocouple is taken for all specimens of that particular combination and is supplemented by one standard deviation at each time step, which is normalised against the heating time required to reach steady state temperature conditions (as explained in Subsection 4.3.1). This way the heating of the samples is compared on the same normalised time axis, even where differences in total heating duration exist, due to different target temperatures of the samples or varying densities (and thereby thermal inertia) of the specimens.

Despite the fact that the three ply samples were larger than the five ply ones (with a depth of 150 mm, instead of 100 mm), the normalised heating development appears to be reasonably consistent between sample configurations. For all heating scenarios it can be seen that (as expected) the solid phase thermocouple closest to the surface heats up faster than the two deeper ones, which both follow a similar pattern of heating. This creates a temperature gradient within the samples which reduced as more heat was transferred into the interior. For heating above 100 °C a plateau can be observed around 100 °C for the deeper temperatures as the evaporation of water acts as a heat sink through the use of thermal energy in the phase change. One peculiar observation that can be made is that the heating of the five ply samples appears to be more consistent between specimens than the three ply samples. This can be attributed in part to the fact that the three ply samples were larger, and therefore required more heat to store significant energy to raise the solid phase timber temperatures in the heating chamber.

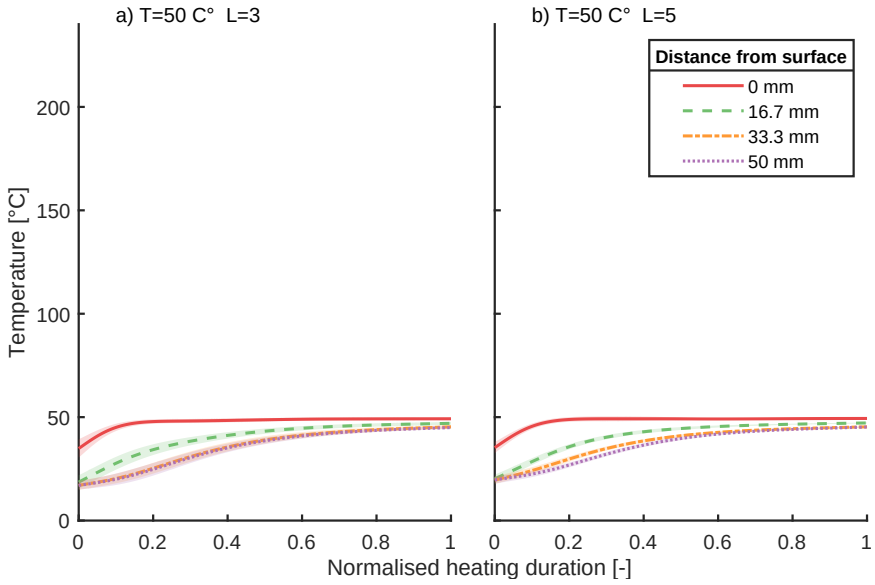

Figure 4.12. Mean and ± one standard deviation summary for thermocouple readings of different samples at fixed distance from the timber surface in experiments with a target temperature of 50 °C and a) three plies and b) five plies.

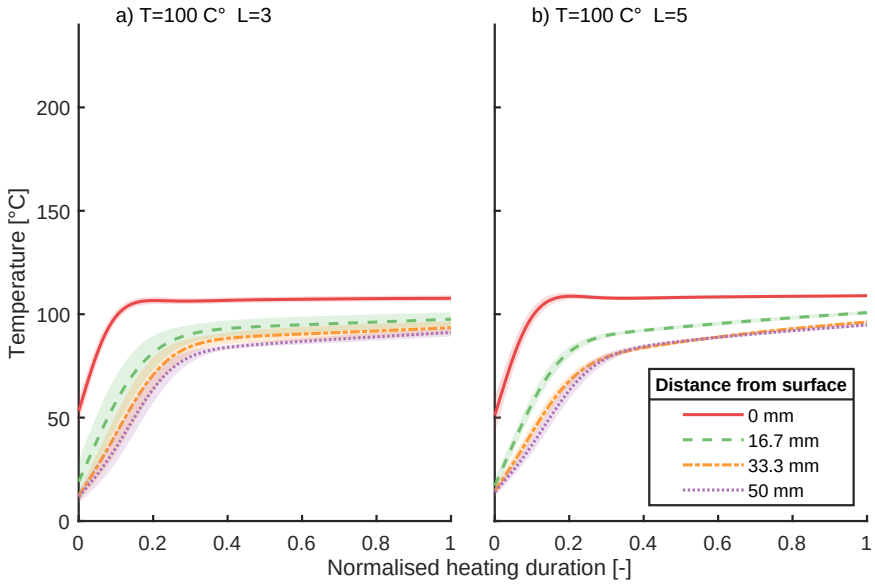

Figure 4.13. Mean and ± one standard deviation summary for thermocouple readings of different samples at fixed distance from the timber surface in experiments with a target temperature of 100 °C and a) three plies and b) five plies.

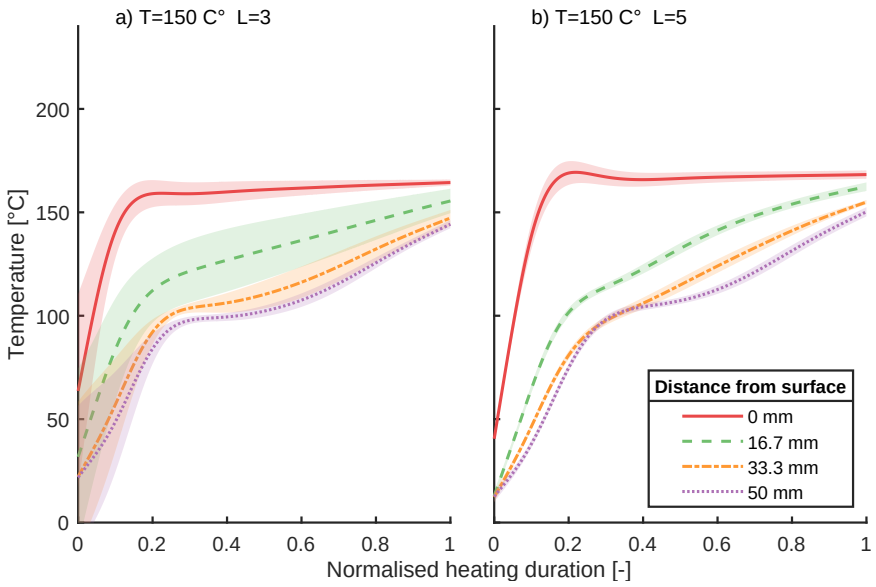

Figure 4.14. Mean and ± one standard deviation summary for thermocouple readings of different samples at fixed distance from the timber surface in experiments with a target temperature of 150 °C and a) three plies and b) five plies.

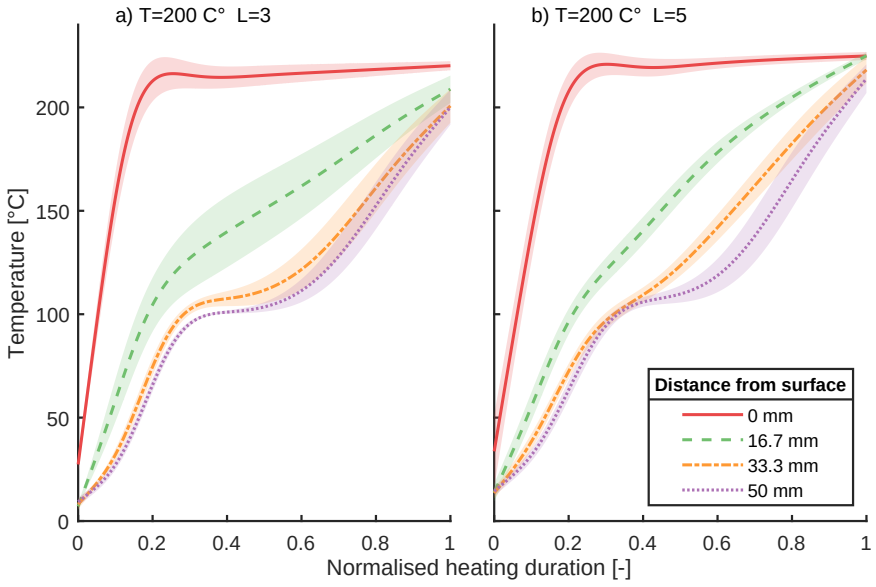

Figure 4.15. Mean and ± one standard deviation summary for thermocouple readings of different samples at fixed distance from the timber surface in experiments with a target temperature of 200 °C and a) three plies and b) five plies.

| **Deflections** | The effective compressive stresses with increases in crosshead stroke for the different configurations at different steady state timber temperatures are shown in Figure 4.16. It can be seen that the higher ultimate stresses, which were observed for five ply samples in comparison to three ply samples at ambient temperatures (refer to Table 4.2 and Figure 4.2), were also present for elevated steady state temperatures. The stress versus crosshead stroke curves follow the same pattern as those for the ambient temperature reference experiments (see Figure 4.2), with an elastic loading phase observed until an ultimate stress limit is reached and subsequent plastic behaviour follows with strain softening. The ultimate strengths reduce with increasing temperatures but then increase between 100 and 150 °C; this is likely linked to the removal of moisture from the samples at these temperatures. For 200 °C samples the retained strength reaches a minimum, indicating that at these temperatures thermal degradation of the timber offsets any strength gains due to drying. From the stress versus stroke plots no discernible difference can be observed for the slope of the elastic response at the different target temperatures, i.e. the elastic modulus, especially in comparison to the differences that arise in ultimate compressive strength, with increasing temperature.

| **Failure mode** | For lower temperatures the typical failure mode of the steady state heated specimens was observed to be similar to the ambient temperature failure mode shown in Figure 4.5, with fibre buckling failure in parallel lamellae occurring at the peak load in a defined failure plane. For higher temperatures the failure mode became more brittle (with more splinters forming rather than wood fibres buckling) and the plies failed in a less interdependent manner than was observed for ambient temperature or low temperature steady state heating. A typical annotated failure mode is shown for a three ply polyurethane adhesive sample in Figure 4.17, where the two observed wood failure points occurred at different loading stages. In addition, a relative movement of the plies can be visually observed from the applied speckle pattern that is highlighted between the two images. A debonding crack can be observed between the left vertical and centre crosswise plies. The observed brittleness for samples at higher temperatures can likely be linked to the loss of moisture in the cell walls and the onset of material degradation due to pyrolysis.

4.3.3.2 Transient heating

| **Temperatures** | The measured temperatures for the experiments where transient heating was applied to constantly loaded samples are shown in Figure 4.18. It can

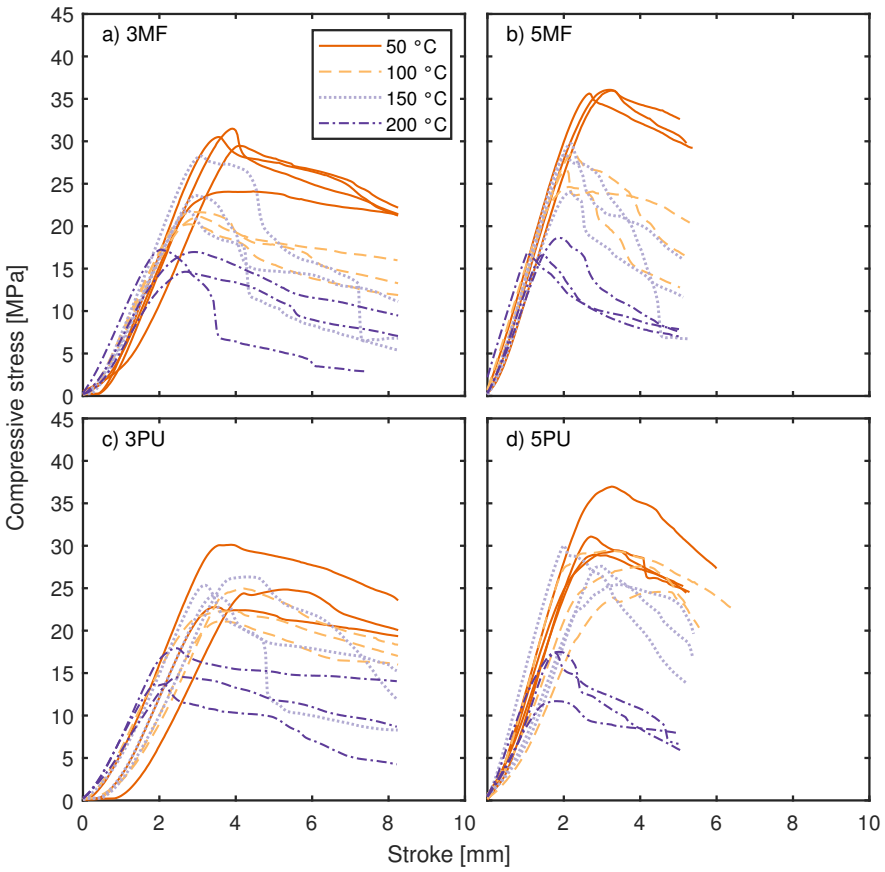

Figure 4.16. Stress response against imposed crosshead stroke for small scale CLT compression samples at elevated steady state temperatures for the four different ply and adhesive configurations assessed.

be seen that the standard error and therefore the deviation of temperatures between different experiments was small. A difference between the three thermocouples can be identified, however, as would be expected considering their positioning at the edge of the specimen, the difference is only marginal and far less obvious than for the centrally located thermocouples that are shown in Figure 4.12 through Figure 4.15.

| **Deflections** | The measured stroke deflections for all transient experiments are shown in Figure 4.19 against the mean temperature in the failure region. For this the mean temperature at failures of thermocouples in the vicinity of the visually observed failure zone were calculated. The failure zone refers to either the row of thermocouples at mid-height of the specimens, or the additional sensors that were placed near the bottom (refer to Figure 4.10). The display of these results is organised by heating

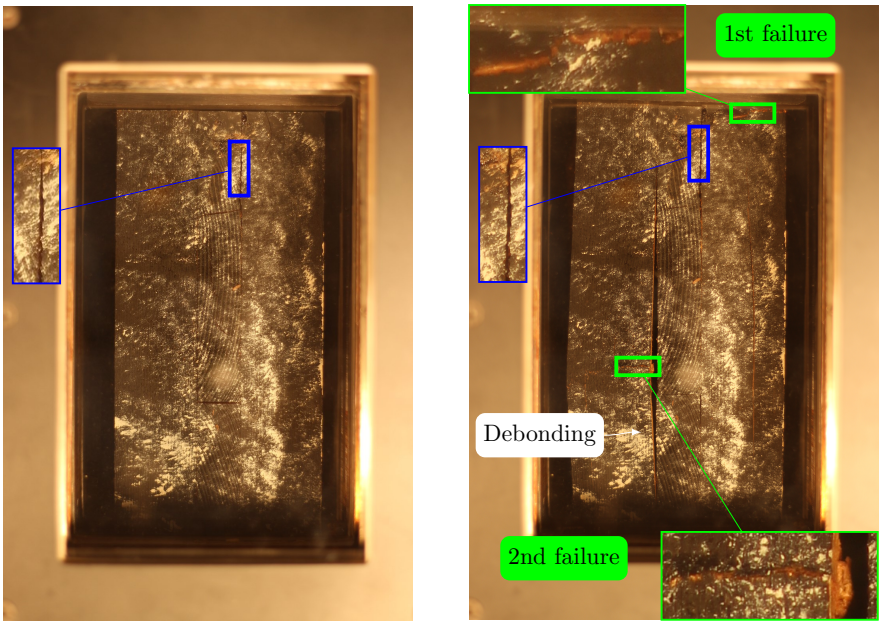

Figure 4.17. Typical failure mode for samples steady heated to 150 °C or higher, here shown for a three ply polyurethane sample heated to 200 °C. Observed wood failures are highlighted as well as relative movement between lamellae as shown by shear shift in speckle pattern.

rate and load applied (refer to Table 4.1 and Figure 4.9). As expected, it is observed that, for the higher loading ratio of 50 % of the mean ambient temperature capacity, runaway deflections and failure occur at lower temperatures than for the lower loading ratio of 25 %. The differences between the failure temperatures for the two assessed heating rates is less pronounced than the difference between the temperatures at failure for the different load ratios. For the higher loading ratio the stroke rate increases until failure occurs while the samples loaded to 25 % experience a reduction in the rate of stroke after an initial increase. For the faster heating rates it can be observed that the samples bonded with polyurethane adhesive tend to fail at lower temperatures than the samples bonded with melamine formaldehyde (MF) adhesive. While this also seems to apply to some individual samples subjected to slow heating, this effect cannot be confirmed without a more thorough investigation of the failure loads and temperatures; this is done in Subsection 4.3.5.

| **Failure mode** | The failure mode for the transient samples varied depending on the heating and loading conditions. For samples that failed during the heating phase

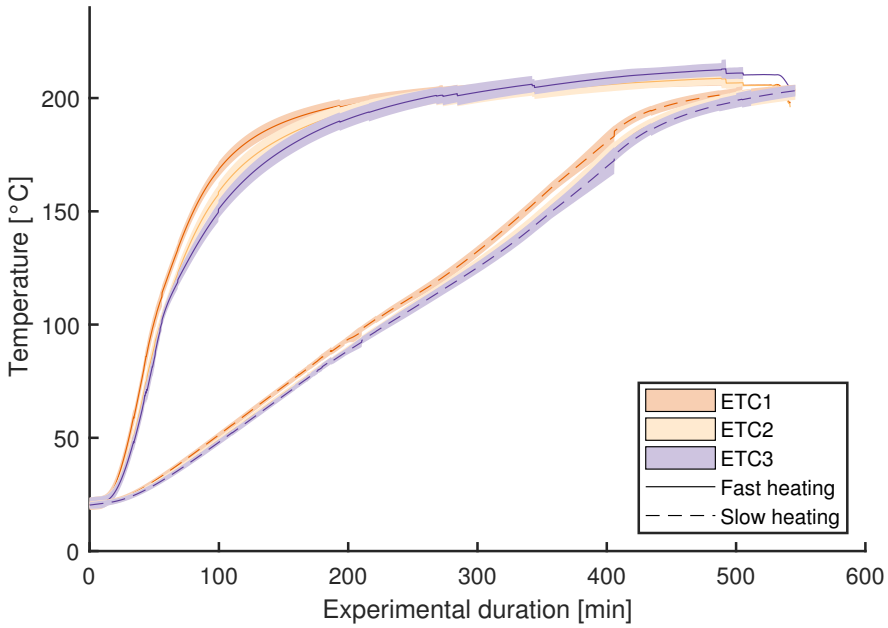

Figure 4.18. Mean and 95 % confidence interval of measured timber temperatures from additional thermocouples 10 mm from specimen bottom (refer to Figure 4.10) for fast and slow gas heating rates.

and before the sample dried out, the failure mode mostly occurred locally near the bottom of the sample where moisture accumulated and softened the timber (due to the tendency of cellulose to become more pliable with increasing water content of the cell walls [40]), which led to crushing and subsequent propagation of failure along the lamellae interfaces. This 'soggy bottom' failure mode was confirmed by examination of the sample immediately after termination of the experiments. An example of this failure mode is shown in Figure 4.20 alongside the loaded sample before any heating was applied. Samples which dried out before structural failure was observed and subsqeuently failed in dry conditions showed the same typical failure modes as steady state samples, as shown in Figure 4.17.

4.3.4 Additional experimental observations

4.3.4.1 Mass loss

The mass of all heated samples in this experimental series was measured before and immediately after each experiment. The percentage of mass loss in terms of the final weight was then calculated according to Equation 3.1, and is plotted against the mean

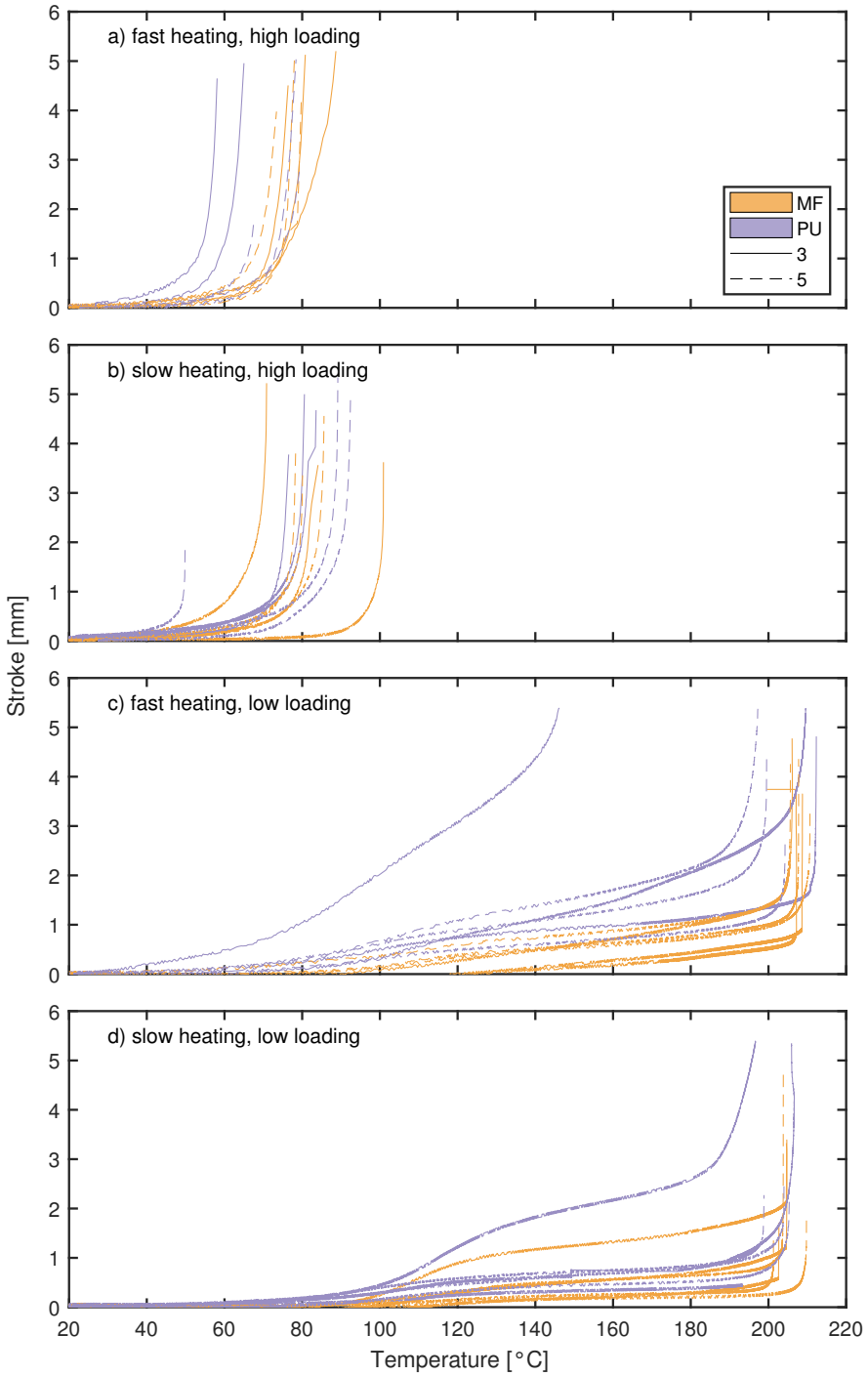

Figure 4.19. Stroke deflection with temperature of transiently heated CLT samples under constant load.

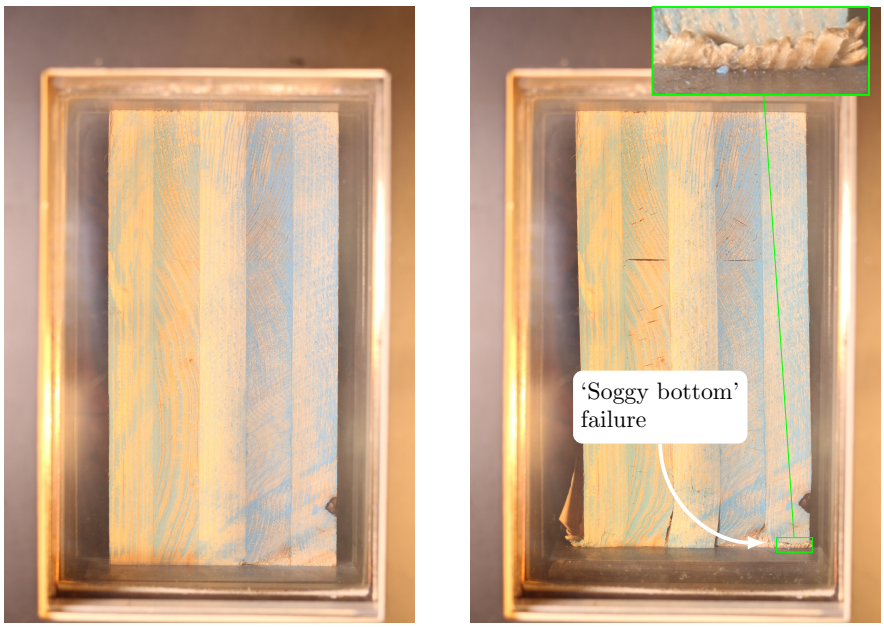

Figure 4.20. Typical failure mode for transient samples with softening of fibres due to moisture accumulation. Shrinkage cracks can be observed in the crosswise layers. Note that blue chalk was used on these samples to increase contrast for image correlation.

timber temperature at failure in Figure 4.21, which also shows the expected mean moisture content as described in Chapter 3. Because the mass loss percentage is calculated based on the same principle as the moisture content (i.e. as a fraction of 'dried' mass) the plot can be interpreted as the moisture content at the end of the experiment and any values above the expected moisture content indicate mass loss beyond the evaporation of moisture. It can be seen that the expected moisture content approximately divides the mass loss into two regimes. An exponential increase in mass loss up to 100 °C followed by a linear increase in the mass loss with increasing temperatures for samples heated to 150 °C or above. From this it can be postulated that mass loss up to 100 °C is driven by the loss of moisture, and for samples heated above 100 °C the expected moisture content mass loss is caused by pyrolysis in the timber, which can therefore be considered to act in specimens heated to 150 °C or above.

4.3.4.2 Self-heating

At high experimental solid phase temperatures the measured temperatures at the centre of some the samples continued to rise beyond the set gas phase temperature and continued to do so even as the oven was switched off and the samples were removed

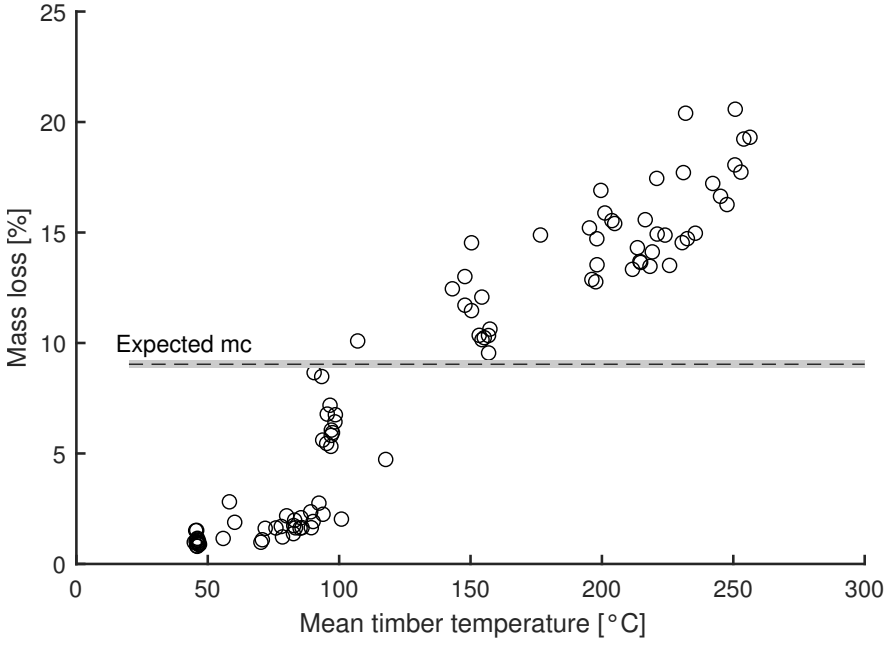

Figure 4.21. Mass loss of samples due to heating versus mean measured timber temperatures.

from the environmental chamber. This is shown for experiment TX3PU_11 in Fig 4.22. It can be seen that the internal temperatures in the timber keep rising above the set gas temperature, indicating that self heating is occurring in the timber. This was also confirmed from the observation of pyrolysis gases emerging from the specimen centre after the sample was removed from the environmental chamber. The self heating of timber that led to thermal runaway at its centre has previously been documented by Cuzzillo [214], who observed self heating at oven temperatures of 200 °C for wood cubes of 89 mm, hence the conditions observed herein can be viewed as equivalent or even more favourable to induce thermal runaway. Babrauskas [215] previously also summarised reports that indicated that self-ignition of timber can occur at temperatures as low as 77 °C, although he also stated that these cases of relatively low temperatures occurred under different thermal and chemical considerations than what was considered by Cuzzillo and that the time scales in this case would be months or even years. While the occurrence of smouldering in timber is neither the focus of this study nor for this thesis, this should be seen as a reminder that timber is not an inert material and once heated to sufficiently internal temperatures pyrolysis and smouldering will contribute additional heat energy to the timber, which poses additional challenges for the structural integrity as well as for extinguishment.

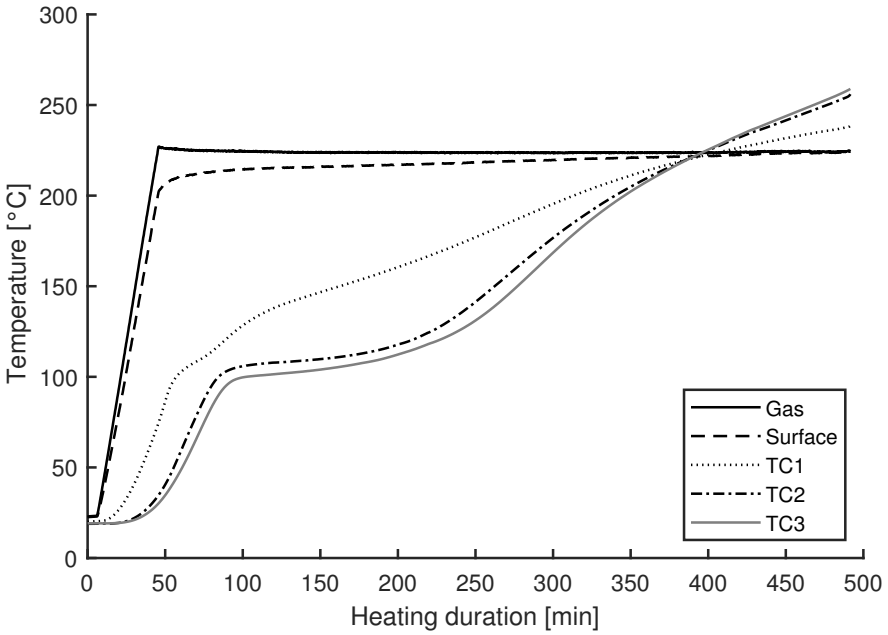

Figure 4.22. Temperature measurements for experiment TX3PU_11 (transient heating of 3-ply polyurethane bonded CLT) showing internal self heating.

4.3.5 Ultimate compressive strength

The effective ultimate compressive strength of samples is plotted against the solid phase temperature for each adhesive type and number of lamellae in Figure 4.23. Note that the temperature values for ambient experiments are jittered (i.e. shifted randomly) by up to ± 5 K for visual clarity, but the nominal assumed temperature for these experiments is 20 °C for all ambient temperatures. The temperature at failure is taken as the mean temperature measured at the time of failure (i.e. peak strength) in the region where failure was observed to initiate. The errorbars denote the minimum and maximum measured temperature in the timber solid phase. As the temperatures are plotted in absolute terms, it is not surprising to see increasing temperature variations for increasing steady state temperatures and the largest temperature variations for transient heating. Overall the errorbars are sufficiently small to justify the use and distinction of mean temperatures from the thermocouples where failure was identified. It can be seen that the increased strength of the five ply samples that was observed for ambient reference experiments is also present for higher steady state temperatures, however this lamination effect does not seem to influence the results from transient heating.

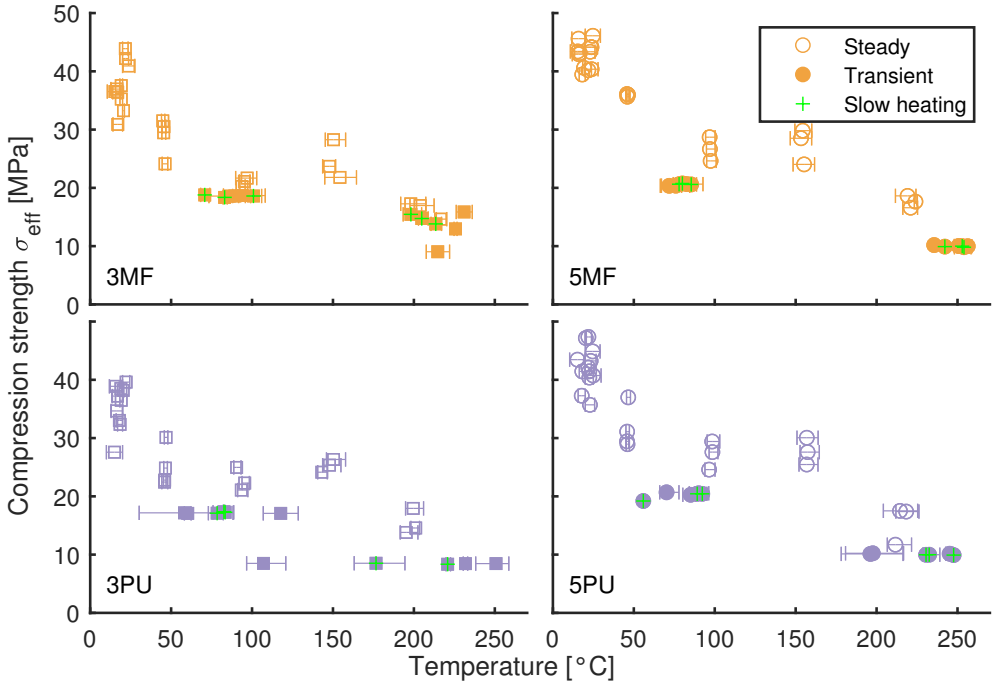

Figure 4.23. Measured ultimate effective compressive strengths for increasing temperatures, arranged by adhesive and number of plies.

An improved comparison of the effect of heating on the axial compressive strength of CLT can be made by normalising the results with respect to their ambient capacity. For this, the mean ambient strength for each configuration (see Table 4.2 is calculated and used to normalise all other data points in this configuration. The resulting normalised compressive strength is plotted against the mean failure solid phase temperature in Figure 4.24. Note that the error bars denoting temperature ranges are omitted for clarity since they are not expected to change with normalisation and can be observed in Figure 4.23. The commonly used reduction curve from EN 1995-1-2 (EC5) [145] for strength of timber in compression is shown for comparison.

Multiple observations can be made from the normalised strength plot in Figure 4.24. The steady state results are clustered relatively closely together and no obvious effect of either glue or ply configuration can be seen to influence the strength with increasing temperatures. It can be seen that the effect of temperature on the steady state results is non linear and that an increase in normalised strength is observed for temperatures above 100 °C. This can be attributed to the removal of moisture as steady state temperatures are approached within the sample and water is driven out of the cell walls. The steady state results are in contrast to the transient results, which follow a significantly

different path. At very high temperatures the transient results converge onto the same path as the steady state specimens. This occurs for transient experiments with a low load and a long heating duration, meaning that if the combined effects of moisture and heat do not sufficiently weaken a transiently heated sample to the point of failure the sample will dry out and effectively act as a steady state sample.

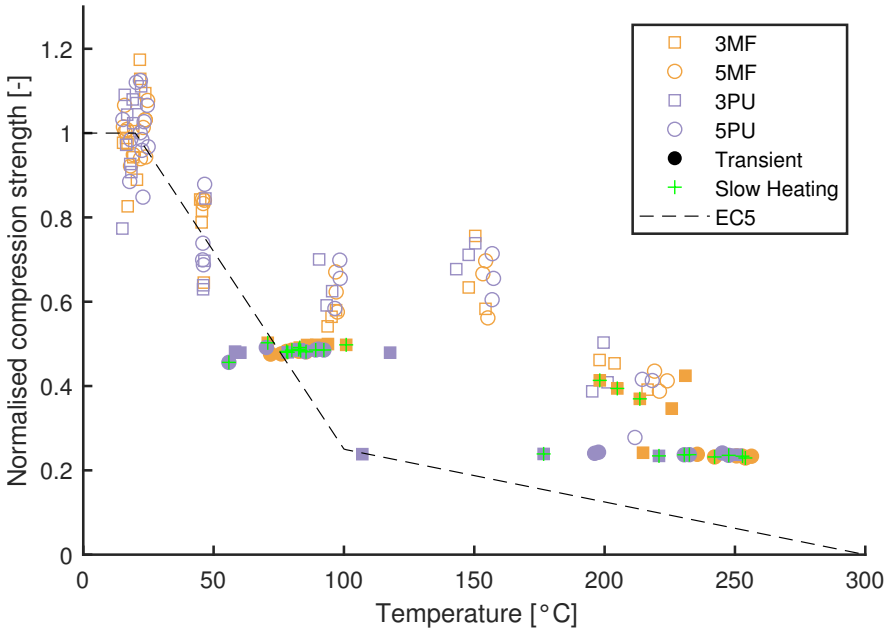

Figure 4.24. Normalised ultimate effective compressive strengths with increasing temperatures for both steady state and transient heating.

4.3.6 Elastic modulus

The absolute elastic moduli with increasing timber temperatures for the four configurations tested are shown in Figure 4.25. Note that, due to the variation in temperature in transiently heated samples it is not possible to obtain meaningful values for the elastic modulus from transient heating experiments. For steady state samples tested at elevated temperatures it can be seen that for samples bonded with melamine formaldehyde the values are somewhat erratic and it is difficult to identify a clear pattern with heating. As for the ambient values, the specimens consisting of five plies have a higher elastic modulus at elevated temperatures than those with three plies. For the specimens bonded with the MF adhesive an initial reduction in elastic modulus is followed by an increase above 100 °C, which is likely linked to the removal of moisture at these

temperatures. This increase in elastic modulus with drying is not evident for the specimens using the PU adhesive type as bonding agent, and also the initial decrease is not as severe as for the MF bonded samples.

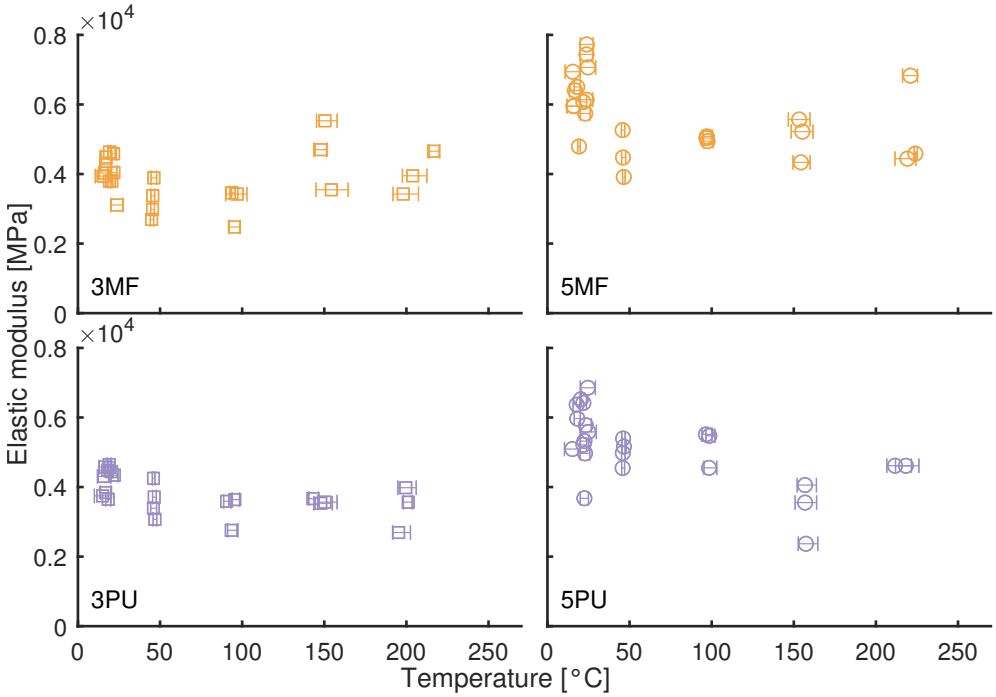

Figure 4.25. Measured elastic modulus for increasing temperatures, arranged by adhesive and number of plies.

The combined plot for the elastic moduli normalised against the configuration mean for samples heated to steady state is shown in Figure 4.26. As could be expected from the absolute values it is difficult to discern patterns from the data. The majority of data points appear to follow a linear reduction that is less severe than the proposed reduction in elastic modulus from EC5. This is not suprising since the recommended reduction is based on transient heating to implicitly account for moisture movement [108] whereas the assessed data herein is based on steady state heating.

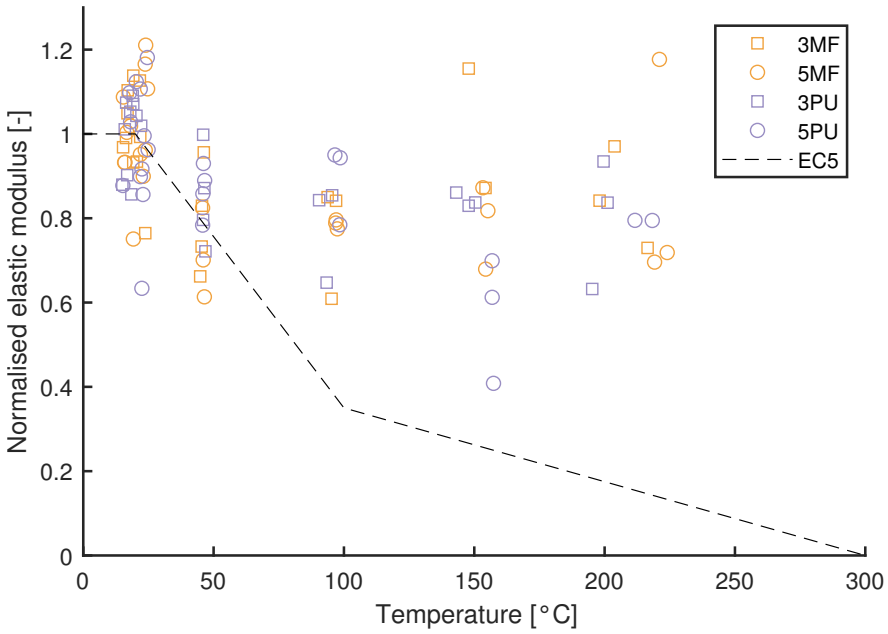

Figure 4.26. Normalised elastic modulus with increasing temperatures for steady state heating.

4.4 Discussion of results

4.4.1 Effect of temperature on strength

Considering the combined results of the steady state and transient tests it becomes clear that transient heating has a more detrimental apparent effect on the load carrying capacity of timber than steady state heating. The major factor causing this is the movement of moisture within the timber. It is known that an increase in moisture will reduce the strength and stiffness of timber significantly, especially in combination with heat [40, 170]. The following section investigates the effect of increasing temperatures on the strength of timber with a special focus on the influence of adhesives and number of lamellae for CLT.

4.4.2 Statistical analysis of temperature effects

4.4.2.1 Multivariable regression analysis

Multivariable linear regression analysis can be used to investigate the changes in strength retention (the normalised stress) with increasing temperatures, and to assess the validity of the resulting model in statistical terms. A first regression analysis can be described by Equation 4.2. This formulation assesses the influence of temperature and the effect of its possible interaction (denoted by ': ') with three other explanatory variables on the normalised compressive strength. The resulting adjusted R^2 value of this model is 0.72 and the resulting statistical output is shown in Table 4.6. It can be seen that there is a significant reduction in retention of compression strength with increasing temperature, with a p-value of 1.6 %. It can also be seen that as temperature increases there is a negative effect on strength retention if polyurethane is used as adhesive and no effect if five instead of three layers are used, however, neither of these effects is statistically significant, which is also highlighted by the relative sizes of the respective standard errors for these two parameters.

$$Norm.Strength \sim T + T\colon Adhesive + T\colon Layers + T\colon Density \tag{4.2}$$

Table 4.6. Multiple linear regression on all data

	Estimate	Std. Error	t value	Pr(>|t|)
(Intercept)	0.9568	0.0201	47.67	0.0000
T	-0.0041	0.0017	-2.45	0.0156
T:AdhesivePU	-0.0002	0.0002	-1.15	0.2533
T:Layers5	0.0000	0.0002	0.24	0.8078
T:Density	0.0000	0.0000	0.74	0.4608

The resulting linear reduction is shown in Figure 4.27. It can be seen that the confidence interval for this fit is large and the fit is therefore not very useful to describe the reduction in normalised strength with increasing temperatures. This also serves as a reminder that a relatively high R^2 value and statistical significance cannot automatically denote a model as 'good'. There are two problems with the fit shown in Equation 4.2: (1) the fit uses all the available data, despite the fact that transient and steady state results clearly differ in response as heating progresses, and (2) the fit attempts to model the data through a linear regression when the data clearly shows a multi linear pattern. Note that if the explanatory variables for adhesive and layers

are omitted from Equation 4.2 then the confidence interval for the regression against temperature shrinks significantly, however, there is not much information to be gained from such a model beyond what is already known: that timber loses strength when heated.

Instead of focusing on all the data, the reduction in strength can be better assessed if steady state heated samples are separated from transient data points. Below 100 °C the steady heated samples still contain moisture and these samples will therefore be included in the transient data analysis that follows. Steady state samples heated to 100 °C or above will not be considered further for regression analysis as these conditions are unlikely to occur in practice and the results are therefore of lesser interest than the data points which capture the transient effects of moisture in the timber. While the duration of heating for steady state samples heated to a target temperature of 50 °C will differ from transiently heated samples they will still contain moisture (see Figure 4.21, and will therefore to some extent capture the interaction of heat and water in timber cells, and are therefore included in the following analysis.

There is not a wide range of suitable subroutines available for a bilinear regression fit. Multiple linear regression splines (MARS) are overly complex where only one output variable is fitted and the results are not readily open for interpretation. One alternative option is the 'segmented' package [216] in R, however, from exploratory analysis of this model, it appears to be more suited for models with multiple *unknown* breakpoints, rather than one predetermined breakpoint.

4.4.2.2 Bilinear breakpoint assessment

For a bilinear model concerning the strength reduction with heat there are some limitations that are not adequately captured by the regression approach presented above. The reduction in strength should only onset above ambient temperatures (herein taken as 20 °C) and at 300 °C the strength should be zero, since char is assumed to have no mechanical strength. Shape Prescriptive Modelling [217] allows linear or higher order fits over multiple predetermined segments and is therefore used in the following to create bilinear fits for the compressive strength data. This is paired with a bootstrap approach to determine the variance of the determined parameters. For a bootstrap the same data is sampled *with replacement* in repeated calculation steps and for a sufficient number of repetitions this allows for an estimation of the mean and confidence intervals of the underlying population.

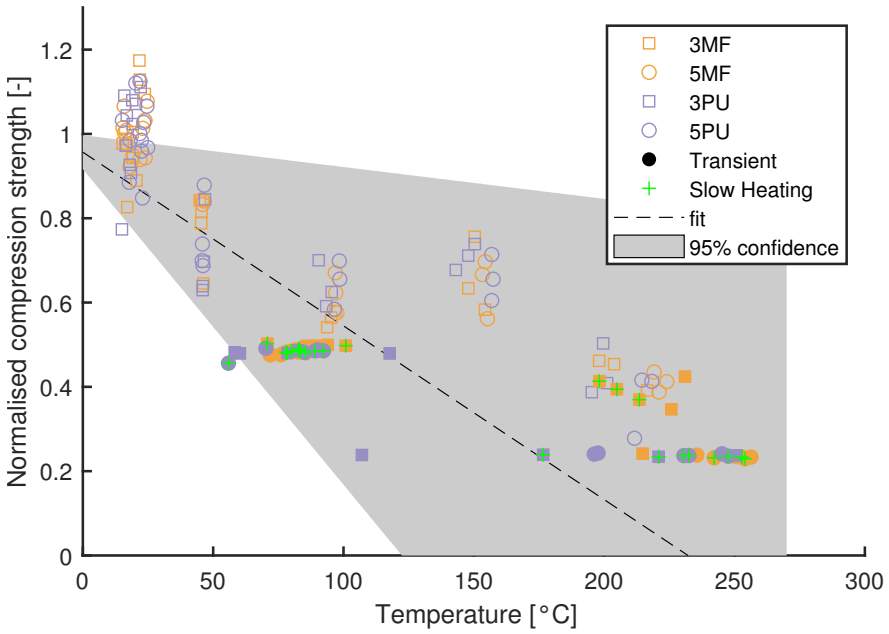

Figure 4.27. Linear regression fit for normalised compressive strength data according to Equation 4.2.

A bilinear fit for the available data is forced through break points at 20, 100, and 300 °C with retained strength fraction set to zero at 300 °C. The breakpoint at 100 °C is determined for the four configuration variables in this study from repeated bootstrap samples. A generalised flowchart of this procedure is shown in Figure 4.28. The resulting histograms for the breakpoints, which denote the strength retention at 100 °C are shown in Figure 4.29.

The resulting breakpoints are normally distributed and it can be seen that, a potentially statistically significant difference exists between PU and MF samples. This can be confirmed by assessing the difference between the two variables through subtraction of the PU data from the MF data. This returns a range of values with a median of 0.087 and 95 % confidence bounds of 0.003 and 0.186. Since these bounds do not contain zero, it can be stated with a 95 % confidence that a difference in strength retention between polyurethane and melamine formaldehyde adhesives exists at 100 °C for the imposed bilinear reduction. This assessment does not hold for the 99 % confidence interval. For the number of layers of the CLT, five ply samples have a slightly reduced retention factor, however the confidence for this difference reflecting the underlying population data lies below 50 % and this is therefore more likely caused by random variation betweens specimens rather than a systematic property of the underlying population.

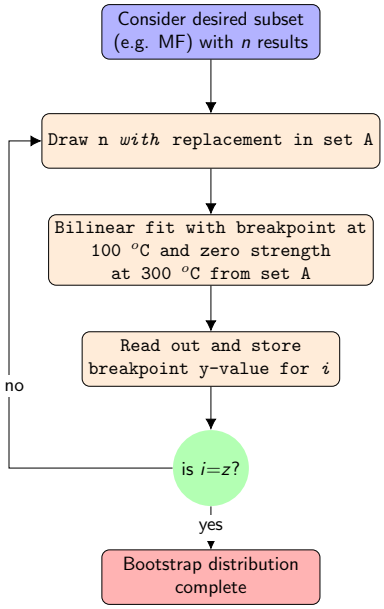

Figure 4.28. Flowchart detailing process for bootstrap distribution of size z.

The correlation matrix for the data in Figure 4.29 is shown in Table 4.7 and it can be seen that no correlation exists between the variables and therefore that no compounding interactions are expected between the data.

Table 4.7. Correlation matrix for breakpoint data.

	MF	PU	Three	Five
MF	1.00	-0.03	-0.00	0.01
PU	-0.03	1.00	-0.00	-0.01
Three	-0.00	-0.00	1.00	-0.02
Five	0.01	-0.01	-0.02	1.00

The determined reduction curves for the two adhesive formulations are plotted alongside the data against temperature in Figure 4.30 with ambient temperature data points jittered between 15 and 25 °C for visual reasons. As determined it can be observed that the PU reduction leads to a lower strength retention at 100 °C with minimal overlap of the confidence intervals. The reduction in strength retention as recommended in Eurocode 5 [145] is plotted for comparison and it can be seen that it provides a lower bound below the 2.5 % percentile for the PU samples.

It is not entirely clear why the adhesive should have a significant effect on the strength

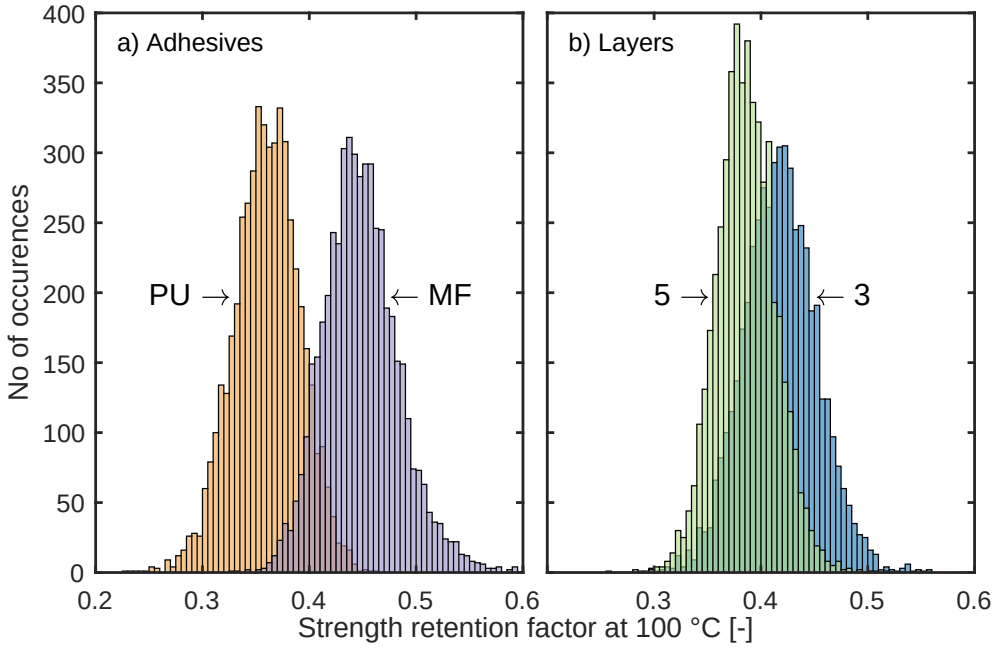

Figure 4.29. Histogram of strength retention factors at 100 °C (i.e. breakpoints) determined from a 5000 sample bootstrap by a) Adhesive and b) No of lamellae in CLT samples.

of heated CLT in this compressive experimental set-up. Past research [70, 174] has identified that polyurethane adhesives often perform worse in terms of shear strength and creep compared to melamine based adhesives. However, from a structural engineering point of view, even if the bonding of the adhesive ceases to act completely, the individual layers should continue to displace at the same rate, thereby maintaining the same strain and stress, since the individual cross-sectional areas resisting the applied forces do not change. The second moment of area, on the other hand, for a specimen with no adhesion between lamellae left is significantly lower than for a fully bonded sample, so the occurrence of small bending moments or buckling in the samples could explain the failure at lower temperatures for PU samples compared to MF ones. Internal moments could be caused by non-uniform heating, as is the case for the transiently heated samples, however, this does not explain why there is also a difference for the steady state samples heated to approximately 50 °C. Another possible explanation, independent of the occurrence of moments in the specimen, could be the loss or weakening of the lamination effect, which is shown to significantly improve the strength for

five plies at ambient capacity. There also remains a slight probability that the reduced strength retention for polyurethane is driven by chance, especially when considering that only a limited number of data points are available at each temperature.

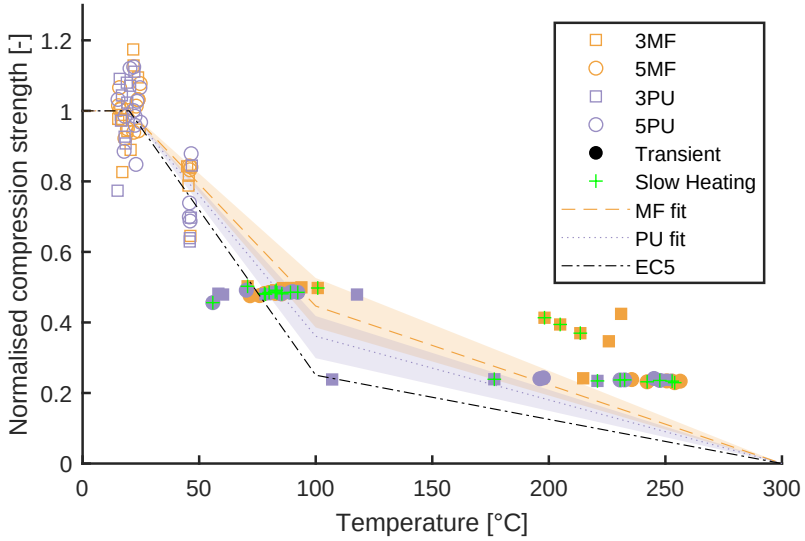

Figure 4.30. Reduction in retention factors with 95 % confidence intervals as shaded areas for different adhesive formulations determined from multi-linear fits with fixed boundary conditions at ambient temperature timber and fully charred conditions.

4.4.3 Effect of temperature on elastic modulus in compression

The normalised reduction of elastic modulus is shown in Figure 4.26. Due to the visible large scatter of the results any advanced statistical analysis will be inherently flawed and is therefore omitted herein. For the accurate determination of elastic modulus a stiffer reaction frame is recommended to reduce the influence of movement of the supporting structure thereby also inducing out of plane movements of the sample.

4.5 Conclusions

This chapter described the set-up, execution, results, and analysis of tests on 143 small scale CLT samples that were subjected to different loading and heating conditions in

axial compression. From ambient temperature reference experiments it was shown that neither for compressive strength nor for compressive elastic modulus did significant differences exist at ambient temperature between samples bonded with one of two different adhesives types. For a difference in the number of lamellae used in the sample it was found that samples made of five plies were able to sustain higher ultimate compressive stresses before failure occurred.

For samples subjected to heating, either through steady state heating followed by loading to failure or transient heating on samples subjected to constant load, a significant difference was observed in the strength reduction between steady state and transient heated experimental conditions. For the former, an initial reduction in strength was followed by an increase for temperatures around 100 °C. No significant differences in the reductions in strength or elastic moduli with increasing temperature were observed for steady state heating. Samples that were heated transiently were observed to fail at comparatively lower temperatures than steady state samples for samples loaded to 50 % of their ambient capacity, while the majority of lower loaded samples (load ratio of 25 %) dried out and subsequently failed at temperatures in line with reductions observed for steady state heated samples. This differing trend between transient and steady state samples was attributed to the movement and accumulation of moisture since the failure mode in transient samples was likely caused by the accumulation of water at the edges of the sample, causing localised softening and failure.

A bilinear model with a predetermined breakpoint at 100 °C was fitted to transiently heated samples as well as steady state sample with remaining moisture and a difference in retention factor was found to lie in a 95 % confidence interval between the two assessed adhesive formulations with polyurethane adhesive having a median breakpoint of 0.09 lower than melamine formaldehyde adhesive samples. From the available experimental data, the underpinning mechanical forces causing this effect could not be identified.

The currently recommended strength reduction curve from EN 1995 1-2 [145] was observed to provide a conservative lower bound for most samples in this experimental study and is therefore likely suitable for use on laminated timber systems subjected to either transient or steady state heating conditions.

For the elastic modulus only samples heated to a steady state temperature were assessed and a reduction with temperature was observed, although the wide scatter of the data, which is in large parts attributed to noise induced, prevented meaningful deeper analysis.

The following chapter will aim to illuminate the effect of layers and adhesives at elevated temperatures further through experiments in bending, with an explicit focus on shear and shear deformations.

This page is intentionally left blank.

CHAPTER 5

Effect of transient slow heating on cross-laminated timber in flexure

This page is intentionally left blank.

This section describes an experimental series performed on uniformly heated cross-laminated timber (CLT) beams in bending in order to better describe and understand the effects of shear between plies in CLT and its consequences both for the deflections induced by combined load and heat, and the load bearing capacity. Debonding describes the loss of bond between two adjacent timber plies due to the combined influence of heat, shear forces and/or normal 'peeling' forces (see also Subsection 2.4.2). This should not be confused with delamination or 'loss of stickability' which describes fall off of charred timber and therefore only has secondary (increased charring rate) effects on the load bearing capacity.

5.1 Motivation

Due to the prevalence of fire resistance compliance testing trough standard time temperature exposure in furnaces, there is little understanding on the occurrence and consequence of debonding in laminated timber elements when shallow thermal gradients lead to elevated glue line temperatures. Debonding will reduce the composite action between adjacent timber plies and thereby reduce the effective stiffness and load bearing capacity of the element. The experiments described herein imposed slow and spatially uniform increases of the gas phase temperature surrounding the CLT beams in order to induce heating of the timber with a relatively shallow thermal gradient at temperatures less than those required for charring, and that minimise pyrolysis of the timber so that the effects of elevated temperatures of the adhesives, as well as prolonged heating of the timber, can be assessed.

This study is the first to look in detail at the structural consequences for CLT with different adhesive types and ply depths at elevated temperatures. A detailed three step experimental series helped to illuminate the roles that adhesives and their bond strength play in the deflection of cross-laminated timber in bending at elevated temperature.

5.1.1 Experimental overview

The experimental matrix detailing the 25 experiments that are described and analysed in this chapter is outlined in Table 5.1. As with the other experimental series described in this thesis the specimens were grouped into samples by the different ply number and by adhesive type used, as described in Chapter 3. In addition, the samples were separated by the temperature exposure (either ambient reference or transiently heated)

and the applied load level. The applied load levels are marked as high (H) for 50 % applied mean failure load and low (L) for 30 % applied mean failure load. For the high applied mean failure load the heating was applied until failure was observed, which did not occur for all experiments from this series. Therefore, since failure would be less likely to occur for the lower loaded samples, it was decided to heat for a fixed time period of three hours, followed by a cooling phase of three hours for the low loaded experiments. This was done to better understand the potential for recovery of deflections in heated beams.

For each combination of loading, heating, and CLT configuration type two repeat experiments were performed. An additional experiment was run for the heated 5PU sample with high loads, as the initial two specimens for this sample showed a clear deviation from one another.

Table 5.1. Experimental matrix for beam elements subjected to four point bending.

	Adhesive	**Layers**	**Temperature**	**Heating duration**	**Load ratio**[a]	**Number of specimen**
Group Name	-	-	[°C]	[h]	[%]	-
B3MF020	MF	3	20	-	0-100	2
B3PU020	PU	3	20	-	0-100	2
B5MF020	MF	5	20	-	0-100	2
B5PU020	PU	5	20	-	0-100	2
BTX3MF_H	MF	3	150	to failure	50	2
BTX3PU_H	PU	3	150	to failure	50	2
BTX5MF_H	MF	5	150	to failure	50	2
BTX5PU_H	PU	5	150	to failure	50	3
BTX3MF_L	MF	3	150	3	30	2
BTX3PU_L	PU	3	150	3	30	2
BTX5MF_L	MF	5	150	3	30	2
BTX5PU_L	PU	5	150	3	30	2

[a]Samples at ambient temperatures are subjected to load increases until failure is observed. For heated samples a proportion of the mean failure load at ambient temperatures is applied.

5.2 Ambient reference experiments

To assess the effects of elevated temperatures on the bending behaviour of CLT beams, it is first necessary to characterise this behaviour at ambient temperature for the CLT

configurations in this study, and thereby to generate baseline data. This section describes four point bending experiments performed on eight CLT beams (two repeats for each configuration) at ambient temperature and presents and analyses the obtained results.

5.2.1 Experimental set-up

Four point crosshead stroke controlled loading was applied to CLT beams with dimensions of 3000, 300 and, 100 mm of length, width, and thickness respectively until failure was observed. The free span of the beams was 2700 mm and the constant moment section at the longitudinal centre of the beam was chosen as 500 mm. Note that this constituted a relatively small section of constant moment in the midspan region relative to the free span. This was chosen to favour a bending failure mode by tensile rupture rather than rolling shear failure in the shear region at ambient temperature. A drawing of the plan and elevation views of the beams is shown in Figure 5.1. The connections were designed to act as pinned connections at all contact points; these consist of steel rollers contacting steel plates, and the stroke was imposed via a 250 kN Instron servo hydraulic actuator [218] with a set crosshead deflection rate of 2 mm/min.

5.2.1.1 Instrumentation

The imposed crosshead stroke displacements were logged through the Instron system. A built in load cell was used to determine the applied load at each stroke increment. A linear potentiometer (LP) was placed at midspan to record vertical deflections. At midspan and near the support a speckle pattern was added to the side of the beams to enable digital image correlation (DIC) [209] to be performed based on images recorded by two cameras at five second picture intervals of both the midspan section and the vicinity near the support; this allowed for complementary deflection measurements and was also used to monitor the strain states on the side surface of the timber. For the first beam the DIC tracking pattern was applied with blue chalk, since this had previously provided satisfactory correlation to track pixel clusters in small scale compression elements without obscuring details of the timber surface. However, due to vibrations in the beam during testing, the chalk was observed to fall off the timber, thereby making tracking after either local or global failure less reliable; for all subsequent beams in this series the speckle pattern was therefore applied as white (eggshell) paint speckles on a matt black spray paint substrate.

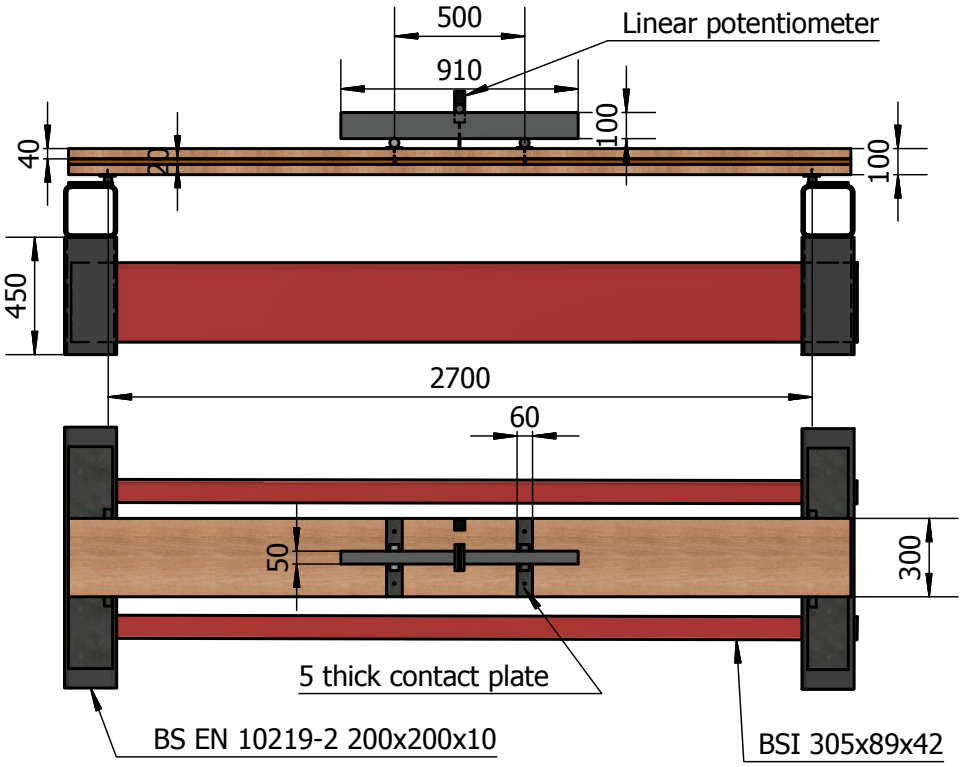

Figure 5.1. Elevation and plan view of the experimental set-up for ambient CLT beams in four point bending.

5.2.2 Experimental results

5.2.2.1 Load – deflection curves

The load applied to the eight tested CLT beams is plotted against the midspan deflection obtained from DIC data in Figure 5.2. The deflection data from DIC was chosen as it did not run out of travel, which was observed for some of the LP data at large deflections. For all beams a similar behaviour can be observed: an initial linear elastic loading response is followed by slight non-linearity, likely caused by plasticity of the compression zone (Tiemann [40] previously related the elastic limit to the compression stress), and a sudden drop in load due to brittle failure. Most of the curves follow a

near identical initial load deflection path, however, for each of the ply numbers, one of the specimens displays a significant lower elastic stiffness than the other three; no obvious explanations for these reduced stiffness values could be made, other than timber being a variable material.

Since, for the three ply samples more timber was placed with fibre direction orientated parallel to the main stress direction these samples were able to sustain higher loads before failure. One interesting point of note can be observed for Specimen 1 for the five ply melamine formaldehyde configuration (5MF_01). The load drops at a deflection of around 40 mm before resuming to increase and reaching its ultimate load. This can be attributed to the fact that the strength and stiffness of the individual boards, even though they are attributed to the same strength class, are random variables. If an individual board fails the overall load carrying capacity reduces but load can be redistributed across different boards and different layers.

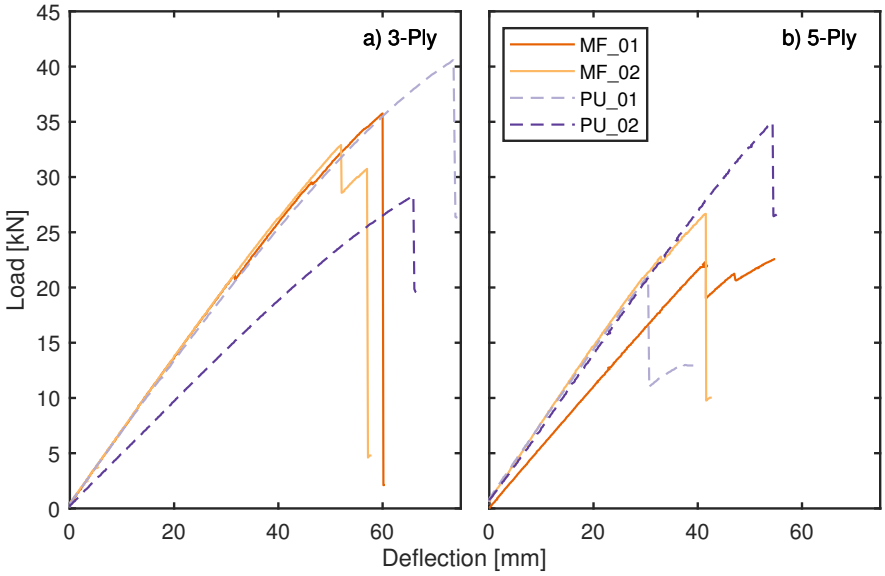

Figure 5.2. Load response of CLT beams with increasing midspan deflections for a) three ply and b) five ply configurations.

5.2.2.2 Mechanical properties

The modulus of rupture (MoR) can be computed according to Equation 5.1 which results in a comparable measure of bending resistance by accounting for the different lamellae layup of the three and five ply beams through calculation of the second moment of area (I). It should be noted that MoR is a simplification of the actual stresses in

timber beams at failure, since the stress distribution will be influenced by plasticity in the compression zone, which are assumed to be equal to the ultimate linear elastic stress at failure in the tension zone.

$$\sigma_b = My/I \tag{5.1}$$

The elastic modulus can be calculated from the measured midspan deflections as shown in Equation 5.2, where m is the load deflection slope, l is the span of the beam between the supports, a is the distance between the supports and the load points and I is the effective second moment of area. The elastic modulus is calculated between 20 and 50 % of the peak load.

$$E = m \cdot \frac{a}{48I} \cdot (3l^2 - 4a^2) \tag{5.2}$$

The modulus of rupture and the elastic moduli for the ambient beam samples are shown in Figure 5.3, grouped by adhesive and ply number with underlying calculations based on assumption of an effective cross-section (see Subsection 2.2.1). For the MoR values it can be seen that the medians between different adhesives and different ply configurations do not differ by much and that the difference observed is likely due to natural variability of the timber. This can be confirmed numerically by performing an analysis of variance (ANOVA), the results of which are shown in Table 5.2. It can be seen that, for the MoR, the null theory is not rejected for either adhesives or layers, meaning that no difference in the underlying populations should be expected between these parameters. From Figure 5.3 a) it can also be seen that the variability of the MoR for MF samples seems to be smaller than those for PU samples; from the limited sample size no obvious reason for this increased variability can be identified and it could simply be coincidental.

For the elastic modulus in Figure 5.3 b) no significant difference can be discerned between median values for the adhesive types and this is confirmed by Table 5.2, however, a statistically significant difference (at the 5%ile significance level) in elastic modulus can be observed between three and five ply sample groups. This does not necessarily reflect the material properties of the timber but rather the experimental conditions. For the three ply sample the effective length to depth ratio is smaller and the cross-layer in the centre is subjected to higher shear stresses, hence it is reasonable to expect that the shear deflections and therefore the overall deflections are larger for these beams. For this analysis it should be remembered that each group in Figure 5.3 consists

of four specimen only and the statistical power is low, i.e. there is chance for type II errors to occur. For comparison, to determine a large effect size (according to Cohen) for ANOVA with a target power of 0.8 and a targeted significance level of 0.05 the sample size is recommended as 26 samples per group, i.e. 52 experiments would be required to reach a power of 0.8, which is not feasible for ambient reference experiments of this scale. The presented p-values should therefore be considered with the appropriate scepticism in light of the relatively small sample size. The quantification of the p-values still offers valuable insights, especially when considering the relative magnitude between them, indicating that adhesives do not significantly influence the ambient behaviour and that the effective elastic modulus is affected positively by an increase in layers, with a 31 % increase in median elastic modulus measured for five compared to three layers. Both of these effects can also be expected based on consideration of the underlying mechanics.

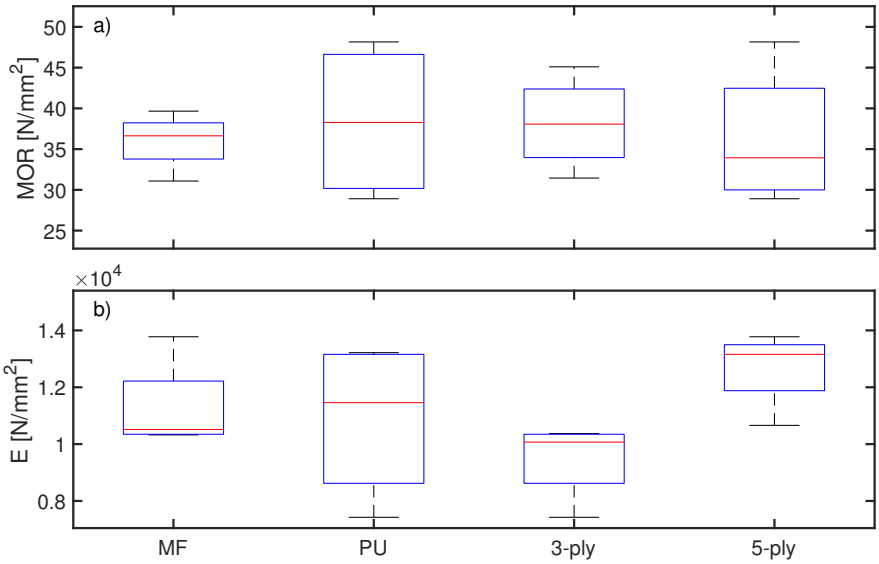

Figure 5.3. Box plot comparison of a) modulus of rupture (MoR) and b) elastic modulus (E) for different sample configurations of CLT beams

Table 5.2. ANOVA p-values summary for beams at ambient temperature.

	Adhesives	Layers
Modulus of rupture	0.68	0.73
Elastic modulus	0.74	0.03

5.2.2.3 Bending strains

Digital image correlation at midspan can be used to determine the longitudinal strain that was induced with increasing curvatures from bending. This is shown in Figure 5.4 with the computed strains superimposed on the surface of a specimen. In addition the longitudinal strain distribution is plotted along the distance from the neutral axis at midspan in Figure 5.5. It can be seen that the strains follow a linear gradient, increasing towards to extreme fibres of the beams, with a neutral axis of zero strain near centre. This shows that *'plane section remain plane'* and that beam theory can be supposed to apply to CLT in bending where no excessive shear strains act. It can be noted that the tension (positive) strains in Figure 5.5 reach higher magnitudes than the compressive strains; this is caused by an apparent shift in the neutral axis away from the geometrical centre of the beam, which can be seen in Figure 5.4 to appear closer to the top compressive edge than the bottom tension edge of the beam. The exact cause for this is not clear, it could be due to an uneven distribution of the mechanical properties of the boards, since boards should adhere to the same strength grade but will naturally show some deviation within this grade.

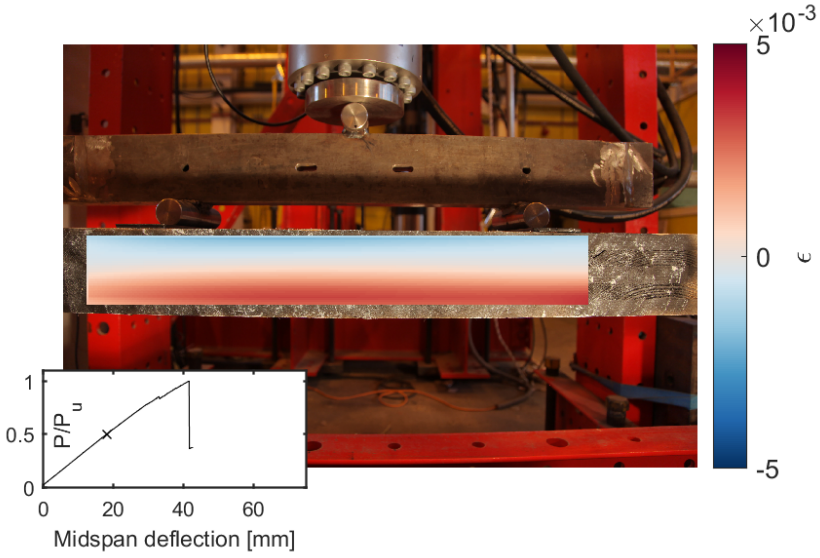

Figure 5.4. Longitudinal strains at midspan at 50 % of ultimate load for CLT bonded with melamine formaldehyde adhesive type and five plies.

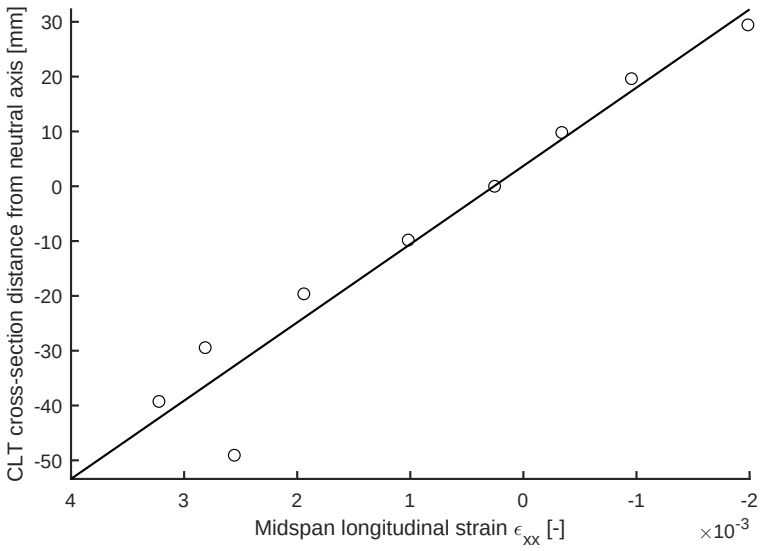

Figure 5.5. Longitudinal strain plotted against distance from the neutral axis at midspan for strain distribution shown in Figure 5.4.

5.2.2.4 Shear strains

From the DIC measurements shear strains were calculated via linear strain triangles that are fitted between the pixel clusters in each image (refer to Section A.2 for a more detailed description). The absolute shear strains with increasing load for a three and five ply beam are plotted in Figure 5.8a and Figure 5.8b, respectively. For both beams the shear strains can be observed to increase as the load and the midspan deflections increase. It can also be observed that the shear strains were concentrated in the plies that are orientated perpendicular to the main loading direction, as expected.

It should be noted that, while these shear strain surface plots are a useful qualitative tool, they can be difficult to interpret quantitatively because the data is spread over a large number of points, and it is difficult to summarise these area measurements into spot measurements; an attempt to quantify these values against the theoretical shear strain distribution in the CLT cross-sections is described below.

The shear strains in Figure 5.8 can be compared with the theoretical shear distributions that arise in CLT cross-sections where shear acts. Figure 5.6 a) and b) show the shear stresses at ultimate load for the three ply beam in Figure 5.8a and the five ply beam in Figure 5.8b respectively; the shear stresses are calculated in accordance with Equation 5.3, where V is the applied shear force, A^* is the area above or below the cross-section depth where shear strain is evaluated, $\bar{y}$ is the distance between the centroid of A^* and the effective cross-section centroid, b is the width of the beam and I_e is the effective cross-section second moment of area. From the shear stresses the shear strains can be calculated through Equation 5.4, where τ is the shear stress and G is the shear modulus, which varies between parallel and cross-wise orientated plies. For the parallel plies a shear modulus of 690 MPA [96] is assumed and the rolling shear modulus of the cross-wise boards is taken as 100 MPa [95]. The coefficient of variation is assumed as 0.13 for the lognormal distributions of both the elastic modulus, and the shear moduli, and they are assumed correlated by a factor of 0.6 [201]. The resulting shear strain distributions are shown alongside the DIC results in Figure 5.7 and agree well with the pattern of high shear strains in the cross layers that can be seen in Figure 5.8. The respective magnitudes of the theoretical shear strains also seem to provide reasonable agreement with those measured by the DIC. Both the three and five ply theoretical shear strains appear to underestimate the measured shear strains. The theoretical shear strains are of course subject to uncertainty, as the real shear modulus is not known for these specimens. In reality the properties will also vary between different boards, introducing local strain discontinuities at the bond lines.

$$\tau = V \cdot \frac{A^* \bar{y}}{bI_e} \tag{5.3}$$

$$\gamma = \frac{\tau}{G} \tag{5.4}$$

5.2.2.5 Failure modes

The majority of beams failed due to rupture of one or two boards on the tension side, and a typical failure mode is shown in Figure 5.9; this tensile rupture was often accompanied by rolling shear failures propagating from the tensile rupture into the shear spans. For some samples compression failure was observed after the experiment in the fibres on the compression side, and this explains the plastic load deflection behaviour that can be observed in Figure 5.2, as the ultimate load is approached. However the ultimate cause of failure (denoted by a steep drop in load) was still a tensile rupture of timber in the layers on the tension side. The plastic deformation of timber in the form of buckled wood fibres on the compressive side is shown in Figure 5.10. One sample failed in shear and the shear crack was observed to propagate along a glue line across the shear span of the beam.

5.2.3 Discussion of results

The mean ultimate loads of the CLT beams at ambient temperature for the four point bending experiments described were measured as 26.3 and 34.3 kN, with standard deviations of 6.3 and 5.2 kN, for five and three ply beams respectively. No significant difference was observed between the two adhesive types; therefore these loads can be used to determine applied loads for beams subjected to heating, i.e. the loads applied to the heated beam experiments are distinguished by ply number, but not by adhesive type.

The shear strains shown in Figure 5.8 were concentrated in the crosswise plies of the CLT beams. This is to be expected, as the rolling shear modulus, or G-modulus of the crosswise plies, is generally assumed to be significantly (between 7 to 14 times [95, 96]) lower than the G-modulus of timber in the parallel direction. It can also be observed that the shear strains in the beam consistent of three plies are up to three times higher than the strains in the five ply sample. The three ply beams have a crosswise layer at their centre and it is therefore unsurprising to see the shear strains there to be larger

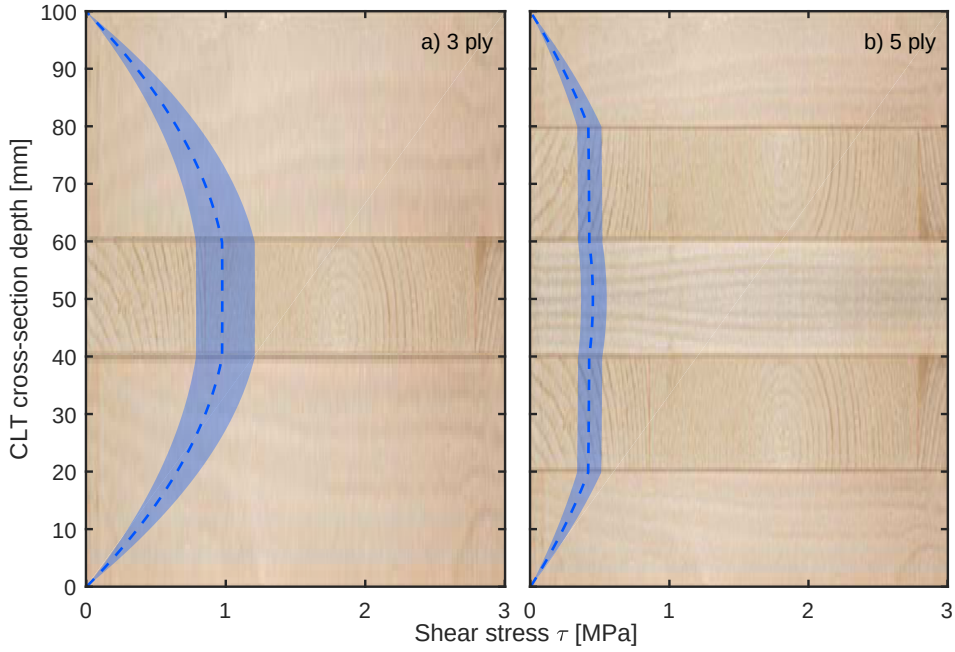

Figure 5.6. Shear stress distribution through CLT cross-section with a) three plies and 20.3 kN shear force and b) five plies and 10.5 kN shear force applied.

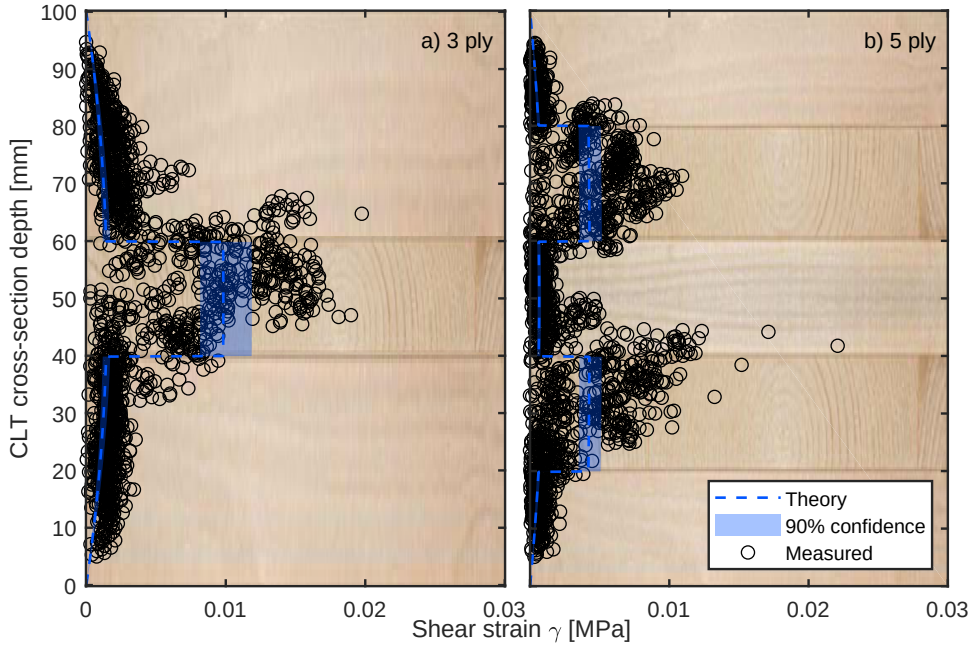

Figure 5.7. Shear strain distribution through CLT cross-section with a) three plies and 20.3 kN shear force and b) five plies and 10.5 kN shear force applied.

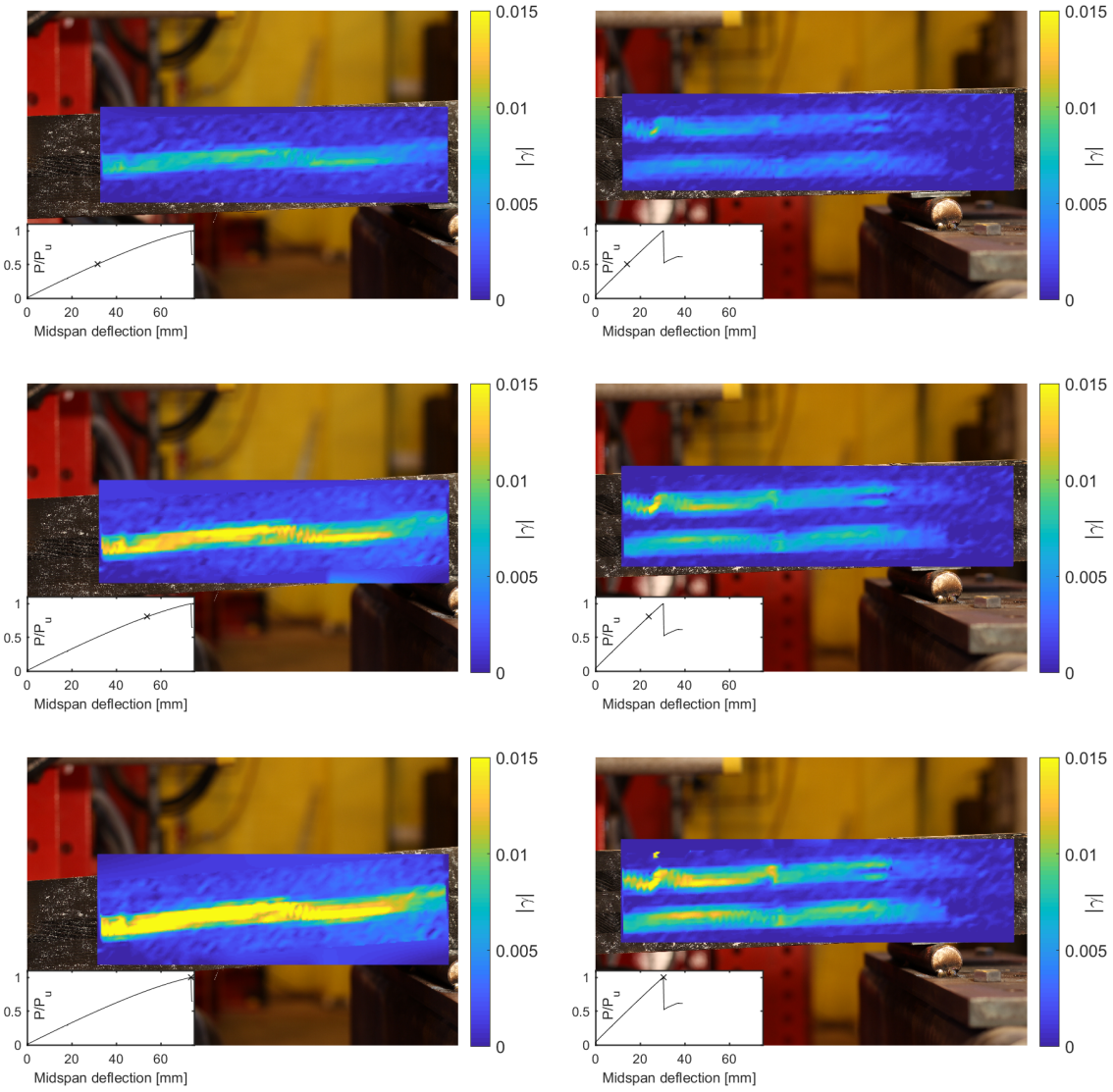

(a) Three ply (b) Five ply

Figure 5.8. Absolute shear strains γ at 50%, 80% and 100% of ultimate load near support for CLT with polyurethane and a) three plies and b) five plies.

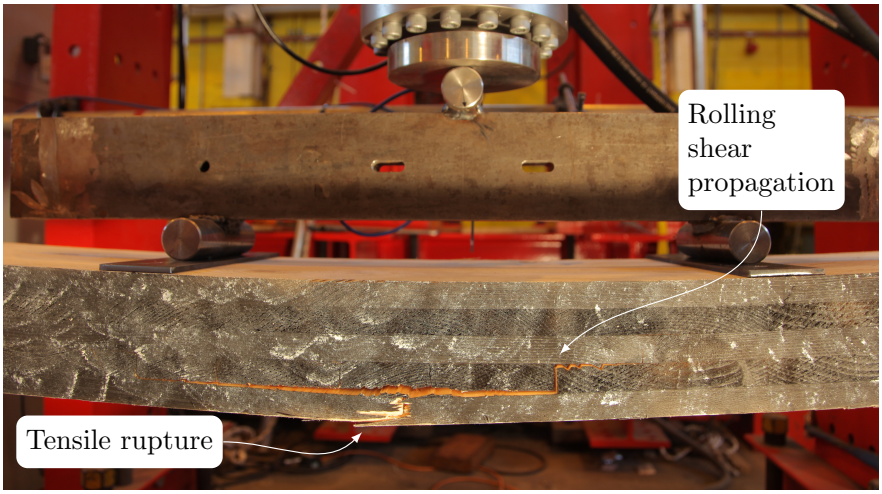

Figure 5.9. Typical failure mode in bending, here shown for a five ply polyurethane sample, with rupture of fibres in tension, followed by a propagation of shear failure along glue lines and rolling shear in cross layers.

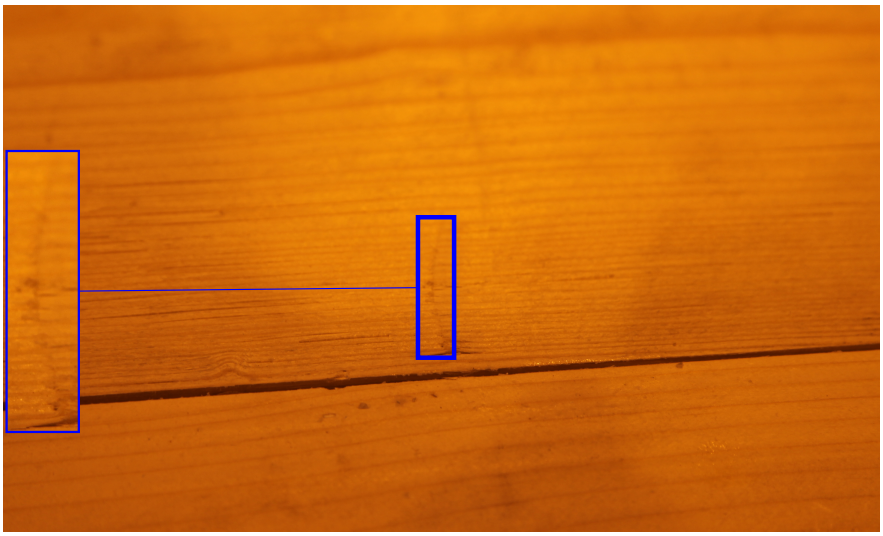

Figure 5.10. Compressive yielding indicated by buckled fibres on compressive (top surface) of a three ply melamine formaldehyde sample.

than for the five ply, as beam theory suggests that shear stresses are largest at the centre of a cross-section. This also explains why the three ply samples experience higher shear deflections and therefore a reduced effective elastic modulus (see Figure 5.3).

5.3 Heated beam experiments

This section describes the experimental configuration used for elevated temperature experiments on 17 CLT beams with the same dimensions and loading conditions as the ambient temperature reference experiments presented in the previous section. The experimental set-up for simultaneous heating and loading, and the installed instrumentation, is explained, followed by a description of the experimental outcomes, which encompass measured temperatures, deflections, shear strains, and experimental observations.

5.3.1 Experimental set-up

CLT beams with dimensions of 3000, 300 and 100 mm of length, width and thickness respectively were placed in a custom thermal chamber, loaded to a proportion of their expected ambient failure load and subsequently heated either to failure or for a predetermined time period with a subsequent cooling phase; this was done in order to instigate shear between the lamellae, and to observe the flexural consequences of slow uniform transient heating of the timber. Part of the beam was observed through a large glazed viewport, allowing digital image correlation analysis to be undertaken to monitor the deformation of adjacent plies, and to measure shear strains near the supports. An annotated photo of the experimental set-up is shown in Figure 5.11.

5.3.1.1 Heating chamber

The main piece of equipment used for the experiments described in this section was a bespoke heating chamber that was built around a large reaction beam to expose construction elements with lengths of up to 3000 mm to elevated gas phase temperatures. Drawings of this set-up are given in Figure 5.12. The heating chamber was previously constructed to both cure and assess the bond strength of carbon fibre polymers used as strengtheners for steel beams [219] and was refurbished for the experiments described herein. It was fitted with two heaters at each end which were placed in line with a

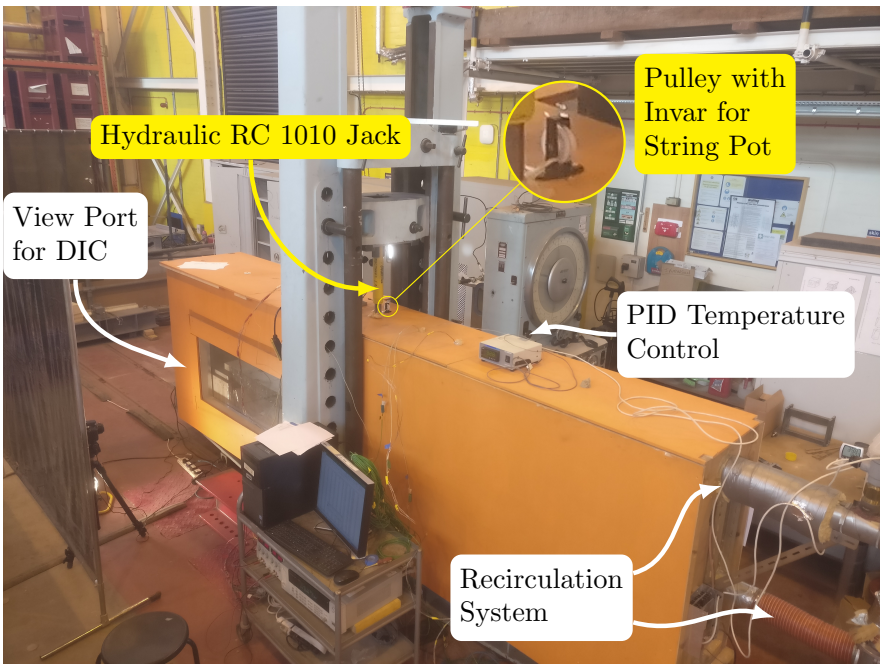

Figure 5.11. Annotated experimental set-up of heating chamber.

closed circulation system that was driven by an external fan. The heaters were controlled by a PID temperature control system connected to a resistance thermometer (RTD), which provided temperature readings at mid height above the specimens in the centre of the chamber, thereby controlling the gas phase temperature within the chamber. The chamber boundaries were constructed from plywood, followed by a layer of PIR insulation and one layer of gypsum board. At one end, two view ports were fitted consisting of two panels of glass each (i.e. providing a form of 'double glazing'). The chamber was built around a reaction beam, which was part of an Avery loading set-up that also encompasses a large reaction frame and a hydraulically driven floor plate. The pinned supports of the reaction beam were exposed within the chamber. The box was opened or closed via four ceiling panels constructed in the same way as its walls and floor. The panels contained small holes through which instrumentation and loading can be applied. Holes that were not used for instrumentation were closed using mineral wool insulation.

5.3.1.2 Loading

The beams were loaded at two load points, 250 mm from midspan, in four point bending using the same spreader beam as the ambient reference experiments shown in

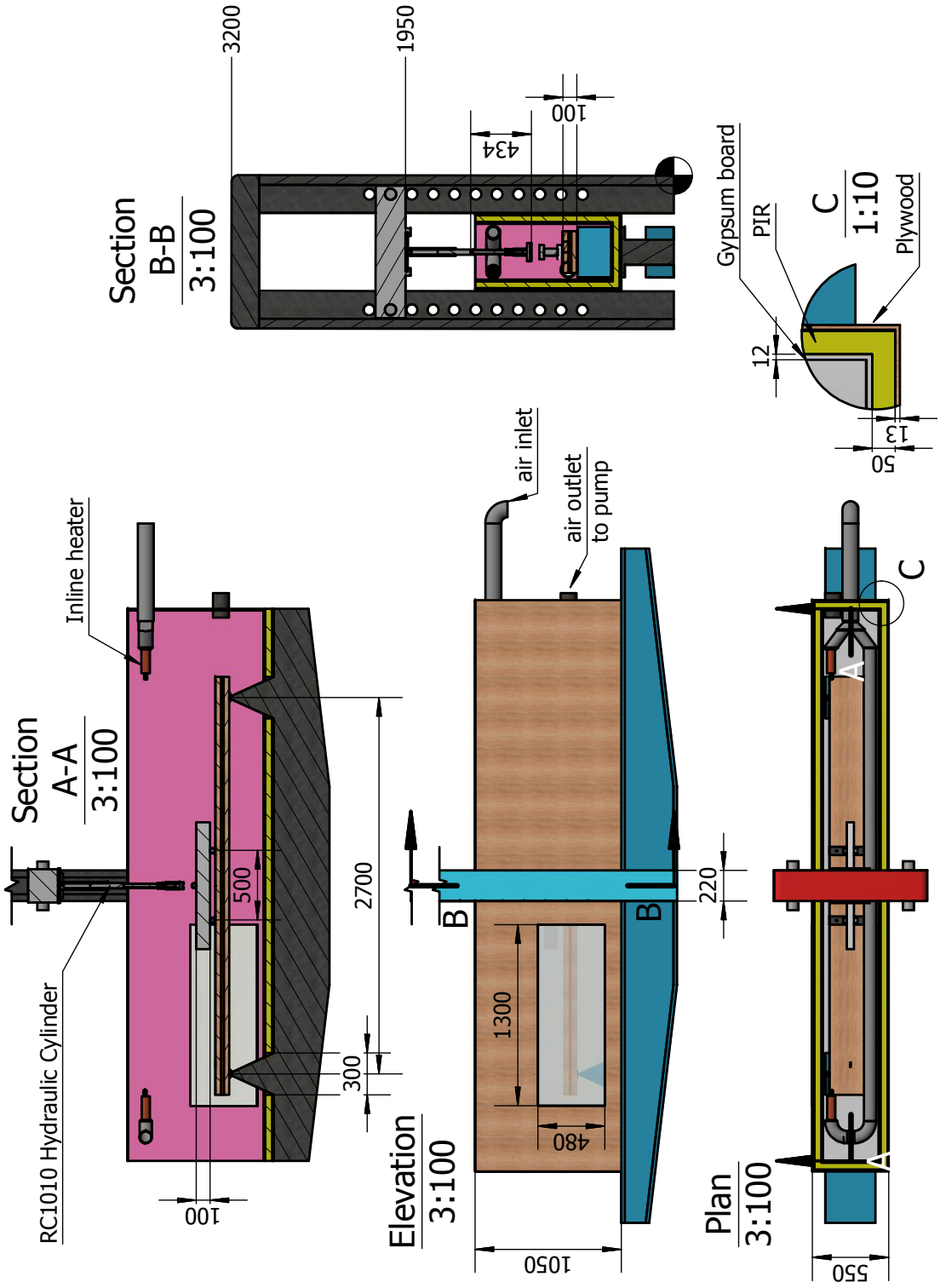

Figure 5.12. Elevation, plan, section, and detail views of the experimental set-up for CLT beam bending in the O-105 heating chamber [219].

Figure 5.1. The load was applied via a hydraulic jack that was fitted within a slot in the 1000 kN Avery load frame. The reach of the hydraulic jack was elongated using a bespoke extension rod that was threaded into the cylinder of the jack. This loading arrangement ensured that loads could be applied to the beams whilst the cylinder of the jack remained outside the heating chamber and not exposed to direct heating. The hydraulic jack was driven by an electric hydraulic power pack which was ramped up to a target pressure that was subsequently held constant during heating (and cooling); as a consequence, when the beam deflected, additional hydraulic fluid was pumped into the cylinder to maintain the pressure. Similarly, pressure was reduced when additional loads increased, either due to strength recovery of the timber in cooling or due to thermal expansion of the loading rod. In addition to the pressure regulation the pump was also fitted with a pressure relief valve, which was set to a maximum pressure, thereby guaranteeing that a set maximum pressure, and hence applied load, could not be exceeded. The application of the load followed a target loading rate of 3 kN/min, which was achieved through alignment of pressure increases with readings from the connected pressure transducer.

Two sets of experiments were run. One with a high loading ratio of 50 % of the mean ambient ultimate load capacity and one with a lower load ratio of 30 % of the mean ambient load bearing capacity. For the 50 % loaded samples the experiments were run until structural failure was observed or until the hydraulic jack exceeded its maximum travel distance due to excessive deflections. For the 30 % load ratio, the samples were heated for three hours and then subsequently cooled for three hours in order to gain insights into the recovery of deflections in the beams as they cooled.

5.3.1.3 Thermocouple placement

Both gas and solid phase temperatures were read throughout the experiment at multiple locations. For gas phase measurements fibreglass sheathed K-type thermocouples (TCs) were placed at multiple heights at the longitudinal centre of the box. In addition one of these gas phase thermocouples was placed around 100 mm above the beam at either of its ends to determine the longitudinal distribution of the gas phase temperatures in the box. For the solid phase measurements, inconel sheathed 1.5 mm K-type thermocouples were placed at the longitudinal centre at a depth of 50 mm and spaced at 75 mm along the width of the sample. At the end of the beam close to the view port thermocouples were placed at varying depths from the surface (17, 33 and 50 mm) 200 mm from the longitudinal the beam edge, spaced 15 mm longitudinally along the centre line. The

positioning of the drilled holes for the TC placements both at midspan and near the support are shown in Figure 5.13.

5.3.1.4 Displacement measurements

The displacements at midspan were measured using a string pot gauge that was extended into the heating chamber using Invar wire, an alloy with a very low thermal expansion coefficient of approximately $1.2 \cdot 10^{-6} K^{-1}$, thereby minimising the influence of thermal expansion of the wire on the deflection measurements; This low thermal expansion coefficient meant that the estimated maximum thermal expansion of the Invar in the chamber was 0.1 mm, and thermal expansion was therefore ignored in any of the following measurements and their analysis. The string pot itself was mounted on a piece of timber that was fastened on top of the lid of the heating chamber and a pulley over a small hole (refer to Figure 5.11) was used to ensure that the Invar was guided vertically onto the beam and that it could run freely. As a backup measurement an additional string pot gauge was attached to one end of the spreader beam.

Two cameras (one on either side of the heating chamber) were placed next to the view ports to take pictures during the loading and heating phase in order to utilise DIC to investigate strains near one support.

5.3.1.5 Heating regime

For both sets of experiments (i.e. high load and low load) the PID, which controlled the heaters on both sides of the chamber, was set to 150 °C with no ramp specified. No ramp was chosen because the large thermal mass of the beam was a limiting factor in heating up the chamber and the beam and the temperature ramp was therefore *as fast as possible*. Example gas temperature development is shown in Figure 5.14 for two experiments, a) one with a load ratio of 50 % and b) for a load ratio of 30 % with a cooling phase. Curves labelled C denote gas phase temperatures at the centre of the heating chamber at corresponding heights in cm from the base of the heating chamber. In addition the temperatures for the gas phase above the beam at the view port end and at the inlet end are shown. It can be seen that a difference in temperature exists with height for the centre temperatures, with the highest temperatures closest to the top of the box. These vertical temperature differences are small enough to be negligible and it can therefore be assumed that the thermal boundary conditions of the beams do not differ much as far as their top and bottom faces are concerned. The

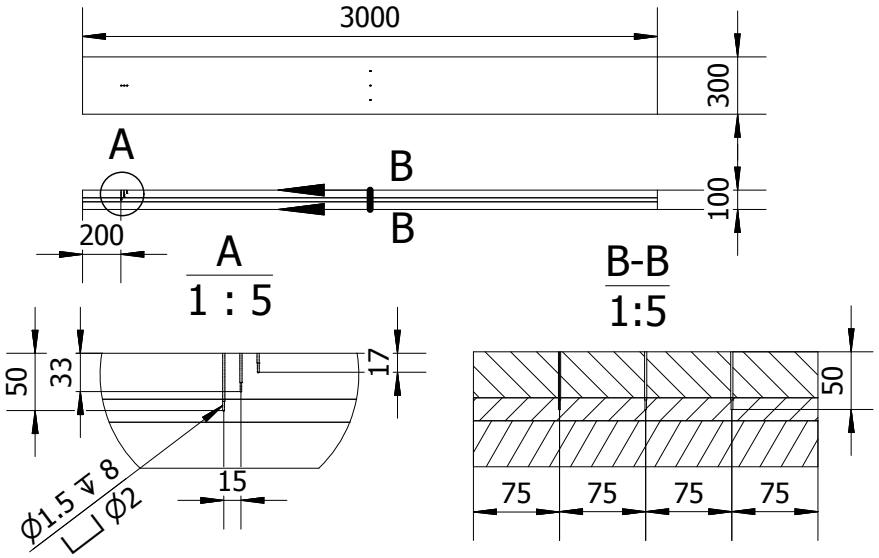

Figure 5.13. Drawing of solid phase thermocouple hole position, depth and bore diameters along heated beam experiments.

temperatures near the inlet of air closely followed the centre temperatures and it can therefore be assumed that the halves of the beams that were facing the inlet were subjected to similar thermal conditions than the midspan regions. It is obvious that this assumption does not hold for the sides of the beams that were facing the view port. The gas temperatures for this region were significantly lower than the other gas temperatures. There was no certain explanation for this; one option could be heat losses through the view ports, as they are less insulated than the rest of the box and heat losses occurred there, however, since the air is mixed, these heat losses should (in theory) be distributed through the chamber. The gas temperatures at this section also appeared more erratic, hinting at different mixing conditions of the gas phase. As the centre gas phase temperatures reached 150 °C it can be seen in Figure 5.14 that they became slightly more erratic, which is due to the PID control turning the heaters on and off, as required to hold the temperature at a quasi steady state.

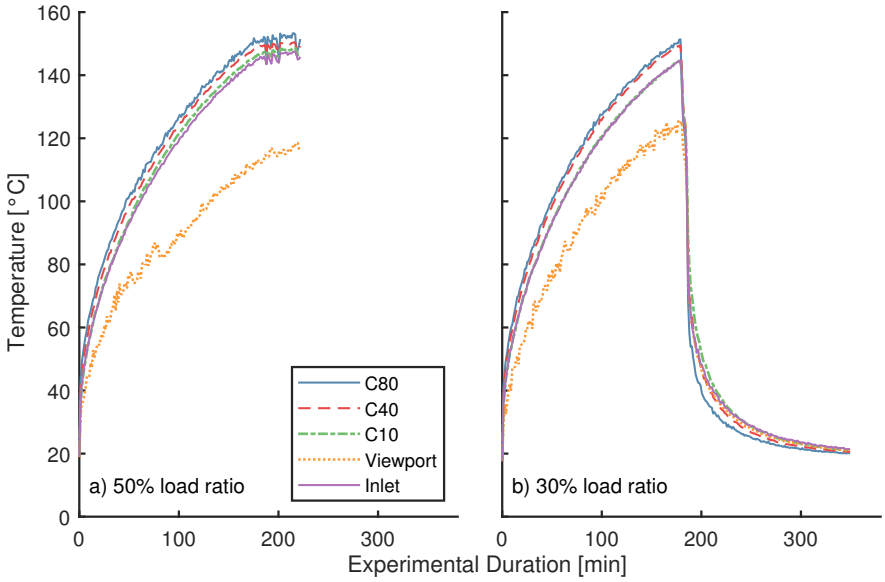

Figure 5.14. Gas temperature development at multiple positions in the heating chamber for a) an experiment loaded to failure and b) an experiment with low applied load and a fixed heating and cooling time.

5.3.2 Experimental results

5.3.2.1 Heating of timber

The mean of the measured timber temperatures for each thermocouple for the experiments loaded to 50 % until failure are displayed alongside one standard deviation in Figure 5.15. As would be expected, considering the gas temperatures in Figure 5.14, the timber near the support heated up more slowly than timber at midspan, the extent of which can be seen by comparing the temperatures at 50 mm between Figure 5.15 a) and b). The deviation in temperatures between experiments was larger for temperature measurements near the instrumented support, however, overall the deviations are not large. Small jumps in the temperature development can be seen for the measurements near the support. These arose when individual beams failed and the experiments ended, thereby causing a shift in the calculated mean temperatures.

For the experiments loaded to 30 % of the ambient temperature capacity the temperature increase in the timber above ambient temperatures are shown in Figure 5.16 for the heating and cooling phases of three hours each. Similarly to the high load experiments the increases in timber temperatures at the instrumented support was less than at midspan, due to either suspected heat losses through the view ports or uneven gas

mixing conditions. As would be expected the temperatures closer to the surface of the timber increased more rapidly in the heating phase and cooled down more rapidly in the cooling phase. It can also be observed that the variation in temperatures for the heating and cooling phase near the support was less across experiments, as compared to the highly loaded experiments, especially for the thermocouple at 50 mm depth. The reasons for this difference in variation are not clear. One potential explanation could be that for the high loads the deflections were larger and that this influenced and coincided with variable mixing conditions in the chamber, however, this is conjecture.

5.3.2.2 Applied loads

The pressures applied to the hydraulic jack by the hydraulic power pack were measured throughout each experiment by a pressure transducer, and this pressure was then translated in combination with the cross-sectional area of the hydraulic jack into the load applied to the beams. The applied loads are shown in Figure 5.17 as smoothed lines ± one standard deviation of the load magnitude throughout the experiments. It can be seen that the applied loads were consistent between the different ply numbers and targeted load levels. Cyclic variation in the loads arose from the weakening of the beams and therefore a drop in the applied pressure until a minimum set pressure was reached and the pump again increased the pressure to the set maximum. From the magnitude of the standard deviations it can be seen that the cyclic load variations were within reasonable bounds considering the applied load levels. For one 5PU specimen under a constant high load, a decrease in load can be observed for the first eighty minutes; this can be attributed to the pump not reaching its minimum set pressure and the automatic pressure regulation was therefore not activated for that time period. This error was rectified when it was noticed, which brought the applied loads to comparable levels for the remainder of that experiment. For the five ply samples at the lower load ratio an increase in the mean applied loads can be observed after around 120 minutes of heating. This is caused by a stabilisation of the applied pressure that, for the remainder of the experiment remained close to the set upper limit without any cyclic reduction in pressure, thereby causing a slightly increased average applied load. While this should not unduly influence the overall results, it is not exactly clear what is causing this phenomenon as it occurs about an hour before the heating is switched off and only occurs for five ply samples subjected to a low load ratio and none of the other sample configurations.

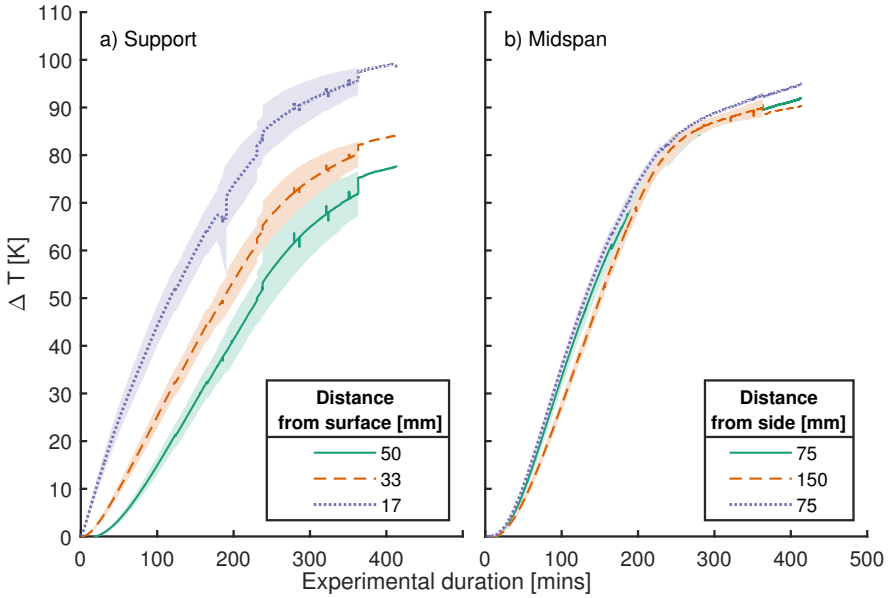

Figure 5.15. Mean and one standard deviation of solid phase temperature increase above ambient for samples loaded to 50 % of ambient capacity for a) temperatures above the support at different depths and b) temperatures at midspan at 50 mm depth through the width of the beam.

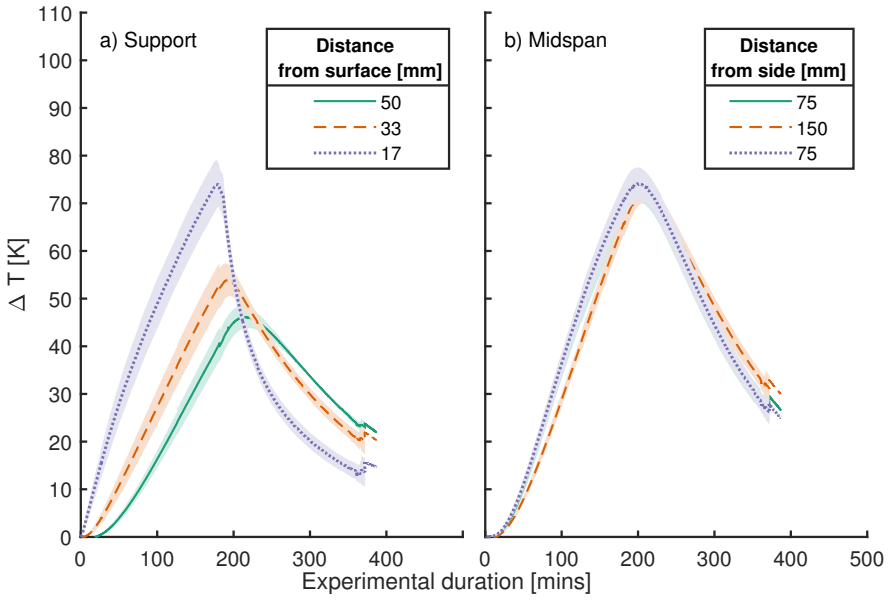

Figure 5.16. Mean and one standard deviation of solid phase temperature increase above ambient for samples loaded to 30 % of ambient capacity for a) temperatures above the support at different depths and b) temperatures at midspan at 50 mm depth through the width of the beam.

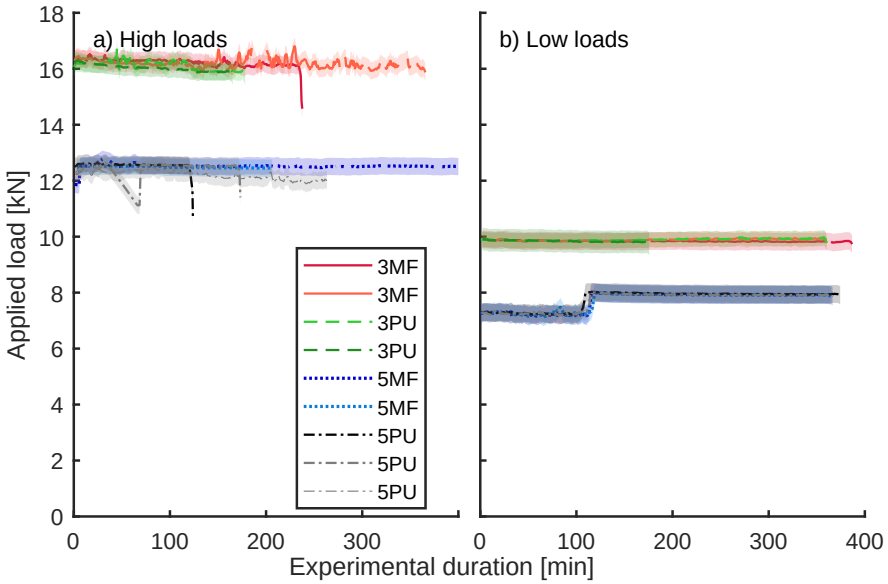

Figure 5.17. Mean applied loads with one standard deviation shown as shaded area for experiments with applied load level of a) 50 % and b) 30 % of mean ambient temperature capacity.

5.3.2.3 Deflection curves

The measured midspan deflections in the heating chamber for samples loaded to 50 % of the mean ambient capacity are shown in Figure 5.18 versus the time from the start of heating and versus the temperature at the centre of the beam at midspan in Figure 5.19. For all specimens it can be observed that heating caused the beams to deflect. For some of the specimen sudden increases in deflection can be observed, highlighting local timber failures. While these failures increased the deflections the load bearing capacity was maintained and deflection continued to increase at a seemingly steady pace until a total loss of the load bearing capacity led to runaway deflections. Note that two specimens (one 3MF and one 5MF) did not exhibit any failure in the observed experimental duration and had to be terminated as the experiments could only be run during official lab opening times and were therefore subject to a time limit. One of the 5PU specimens could be observed to deflect at the highest rate and failed earliest; this sample was observed to contain visible material defects (timber missing in a finger joint on the compressive surface) before the experiment and its behaviour was therefore unlikely to be representative of intact specimen of this configuration group. An additional repeat

was run for this configuration and did not exhibit this early onset of failure. The defect 5PU specimen will not be included in any analysis or commentary in the following sections.

The highest deflection rates and earliest failures can be observed for the two three ply CLT specimens that utilised polyurethane as adhesive. All other specimens initially followed similar deflection paths before they were distinguishable by the occurrence of localised material failures.

The midspan deflections plotted against time and against temperature for the beams loaded to lower load ratios and subjected to a three hour heating followed by a three hour cooling phase are shown in Figure 5.20 and Figure 5.21, respectively. The deflection paths for each of the repeat experiments for the four configurations closely follow each other; and the different configurations appear grouped by adhesive type and ply number. Apart from one of the 3PU specimen, which failed a few minutes before the cooling phase was instigated, none of the other specimens experienced structural failure and deflections remained constant as the temperature was reduced. For all specimens a sudden increase in midspan deflections was measured at the onset of the cooling phase. This was likely caused by the sudden inflow of ambient temperature air into the thermal chamber and resulting rapid cooling of the compression surface of the timber; the deflections caused by this are negligible in the context of the overall measured deflections

5.3.2.4 Shear strains

As for the ambient temperature reference experiments, the shear strains on the surfaces of the beams near the support were measured using DIC. The obtained absolute shear strains near the support of beams subjected to the lower constant load level of 30 % of the mean ambient structural capacity are shown in figures 5.22 and 5.23 for three and five ply CLT respectively. For each number of plies the shear strains are shown for CLT bonded both with a) polyurethane adhesive and b) melamine formaldehyde adhesive types. It can be seen that the shear strain distributions are not as clear as those for ambient temperature tests in Figure 5.8; this can be attributed to a multitude of effects: (1) the heated experiments were of longer duration, so changing light conditions have a larger effect, (2) the images were taken through the glazed view ports, which showed reflections and accumulations of dust, and (3) the timber did not only deform physically but also changed its colour and moisture content, which led to water drips and later drying cracks on the surface of the timber. All of these effects are challenging for the

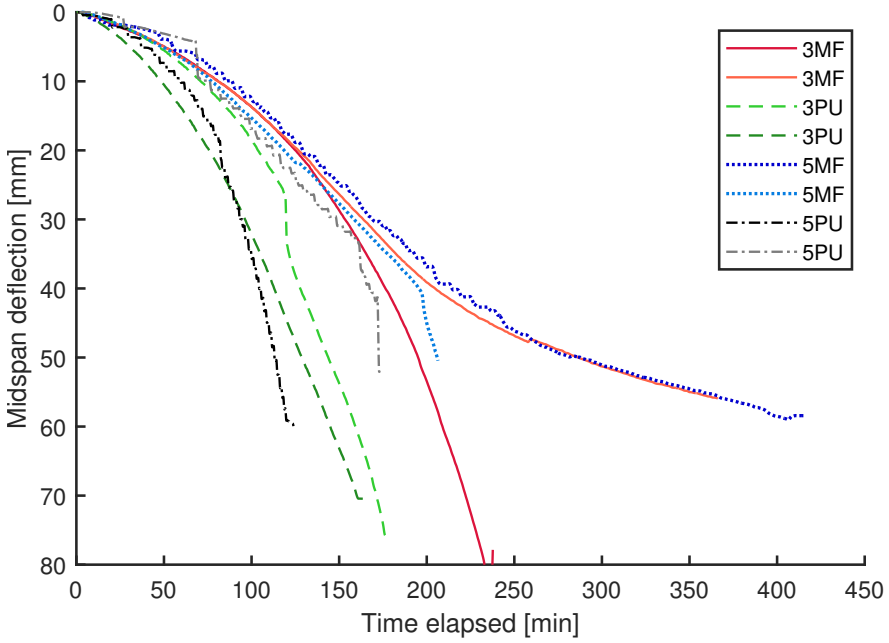

Figure 5.18. Midspan deflections against heating time for CLT beams loaded to 50 % of their ambient temperature capacity.

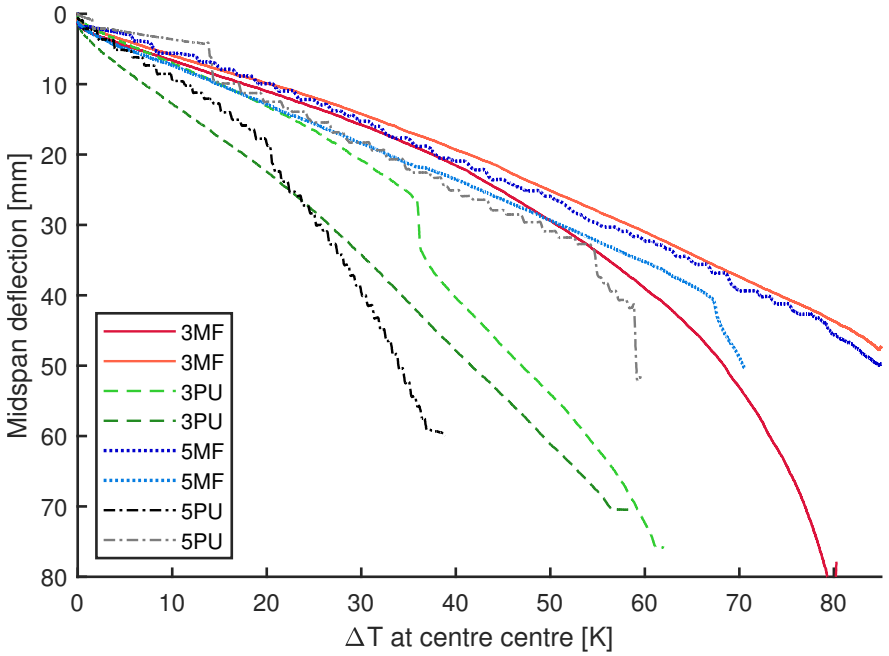

Figure 5.19. Midspan deflections against temperature increase at midspan for CLT beams loaded to 50 % of their ambient temperature capacity.

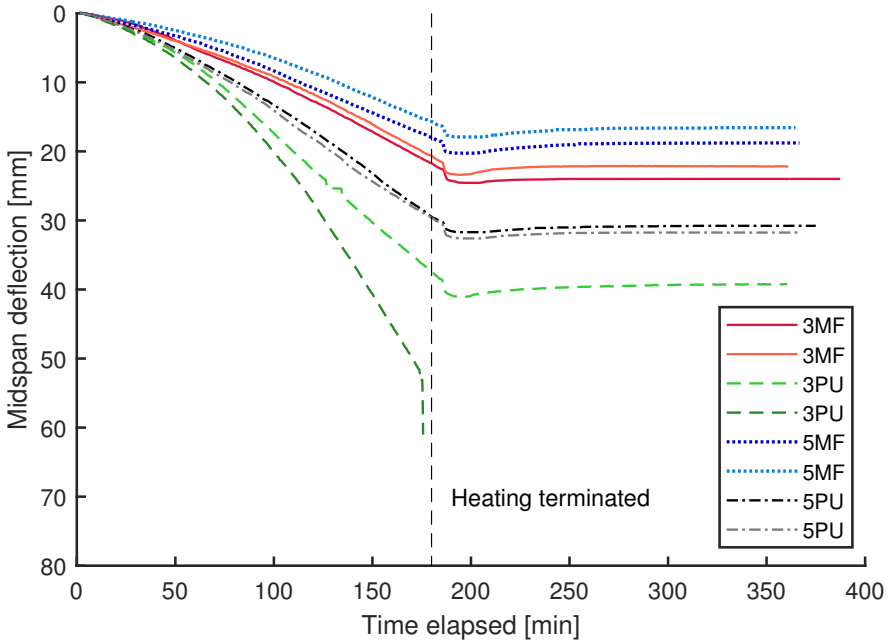

Figure 5.20. Midspan deflections against heating time for CLT beams loaded to 30 % of their ambient temperature capacity and subjected to heating and subsequent cooling.

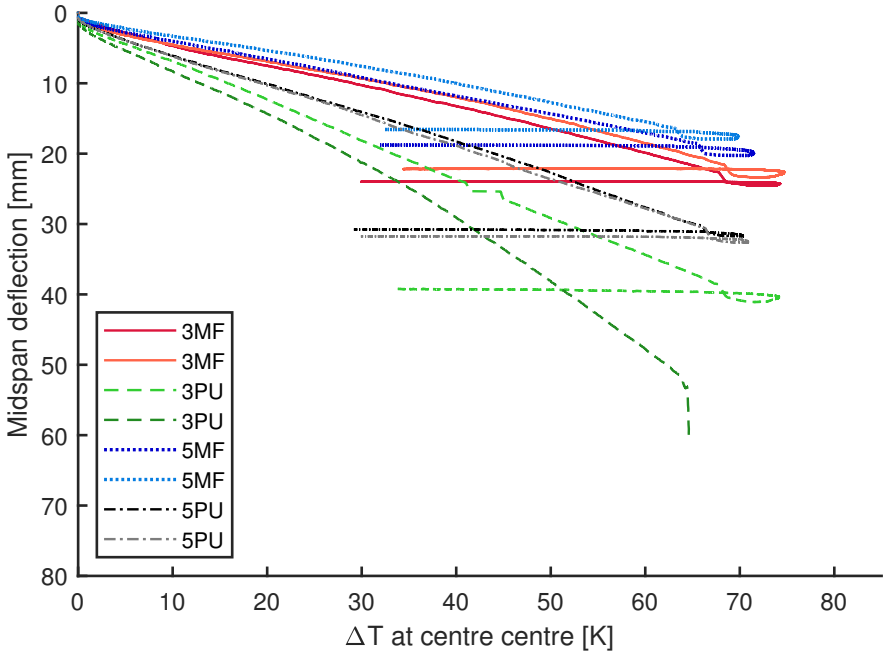

Figure 5.21. Midspan deflections against temperature increase at midspan centre for CLT beams loaded to 30 % of their ambient temperature capacity and subjected to heating and subsequent cooling.

DIC strain calculations as they show change in the taken photographs that are not actually strain related.

For all specimens a similar pattern to the ambient shear strains can be observed, with crosswise orientated layers clearly marked out by higher strains. It should be noted that the maximum shear strains on the colorbars have been increased to 0.025 for the heated beams compared to 0.015 for the ambient temperature cases in Figure 5.8. This was necessary to capture the distribution of the higher shear strains for the heated beams properly.

It can be observed that for both the three and the five ply CLT samples the specimens bonded with the PU adhesive type experienced larger shear strains. This is to be expected, since these samples also experience higher deflections with increasing heating (see Figure 5.20). On closer inspection it can also be observed that for the PU bonded specimens the shear strains were more concentrated in specific locations. While rolling shear strains still occurred in the crosswise layers these shear strain concentrations appeared more prominently around the adhesive line.

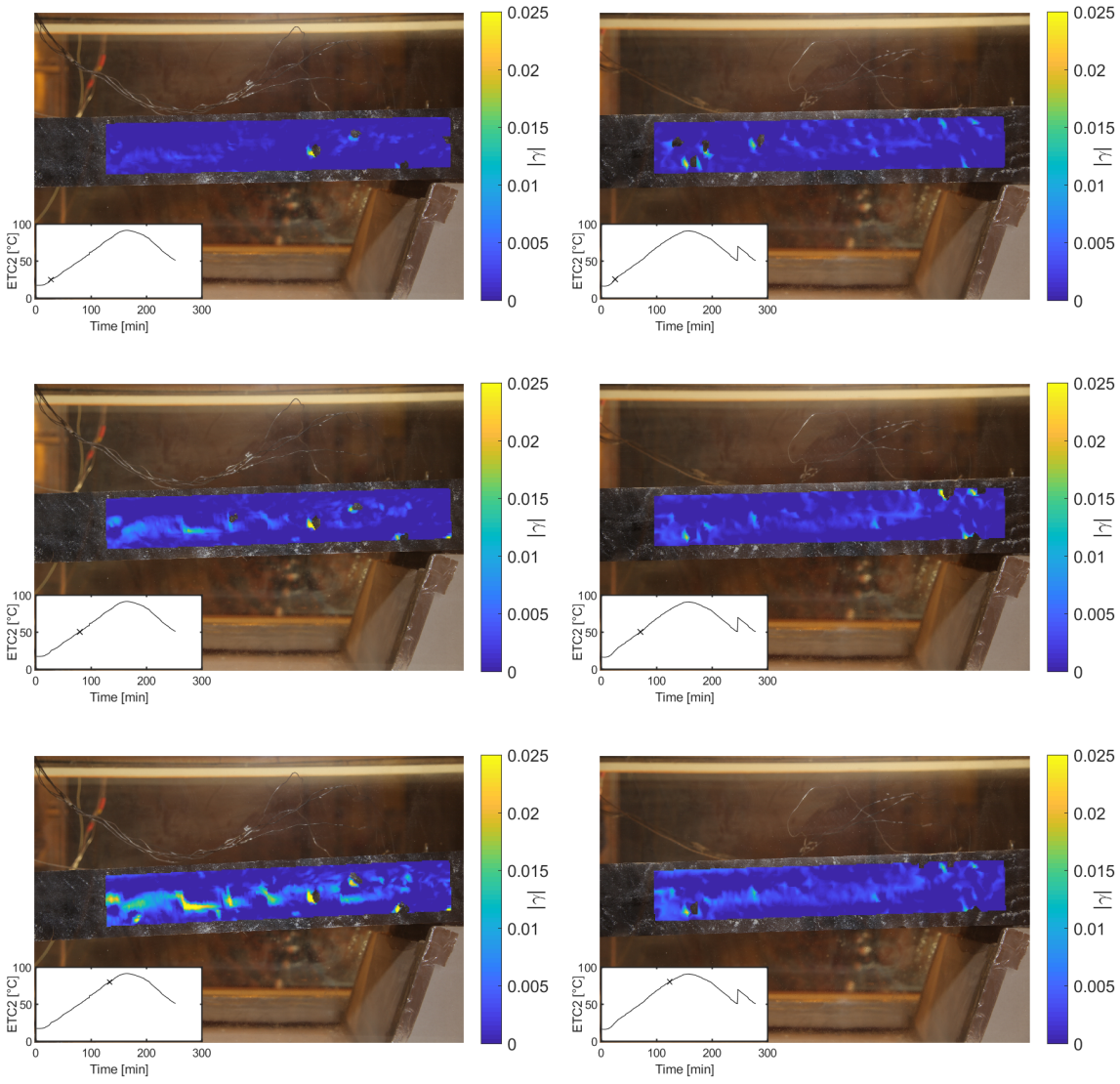

(a) PU (b) MF

Figure 5.22. Absolute shear strains γ near support at midspan centre temperatures of 25, 50, and 80 °C for three ply CLT with a) polyurethane (PU) and b) melamine formaldehyde (MF) adhesive type.

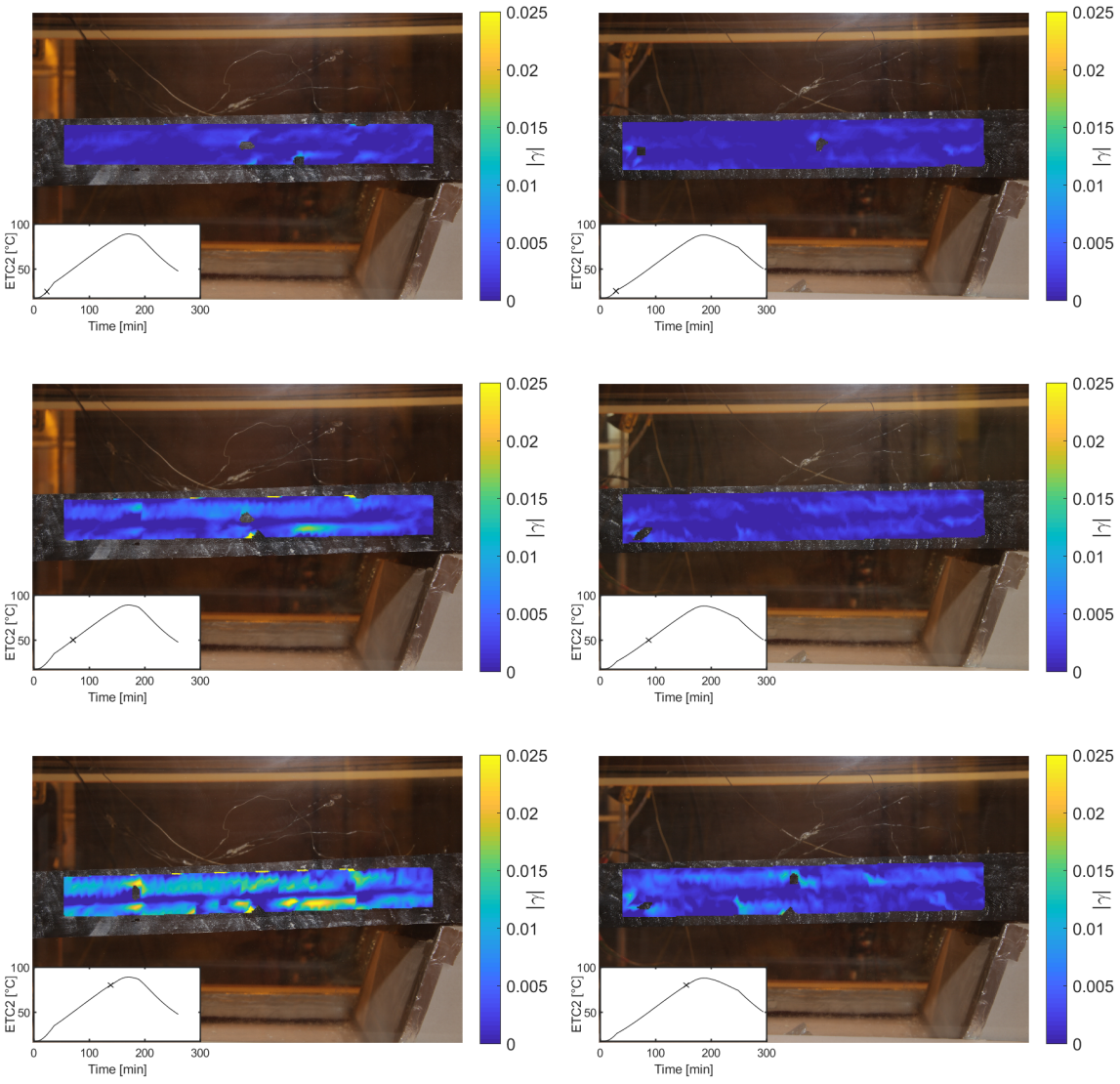

(a) PU (b) MF

Figure 5.23. Absolute shear strains γ near support at midspan centre temperatures of 25, 50, and 80 °C for five ply CLT with a) polyurethane (PU) and b) melamine formaldehyde (MF) adhesive type.

5.3.2.5 Failure modes

The heating chamber required high thermal insulation to sufficiently heat the CLT samples; therefore it did not allow for visual observation of ongoing experiments, other than through the view ports near one of the supports. Therefore the determination of local and/or ultimate timber failure could only be approximated from sounds from the chamber (which were also diminished due to the high insulation), from observations of the failed samples, or from the deflection measurements.

Inspection of samples after the experiments and their removal from the box showed bending failures due to tensile rupture for most of the specimens near their midspan. These tensile ruptures either occurred in knots or other defects, or in finger joints (as shown in Figure 5.24). These failures were, in some instances, accompanied by debonding failures propagating along the failure cracks and causing rolling shear failures of the crosswise layers. It cannot be determined with 100 % certainty which failure mode was the original failure mode; however, since these bending failures occur mostly at midspan, (where shear forces are expected to be zero), the bending failures were more likely to be the cause of failure for the beams and the shear failures were further consequences from the bending failures. Independently of the respective material failures, debonding was observed after the experiments at ply interfaces; an example of this is shown in Figure 5.25. This was observed to occur for both adhesive types and ply configurations.

For the samples loaded to 30 % of the mean ambient temperature ultimate capacity structural failure (denoted by a drop in load and run away deflections) occurred only for one specimen. All other beams deflected but continued to carry load throughout the cooling phase. The only visible 'damage' to these samples was a permanent curvature. The one sample that did fail structurally (BTX3PU_L_02), failed due to tensile rupture accompanied by rolling shear, similar to the samples loaded to 50 %.

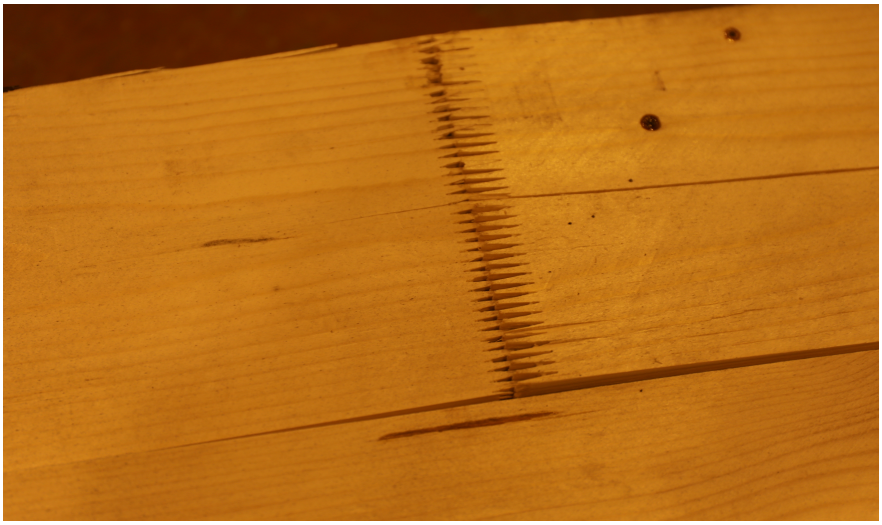

Figure 5.24. Combined timber and adhesive failure in a finger joint for a five ply polyurethane sample.

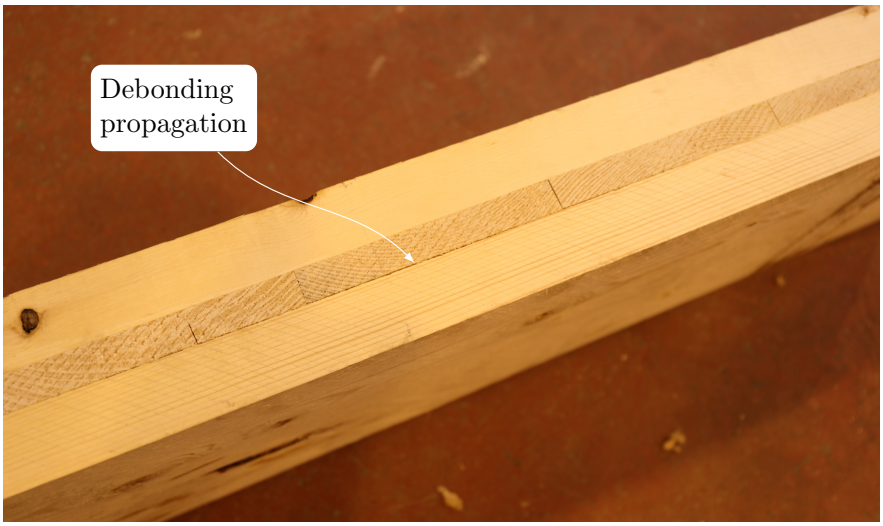

Figure 5.25. Debonding between lamellae observed after heating for a three ply polyurethane sample subjected to 50 % load.

5.4 Discussion of results

5.4.1 Influence of glue and lamination configuration set-up on bending stiffness and flexural capacity at elevated temperatures

From the results in figures 5.18 and 5.20 it is clear that a difference in deflection rates with increasing temperatures exists between the assessed configurations. Samples bonded with polyurethane adhesive type consistently perform worse when heated than their respective melamine formaldehyde counterparts. Since this effect was not evident for the ambient reference samples, it is very likely that the effect of heat on the adhesion between plies contributed to the deflections, potentially due to a reduction in composite action between plies.

For the samples with low load ratio the measured deflections are distinguishable by the configuration groups, but for the highly loaded experiments this distinction is harder to make (apart from the 3PU specimens). This can be explained by the fact that, at 50 % load, small defects in the timber were more likely to cause material failure as the timber was weakened by increasing temperatures, while for the 30 % loaded samples no material failure occurred and the response was therefore not influenced by local timber defects and this allows a better focus on the driving mechanisms. From a design point of view this might be interpreted to the extent that the different configurations are of less relevance to the load bearing capacity in heating as indicated by Figure 5.20 as material failures and accompanying collapse are more important in fire cases than accelerated deflection rates [83]. However, for some loading scenarios an increase in deflections will also ultimately cause earlier failures due to the creation of additional stresses from P-Delta effects. This is further investigated in Chapter 6 where CLT wall elements are exposed to heating from one side and the lateral deflections ultimately lead to earlier failure for samples with a higher deflection rate.

The deviation in deflection between the different sample groups are larger than the deviations amongst specimen of the same configuration. This means that the observed differences are systematic and that the observed deflections are dependent on the adhesive and lamellae configuration. A clear hierarchy of performance (with the assumption that less deflection indicates a better performance) upon heating can be identified in Figure 5.21 for the configuration groups. This is summarised in Figure 5.26, which shows the heat induced deflections in beams subjected to the lower load level after 180 minutes of heating. The 3PU specimen that failed structurally is not included in this comparison, as it failed before 180 minutes of experimental duration. The clear

difference in flexural behaviour between the adhesive types can be observed with a 40.6 % reduction in mean deflections for MF bonded specimens compared to those bonded with PU. For the layers the difference between mean deflections was 15.0 %; this suggests that these heat induced deflections were mainly driven by the adhesive type. The ANOVA p-values in Table 5.3 show that both the effect of the adhesive type and of the number of layers can be considered statistically significant. In summary it can be said that the configurations bonded with MF perform better than the ones with PU and specimen with five plies perform better than three ply ones, in this order.

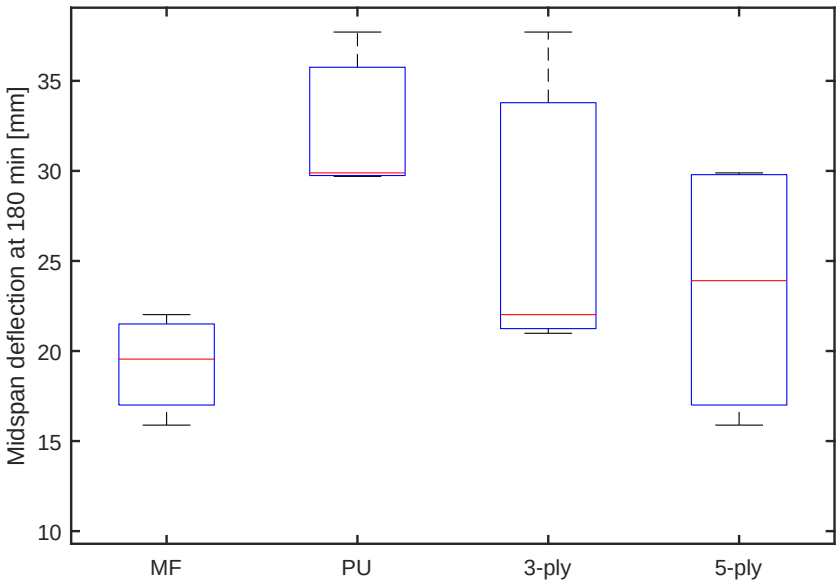

Figure 5.26. Boxplot comparison of midspan deflections after 180 minutes for beams subjected to 30 % of their expected ambient load bearing capacity.

Table 5.3. ANOVA p-values summary for influence of adhesives and ply numbers on fraction of deflection after 180 minutes of heating for beams subejcted to low load level.

	Adhesives	Layers
Pr(>F)	2.41E-04	5.48E-03

5.4.2 Occurrence of debonding

Debonding between adjacent lamellae (for which grain angles vary by 90 ° in this CLT) was observed in beams after the experiments were terminated for both adhesive types.

This separation of adhered timber surfaces along bond lines can be caused by either weakening of the adhesion due to heat, rupture of the bonds due to excessive shear stresses, or a combination of these factors. An alternative cause of debonding can be differential shrinkage parallel and perpendicular to the longitudinal timber fibres, which can occur at temperatures around 100 °C as moisture in timber cells evaporates and/or migrates to cooler regions.

From DIC images in figures 5.22 and 5.23 it could be observed qualitatively that shear strains predominately occurred in the cross-wise orientated plies for CLT specimens at elevated temperatures, similar to what was observed for ambient temperature reference experiments (see Figure 5.8). It was also observed that the shear strains for specimens bonded with polyurethane were visibly higher than for melamine formaldehyde ones at equal temperature increases. In addition, it was observed that for the polyurethane bonded CLT beams the highest shear strains concentrated close to the adhesive bond lines between adjacent plies. This suggests that debonding between plies occured at these spots of concentrated shear strains, indicating either a separation between the plies or interlayer slip due to excessive shear deformations. If this behaviour was simply caused by drying cracks or differential shrinking then these shear strain concentrations would be expected to have a similar magnitude between specimens bonded with PU and MF adhesive types. Since this was not observed for the experiments described herein, these shear strain images suggest (qualitatively) that timber bonded with polyurethane may have reduced adhesion between plies at elevated temperatures compared to those bonded with melamine formaldehyde. This observation also agrees with literature which has generally reported a higher reduction in shear resistance for PU adhesives compared to MF ones [70, 174], and it has also been reported that the proportion of wood failure in heated experiments is on average higher for MF compared to PU adhesive bonded timber samples [174, 179]. These adhesion losses will reduce composite action between the plies and thereby increase the overall deflections, which explains why the heat induced midspan deflections in Figure 5.20 are distinct between sample groups and higher for polyurethane samples.

One additional interesting observation is that the observed shear strain concentrations were non-continuous along the glue lines, indicating that bonding was not lost completely (which would mean that adjacent plies could theoretically simply slide past one another, barring timber friction) at elevated temperatures but that debonding and interlayer slip were limited to localised portions of the glue line. Timber to timber bond lines represent complex interactions between adhesives and wood cells, and a loss in shear modulus in the adhesive would not automatically indicate a complete loss of

bond shear resistance. Instead, debonding occurs in regions of elevated shear stresses and the resulting loss in composite action should be seen as a boundary condition that could be placed somewhere between either perfect bonding (which is generally expected at ambient temperature conditions), and a total loss of bonding. In addition, the provided DIC shear strain distributions can only inform about the surface conditions and for these experiments; they give no insight into the bond line throughout the width of the tested beams, where localised loss of adhesion could either have been more, or less pronounced than near the edges.

5.4.3 Occurrence of rolling shear

While Emberley et al. [93] observed rolling shear as a primary failure mode propagating from debonding cracks in slowly heated CLT beams in bending. This was not observed for the experiments described herein. One potential reason for this difference in failure modes is that, with a length of 1500 mm, Emberley et al.'s beams were significantly shorter than the 3000 mm long beams from this study, resulting in a lower length to depth ratio. In addition, the shorter beams in Emberley's study were heated with a radiant panel before loading was applied, so occurrence of creep from combined loading and heating would not have been captured by their experimental set-up; this meant that their experiment was driven by transient load increases instead of transient heating, which might also explain why rolling shear was not observed as a dominant failure mode for the results presented in this chapter, as deflections induced by slow transient heating are subject to a much slower rate of deformation, compared to load controlled experiments.

5.4.4 Mechanical properties of cooling CLT

For the samples subjected to a heating and a subsequent cooling phase, no recovery of deflections was observed upon cooling of the timber. This indicates that either, (1) the reduction in elastic modulus upon heating is irreversible, or (2) that the deflections are caused predominantly or partly by creep, rather than simply a change in elastic modulus. The achieved timber temperatures (see Figure 5.16) were significantly less than 200 °C, which is often considered as the temperature for the onset of timber pyrolysis (refer to Subsection 2.3.2). Therefore no significant chemical decomposition of the material would be expected, although material changes (e.g. formation of new bonds) may occur below these temperatures.

The deflections at midspan of beams loaded to 30 % are shown in Table 5.4 for different experimental stages. It can be observed that the ratio of the recovered load after loading was removed to the maximum achieved deflection during heating is relatively constant across all experiments, showing that a mean of 60 % of the total induced deflection remains present for all samples, i.e. on average 40 % of the total deflections are recovered when both heat and load are removed. It is interesting that this also applies to BTX3PU_L_02, which experienced structural failure before the cooling phase was induced, indicating that high flexural deflections (even to the point of tensile material rupture) can be recovered but nearly all of the heating induced deformation is maintained within the sample.

Table 5.4. Deflections at midspan for low loaded beams after loading, heating, and unloading after cooling.

	δ **Load**	δ **Heating**[a]	δ **Unloading**	δ **Unloading / δ Heat**
	[mm]	[mm]	[mm]	[-]
BTX3MF_L_01	13.55	37.58	22.76	0.61
BTX3MF_L_02	15.36	37.56	20.32	0.54
BTX3PU_L_01	17.11	56.56	37.28	0.66
BTX3PU_L_02	23.21	94.22	56.83	0.60
BTX5MF_L_01	13.35	32.03	19.34	0.60
BTX5MF_L_02	9.76	26.43	13.85	0.52
BTX5PU_L_01	15.14	45.89	29.41	0.64
BTX5PU_L_02	14.01	45.91	28.72	0.63

[a] includes deflection from loading

From previous work on adhesives (see Subsection 2.4.2) multiple researchers [70, 174] have found a difference in shear strength and creep resistance with increasing temperatures between polyurethane and melamine formaldehyde adhesive types. The practical implications from these findings were not always clear, since a weakening of an adhesive does not automatically translate into weakening of an adhesive bond in timber, or these findings had previously been dismissed as non relevant for the load bearing capacity of timber in standard fires in furnaces [185]; this was based on numerical calculations that showed that normal bending stresses dominated the cause of failure even for an extreme weakening of the adhesive in glue-laminated timber, because the shear stresses

in the bond lines were calculated to remain low. These considerations did not account for the importance of increasing deflections and resulting instability failure. From the results presented herein there is clear evidence that heat induced deflections in CLT are increased for samples that are bonded with polyurethane adhesive. With lower shear resistance at elevated temperatures, the bonding strength between plies is reduced, thereby increasing shear deflections and due to a loss in composite action the second moment of area is also reduced, which contributes to increased deflections.

5.5 Conclusions

This chapter described experiments performed on one way spanning CLT beams with different adhesives used to bond timber lamellae of varying thickness. From ambient temperature reference experiments, no difference in the modulus of rupture was found between either of the two different lamellae thicknesses or the two different adhesive types. For the elastic modulus, reduced values were found for three ply CLT elements compared to their five ply counterparts. This was attributed to the increased effect of shear deflections for the three ply samples which have thicker outer lamellae and therefore a lower effective length to depth ratio.

Experiments with transient uniform heating of the gas phase surrounding the specimens to a maximum of only 150 °C were performed on samples that were subjected to constant four point bending loading of either 50 or 30 % of their respective mean ambient temperature capacity. The measured midspan deflections increased for all samples with increasing heating. For the higher loaded samples accelerating deflections eventually culminated in material failure due to tensile rupture caused by bending. Some samples did not experience failure and the increase in deflections reduced with progressing heating time until these experiments were terminated without observation of loss of structural load bearing capacity.

For samples subjected to the lower load ratio of 30 % there was a clear difference in deflection behaviour both between different adhesive types and the number of plies. Samples bonded with a polyurethane adhesive type displayed heating induced deflections that were on average (mean) 40 % higher than for those bonded with a melamine formaldehyde adhesive and samples with three plies deflected 15 % more than their five ply counterparts. For these samples with lower applied load ratio the heating was halted after three hours and three hours of cooling was induced. Only one of these CLT

beams (a three ply polyurethane adhesive bonded specimen) experienced material failure and a loss of load bearing capacity during the heating phase. For all the other samples no recovery of the deflections was observed upon cooling and only an average of forty percent of the overall deflections were recovered after all structural loading was removed. It was interpreted that the majority of heat induced deflections in these beams were caused by creep and were non-recoverable. It was not clear whether the observed creep deflections were caused by the timber or by the adhesive, or a combination of both. Further studies with experiments on small scale samples are recommended to illuminate the driving factors and conditions for these creep deformations.

A qualitative investigation of strain distributions over the specimens' sides showed that for CLT bonded by polyurethane adhesive types the shear strains were partially concentrated near the adhesive lines between plies; this was not observed for specimens bonded with the melamine formaldehyde adhesive. Since there were no other variations between these sample groups, this was interpreted as a weakening of the polyurethane adhesion causing interlayer slip and debonding between adjacent timber plies and thereby explaining the accelerated midspan deflections for specimens bonded with this adhesive compared to their MF bonded counterparts.

The results from this chapter clearly indicate that significant heat induced deflections and structural failure may occur for CLT in low heating (relative to conditions that may arise in compartment fires) conditions. It is also clear that significant influence of the adhesives exists on the flexural response of heated CLT beams and it can therefore be concluded that the behaviour of CLT (and likely other types of engineered timber products) has to be considered separately from sawn solid lumber when fire safety is considered. These results may also in part explain why the often utilised zero strength layer of 7 mm [122, 145, 191], to account for the effect of heated timber below the char layer, does not agree well with measurements and observations on CLT [141, 186, 190]. It is clear that either more research to understand the effects of adhesives on the fire safety of CLT is necessary or more precautions in the form of more conservative design must be taken, which will increase the overall project costs for structural timber buildings. Of course the heating conditions for the beams in this chapter are unlikely to occur in practice and steeper temperature gradients are generally expected in real fires, however the results are still relevant for heated timber below the char layer, which will be exposed to shallow temperature gradients in a decaying fire [173]. The effect of the findings in this chapter on the load bearing capacity of CLT walls at heat exposure more akin to compartment fire exposure are further explored and described in the next chapter.

This page is intentionally left blank.

CHAPTER 6

Axially loaded CLT wall experiments

This page is intentionally left blank.

This chapter describes results and their analysis from experiments on CLT wall strips under sustained load to a proportion of their ambient capacity and exposed to a radiative heat flux over a distance of 300 mm at their mid height.

6.1 Motivation

Instability is a major consideration for the structural performance of timber compression elements in fire, especially as charring and heating of timber in a fire will increase the slenderness and applied load eccentricity of exposed elements. The publicly available test data for CLT walls is limited (see Subsection 2.5.3) and no comparative test results of the influence of adhesives for CLT compression elements in fire have been discussed in the academic literature. The experimental series presented in this chapter assesses the stability of simply supported, slender cross-laminated timber wall strip elements subjected to one sided radiation exposure at their mid height in a novel experimental configuration. The results shed further light on the structural load bearing capacity of CLT walls in fire and highlight the importance of a number of variables: the heat exposure intensity and duration, the adhesive type used for bonding of the CLT plies, and the number and thickness of the plies.

6.2 Samples used

All samples described in this section had a thickness of 100 mm, a width of 300 mm and a length (height) of 1700 mm. Four configurations, varying with adhesive type and lamination build up, were investigated for their response to radiative heating when loaded.

The experimental matrix is shown in Table 6.1. Four different heating regimes, of eight experiments each with two repeats for each configuration, were applied to the samples: (1) ambient reference tests to failure with no heat applied, (2) exposure to a "high" radiative heat flux (i.e. above the critical heat flux to sustain burning) until failure, (3) exposure to a "high" radiative heat flux for a fixed amount of time and a subsequent cooling phase with no heat applied, and (4) exposure to a "nominally low" heat flux (i.e. below the critical heat flux for autoignition) until failure to observe the reduction in load bearing capacity from pyrolysis of timber that is not flaming. The load for the heated samples was kept constant for all the experiments. It should be noted that the load ratios shown were not equivalent between the ambient and heated experiments,

since the ambient load ratios refer to the ultimate capacity, i.e. samples were tested until failure, and the load ratios for heated experiments thus refer to the ratio of applied load during testing to the manufacturer recommended load capacity (which is based on design code calculations [88]). This is elaborated further in the experimental set-up section on heated samples (Subsection 6.4.1).

Table 6.1. Experimental matrix for wall elements subjected to compression.

Group Name	**Adhesive** -	**Layers** -	**Heat flux (approx.)** [kW/m^2]	**Heating duration** [min]	**Load ratio** [%]	**Number of specimens** -
C3MF020	MF	3	0	-	0-100[a]	2
C3PU020	PU	3	0	-	0-100[a]	2
C5MF020	MF	5	0	-	0-100[a]	2
C5PU020	PU	5	0	-	0-100[a]	2
C3MF050	MF	3	50	to failure	50[b]	2
C3PU050	PU	3	50	to failure	50[b]	2
C5MF050	MF	5	50	to failure	50[b]	2
C5PU050	PU	5	50	to failure	50[b]	2
C3MF050P	MF	3	50	15	50[b]	2
C3PU050P	PU	3	50	15	50[b]	2
C5MF050P	MF	5	50	25	50[b]	2
C5PU050P	PU	5	50	25	50[b]	2
C3MF015	MF	3	15	to failure	50[b]	2
C3PU015	PU	3	15	to failure	50[b]	2
C5MF015	MF	5	15	to failure	50[b]	2
C5PU015	PU	5	15	to failure	50[b]	2

[a] tested monotonically to failure in load control.

[b] based on manufacturer recommended design load load capacity. Equivalent to 25 % allowable stress design (ADS).

6.3 Ambient Reference Experiments

To understand the behaviour of CLT walls in fire situations, it is essential to first characterise and observe the load deflection behaviour and failure modes of reference samples at ambient temperatures.

6.3.1 Experimental Set-up

Two wall strip samples were loaded to failure at ambient temperature for each of the four assessed configurations of CLT. Special mounting brackets were manufactured to load the columns through notionally pinned connections at top and bottom. Drawings of the experimental set-up are given in Figure 6.1. Load was applied through a hydraulic jack which was powered by an electrical hydraulic power pack. Three linear potentiometers were used to measure the lateral deflections of the specimens. In addition a speckle pattern was applied to the sides of the wall strips to track their movements with digital image correlation (DIC); GeoPIV_RG [209, 220] was used for DIC calculations for the ambient temperature wall experiments.

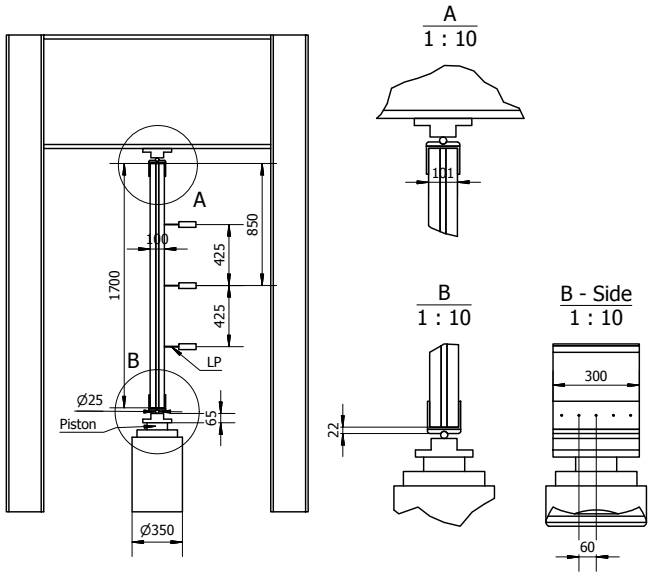

Figure 6.1. Drawings of experimental set-up for ambient experiments on cross-laminated timber wall strips.

The loading rate for the ambient reference experiments was set at 20 kN/min and was controlled manually. The actually achieved loading rates (measured from a linear fit between test start and maximum load) are shown in Table 6.2, where it can be seen that a consistent loading rate with maximum deviation of 3 % from the target loading rate was achieved.

6.3.2 Ambient results

6.3.2.1 Load – deflection curves

The lateral displacements at mid height of the wall strips from digital image correlation measurements are plotted in Figure 6.2 a) and b) for three and five ply CLT respectively. For all specimens a buckling failure mode with increasing lateral runaway deflections, culminating in a critical buckling load, was observed. The ultimate loads achieved are shown in Table 6.2 and varied quite widely, as did the specific manner of failure. The highest failure load of 956 kN was achieved for a three ply MF adhesive sample, and for this sample the lateral deflections only increased minimally until sudden failure occurred (note that for this sample the lateral deflection measurements stopped abruptly, which can be attributed to the rapid deflections at failure which were not captured by the five second data capture interval that was set for the DIC). With almost zero lateral deflection and then a sudden bifurication of the load deflection path and failure, this specimen failed similarly to a 'pure' Euler failure mode. Conversely the element with the lowest failure mode was a three ply specimen bonded with PU adhesive, for which lateral deflections were observed to occur and follow a non-linear path from the outset of the applied load increase until a failure load was reached. This stark difference in the load deflection behaviour is most likely caused by different initial eccentricities. One issue with this experimental set-up was that the steel brackets that were used to apply load to the CLT were manufactured to fit one size, with 2 mm of tolerance allowed for the sample thickness. It was observed that the thickness for some of the specimens in this test series varied by up to a millimetre, and therefore small eccentricities of up to 2 mm were introduced when the holding brackets were fitted onto the columns. These eccentricities, in addition to built in eccentricities due to global geometric imperfections, can partially explain the differences in the load deflection behaviour.

6.3.2.2 Failure modes

From a structural mechanics point of view, all specimens failed in global buckling, i.e. a loss of stability. This was accompanied by excessive lateral deflections which increased bending stresses in the timber and ultimately led to material failure. Upon inspection of the failed samples and review of experimental videos, multiple material failures were observed. Some specimens showed up to three different kinds of material failures. This is shown in Figure 6.3 with compressive buckling of timber fibres, rolling shear, and

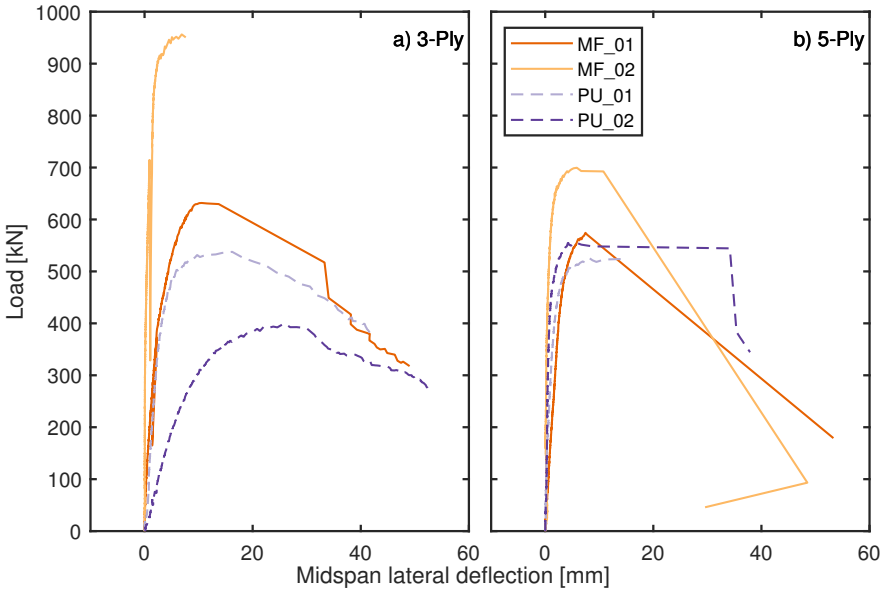

Figure 6.2. Midspan lateral deflections of CLT wall strips at ambient temperatures versus increasing applied compressive loads.

bending rupture on the tension side all being visible.

The released failure energy (from observations of the failure modes) increased with the buckling load, especially for samples where lateral deflections remained small until buckling occurred, since for these samples a larger amount of elastic energy was stored in the columns, and subsequently released upon the bifurcation of the load deflection path. For one specimen (5PU020_01), this caused the column to snap in half at midspan, where finger joints lined up on both compression and tension side. This is shown in Figure 6.4, it can be seen that, for the finger joints on the tension side, the wooden 'fingers' remain intact, indicating a failure of the joint's bond. On the compression side timber failure can be observed in the joint.

6.3.3 Discussion of ambient results

The buckling failure loads were found to vary greatly in a range between 400 and 956 kN, and higher failure loads were measured for samples bonded with melamine formaldehyde (compared to their respective PU counterparts). This effect seemed to be especially pronounced for three ply samples. This finding is unexpected since timber bonding adhesives are generally assumed to have similar properties at ambient temperatures. In Table 6.3 the ANOVA p-values for the failure compressive stresses

Table 6.2. Ambient wall results.

Name	**Load rate** [kN/min]	**Density** [kg/m^3]	**Ult. failure load** [kN]	**Compression stress** [MPa]
C3MF020_01	20.0	-	631.8	26.1
C3MF020_02	19.8	469.8	956.3	39.5
C3PU020_01	19.7	470.2	537.7	22.2
C3PU020_02	19.4	454.0	400.0	16.5
C5MF020_01	19.8	466.6	574.3	31.2
C5MF020_02	19.9	476.2	699.6	38.0
C5PU020_01	19.8	499.1	525.6	28.6
C5PU020_02	19.7	470.8	555.6	30.2

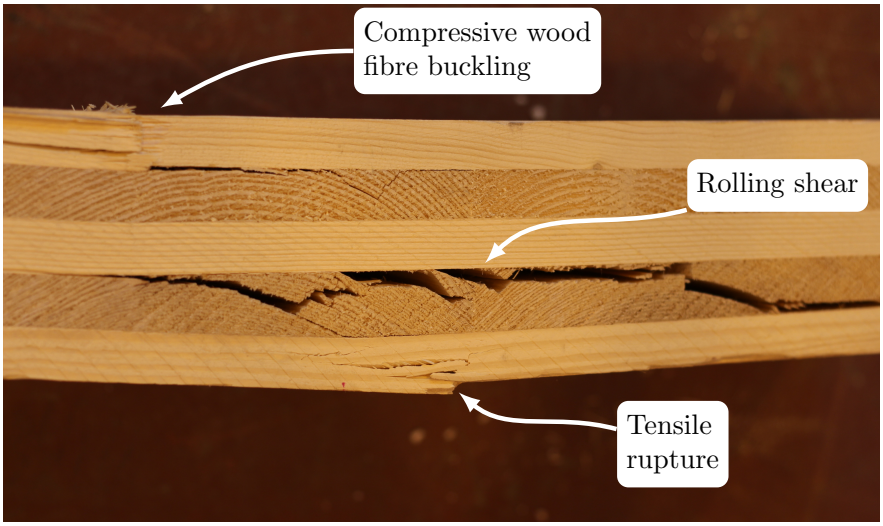

Figure 6.3. Multiple different material failure modes in buckled CLT wall strip.

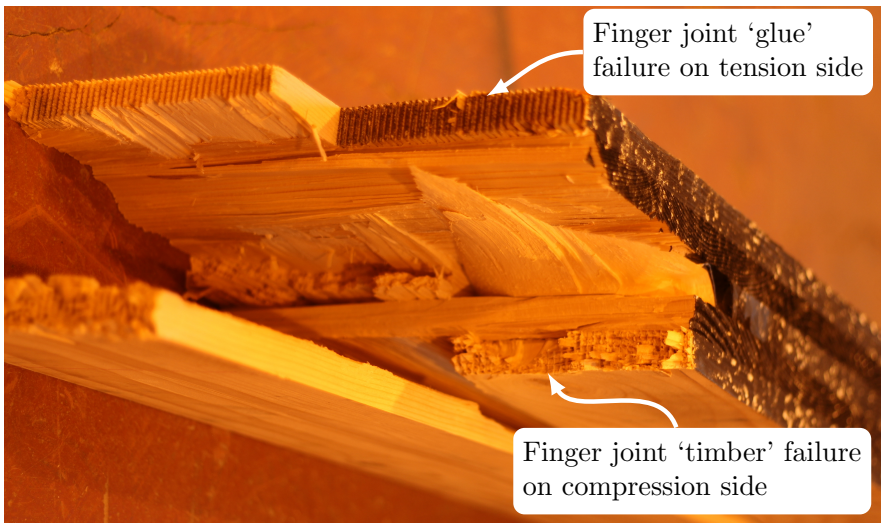

Figure 6.4. Multiple different material failure modes in buckled CLT wall strip.

in Table 6.2 show that the variation between both the adhesives and ply number are above what is commonly considered as statistically significant (p<0.05), indicating that any differences in ultimate load between the specimens is likely caused by chance, rather than differences in the underlying populations of CLT with different adhesive types and layer configurations. A more likely explanation for the varying failure loads, other than differences in layers and adhesives, that can be drawn from the development of the lateral deflections at midspan is that inherent eccentricities in the timber and the loading brackets caused P-Delta effects, leading to excessive deflections and larger stresses at increasing loads, thereby causing progressive global buckling failure.

Table 6.3. ANOVA p-values summary for influence of adhesives and ply numbers on compressive failure stress.

	Adhesives	Layers
Pr(>F)	6.98E-02	2.04E-01

Because of the large variability in ultimate loads, these ambient reference experiments had limited usefulness, both for the design as well as the analysis of wall elements subjected to fire. For future experiments a significant improvement of the experimental set-up could be made through the introduction of significant initial eccentricities into the loading set-up. Such imposed eccentricities would then render effects from much smaller inherent and unintended eccentricities less important, thereby potentially creating more uniform and less variable experimental conditions between samples.

Note that this effect also means that the eccentricities that were observed for the ambient experiments are unlikely to have a large effect on the experiments exposed to one sided constant heat flux, as heating and charring of timber will create eccentricities that are significantly larger than inherent eccentricities in the timber or the connections.

6.4 Wall strips exposed to heat

6.4.1 Experimental set-up

6.4.1.1 Loading set-up

A bespoke steel frame was fabricated to place and load the wall strips to a sustained fraction of their ambient temperature capacity before exposing them to different heating scenarios. The frame was welded together from standard steel sections (SHS 120x120x8 for cross beams and SHS 80x80x4 for columns) and fitted with stands at its base to maintain stability. The frame was the same as was used for the experiments described by Wiesner et al. [190] in 2017 and was designed to withstand an ultimate load of 100 kN, with an additional safety factor of 2 applied. The steel of the frame facing the radiant panels was protected by encapsulation with 25 mm layer of mineral wool. The top and bottom ends of the wall strips were fitted with steel brackets, which were fabricated from two L channel sections that were welded together and fitted with a roller to act as pinned connections. The wall strips, fitted with their steel mounting brackets, were placed on the hydraulic jack, which was equipped with a female pinned connection section, and the hydraulic jack was extended to secure the specimen in place in the steel frame. Drawings of the experimental set-up are shown in Figure 6.5 and an annotated image of the set-up is shown in Figure 6.6.

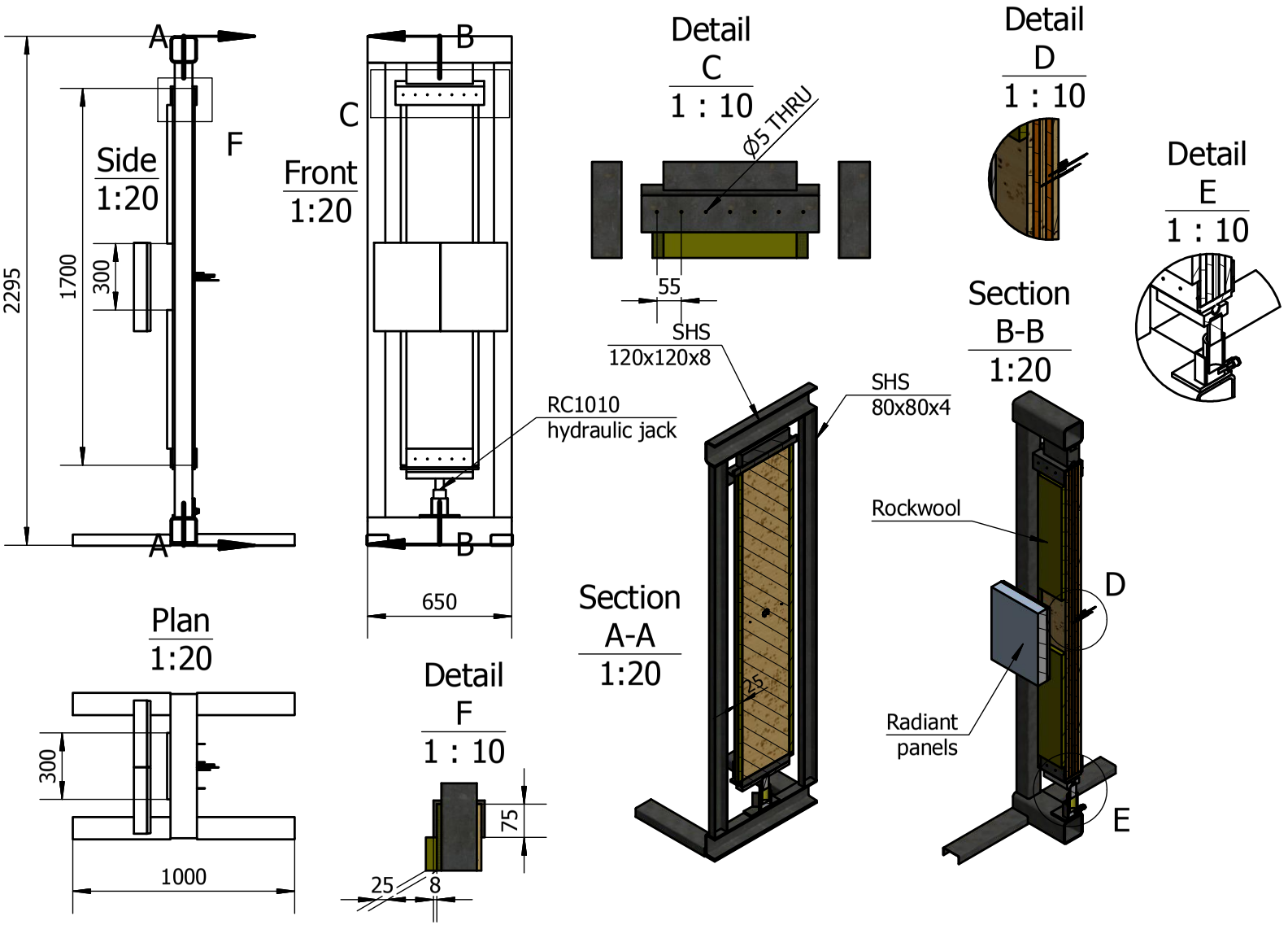

Figure 6.5. Drawings of elevation, plan, section and detailed views for the experimental configuration for the experiments described in this chapter.

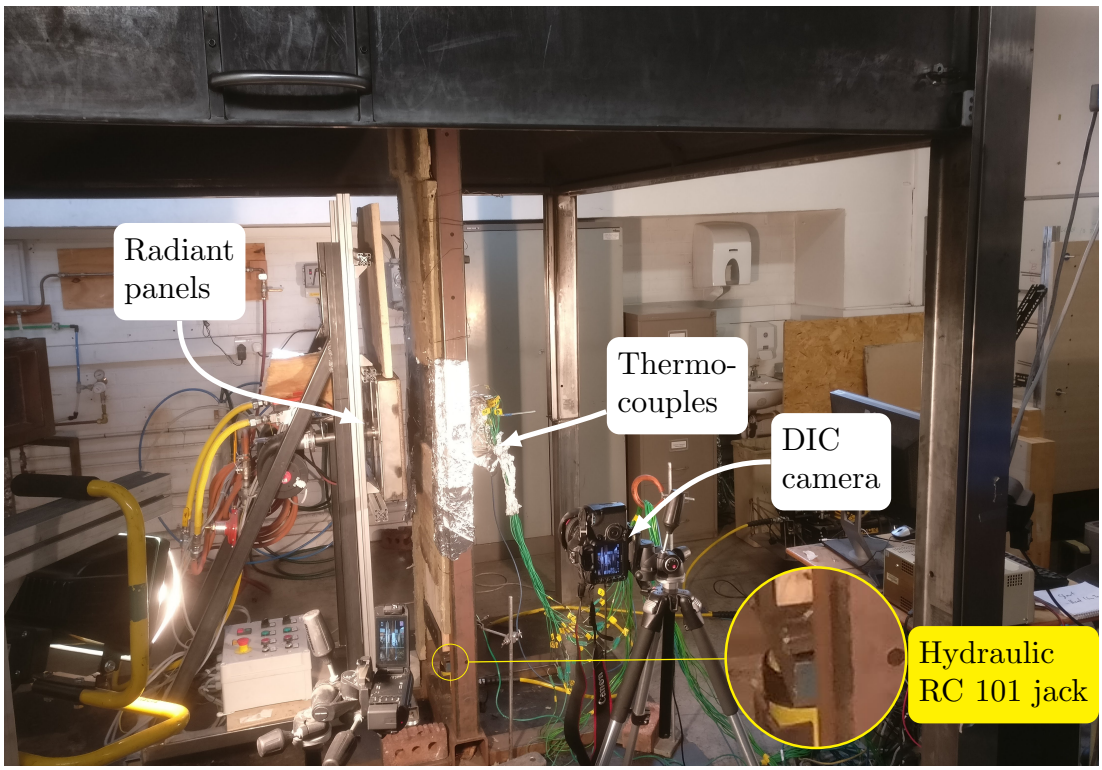

Figure 6.6. Annotated image of the experimental set-up, showing a CLT wall in the loading frame, faced by the radiant panel system.

6.4.1.2 Applied Loads

Due to the considerable variability in ultimate failure loads observed during ambient temperature reference tests (see Table 6.2), the applied load for the heated wall strips was determined from recommended loads from the manufacturer [88], rather than from observed ultimate ambient failure loads. This recommendation is for the applied compressive load on CLT under consideration of a wind load of 1 kN/m^2 and has been reproduced for the two investigated configurations in Figure 6.7. The load is chosen for a wall height of 1.7 m and a wall width of 0.3 m. The chosen load is then further multiplied by a factor μ to account for the fact that the expected fire load case will only correspond to a fraction of the assumed ultimate failure load, based on the low probability of an ultimate loading scenario coinciding with a fire. Note that μ is recommend as 0.6 in EN 1995-1-2 [145] but herein, due to considerations of the ultimate capacity of the loading frame, a value of 0.5 was assumed instead. From this, the ultimately chosen applied loads for the three and five ply wall strips were 60 and 78.4 kN respectively.

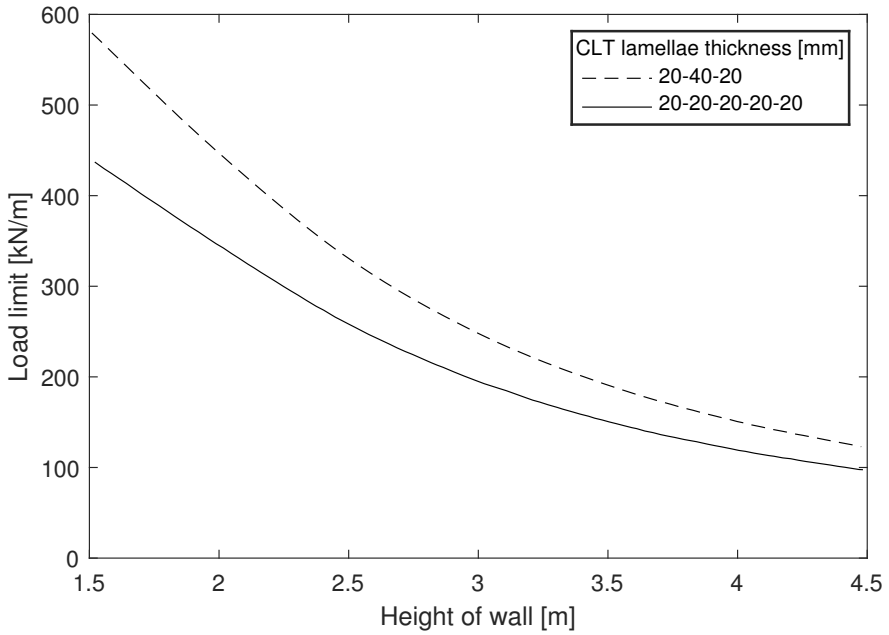

Figure 6.7. Recommended applied loads for two CLT lamellae configurations [88].

The chosen applied sustained loads can be placed into context by considering recommended loads in PRG 320 [208] for a qualification test for adhesives, where a representative load is recommended as 25 % of the allowable stress design (ADS) value. If the timber used for this study is assumed to be equivalent to a quality class of E1 in PRG 320 [208], then the recommended load would lie between 55.8 (if only parallel layers are considered active) and 69.24 (if all layers are considered active) kN for the five ply samples and between 74.4 (parallel only) and 81.12 kN for the three ply samples. Hence, the applied loads can be considered broadly representative of assumed in service loading conditions across several jurisdictions.

6.4.1.3 Thermal exposure

Three different scenarios of heat exposure were assessed in the study reported herein. All scenarios applied a nominally constant incident radiative heat flux to a centre section of 300 by 300 millimetres at mid height of the walls, while the remaining surface of the walls was protected by mineral wool. The first experimental series exposed the walls to a comparably high heat flux until structural failure of the element was observed. This scenario is similar to the thermal assault a building element might be exposed to in a post-flashover fire. The second series utilises the same heat flux on

the sample but the heat flux is set to zero after a specified time. This scenario is used to investigate the effect of stored heat in the sample and the latency of heat transfer (i.e. the "thermal wave") in a material with a low thermal inertia, such as wood. This will give insight into the structural response of timber walls during the decay phase of a fire assuming the fuel load has burned out and gas temperatures in a compartment return to ambient temperatures. The third series, like the first series, also applies heating until failure, but with a reduced imposed heat flux below the critical heat flux for continuous flaming combustion. Note that for all exposures the heat flux to the timber surface will decrease as the specimen surface recesses due to charring and as lateral deflections increase; therefore the incident heat flux is only nominally constant (i.e/ it is not altered with time purposefully).

All heating scenarios described herein were achieved by exposing the timber to the same set of radiant panels, which where placed at a varying standoff distances from the wall strips. The two radiant panels both had a height of 400 and a width of 300 mm and were arranged next to each other, resulting in a total panel width of 600 mm. The panels were fuelled by propane and fitted with fans to provide the necessary air supply. Both panels were fitted with an ignition detector that automatically detected when the panels had ignited and stopped the fitted spark igniters after ignition. The panels used a combined 1.65 g/s of propane as fuel. The radiative heat flux on the exposed face of the wall elements was varied through the standoff distance of the panels with respect to the timber, i.e. for a lower heat flux, the panels were moved farther away from the exposed timber surface. The radiative heat flux from the panels was measured prior to the experimental series using a water cooled Schmidt-Boelter heat flux gauge, which was attached to a modified 3D carving router in order to measure the heat flux at different positions. This set-up is shown in Figure 6.8. The front of the CLT walls facing the panels that was not intended to be directly exposed to radiant heating was protected with 25 mm thick mineral wool panels that were held in place by screws and washers. A square area of 300 mm by 300 mm of the CLT samples was left exposed at mid height of the walls. The edges of the mineral wool panels were sealed with fire cement to minimise the ingress of hot gases.

The measured heat flux for the high heat flux exposure, supplied by the radiant panels at a standoff distance of 100 mm, is shown in Figure 6.9 over the exposed area of at the mid height portion of the timber wall strips. At this relatively close distance between panels and the timber surface two factors caused variation in the heat flux distribution over the exposed area: (1) the angles between parts of the panels and timber that is not directly adjacent are acute, which caused reduced close range view factors across the

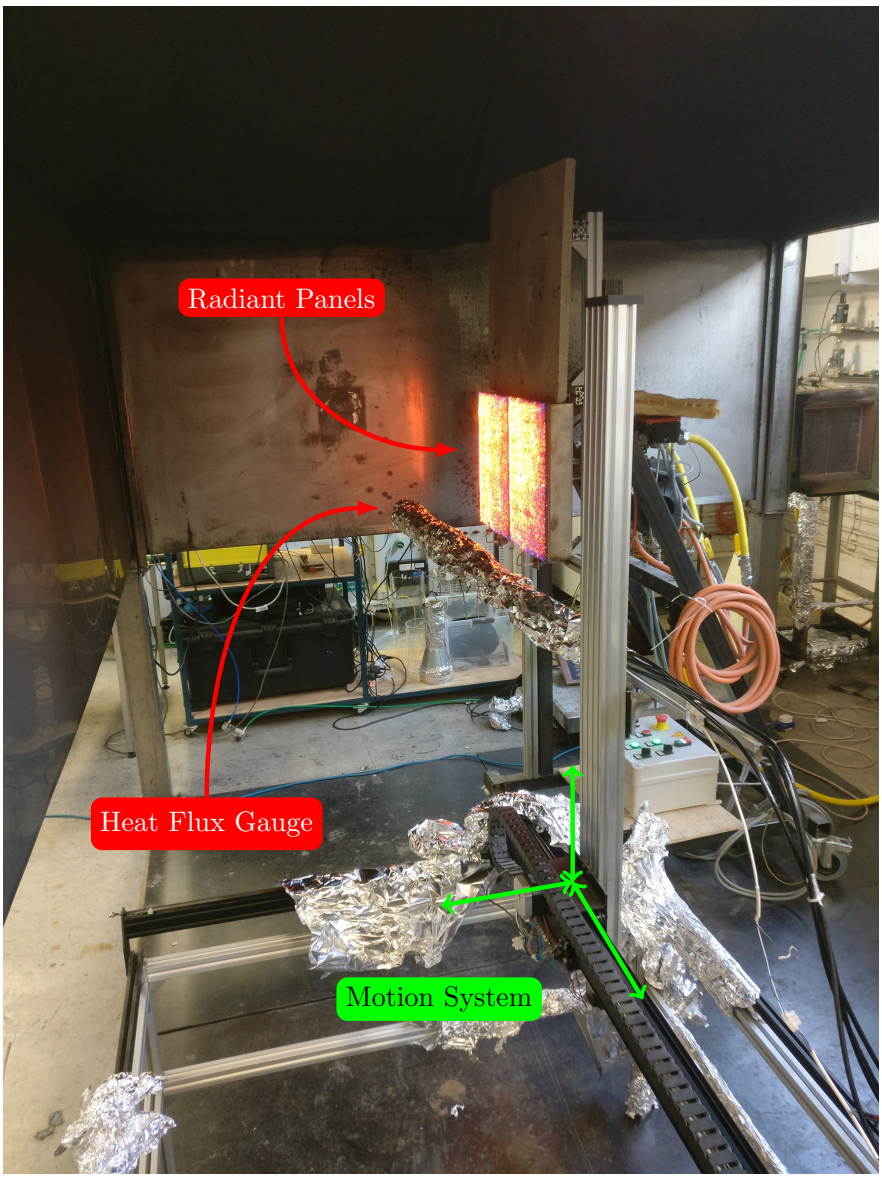

Figure 6.8. 3D linear motion system used to map the heat flux from the radiant panels used.

panels and this caused increased radiative heat flux at the centre portion, and (2) hot air flowing past the panels created a convective flow which added additional convective heat transfer to the upper parts of the exposed surface. The maximum heat flux was measured to be off-centre of the exposure area;this arose from the necessity to place the panels off-centre to the specimen due ot experimental considerations. Overall these effects were not deemed to be critical and a coefficient of variation (CoV) of 13 % from

the mean heat flux of 51 kW/m^2 was measured.

The heat flux distribution at a distance of 400 mm, which is classified herein as a low heat flux, intended to lie below the critical heat flux for autoignition of timber (which is reported to lie below 25 kW/m^2 [221]), is shown in Figure 6.10. It can be seen that, with a mean heat flux of 15 kW/m^2 and a CoV of 6 %, both the magnitude and the variation in heat fluxes over the exposed timber surface is minimised, compared to the higher heat fluxes in Figure 6.9. The reduction in spatial variability can be attributed to the elimination of convective flows from the panel impinging on the timber (which was observed visually during the calibration process) as well as more uniform view factors due to larger view angles between points on the panel and points on the timber surface.

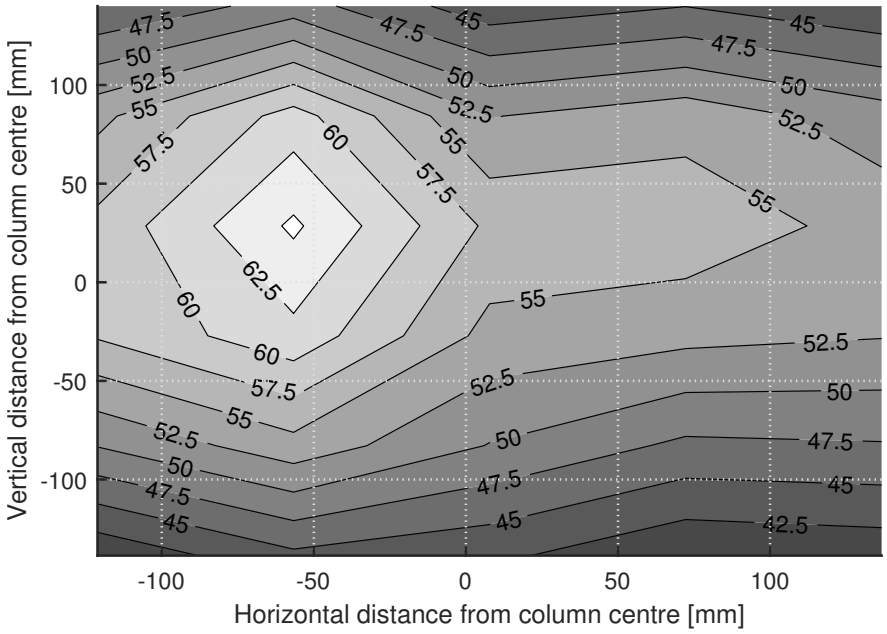

Figure 6.9. Incident imposed heat flux in kW/m^2 over the exposed surface area of the timber specimen at 100 mm distance from the radiant panel surface.

The mean imposed heat fluxes at the surface of the timber against the experimental duration are summarised in Figure 6.11. The actual experimental duration varied as experiments were terminated upon structural failure.

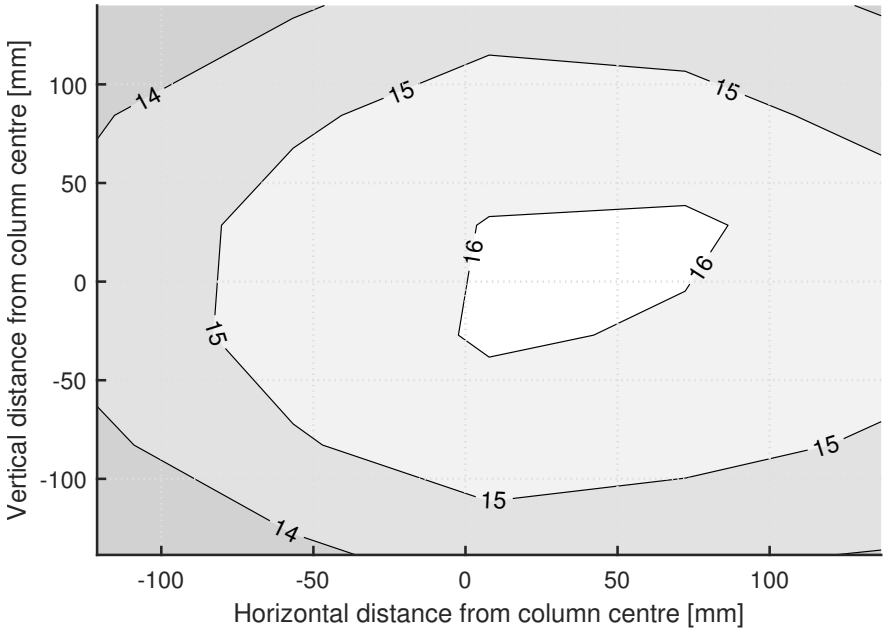

Figure 6.10. Incident imposed heat flux in kW/m^2 over the exposed surface area of the timber specimen at 400 mm distance from the radiant panel surface.

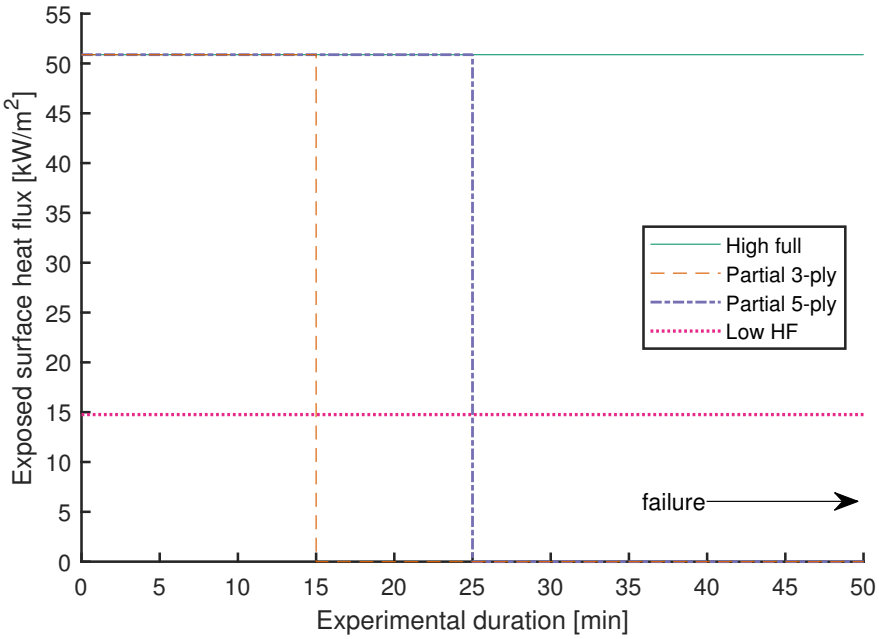

Figure 6.11. Incident mean imposed heat flux in kW/m^2 at the exposed surface of the timber specimen against time of experiments.

6.4.1.4 Thermocouple placement

Inconel sheathed K-type thermocouples (TCs) with outer diameter of 1.5 mm were placed into the timber from the unexposed side to specified depths to monitor the evolution of internal temperatures through the depth of the timber samples. The bottom 8 mm of the holes had a diameter of 1.5 mm and the remaining depth was drilled with a 2 mm drill bit. For the samples in this chapter, the holes to place the TCs were drilled by a CNC machine that was modified to allow the drilling of holes (instead of milling material). A low voltage spindle was equipped with a speed control module, allowing the operator to slow down, increase or halt the speed via a G-code feed. This was necessary to maintain precision when the drill bits were moved between adjacent holes, as high drill speeds can induce vibrations and resonance in thin drill bits such as the 1.5 and 2 mm diameter drill bits used for this study. The drill (see Figure 6.12) followed a predefined grid system of holes at specified coordinates and drill depths. This set-up allowed for rapid specimen preparation and ensured accurate and consistent thermocouple depth and location placement across specimens.

For temperature profile measurements, an ideal measurement set-up measures temperatures at varying depths through the cross-section. For obvious reasons it is not possible to place more than one thermocouple at the exact spatial location along a line through the cross-section when inserting thermocouples from the back of exposed specimens. Instead the aim was to place thermocouples as close as possible to each other whilst maintaining a minimum distance between them in order to minimise the influence of the thermocouples on the adjacent temperature readings. To achieve a tight TC packing density it was decided to arrange TCs as circles inside larger circles; this way the internal circles ensured a minimum spacing between the TCs. The packing was done in accordance with optimal packing density as described by Graham et al. [222], thereby achieving the highest possible proximity of thermocouples whilst maintaining a minimum spacing. The spacing between TCs for these experiments was (in lieu of available specific guidance) somewhat arbitrarily chosen as 10 mm. The resulting layout of the TCs is shown in Figure 6.13, together with the corresponding depth placement from the unexposed surface (i.e. the drill depth). The majority of thermocouples were placed in the geometric centre of the unexposed surface, in accordance with the packing density as described above, and two additional TCs were placed at 50 mm from the specimen edge on either side to monitor the uniformity of heat progression along the horizontal coordinates of the samples.

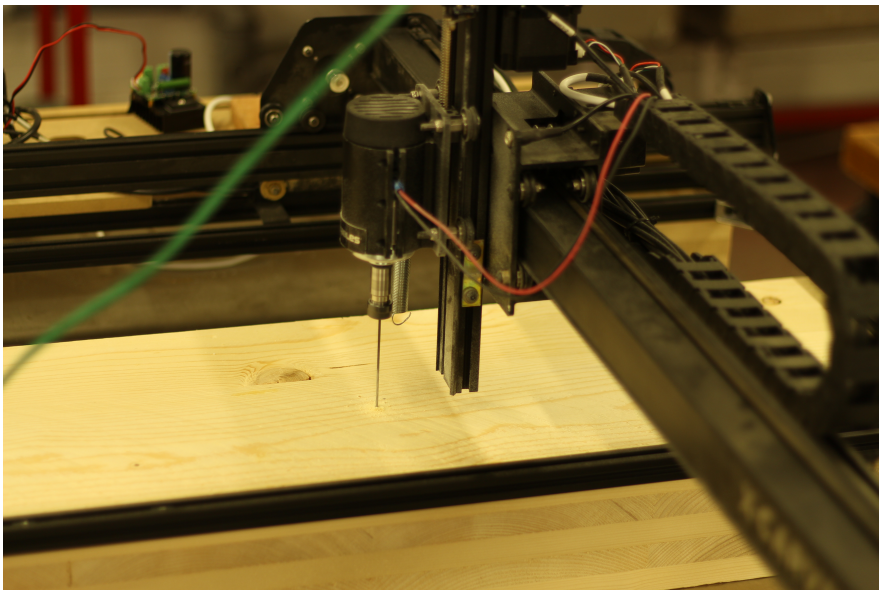

Figure 6.12. Customised CNC router set-up for thermocouple hole drilling.

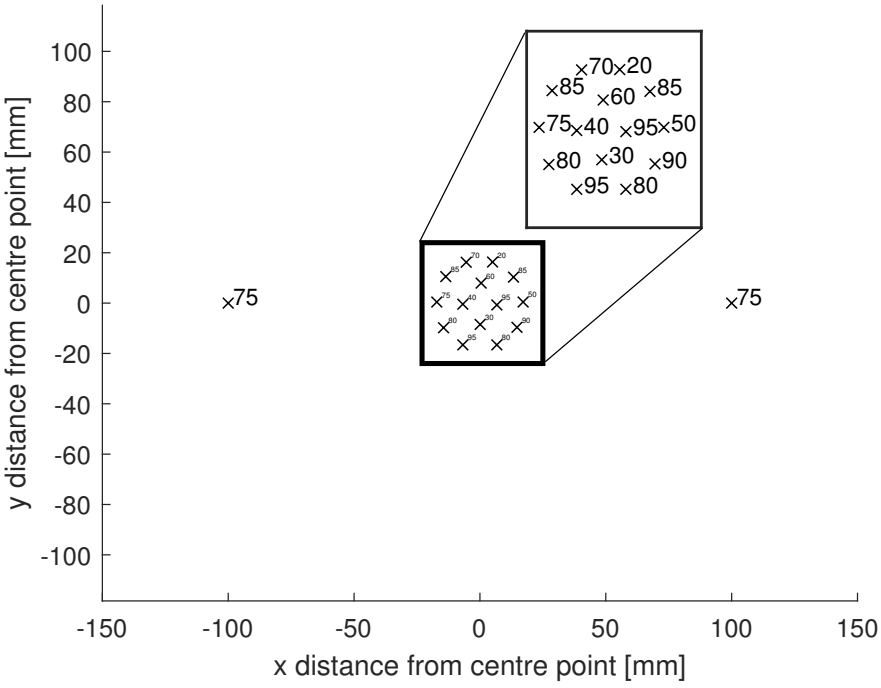

Figure 6.13. Locations of thermocouple holes and corresponding depths on back of exposed sample with respect to geometric centre of the exposed surface.

6.4.1.5 Deflection measurements

The use of image analysis to determine deflections and strain in engineering is well documented and there are powerful and complex image analysis tools available, which are able to supply sub pixel accuracy for determination of movement between two images, for example Geopiv_RG [209, 220], which was used to track deflections for ambient reference walls in Section 6.3. However, due to the high accuracy, very detailed image analysis tools experience difficulties when smoke, flames, and convection currents are present within the area of interest. Since all of these were anticipated to occur for the experiments described herein it was clear that DIC would not be a reliable measurement tool. In addition, only a very small portion of the wall specimens was visible from the side, with the loading frame obscuring the majority of the walls from a side view. To overcome these issues, a new image analysis method was developed for these experiments. The new method relies on the detection of circular shapes in each image, thereby identifying the location of their geometric centre.

Images were taken at chosen intervals (here five seconds) and then analysed individually in MATLAB [223]. Circles in each image were detected through a Hough transformation [224], which relies on the parametrisation of each point that can be distinguished in the image based on its brightness (or lack thereof). To detect circles, three parameters are assessed, forming cones in a three dimensional space. Intersection of these cones by common points indicate that these points are located on the same circle. Black round stickers were placed on the visible portions of the wall specimens and these circles were tracked between all images to obtain their movement in pixels. At the start of each experiment an image of a chequered board with squares of 10 mm was taken and this image was used obtain a calibration to translate pixels to millimetres.

In addition to the "circle analysis", two linear potentiometers (LPs) were used to track deflections. One was placed on the side of the exposed timber surface at midspan in order to track lateral deflections, and the other was placed on the lower connection bracket to measure vertical displacements. One issue was observed for LPs when they were placed on timber; since they are under a small amount of stress they tend to make a small indent on the timber surface. When the wall then moves vertically (i.e. perpendicular to the direction of measurement of the LP) the tip of the LP is dragged along, thereby causing the LP to bend and thereby rendering the readings less accurate. The LPs were therefore mainly included as a backup measurement for the circle analysis and all following results and analysis are based on values from the circle analysis.

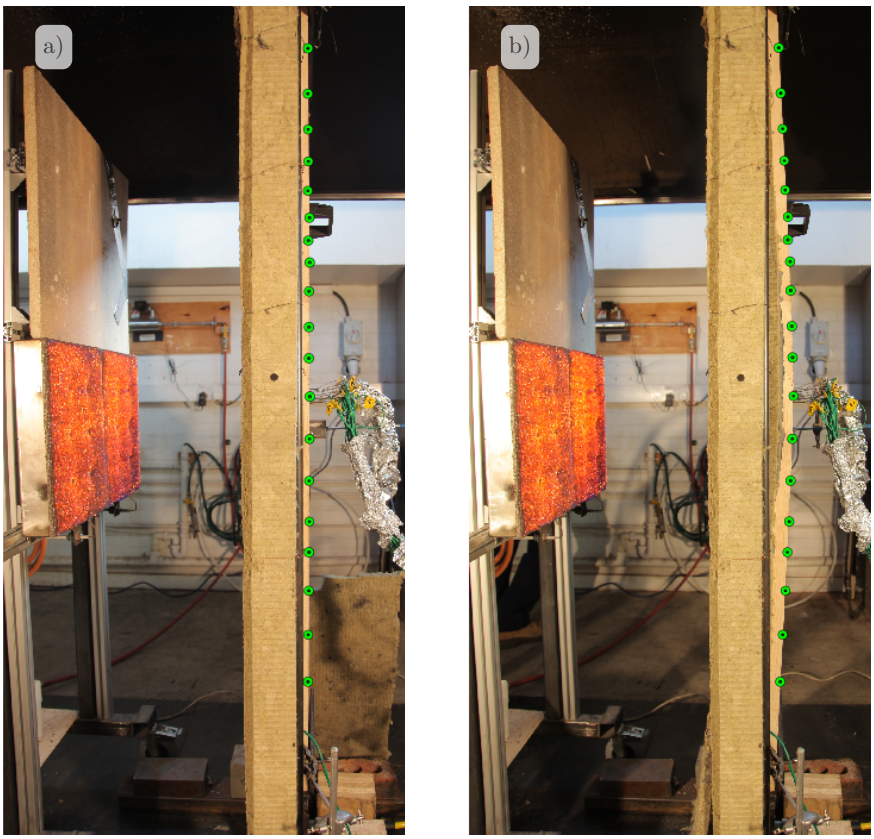

Figure 6.14. Highlighted circles for deflection measurements along the unexposed edge of a CLT wall at a) start of an experiment and b) failure of the specimen.

6.4.1.6 Post experiment

After the experiments ended, the imposed heat flux was removed (if this had not been done already as part of the experimental procedure). This led to auto extinction of flaming timber in all cases. Remaining localised smouldering was then extinguished via the application of water spray. All of the protective mineral wool was removed as quickly as possible to prevent any smouldering below the insulation. All thermocouples were recovered from the unexposed side of the wall strips before the samples were removed from the loading frame. After the samples had cooled down sufficiently the samples were sawn in half at midspan and the depth of the progression of the char front was physically measured in the cross-sections.

6.4.2 Temperature readings

The placement of thermocouples is described in Subsection 6.4.1.4. When analysing the resulting thermocouple data, there are three challenges that need to be addressed to obtain reliable temperature readings: (1) only a limited number of discrete depths are measured, however, it is desirable to have continuous data on the in-depth temperature in the sample since this knowledge will be essential to attempt to model the change in material properties through the cross-section. In addition, there is special interest in determining the 300 °C isotherm to infer the charring rate, and only a few thermocouples will read 300 °C at any given moment. (2) since timber is a natural material its thermal and chemical properties are randomly distributed variables; this introduces noise into the thermocouple data at equal depths, which becomes increasingly pronounced above 100 °C [225], and (3) the influence of high conductivity of the thermocouples relative to the timber, which creates a heat sink and influences the temperature readings of the thermocouple itself. (1) and (2) are common issues in data collection and can be solved via prediction and estimation respectively. For (3) there is a lack of ground truth (the actual temperature of the timber if no thermocouple was present) and this is a complex problem that requires consideration of the underlying physics for a satisfying solution. Solutions to these problems are presented in Section B.2. The uncertainties arising from (1) and (2) are quantified and a simplified procedure for thermocouple corrections to address (3) is explained.

6.4.3 Results for elements exposed to "high" heat flux until failure

6.4.3.1 Deflections

Figure 6.15 shows the horizontal deflection at midspan for eight loaded CLT wall strips (two repeats for each configuration) exposed to the incident initial radiant heat flux shown in Figure 6.9. For the wall strips with a three ply 40-20-40 layup, the two repeats for each adhesive type follow the same deflection trajectory. A clear distinction between the adhesives can be observed, with the PU bonded walls failing after around 20 minutes and the specimens bonded with MF after around 30 minutes. The five ply wall strips (20-20-20-20-20) maintained their load bearing capacity for longer than the three ply ones. The experiment for Specimen C5MF050_1 was stopped before failure as the insulation fell off the sample and the whole front area of the wall started to burn. Nonetheless, reasonable agreement can be seen between the MF bonded 5 ply specimens until 35 minutes of exposure time. As was measured for the three ply

specimens, the PU bonded five ply elements were also observed to maintain their load bearing capacity for a shorter period than those five ply specimens that were bonded with the MF adhesive.

6.4.3.2 Char progression

The char depths that were measured by tracking the 300 °C isotherm for this sample group are plotted against the time of heating in Figure 6.16. In addition, the rates of charring are shown in Figure 6.17. All specimens initially charred quickly, with a peak charring rate visible, before the formation of the char layer caused a deceleration in the charring rates. Overall the progression of the charring depths and the corresponding charring rates does not appear to have varied greatly between the different specimens, with C5PU050_01 being one noticeable exception, with a deeper and faster char progression than all other specimens. This can be linked to periodic increases in the charring rate throughout the experimental duration, which was possibly caused by pieces of char falling-off, thereby increasing the charring rate locally. After the initial peak charring rate the charring rates reduced and followed a trend to reach a quasi steady rate. It should be noted that both the char depth and the charring rates were zero for the first few minutes of the experiment, however, ignition of the exposed surface and accompanying charring was observed a few seconds after the protective shield was removed and the samples were exposed. The delayed observation of the charring rate can be attributed to the fact that the TCs closest to the surface were located five millimetres below the exposure area and therefore would not have registered any heat until the heating front reached these thermocouples. Images of the char profile after the experiments are shown for both ply configurations in Figure 6.18; apart from corner rounding that can be observed near the edges, the char profile appears essentially continuous over the width of the specimens, although accelerated local charring had occurred near gaps between boards (also observed by [75]). In Figure 6.18 b) the char front can be observed to have followed the growth rings of one of the boards, which led to a radially increased char depth.

6.4.3.3 Observations

Failure for all specimens were preceded by accelerating (i.e runaway) deflections, causing visible curvature that increased in a matter of seconds before material failure (as shown in Figure 6.19) occurred in the form of tensile rupture on the wall side facing away from the heat exposure.

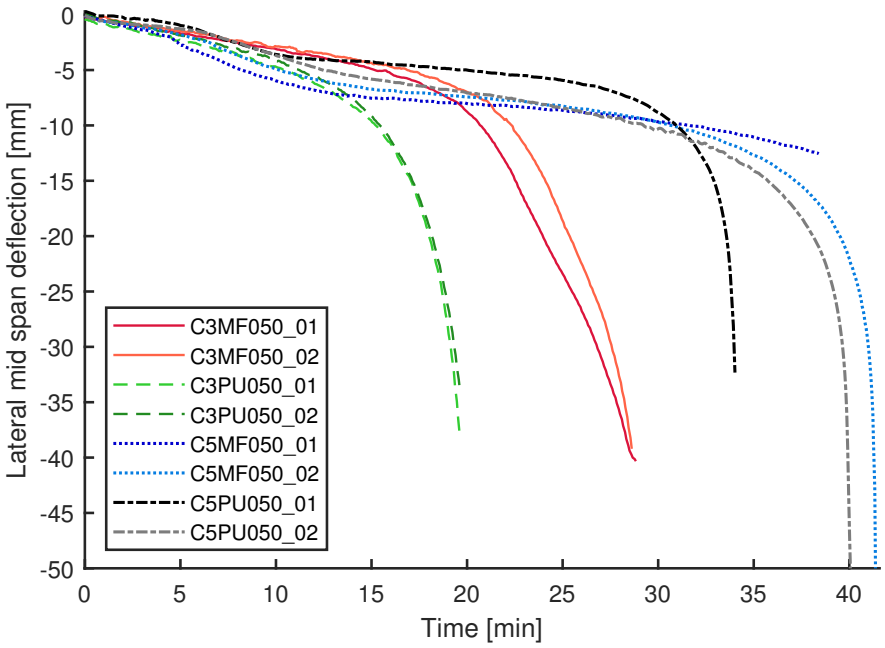

Figure 6.15. Mid-height lateral deflections of wall strips exposed to full radiant heat flux until structural failure

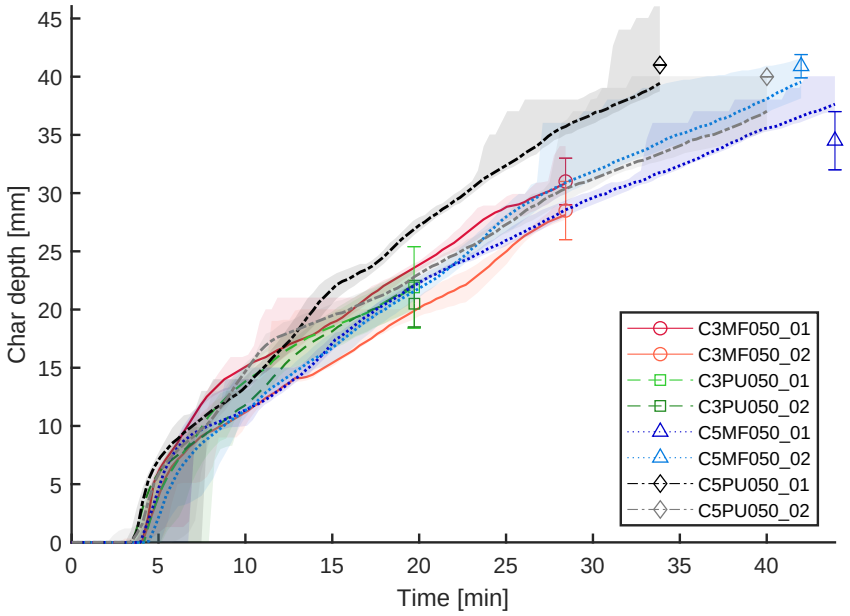

Figure 6.16. Char depths inferred from 300 °C isotherms for specimens heated to failure with the high heat flux scenario.

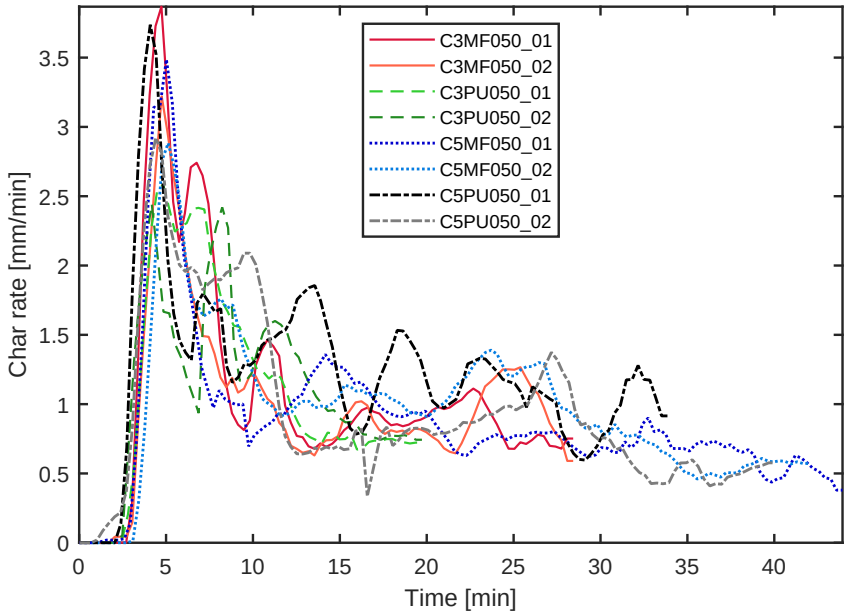

Figure 6.17. Rates of charring inferred from 300 °C isotherms for specimens heated to failure with the high heat flux scenario.

Char fall-off of pieces of charred timber plies were observed for both the five ply samples that were bonded with the PU adhesive type. Char spalling, which manifested itself as small bits of char popping off the char surface was observed for all specimens for this "high" heat flux. Due to the close proximity of the radiation panels to the burning surface, it was difficult to determine the exact moment of char-fall off visually. For specimen C5PU050_01 char fall off was observed 30.6 minutes into the experimental duration. At this time the temperature at the first glue line (at 20 mm from the exposed surface) was measured as 866 °C and 221 °C at the second glue line (40 mm from exposed surface). This indicates that this observed char fall off occurred at the second glue line (since temperatures at the first glue line indicated oxidation of the char). The increase in charring rate for this specimen (see Figure 6.17) indicates that char fall-off could have occurred as early as 13 minutes into the experimental duration, although this was not observed visually. It should also be borne in mind that the analysis of char fall-off in the context of measured temperatures is flawed, as thermocouples can keep char in place at the location where temperatures are measured. For specimen C5PU050_02 char fall-off was visually determined after 37.1 minutes of experimental duration. At this time the temperature at the first glue line (at 20 mm from the exposed surface) was measured as 747 °C and 233 °C at the second glue line (40 mm

from exposed surface).

The key results from this experimental series are summarised in Table 6.4, which confirms the high repeatability for the three ply CLT configurations in this series, which can also be seen in Figure 6.15. The charring rates in this table are calculated as the final char depth, determined from measurements after the experiments' divided by the duration of the experiment (i.e. the failure time).

Table 6.4. Overview of results for CLT wall samples exposed to a "high" heat flux until failure.

Specimen	**Failure time** [min]	**Final char depth** [a] [mm]	**Char rate** [b] [mm/min]	**Char fall off** [ ]
C3MF050_01	28.5	31.0	1.09	No
C3MF050_02	28.7	28.5	0.99	No
C3PU050_01	19.7	21.9	1.11	No
C3PU050_02	19.7	20.5	1.04	No
C5MF050_01	DNF	34.5	-	No
C5MF050_02	41.4	40.9	0.99	No
C5PU050_01	34.0	41.0	1.21	Yes
C5PU050_02	39.8	40.0	1.01	Yes

[a] Measured after experiment.

[b] Final char depth [a] divided by heating duration.

Figure 6.18. Charred profile at mid height cross-section for a) a three ply and b) a five ply sample.

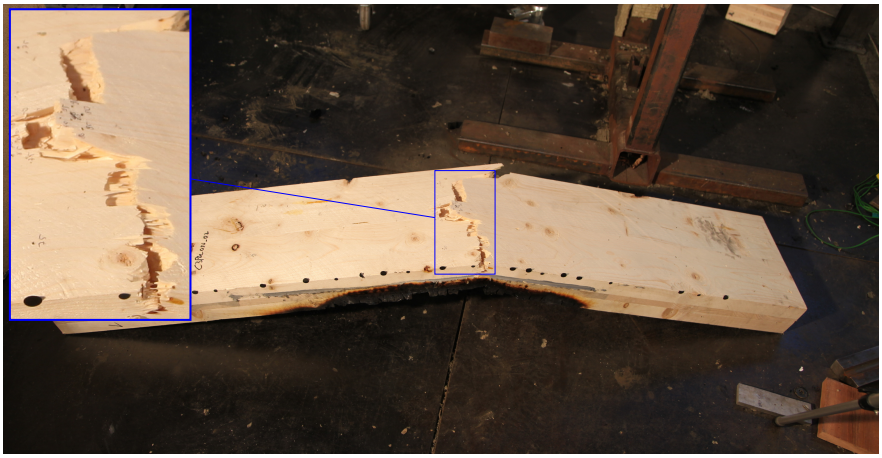

Figure 6.19. Specimen C3PU050_02 after experiment end, showing the tensile rupture on the fire unexposed side of the wall.

6.4.4 Results for elements exposed to high heat flux with subsequent cooling phase

6.4.4.1 Deflections

The measured mid-height lateral deflections for wall strips heated for either 15 or 25 minutes for three and five ply specimens, respectively, are shown in Figure 6.20. The heating times were taken as approximately 75 % (rounded to the nearest 5 minutes) of the lowest failure times for each ply number configuration from the experiments with "high" heat flux exposure until failure. For the three ply samples it was observed that the deflections continued to progress after the radiant panels are switched off, and that the rate of deflection decreased shortly afterwards. Subsequently the walls continued to deflect slowly until the experiments were terminated with no failure observed; although given the slow but continuous deflections those wall strips might have experienced structural failure eventually if the experiments had run for a prolonged time period, however, for safety reasons it was not possible to extend the experimental durations past the laboratory opening times. Within the three ply samples the two specimens bonded with polyurethane initially experienced higher deflections than those bonded with melamine formaldehyde, but after the heating was stopped the deflection rates were similar. For the five ply samples it was observed that the the lateral deflections of the walls experienced a plateau, which continued after the heat was removed before deflections accelerated and ultimately led to structural failure of the samples. The paths to failure can be distinguished between the two adhesive types for the five ply specimens, with PU bonded samples deflecting faster and failing earlier than those bonded with MF, which was observed to reduce in deflection rate before runaway deflections occurred, causing global buckling failure.

6.4.4.2 Char progression

The char depths calculated from the 300 °C isotherm are shown versus the experimental duration for these experiments in Figure 6.21, and the corresponding rates of charring for the first 35 minutes of these experiments are shown Figure 6.22. It can be seen that all specimens, independently of their configuration type, charred at a similar rate at the beginning of the experiments. Once the panels were switched off the progression of the char front stopped and the char depth remained essentially constant for the remainder of the experimental duration, which was also confirmed by the charring rate dropping to zero immediately after the radiant panels were switched off. For the five

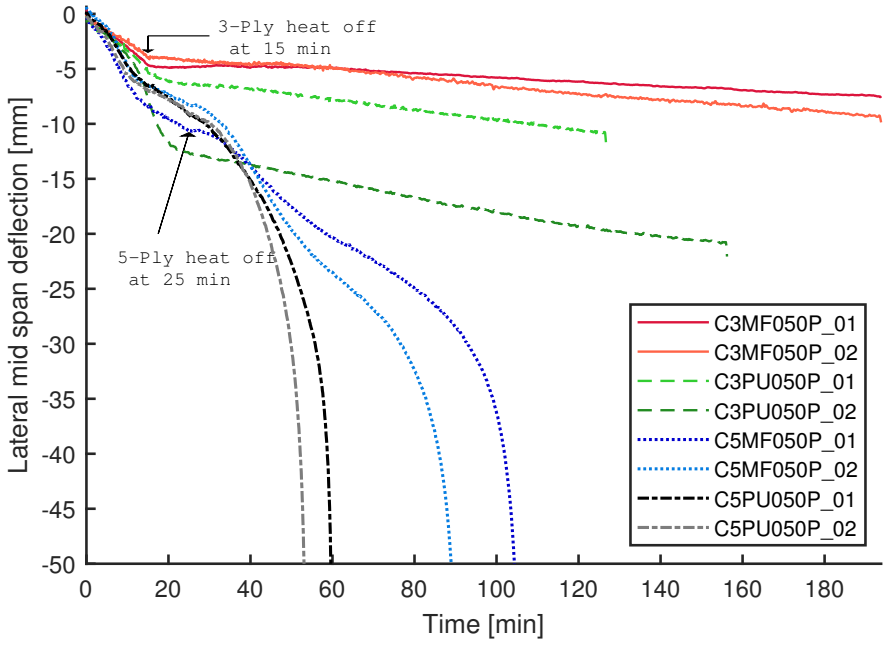

Figure 6.20. Mid-height lateral deflections of wall strips exposed to "high" radiant heat flux for a specified duration of heating and subsequent cooling phase.

ply samples it can be seen that the final char depths ranged between 25 and 30 mm; because the plies have a thickness of 20 mm, this means that the char front was located in a crosswise orientated ply when the heating was stopped; this explains the plateauing of the deflections in Figure 6.20 during this time period since crosswise plies contribute significantly less to the structural capacity and loss of their individual contribution due to progressing heat will cause lower deflections than loss of plies orientated parallel to the direction of loading.

6.4.4.3 Observations

An image sequence of different experimental phases is shown in Figure 6.23. After ignition a long flame was observed, indicating the relatively high burning rate that is also evident from the initial high charring rates in Figure 6.22. This was subsequently reduced, leading to a smaller flame, as shown in Figure 6.23 b), since the growing char layer provided insulation for the timber and limited the flow of pyrolysis gases to the air, where they could burn. For all specimens removal of the external heat flux caused auto-extinction, as shown in Figure 6.23 c), and as would be expected for timber that had already built up a char layer. Afterwards, smoke continued to be emitted from the

specimens in some locations, indicating continuous smouldering combustion, although this was localised to discrete spots on the charred surface were heat below the char was provided with fresh air through small gaps.

Char fall-off was observed for both of the five ply specimens that were bonded with polyurethane adhesive, and this occurred both during the heating (as indicated by increases in the rate of charring in Figure 6.22), and also during the cooling phase for these specimens. For C5PU050_01 the first visual confirmation of char fall-off was at 20 minutes. At this time temperatures of 407 °C and 120 °C were measured for the first and second glue line, respectively. AS for the specimens heated to failure, the charring rate (see Figure 6.22 indicates that fall-off could have occurred between 10 and 15 minutes of experimental duration. Additional char fall-off for this specimen was observed at 49 minutes (254 °C and 130.8 °C, first and second glue line, respectively). For C5PU050_02 the first visually observed char fall-off occurred after 20.5 minutes with glue line temperatures of 502 °C and 137 °C at 20 and 40 mm, respectively. Mild char spalling, wherein small pieces of char pop off the surface of the char, occurred for all specimens.

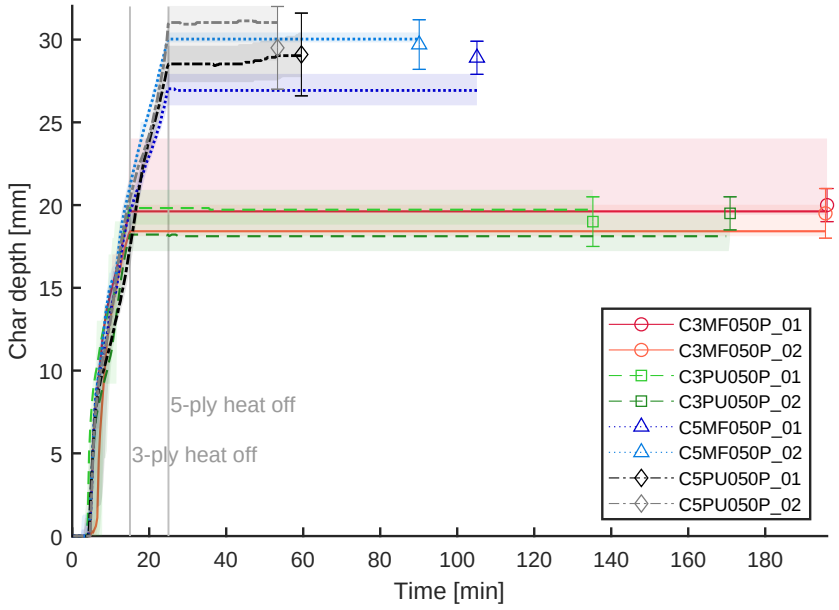

Figure 6.21. Char depths inferred from 300 °C isotherms for specimens heated for a predetermined amount of time.

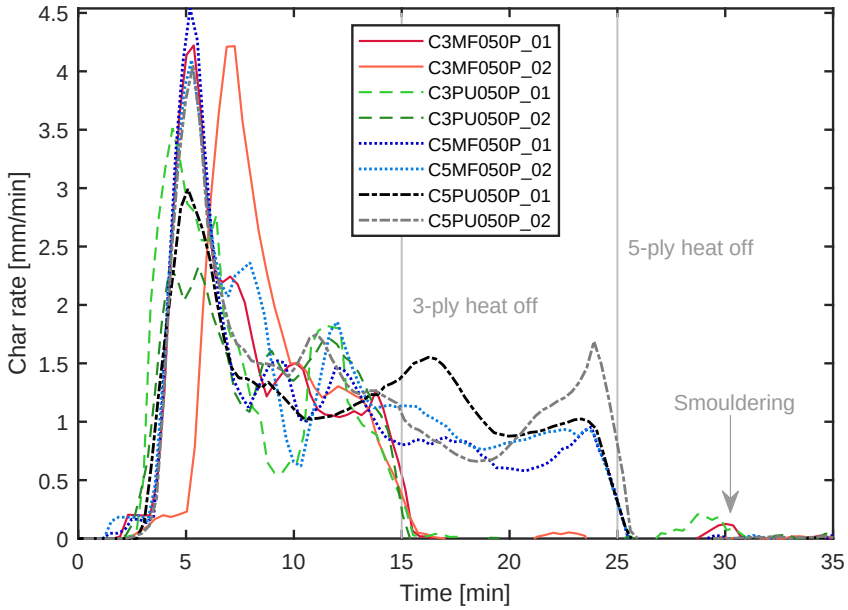

Figure 6.22. Rates of charring inferred from 300 °C isotherms for specimens heated for a predetermined amount of time.

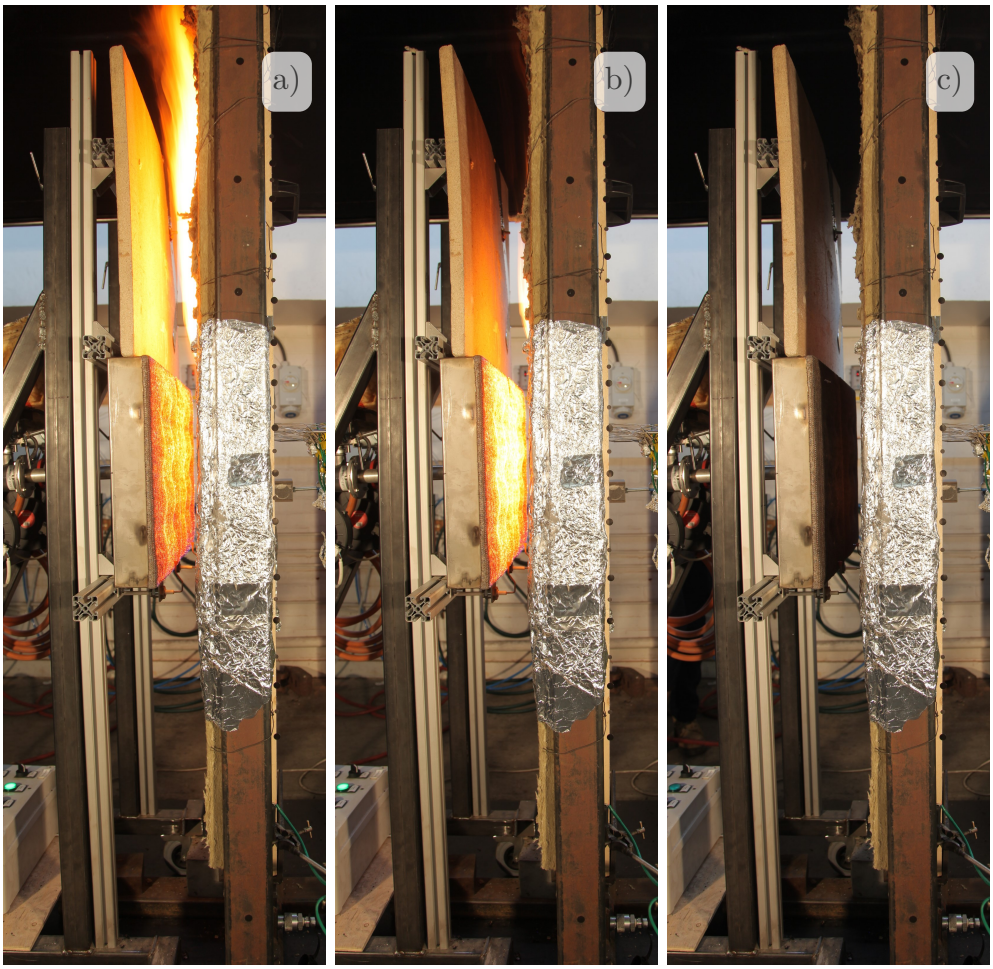

Figure 6.23. Sequence of different stages of an experiment for walls subjected to a "high" heat flux for a predetermined time. a) just after heating exposure began and auto-ignition occurred, b) just before the heat was removed and, c) just after the heat was removed.

Table 6.5. Overview of results for CLT wall samples exposed to a "high" heat flux for 15 and 25 minutes for three and five ply samples respectively.

Specimen	**Failure time** [min]	**Final char depth** [a] [mm]	**Char rate** [b] [mm/min]	**Char fall off** [ ]
C3MF050P_01	DNF	20.0	1.33	No
C3MF050P_02	DNF	19.5	1.30	No
C3PU050P_01	DNF	19.0	1.27	No
C3PU050P_02	DNF	19.5	1.30	No
C5MF050P_01	105.2	28.9	1.16	No
C5MF050P_02	90.2	29.7	1.19	No
C5PU050P_01	59.7	29.1	1.16	Yes
C5PU050P_02	53.3	29.5	1.18	Yes

[a] Measured after experiment.

[b] Final char depth [a] divided by heating duration.

6.4.5 Results for elements exposed to low heat flux until failure

6.4.5.1 Deflections

Figure 6.24 shows the measured lateral deflections at mid height for the CLT panels which were exposed to a nominally "low" heat flux with a mean 15 kW/m^2 across the exposed area. Specimen C3MF015_01 (the first specimen for this series) was exposed to a mean heat flux of around 20.5 kW/m^2; this was done as this heat flux lies below most critical non piloted ignition heat fluxes for timber cited in literature [221]. Initially, no ignition was observed for this specimen (as planned), however, after 4.5 minutes a piece of char spalled off the specimen, bounced off the radiant panels, and ignited the pyrolysis gases as it bounced back towards the specimen surface, thereby causing flaming combustion which sustained itself for approximately nine minutes and approximately 7 mm of char depth progression. This ignition process introduced an unwanted element of uncertainty, and it was therefore decided to reduce the heat flux for subsequent specimens to the average of 15 kW/m^2 shown in Figure 6.10. The deflection path for specimen C3MF015_01 is therefore omitted from Figure 6.24, because its boundary conditions differed compared to the other wall strips. Specimens consisting of three plies and bonded with the polyurethane adhesive type exhibited the shortest times to failure, as was observed for the deflections resulting from the "high" heat

flux in Figure 6.15. The deflection paths to failure exhibited more deviation between repeats than those observed for the walls exposed to a high heat flux. For the other specimens no obvious difference in behaviour could be observed between different CLT configurations and adhesive types, although it was observed that the MF bonded three ply sample's deflection decreased continuously, while the five ply sample experienced a plateau when the heat front (i.e. hotter than ambient temperatures) passed through a crosswise orientated ply.

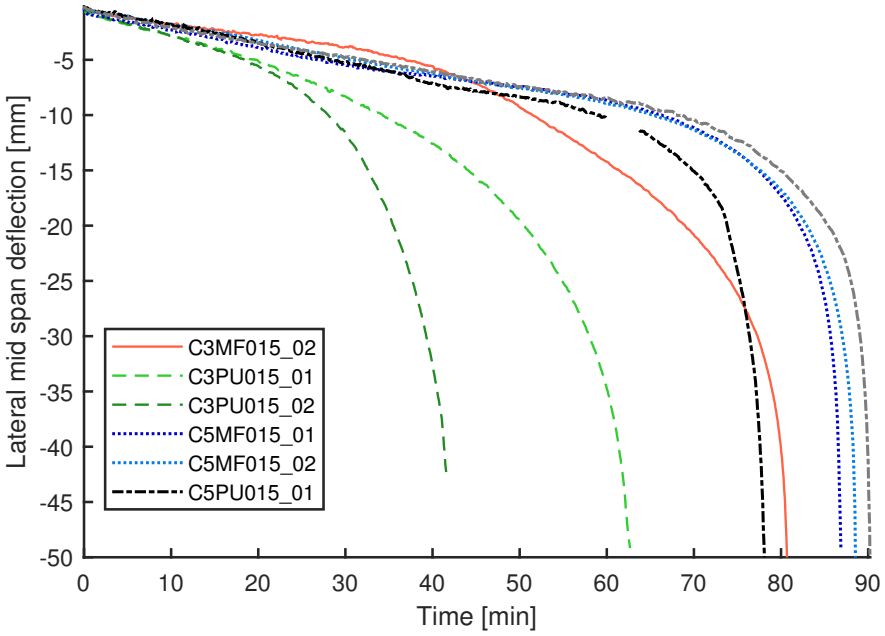

Figure 6.24. Mid-height lateral deflections of wall strips exposed to a low radiant heat flux until structural failure.

6.4.5.2 Char progression

The char depths calculated from in-depth temperature readings for experiments with the "low" heat flux are shown in Figure 6.25 and the corresponding rates of charring for the experimental duration are shown in Figure 6.26. It can be seen that the charring behaviour was similar to that observed for the samples heated with a "high" heat flux, with an early peak in charring followed by a reduction to a quasi steady charring rate. Both the peak and the steady state charring rates were measured to be lower than for the samples exposed to a high heat flux. For the specimens with five plies and bonded with the PU adhesive, two spikes in charring rate were measured during the steady state phase, which is most likely linked to char fall-off after 64 and 76 minutes

for specimens (C5PU010_01) and (C5PU010_02) respectively. In addition ignition and subsequent flaming through cracks in the char surface and in spots where char had fallen-off would have contributed to this increase in charring rate.

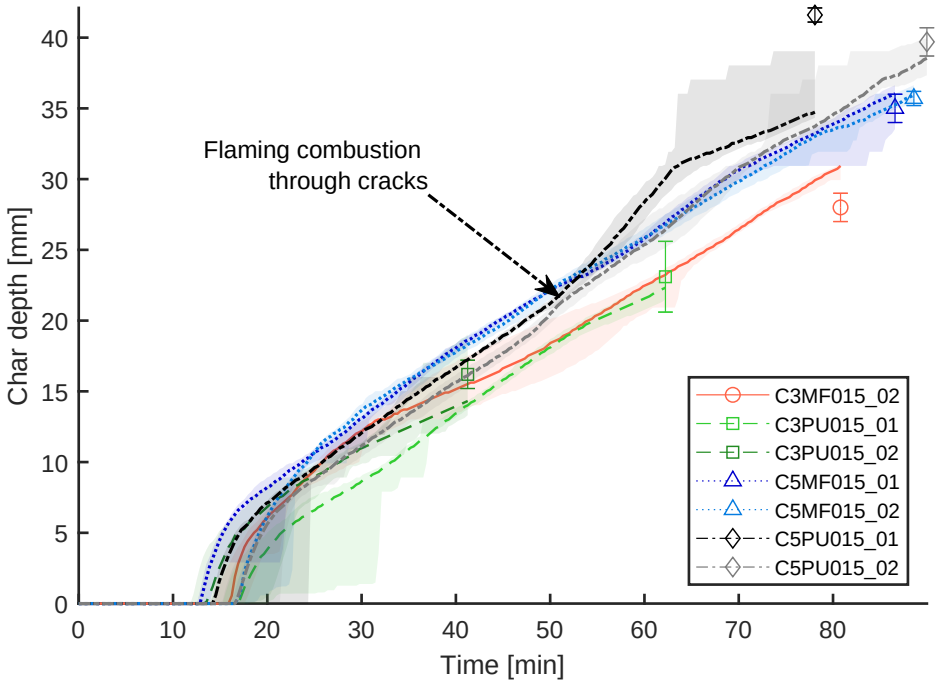

Figure 6.25. Char depths inferred from 300 °C isotherms for specimens heated to failure with a low heat flux.

6.4.5.3 Observations

Apart from specimen C3MF015_01, which was, as described above, exposed to a slightly higher heat flux and experienced flaming combustion, no significant continuous flaming occurred for the specimens in this low heat flux series. For five ply specimens bonded with polyurethane occasional flames spontaneously appeared from cracks that had formed in the charred surface, but this flaming was localised to these cracks and did not form a continuous flame for more than a minute (although repeated flickering of flames in the same spot for one specimen (C5PU010_01) occurred for up to seven minutes and this was also evident from the char depths and charring rates in figures 6.25 and 6.26, respectively, where an increase in charring rate for this specimen is visible after around 50 minutes, when flaming started to occur through gaps, as the char front had reached the first glue line at a depth of 20 mm. Other than the measurable

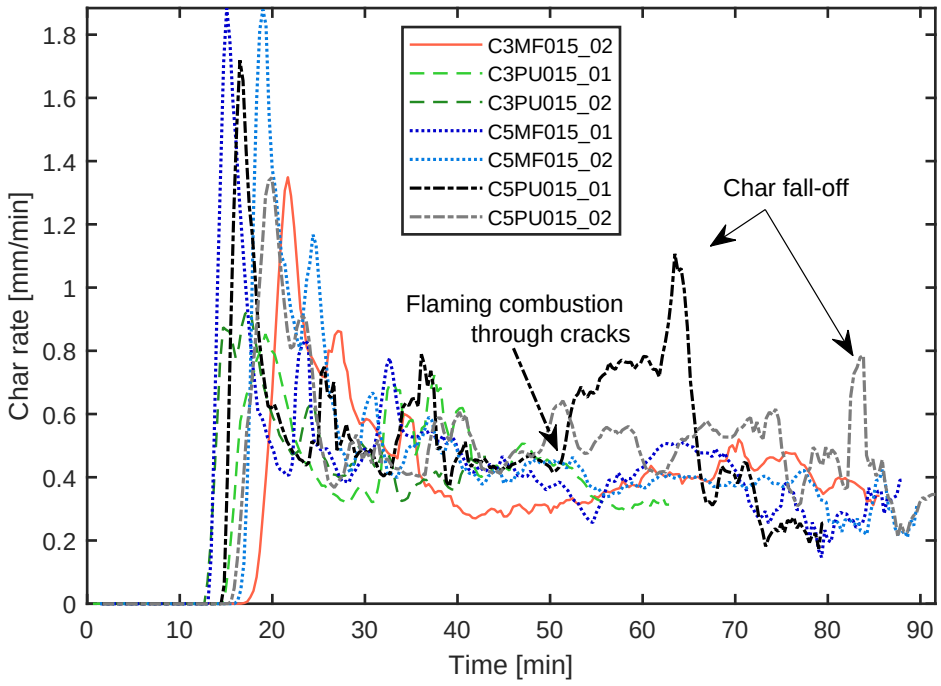

Figure 6.26. Rates of charring inferred from 300 °C isotherms for specimens heated to failure with a low heat flux.

increase in charring rate for this specimen any other occurrence of flaming was not deemed to have influenced the results in a significant way.

Due to the predominant absence of flaming combustion, these samples produced a comparatively large amount of smoke and flammable vapour, especially in the first 10 minutes of the experiments, after which the established char layer reduced pyrolysis, causing a reduction in the charring rate, as shown in Figure 6.26. For CLT specimens made of three plies, water was observed to flow out of the thermocouple holes in the back of the walls trips during testing. This was likely caused by water that was displaced by the progressing heat front which then condensed on the Inconel sheathing of the thermocouples deeper in the timber (where the drilled holes of the thermocouples were wider than near the tip). This flow of water was not observed to occur for five ply samples; potential reasons for this difference are discussed in Subsection 6.5.6.

CLT is made up of multiple boards which form the different plies, and for some specimens in this series it was observed that the physical appearance of the charring on the exposed surface was visibly distinguishable between different timber boards, as shown

in Figure 6.27, however, this did not seem to influence the in-depth temperature measurements, and the char depth was visually observed to be essentially uniform between the two boards.

As for the "high" heat flux exposure, both to failure and for a predetermined time, fall-off of char from the exposed charred surface was observed for both of the five ply PU specimens for the "low" heat flux exposure. This occurred after around 64 minutes for specimen C5PU010_01 and 76 minutes for C5PU010_02. For the former, flaming ignition at a small gap in the char layer was observed before the fall-off, which then led to more flaming. For the latter, flames were only observed after fall-off occurred. The occurrence of char fall-off and its effects are also highlighted in Figure 6.28, which compares the charring pattern on the surface of five ply specimens bonded by MF and PU adhesives; for the specimens using the PU adhesive type the char pattern was observed to be less uniform, and large gaps where fall off occurred were identified.

Table 6.6. Overview of results for CLT wall samples exposed to a "low" heat flux until failure was observed.

Specimen	**Failure time** [min]	**Final char depth** [a] [mm]	**Char rate** [b] [mm/min]	**Char fall off** [ ]
C3MF015_01[c]	47.0	24.3	0.52	No
C3MF015_02	80.9	28	0.35	No
C3PU015_01	62.5	23.1	0.37	No
C3PU015_02	41.6	16.2	0.39	No
C5MF015_01	86.7	35	0.40	No
C5MF015_02	88.7	35.7	0.40	No
C5PU015_01	78.1	41.6	0.53	Yes
C5PU015_02	90.3	39.7	0.44	Yes

[a] Measured after experiment.

[b] Final char depth [a] divided by heating duration.

[c] Specimen exposed to a mean heat flux of 21 kW/m^2.

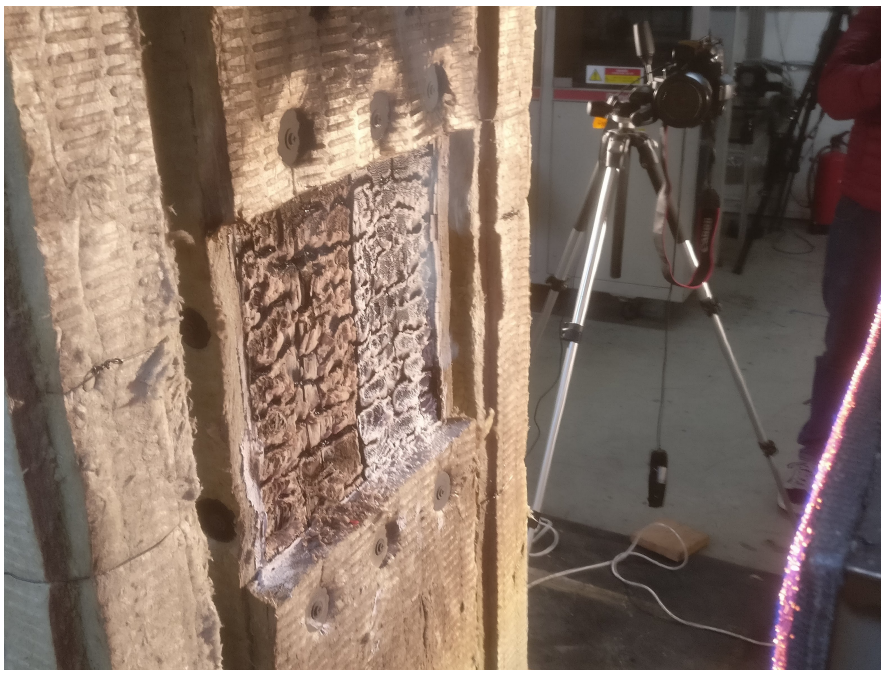

Figure 6.27. Charring of CLT wall exposed to a 'low' heat flux of 15 kW/m^2. Different timber boards are clearly distinguishable.

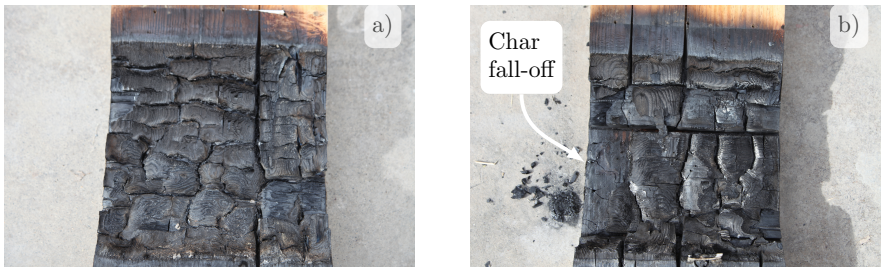

Figure 6.28. Comparison of char pattern of exposed timber surface for five ply specimens bonded with a) MF and b) PU adhesive type after experiments with low heat flux exposure. Char fall-off is clearly visible for PU bonded CLT but not for that with MF.

6.5 Discussion of results

6.5.1 Influence of adhesives and ply configuration

Considering all specimens which failed structurally, it can be seen in figures 6.15, 6.20, and 6.24 that all (but one) of the CLT wall strips which were bonded with the

polyurethane adhesive failed earlier than their respective counterparts using melamine formaldehyde adhesive. This difference was especially distinguishable for the three ply samples exposed to a high heat flux until failure in Figure 6.15. The paths and times to failure for these samples are clearly separated by the different adhesive types and only very little variation can be observed between the curves belonging to each adhesive type. The mean time to failure for these samples was 31 % higher for those bonded with MF, compared to those bonded with the PU adhesive type. If variation in the mechanical properties of timber of these specimens or initial eccentricities (as postulated for the ambient reference experiments) had a significant influence, this would be expected to be clearly exhibited via larger variation in the results within the two adhesive types. It can also be stated that the earlier failure times for the PU bonded CLT are not caused by accelerated charring where char fall-off occurred, because no char fall-off was observed for the three ply specimens that were bonded with PU, yet, as described above, they failed up to 45 % earlier than their MF bonded counterparts. This demonstrates that the adhesives used to bond the experimental wall strips had a clear influence on the load bearing capacity in heating.

All specimens were subjected to an equivalent load ratio of their nominal ambient load bearing capacity. For the sample groups heated to failure, those that were made up of the 40-20-40 three ply configuration in general failed earlier than those of the 20-20-20-20-20 five ply configuration, under the same loading ratio as proportions of ambient temperature design load capacity.

The effect of ply number and adhesive type on the failure times can be assessed statistically by normalising the time to failure for each specimen against the mean failure time of its exposure group, i.e. high, partial, and low heat flux exposures. This assigns each experiment a fraction of the mean expected failure time for its group. Specimens with a value below unity perform worse than average and specimens above unity perform better.

The results of this analysis are shown as a box plot in Figure 6.29, from which the findings above are confirmed: Polyurethane bonded CLT walls fail on average (median) 20 %age points earlier than what would be expected if all specimens were bonded with an 'average' adhesive. Similarly, the median value for the three ply sample group is 17 %age points lower than what would be expected for a specimen with no ply influence. Table 6.7 shows that the p-values from ANOVA lie below the often utilised threshold of 5 % and that these results are therefore unlikely to have arisen by chance, but instead indicate differences in the load bearing capacity in fire that are inherent within the underlying populations.

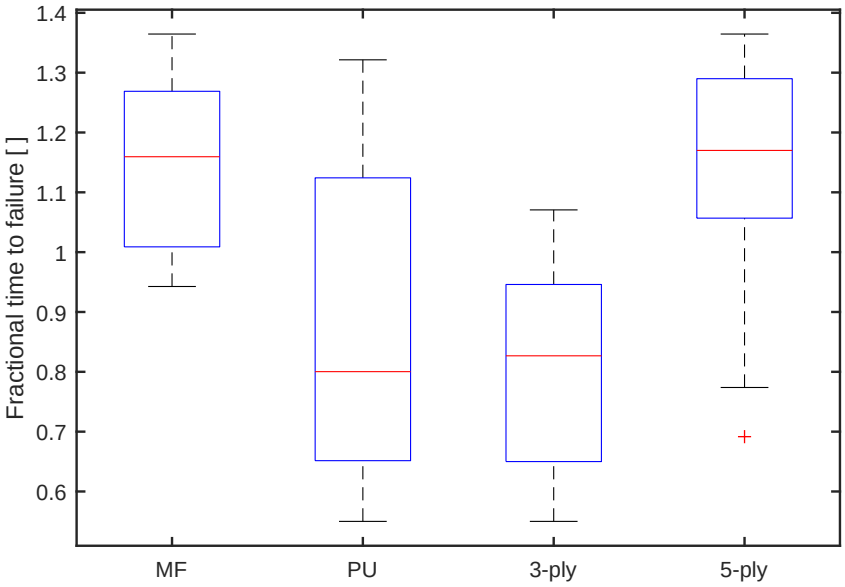

Figure 6.29. Comparison of failure times normalised against mean failure time for each exposure type. Assessed by adhesive type and number plies.

Table 6.7. ANOVA p-values summary for influence of adhesives and ply numbers on fraction of mean failure time.

	Adhesives	Layers
Pr(>F)	4.02E-03	1.42E-03

The differences in load bearing capacity in fire between three and five ply CLT wall strips had previously been highlighted by Wiesner et al. [190], and the results herein corroborate this. The configuration of 40-20-40 is arguably an extreme case, with a large proportion of parallel timber placed in the outer plies; this was chosen deliberately by the author to illuminate the reduction in capacity compared to a ply configuration with more, thinner, plies. For the three ply walls more load bearing material is placed in the outer plies, which means that 50 % of the total available material that is supporting the applied load is comparatively rapidly exposed to fire at an early stage. In contrast, for the five ply samples, as the first outer layer is damaged by the heat, only one third of the parallel timber is affected and any losses in mechanical properties in the cross-wise layers do not contribute significantly to the overall load bearing capacity, as confirmed from the deflection plateaus that were observed for five ply specimens in figures 6.15, 6.20, and 6.24. In addition, as observed in Chapter 5, the three ply

specimens with thicker outer layers were subjected to higher shear deflections, where shear forces were present. As the lateral midspan deflections increased, so did the shear forces, which would then cause additional shear deflections. This would be more severe for three ply compared to five ply specimens. From a structural design perspective, these observations cause a dilemma; from a an ambient temperature structural perspective thicker outer layers are beneficial, because this maximises the load bearing capacity with respect to the foot print of an element and its resistance to stability failures. From a fire dynamics point of view, thick outer plies are also desirable, since this is likely to increase the time to char-fall off in a real fire, thereby increasing the chances of achieving burnout and auto-extinction before char-fall off leads to a second flash over in a compartment [129, 131]. However, from a structural fire engineering perspective, thicker outer layers reduce the time to failure for CLT walls in a fire, as outlined above. This highlights the opportunity for multiple parameter design optimisation (and the need for compromises), and the possible advantages gained by including fire engineering considerations at an early design stage for CLT buildings.

Considering adhesives used in CLT production it has been shown that the use of the polyurethane adhesive type reduces the time that the load bearing capacity of a CLT wall can be maintained under heating. One of the presumed reasons for this is a reduction in bonding strength as the temperatures of the adhesives are increased. This was demonstrated in bending Chapter 5 and manifested in accelerated heat induced deflections. In the fire exposed wall strips this means that the P-Delta effects which arise from heat induced eccentricities are likely increased due to a weakening of the glue line, which will reduce composite action between lamellae and lower the effective second moment of area of the wall strip. While accelerated deflections are not a primary design concern for the fire limit stage in floor systems, they significantly lower the structural performance of walls in fire for the reasons outlined above. This suggests that designers of buildings incorporating CLT walls can significantly increase fire performance through selection of the appropriate adhesive type. Current codified guidance documents do not recommend the consideration of adhesive strength in fire, and the choice of adhesive is currently only considered for the potential occurrence of char fall-off, and only in some jurisdictions [192, 208]

Adhesives in the timber industry undergo constant development, and in theory this leads to a number of available choices of bonding agent for the production of CLT. In reality, since CLT elements are factory produced by a relatively small (albeit growing) number of manufacturers, the choice of available CLT products can be limited and engineers might not be able to obtain CLT with a preferred adhesive type due to a

lack of availability. Different adhesive types result in different manufacturing set-ups and this means that the specification of an adhesive type should be a well thought out proposition, incorporating all aspects relevant to building design and performance. The findings from this thesis should therefore not be reduced to *'melamine formaldehyde good, polyurethane bad'* but should prompt a deeper look at how the fire performance of CLT can be improved at the production stage and suggests that adhesives should be considered when assessing the performance in fires. As with the number of plies in CLT, this becomes an optimisation problem, since adhesives will also have performance criteria not related to fire safety. For example, due to health reasons many jurisdictions limit the amount of formaldehyde that building products may contain; the acceptability to prevent 100 deaths in fires through the choice of a different adhesive but to cause 1000 more due to cancer must be assessed. To answer these questions is not within the remit of this thesis, but the research herein is a contribution to knowledge to enable a better understanding of these considerations, and to make more informed decisions.

6.5.2 Charring

The average charring rates in Table 6.4 and Table 6.5 show that the charring rates for the experiments that were stopped after a specific period of time are higher than those that were measured until failure was observed, despite the use of the same heat flux exposure for both these experimental series. This difference occurred because the considered heating time over which the charring rate was calculated is shorter for the partial exposure results, causing an initial peak in the charring rate to weigh more heavily on the overall mean charring rate; this also explains why the mean calculated charring rates are higher for the three ply samples in Table 6.5, which were subjected to shorter durations of heating.

The influence of the above noted initial charring peak was observed to be less with longer heating durations, since the charring rate stabilised to a steady state. Structurally this peak is also relevant since it occurs at the beginning of the fire and therefore rapidly removes load bearing capacity from the outer ply, which contributes most significantly to the load bearing capacity, especially for the three ply samples, as discussed previously.

The mean charring rate was measured as 1.06 mm/min for the samples subjected to a "high" heat flux of 51 kW/m^2, and as 0.36 mm/min for the samples subjected to a "low" heat flux of 15 kW/m^2. The ratio of the two heat fluxes was 3.4, and the resulting ratio of the mean charring rates was 2.9. From the plots in figures 6.17 and 6.26 it can

be seen that this difference was driven in part by the peak charring rate as the steady state charring rates stabilised around 0.65 and 0.4 respectively. It can therefore be postulated that the relationship between imposed heat flux and steady state charring rate is non linear. On the one hand this can be interpreted as suggesting that there is an upper bound for the steady state charring rate. On the other hand these results indicate it should also be taken into account that a significantly lower heat flux would not scale linearly to a significantly lower charring rate, unless the imposed heat flux is below a threshold value below which no pyrolysis is expected to occur. It should also be considered that the actual heat flux on the timber surface for the high heat flux experiments would have been larger than the heat from the radiant panels alone, since these experiments also maintained flaming combustion throughout the experiments, which would provide an unknown amount of additional heat flux to the timber surface.

6.5.3 Char fall-off

Char fall-off (refer to Subsection 2.3.2), which is also often referred to as delamination, denotes the loss of pieces of char and is suspected to occur when the heat or char front reaches the adhesive line and thereby reduces the adhesion between char and underlying timber. The exact temperature conditions to induce charring are unknown but previous research [173] indicates that it could happen before the char front (denoted by the 300 °C isotherm) reaches the glue line. While it has little effect on the structural load bearing capacity (as char is assumed to have negligible strength and stiffness), char fall-off is consequential for the fire dynamics and can, through the exposure of 'fresh' timber, prolong the fire duration, cause increased gas phase temperatures, and increase the intensity of external flaming, in a timber lined compartment.

Char fall-off was observed for six specimens in the experimental series in this study, all of them were five ply CLT wall samples bonded with the polyurethane adhesive. For the three ply samples, no char fall-off was observed for either adhesive; this can be attributed to the fact that the outer timber plies for these samples were 40 mm thick, and the char front therefore did not reach the first glue line before failure occurred or the heating was stopped.

6.5.4 Failure modes

The failure modes for all specimens that failed structurally (i.e. were no longer able to support the applied load) were observed as global buckling, with rapidly accelerating

deflections and tensile rupture on the unexposed sides of the walls. The ultimate failure of the *material* was tensile rupture on the unexposed side due to secondary bending moments arising from P-Delta effects. It is important to recognise that this rupture ultimately failed the material, but that structural failure occurred earlier, when the deflections grew too large to be sustained by the weakened wall, thereby causing larger bending moments and accelerating deflections. At these deflections points of no return were reached and from the accelerating deflections it can be concluded that the bending moments and thereby the tensile stresses in the unexposed side of the walls would trend towards infinity; therefore, even if the specimens had been fabricated from timber with higher tensile strength they would have failed soon after the walls started to buckle. From the rapidly increasing deflections before failure, which occurred with no audible tension failures, it can also be postulated that compressive yielding (i.e. plasticity) occurred in the heated timber in compression, which would lead to the failures observed for a simply supported wall. This is important to recognise, since fire resistance for CLT is most often determined for floor systems in pure bending, where the modulus of rupture is a major contributing parameter to the load bearing capacity in bending, while the compression strength will often not exert a major influence as extreme compressive stresses will only occur at the unexposed face and therefore unlikely to be affected by heat. In addition, design recommendations [83] for CLT often do not address finer details of deflections, as these are considered to be governing for serviceability conditions and therefore not applicable to fire. The failures observed herein show that excessive deflections are likely to be the primary failure cause in CLT wall systems exposed to fire, and that the reductions in effective elastic modulus must be considered by designers. In addition, the occurrence of shear deflections (as observed in Chapter 5) caused by weakening of the adhesive bond lines may matter greatly since the resulting additional deflections are likely to lead to earlier failure.

6.5.5 Decay phase

The decay phase of a compartment fire was simulated by removal of the exposure heat flux after a predetermined time of heating, thereby inducing a cooling phase in some parts of the timber. As shown by the results in Figure 6.20 and Table 6.5, all of the five ply specimens eventually experienced failure after the heat flux was removed after 25 minutes of heating, while all of the three ply samples, which were heated for 15 minutes, maintained their load bearing capacity until the experiments had to be terminated for safety reasons. To better understand the causes of failure for these two cases, the temperature profiles at different heating durations are shown for both the three and

five ply samples in Figure 6.30. After 15 minutes, when the heat was switched off for the three ply samples, the temperature profiles for all specimens followed similar distributions within the cross-sections, as seen in Figure 6.30 a) and e). After ten more minutes, when the heat was removed for the five ply samples, it can be seen that the three ply samples had cooled down to between 150 and 200 °C, while the temperature profiles for the five ply samples had shifted deeper into the cross-section, as would be expected under the continuous heating. After 45 minutes from the start of the experiments, (i.e. 30 and 20 minutes beyond the point that that the heat flux had been switched off for the three and five ply samples, respectively) the uncharred timber of the three ply samples had cooled further to maximum temperatures around 100 °C. For the five ply specimens in Figure 6.30 g) the temperature did not reduce to the same degree. Instead, while the surface cooled significantly, considerable heat remained within the char and pyrolysis zone; this enabled more heat to conduct deeper into the cross-section, thereby heating and weakening previously cool timber.

From a load bearing capacity perspective the cooling surface zone is irrelevant, since this timber had been heated to over 300 °C and therefore turned to char with no remaining contribution to the load bearing capacity of the wall strips. After an additional 15 minutes, the temperatures within the char layer remained between 250 and 300 °C for the five ply PU specimens, which failed or had failed at this point structurally (i.e. the shown temperature profiles refer to the profile at failure after 59.7 and 53.3 minutes for C5PU050P_01 and C5PU050P_02, respectively), while the temperatures for the MF specimens had cooled down to peak temperatures around 120 °C. Despite this cool down the five ply MF specimens went on to collapse 30 and 45 minutes later.

Their respective temperature profiles at failure are shown separately in Figure 6.31. A continuous cool down from ∼115 to 100 °C occurred between 60 and 90 minutes for C5MF050P_02. Similarly the temperature at 60 mm into the timber cross-section reduced from 74 to 67 °C. However, the temperature at 80 mm cross-section depth (the deepest adhesive line) continued to increase in those 30 minutes from 37 to 45 °C. This demonstrates the high sensitivity of the walls strips' structural stability to small temperature increases in previously unheated sections, and also shows the importance of the non-recoverable heat-induced deflections that were highlighted in Chapter 5, since the cooling at 60 mm cannot compensate for the heat increases deeper in the timber.

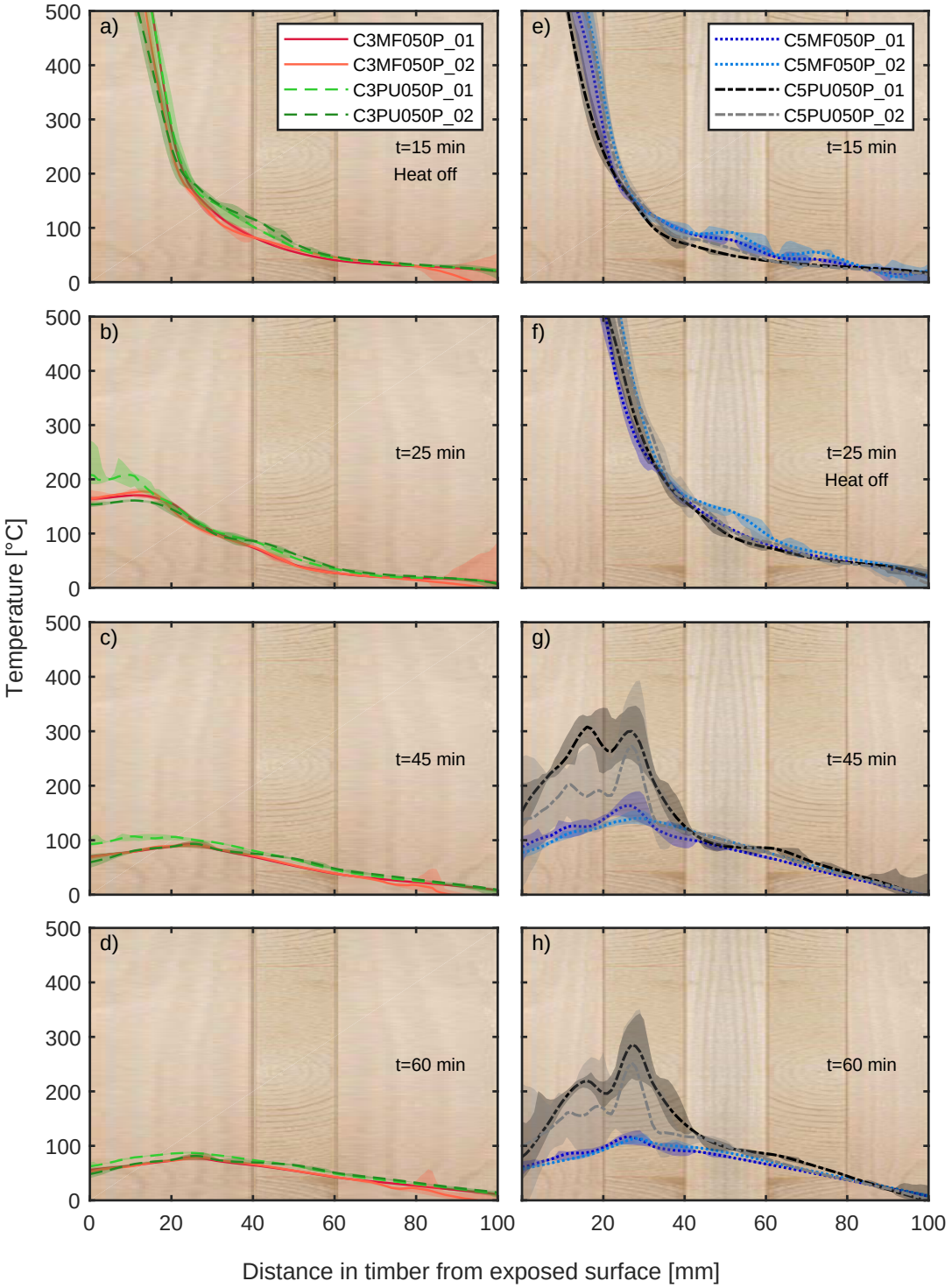

Figure 6.30. Timber temperature profiles versus distance through the cross-section from the exposed surface. 90 % confidence intervals of the temperature profiles are shown as shaded areas.

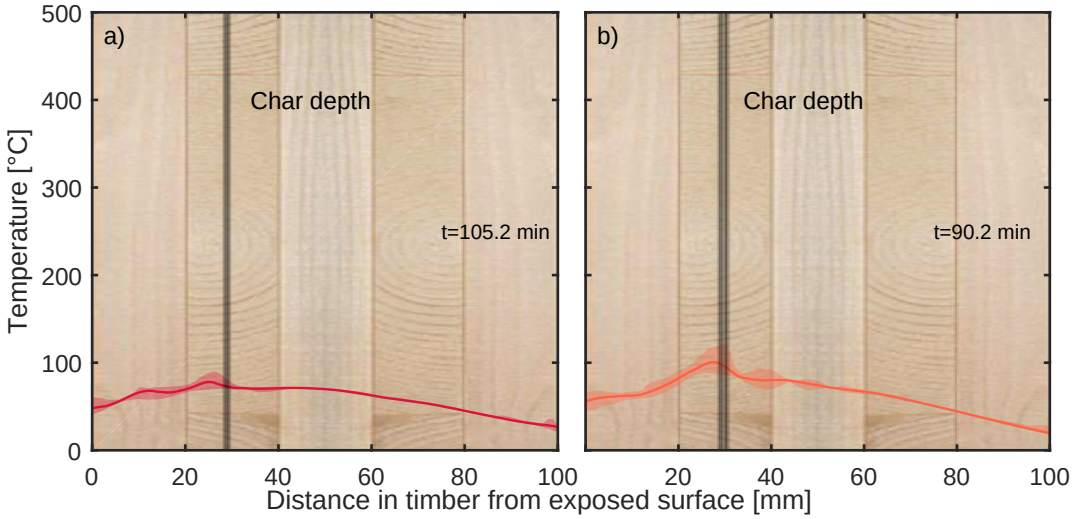

Figure 6.31. Timber temperature profiles versus distance through the cross-section from the exposed surface for a) C5MF050P_01 and b) C5MF050P_02 at their respective times of failure. 90 % confidence intervals of the temperature profiles are shown as shaded areas.

From the plots in Figure 6.30 g) and h) it can be seen that the specimens with five plies and bonded with polyurethane adhesive type retain much more heat during the cooling phase of the timber compared to the specimens bonded with melamine formaldehyde. One possible explanation for this could be that the PU specimens experienced char fall-off, while this was not observed for those bonded with MF. However, any increase in heat into the timber from char fall-off would have to occur before the heat was removed and at this point, as shown in Figure 6.30 g), there was no evidence of a difference in heat profile between the two adhesive types. If anything, a reduction in char layer would aide the cooling process as it would remove insulation from the heated zone. Two possible alternative hypotheses can be put forward for the elevated temperatures in the PU samples in the cooling phase; (1) the polyurethane adhesive itself contributes to heat generation in pyrolysing timber and smouldering char and (2) the occurrence of char fall-off generates inlets for air (and thereby oxygen) to penetrate into the char layer and aides a smouldering combustion process. At this point these hypotheses are merely conjecture and it is not the focus of this thesis to investigate ongoing combustion phenomena in any depth. One argument against (1) is that if the adhesive contributed significantly to heat generation, then this would be expected to show as spikes in temperature near the glue lines, however, this is

not the case in Figure 6.30. Given the relatively small sample size there is also the possibility that the observed temperature increases are coincidental. Whatever the cause for the elevated temperatures in the PU bonded CLT is clearly not beneficial to the load bearing capacity during the fire decay phase, and as seen above as well as in chapters 4 and 5, samples bonded with PU already appeared to be performing worse structurally than their MF counterparts, even under equal thermal conditions. Given the apparent prevalence of one component polyurethane adhesive formulations in CLT production this is perhaps an area that warrants further research on a smaller scale to understand the thermal boundary conditions arising in polyurethane bonded timber products during both the fire growth and decay phases.

The temperature profiles in Figure 6.30 show a reasonable repeatability between specimens and also between different ply configurations and adhesive types (apart from the already discussed deviations in the cooling phase for the five ply samples), highlighting the suitability of this experimental set-up for comparative analysis. It was observed that the 90 % confidence intervals of the temperature profiles were narrow, apart from regions where rapid changes of the temperatures with depth occurred. This suggests that drilling TC holes by robot and the location and spacing of the thermocouples is a suitable method for experiments and analysis such as that presented herein.

6.5.5.1 Implications

The failure of the five ply specimens in cooling shows that the decay phase of a fire should be considered by designers when the possibility of structural collapse is considered, as had been postulated by previous research [147, 148, 173]. The original intent of fire resistance furnace tests was to generate a fire severity that implicitly accounted for burnout, and therefore inherently for a decay phase. Modern fire resistance ratings are based on a perceived risk factor of a compartment based on its occupancy type and height; the decay and subsequent cooling phases of a fire are therefore not necessarily considered. At 15 and 25 minutes of heating duration the heating consisted of about 75 % and 74 % of the lowest observed failure time from experiments heated to failure for three and five plies respectively. This constitutes a relatively long heating duration (relative to the failure time) and it could be argued that fire resistance times from furnace tests will have sufficient margin of safety on the fire severity to ensure that CLT walls will survive a cooling phase. There are two counter points to this: (1) this supposed margin of safety arising from fire resistance testing in furnaces is not quantifiable in engineering terms, and (2) the fraction of applied heating duration for

the five plies (which all collapsed) to the longest time to failure from the experiments to failure (see Table 6.4) was 60 %.

It can be postulated that the fractional heating time required to induce failure in the cooling phase is not linear to the potential failure time, since both ply sample groups were heated to equivalent fractional heating durations but only the longer (in real time) heated five ply samples passed a point of no return that led to failure. Clearly, a combination of thermal and structural effects makes this a complex problem to consider. As the heating duration increases, more heat is stored in the timber and this will not only cause heating deeper into the timber in the cooling phase but also increases the probability of smouldering to manifest and to generate more heat even after the original fire has decayed. In addition, the occurrence of deflections penalises the load bearing capacity with interest, i.e. at later stages in the fire smaller deflection increments become more critical due to the already existing deflected shape of the wall. The potential for structural collapse during or after the decay phase is not unique to timber, and recent research by Gernay et al. [226, 227] proposed to shift the focus for structural fire safety assessment from a fire resistance concept to a burnout assessment. As seen in the results presented in this study, this problem is considered especially critical for timber because (1) its strength and stiffness retention is affected at relatively low temperatures (as compared to concrete and steel), and (2) it is possible for a structural timber element to keep supplying heat to itself through exothermic reactions, even where flames extinguish.

6.5.6 Moisture movement

For the samples exposed to a low heat flux, water was observed to flow out of the thermocouple holes on the unexposed side for three ply samples but not for those consisting of five plies. This can possibly be attributed to the different thickness between the two ply numbers. For the samples with five plies, the plies had a thickness of 20 mm, compared to 40 mm for the outer boards in the three ply walls. This means that a moving moisture front encountered a cross layer earlier in a five ply than a three ply specimen. The permeability of timber varies with grain orientation and is higher parallel to the grain than perpendicular; in a cross ply the water was therefore given a different 'path of least resistance' to *drain* away from the heat front rather than moving deeper in the timber. In the absence of any moisture measurements for these experiments this theory is conjecture, and the deeper investigation of moisture movements is not an objective of this study. However, this indicates that the ply configuration is another factor to consider for the detailed modelling of heat and mass transfer in CLT.

6.6 Conclusions

This chapter presented details of an experimental series on the load bearing capacity of CLT wall strips during severe heating. Set-up and results from samples with four different heating exposure scenarios were presented.

The simply supported wall strips were concentrically loaded to a 50 % of their manufacturer recommended load limit, resulting in applied loads of 60 and 78 kN for five and three ply CLT respectively, and then exposed to a constant incident radiative heat flux while the load was sustained. Due to the effect of charring and heat the samples developed load eccentricity with increasing experimental durations, which ultimately led to global buckling failure with runaway lateral deflections. The main findings are summarised below.

- A statistically significant influence of the adhesive type in the CLT on the compressive load bearing capacity in fire was observed. Specimens that were using a polyurethane adhesive type consistently failed earlier than those bonded with a melamine formaldehyde adhesive type. The median normalised failure time for PU bonded samples was 20 % less than for a median sample with a nominally 'neutral' adhesive, and 36 % less than a median MF bonded CLT wall strip. In addition, char fall-off was observed for PU bonded CLT but not for the MF bonded samples; it is suggested that this was independent of, and did not cause, the reduced structural capacity in fire for the PU samples.
- Specimens with three plies, which had thicker outer plies, had a reduced time to failure as compared with five ply specimens, with the median normalised failure times for three plies being 17 % less than the overall median failure times. This is thought to be linked to increased shear stresses in the three ply layers. In addition, faster deflection rates and earlier failures in three ply samples were linked to the fact that three ply samples do not have a 'sacrificial' crosswise layer that can slow down the overall loss in cross-section.
- The failure modes for the wall elements were global buckling, and runaway deflections indicated compressive yielding as a cause of failure. This highlights that a loss in stiffness and accumulated lateral deflections, rather than a loss in material strength, should be considered as the primary failure mode for CLT walls in fire.
- Failure in the fire decay and timber cooling phase was observed for five ply samples but not for three ply samples, after both sample groups had been subjected

to heating durations of 15 and 25 minutes for three and five plies respectively, which corresponded to ∼75 % of their expected minimum failure time. Structural collapse in the cooling phase was determined as a complex interaction of thermal and structural factors wherein prior heating both induced eccentricities, which increased the probability of subsequent unstable behaviour, and also caused in-depth heating which then continued to weaken the walls after the initial heat flux exposure was removed.

The results presented in this study showcase a novel experimental approach that resulted in multiple novel findings. The importance of the adhesive type is shown not only for fire dynamics considerations but also for the overall structural capacity of CLT wall systems. This research highlights that CLT is a complex composite system and that its fire behaviour can be improved by careful multi parameter consideration of the individual aspects of the system.

The failure of CLT walls in the fire decay phase was, for the first time, demonstrated through a systematic experimental program; this highlights the need for designers to consider the possibility of failure as heat moves within CLT and the issues arising from an non inert material that can continue to generate its own heat in-depth, even after a primary heat source has self-extinguished.

CHAPTER 7

Analysis

This page is intentionally left blank.

This chapter contains a more in-depth investigation into the findings in Chapter 6 to determine the importance of individual input parameters and to highlight the requirement for critical understanding to successfully model the structural performance of CLT walls or columns in fire.

The chapter reviews some basic concepts of instability and how they can be represented numerically by simplified structural models. A hybrid modelling approach is used to estimate the bending moment and shear force diagrams in the wall strips tested in Chapter 6; this is subsequently used to illuminate the stress distributions within the CLT cross-sections with progressing burning duration, and to highlight areas where additional research may be warranted.

7.1 Buckling Theory and Analysis

All the tested wall strips, both at ambient and elevated temperatures, in Chapter 6 failed due to instability, which could be identified by rapidly accelerating lateral deflections at mid height of the specimens. To better understand this behaviour, the following sections provide a summary of the mechanical considerations that cause global buckling.

Since the boundary conditions for the tested wall strips consisted of continuous pinned connections along their width, the behaviour of the wall strips can be approximated as those of slender columns; the buckling of such columns is best described from the simplest case: a pinned-pinned column, subjected to an axial load, as shown in Figure 7.1 a).

Due to the symmetric support conditions it is assumed that, when a critical buckling load is applied, the column will deflect sideways to follow an alternative bifurcated load path, and that the deflection, v, will have its greatest value at the mid-height of the column. The equilibrium of moments along the height, x, of the column (see Figure 7.1 b)) when buckling occurs can then be described as shown in Equation 7.1. The solution to this second order linear differential equation is shown in Equation 7.2, where α is a summary of the terms involved in Equation 7.1, as shown in Equation 7.3.

$$\frac{d^2v}{dx^2} + \frac{Pv}{EI} = 0 \tag{7.1}$$

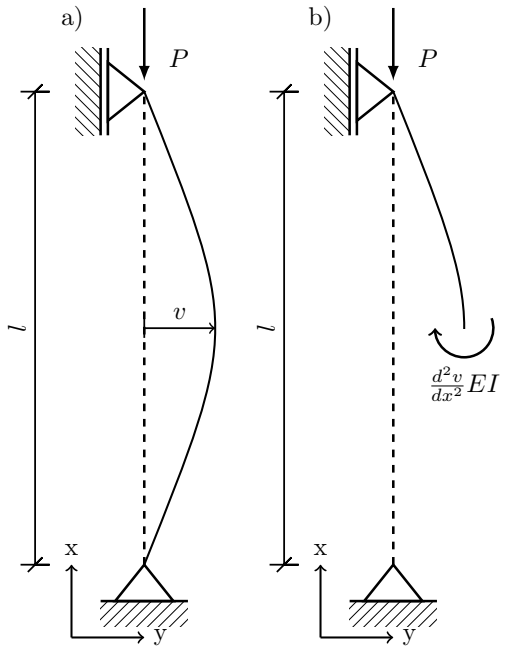

Figure 7.1. a) assumed deflected shape, and b) bending moment equilibrium in a pinned-pinned column at its critical buckling load.

$$v = A \cdot \sin(\alpha x) + B \cdot \cos(\alpha x) \tag{7.2}$$

$$\alpha = \sqrt{\frac{P}{EI}} \tag{7.3}$$

The boundary conditions of a pinned-pinned column necessitate that $v = 0$ at $x = 0$ and that $v = 0$ at $x = l$, giving $B = 0$ and Equation 7.4 as possible solutions.

$$A \cdot \sin \alpha l = 0 \tag{7.4}$$

If $A = 0$ the deflection remains zero for all x, which refers to an unstable equilibrium load path and is of no interest for the problems investigated in this thesis; from a structural point of view the solution of $\sin \alpha l = 0$ is more relevant and this condition is given if Equation 7.5, where n is an integer between zero and infinity, is satisfied. Combining equations 7.3 and 7.5, and recognising that the critical (i.e. lowest) buckling load will occur for $n = 1$, the so called Euler buckling load for a pinned-pinned column can be described analytically by Equation 7.6

$$\alpha L = n\pi \tag{7.5}$$

$$P_{crit} = \frac{\pi^2 EI}{l^2} \tag{7.6}$$

Generally speaking, varying inherent eccentricities will prevent the Euler buckling load from being reached, as these eccentricities will induce increasing lateral deflections as the load is increased and approaches the buckling load [65, 98]. Material failure (due to bending moments arising from P-Delta effects) will eventually cause failure somewhat before the Euler buckling load is reached.

The following paragraphs describe the derivation to obtain an expression for the mid-height deflections in columns or walls subjected to eccentric loading.

Eccentricities arising in walls from a progressing heating (charring) front can be simplified to an eccentrically loaded column, for which the moment equilibrium is shown in Equation 7.7 where e_c denotes the eccentricity between a concentrically applied load and the elastic centroid of the heated section. Applying the same boundary conditions as for the pure Euler buckling described in equations 7.1 to 7.6, the deflection along the wall height can be described as shown in Equation 7.8.

$$\frac{d^2v}{dx^2} + \frac{Pv}{EI} + \frac{Pe_c}{EI} = 0 \tag{7.7}$$

$$v = e_c \cdot \left[\tan(\frac{\alpha l}{2}) \sin(\alpha x) + cos(\alpha x) - 1 \right] \tag{7.8}$$

The highest deflections in a buckled wall occur at its mid height, therefore setting x equal to $l/2$ in Equation 7.8, yields Equation 7.9, which can be used to describe the mid-height deflection of a wall with known eccentricity and known applied load. A variant of Equation 7.9, which is also sometimes referred to as 'the secant formula' has previously been used by Suzuki et al. [113]. Equation 7.9 will be used later in this chapter to inform and validate a proposed simplified modelling approach with regards to the wall strips that were tested in Chapter 6.

$$v_{\frac{l}{2}} = e_c \cdot \left[\sec(\alpha \frac{l}{2}) - 1 \right] \tag{7.9}$$

7.2 Deflected shapes

From Equation 7.1 it is evident that eccentricities, horizontal deflections, and therefore the deflected shape of a wall have a significant influence on its load bearing capacity. This section therefore investigates the deflected shapes from the experiments on wall strips presented in Chapter 6. From the tracked circles along the edge of the wall strips (refer to Subsection 6.4.1.5) the deflected shape can be obtained for each moment in time. The positions of the tracked circles at selected time steps are shown in Figure 7.2 for the two repeats of melamine formaldehyde bonded three ply walls under "high" heating exposure (which consisted of a mean radiant heat flux of 51 kW/m^2, see Subsection 6.4.1.3 to failure. In addition, a sinusoidal curve in the form of Equation 7.10 was fitted to the deflected shape and is also shown, including its confidence intervals. The deflected shapes for three ply walls bonded with a polyurethane adhesive are shown in Figure 7.3. From these figures it can be seen that the fitted sine curves give a reasonable approximation of the deflected shapes, as would be expected from theoretical considerations on buckling outlined in Equation 7.1.

$$v = a \cdot \sin(b \cdot x + c) \tag{7.10}$$

7.2.1 Bending moments along walls

From the deflected shapes it is clear that increasing bending moments will develop along the height of the walls. These bending moments are caused by second order P-Delta effects between the initially concentric applied load and the developing eccentricities. Initial eccentricities are caused by the weakening of the cross-section due to heating and charring, and these initial eccentricities are the cause of initial moments. These cause further deflections, which then cause secondary moments, and further deflections.

The bending moments along the height of the wall strips, caused by the sum of the P-Delta effects just before failure, can be obtained from the deflected shapes that are displayed in figures 7.2 and 7.3. As should be expected, the bending moment distribution at failure in Figure 7.4 follows the same sinusoidal shape along the wall height as the deflected shape. It can be seen that, again as expected, the maximum bending moments occur at mid-height of the columns and these range between 1.9 and 4.6 kNm. More interesting than the actual magnitudes are the shape of the distribution of moments, since this allows an assessment of the shear forces acting along the wall

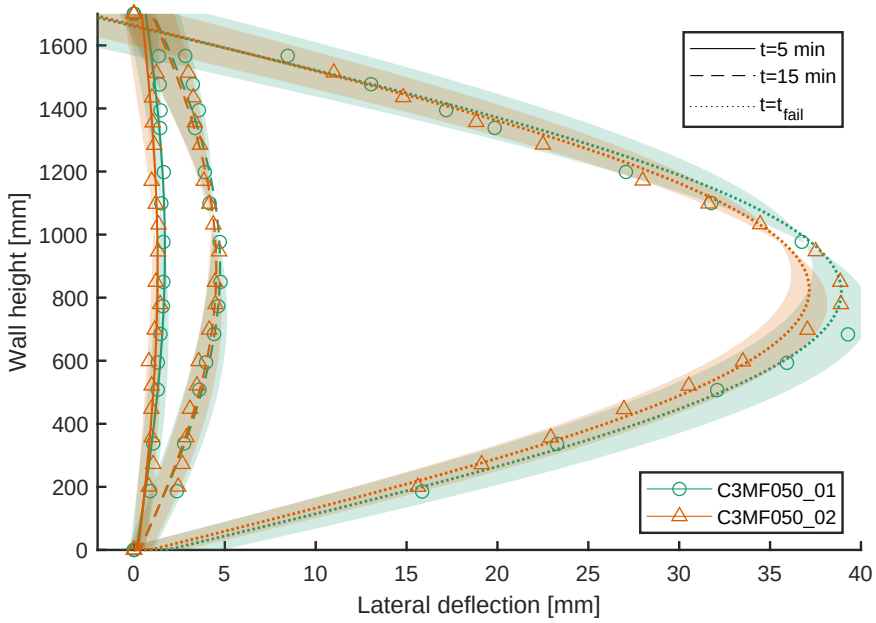

Figure 7.2. Vertical and horizontal position of tracked points on three ply melamine formaldehyde adhesive CLT wall and fitted sine curves at selected time steps.

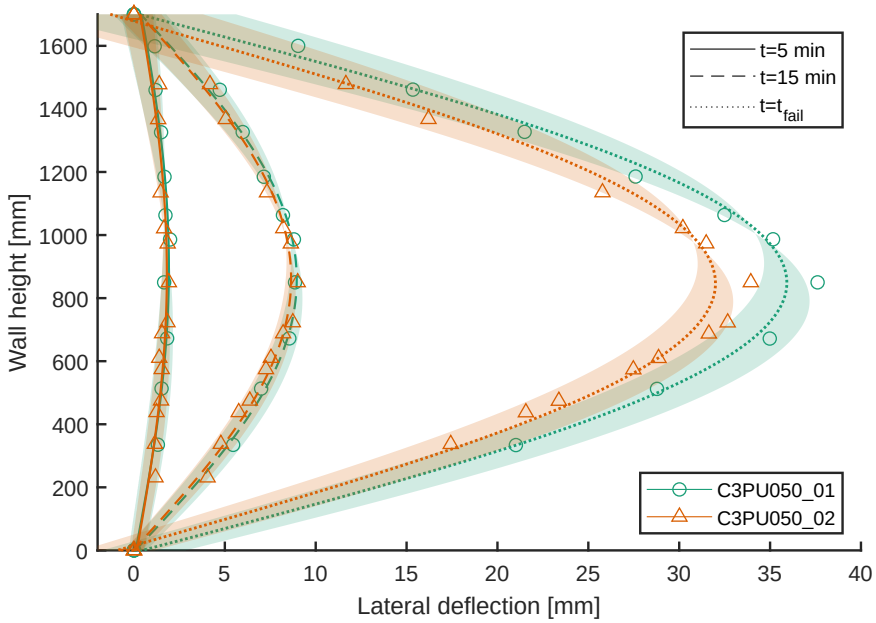

Figure 7.3. Vertical and horizontal position of tracked points on three ply polyurethane adhesive CLT wall and fitted sine curves at selected time steps.

strips.

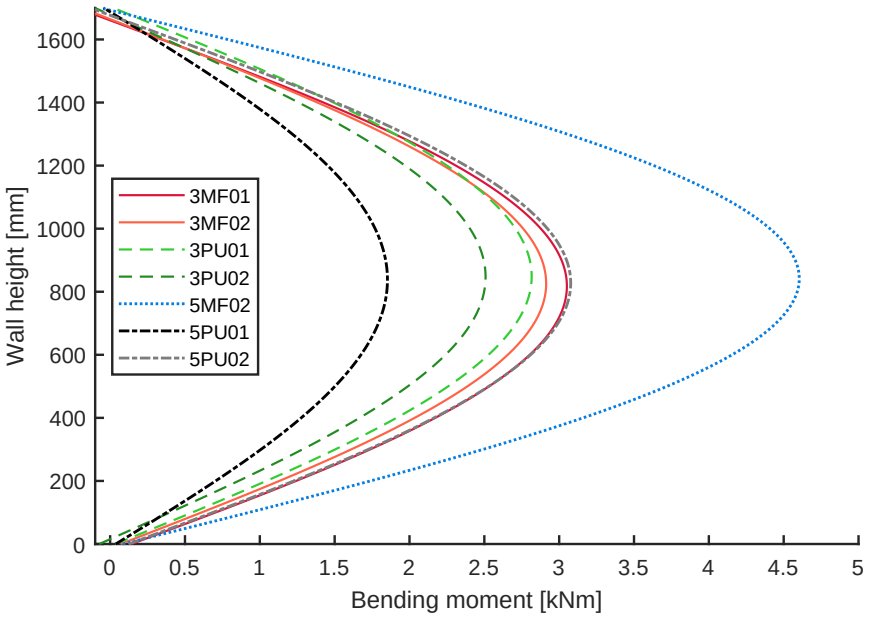

Figure 7.4. Bending moment diagrams from deflected shapes just before failure for walls exposed to "high" heat flux exposure until failure.

7.2.2 Shear along wall height

Elements that are loaded concentrically in plane are not subject to out of plane shear forces, however, this changes with the introduction of eccentricity due to one sided heating. As can be seen in Figure 7.4, the bending moment changes along the height of the wall strips. By definition, this means that shear forces are present in the wall strips to balance forces arising from bending stresses over the height. The shear force, V, can be calculated from the slope of the bending moment, M, along the height, x, of the wall using Equation 7.11. The resulting shear force diagrams from the bending moments in 7.4 are shown in Figure 7.5; it is observed that the highest shear forces occur near the supports and that the shear force is zero at mid height, where symmetry stipulates zero rotation. This means that the highest shear forces do not coincide with the heated region in these tests. The highest shear forces affecting the heated cross-section occur on the edge of the heated section with an absolute value range between 1 and 2.5 kN.

$$V = -\frac{dM}{dx} \tag{7.11}$$

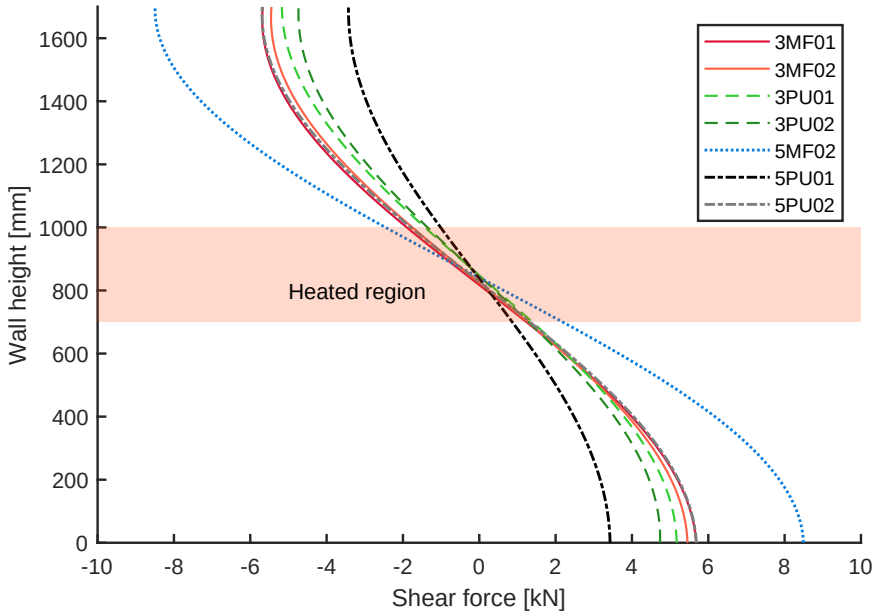

Figure 7.5. Predicted shear force diagrams from deflected shapes just before failure for walls exposed to "high" heat flux exposure until failure.

7.2.3 Stress profiles

The reduction in stiffness of timber is generally assumed to be less severe for tension, compared to compression (refer to Subsection 2.4.1), and this introduces additional complexity into the analysis of timber structures; the elastic modulus distribution in a cross-section will depend on the location of the neutral axis, which in turn depends on the distribution of the elastic modulus in the cross-section.

From the deflected shape along the wall height the curvature κ can be obtained from Equation 7.12, where v is the lateral deflection along the height of the wall, x. Since the applied load was kept constant throughout the experiments it can be used in conjunction with the curvature to determine the stress profile within the cross-section of the walls with increasing heating duration. The stress profile is found from equilibrium of the applied forces, as shown in Equation 7.13. σ denotes the axial stress and is determined by Equation 7.14, where y_i is the distance of each slice in the cross-section from its geometric centre, na is the position of the neutral axis, and E_i is the elastic modulus of timber at this position in the cross-section, according to its temperature, orientation (i.e. parallel or crosswise to the main loading direction), and stress state. Timber in

compression is assumed to follow an elastic-perfectly plastic constitutive relationship, i.e. the stress in fibres, where the stress is equal to or exceeds the yield strength, is set to the yield strength, as shown schematically in Figure 7.6. The yield strength is assumed to vary with temperature in accordance with the strength reduction recommendations from the Eurocodes [145] for timber in compression. This follows a bilinear reduction trend with a strength retention of 25 % at 100 °C and 0 % at 300 °C (char) and above. Similarly the elastic modulus is reduced in accordance with the Eurocodes, with a 100 °C breakpoint of 35 %. The Eurocode reduction curves were chosen over the determined reduction curves in Chapter 4 since no reliable reduction correlation was found for the elastic modulus. The compressive yield strength at ambient temperatures for the stress profiles herein is assumed as 39.7 MPa, determined from experiments presented in Chapter 4. Resulting stress profiles from this hybrid modelling approach are shown in figures 7.7 and 7.8 for a three and five ply wall strip exposed to "high" heat flux, respectively.

$$\kappa = \frac{d^2v}{dx^2} \tag{7.12}$$

$$\sum_{i=1}^{n_s} \sigma_i \cdot A_i - P = 0 \tag{7.13}$$

$$\sigma_i = \kappa \cdot (na - y_i) \cdot E_i \tag{7.14}$$

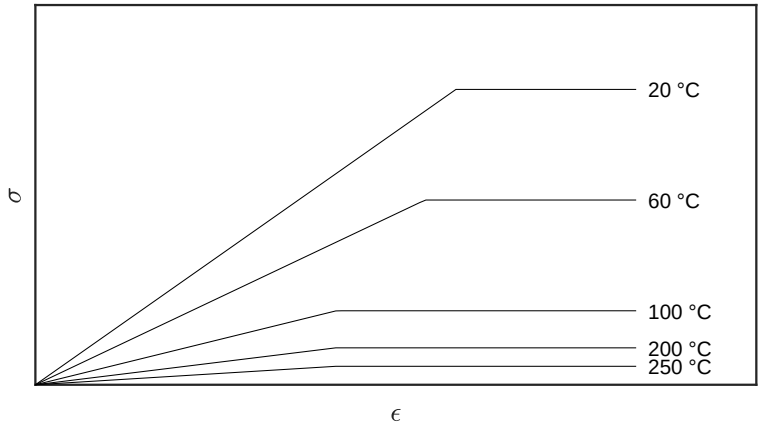

Figure 7.6. Assumed stress strain relationship at multiple temperatures.

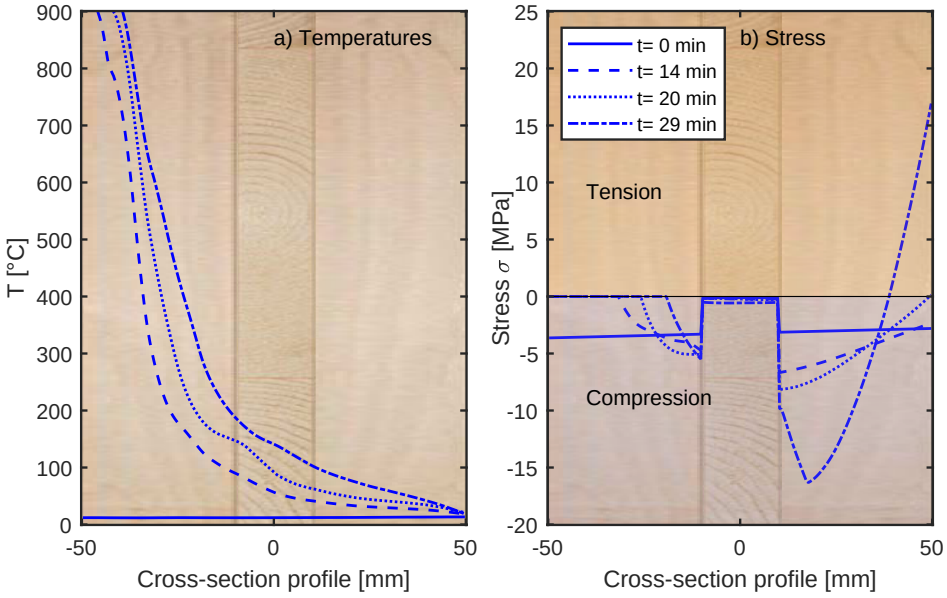

Figure 7.7. Profiles of a) temperature and b) stress through a three ply MF bonded specimen under full exposure at fractional times of 0, 0.5, 0.75 and 1 of the observed failure time.

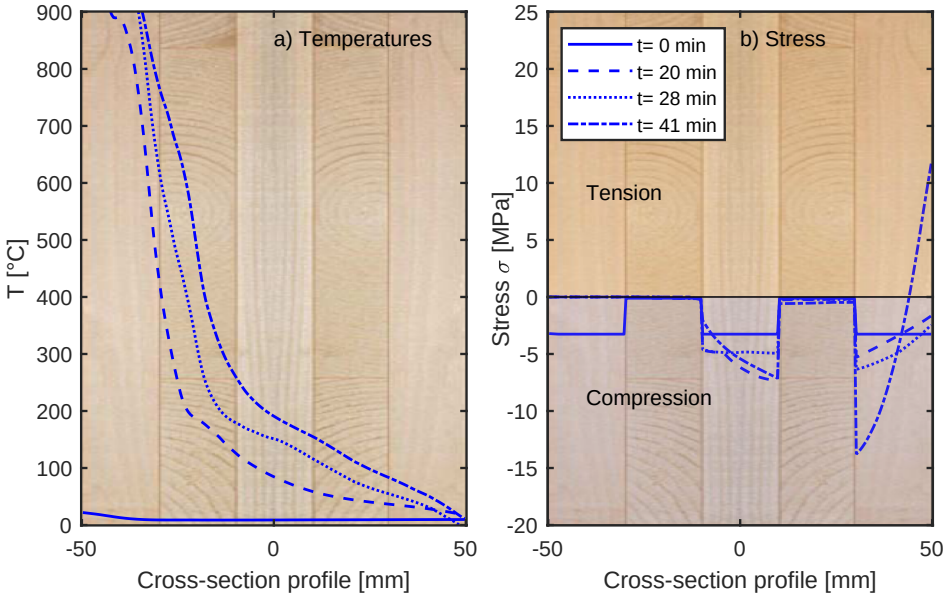

Figure 7.8. Profiles of a) temperature and b) stress through a five ply PU bonded specimen under full exposure at fractional times of 0, 0.5, 0.75 and 1 of the observed failure time.

The detailed consideration of the assumed stress profiles offers multiple helpful insights to better understand the structural behaviour and the special considerations needed to represent the buckling of CLT walls numerically.

7.2.3.1 Significance of stress mode for elastic modulus reduction

As mentioned above, the assumption that the elastic modulus reduction varies between timber in compression and timber in tension excludes exact solutions and introduces the need to iterate towards a 'correct' solution. From the stress distributions in figures 7.7 and 7.8, it can be seen that tension stresses only became significant towards the end of the experiments. At the same time, the temperature profile through the cross-section suggests that the temperature increase in the tension zone was moderate; this raises the question whether the difference in elastic modulus retention is significant to the overall stress distribution or if this can be considered negligible to the overall structural behaviour. The bending moments about the cross-sections' geometric centres resulting from the stress distributions can be computed for two cases: (1) the consideration of both tension and compression in the determination of the reduction in elastic modulus, and (2) the assumption that the whole cross-section is in compression. The relative difference between these two moments is shown in Figure 7.9 for two wall strips.

It is observed that the error between the two calculation procedures remains close to zero for the majority of the experimental time, which has been normalised against the test duration. At some points the error can be seen to jump before reverting to small values again; these peaks occurred when the direction of the moments about the cross-section centre changed, and since this happened at slightly different times for the two procedures, large momentary errors occur. These peaks are more a numerical problem rather than a reflection of the differences in stress, and overall the errors between the procedures are small, suggesting that the distinction between tension and compression for the reductions in elastic modulus can be considered negligible and that the cross-section can be simplified to act in compression only to determine the retained elastic modulus of heated timber.

7.2.3.2 Tensile stress development

The stress profiles from the modelling above can also be used to read and assess the development of tensile stresses on the unexposed face of the CLT and their development within the normalised experimental duration. The extreme fibre tensile stresses for

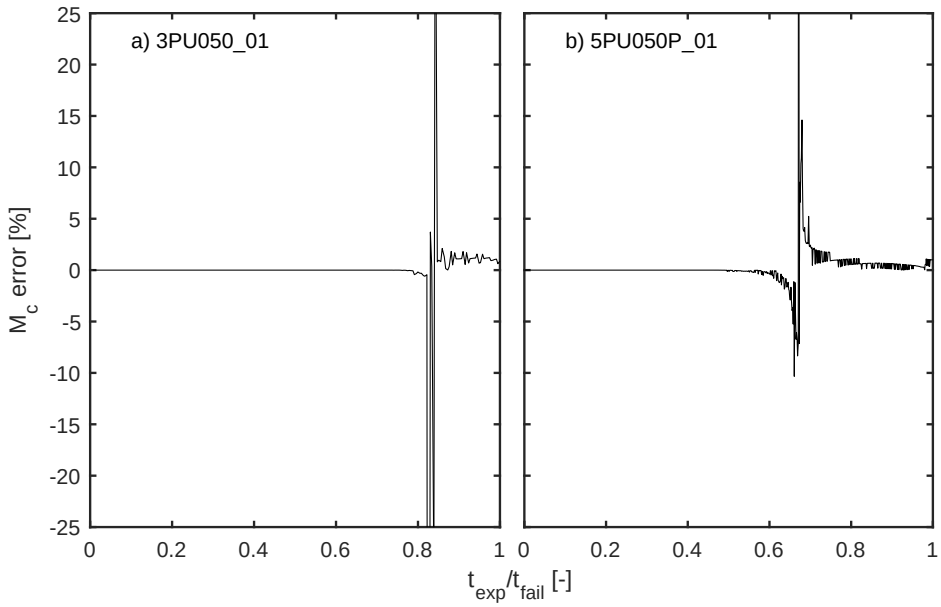

Figure 7.9. Percentage errors between calculation procedures assuming only compression, and separate tension and compression reduction plotted against normalised experimental duration.

selected wall strips of the "high" heat flux exposure to failure series are graphed in Figure 7.10. The exponential increase of tensile stresses during structural failure can clearly be identified and correspond to the runaway deflections that were observed in Chapter 6. The increasing tensile stresses can also be quantified in the context of the normalised time via a slight extension of the exponential fits. A theoretical 5 % increase in experimental duration (to a normalised time of 1.05) causes a 32 % increase in tensile stress for specimen 3MF050_01 and a 598 % increase for 5MF050_02. These assessments suggests that, to successfully assess failure for axially loaded CLT walls in fire, the failure criterion should be based on the lateral deflection and compressive yielding, rather than exceedance of the modulus of rupture or tensile strength.

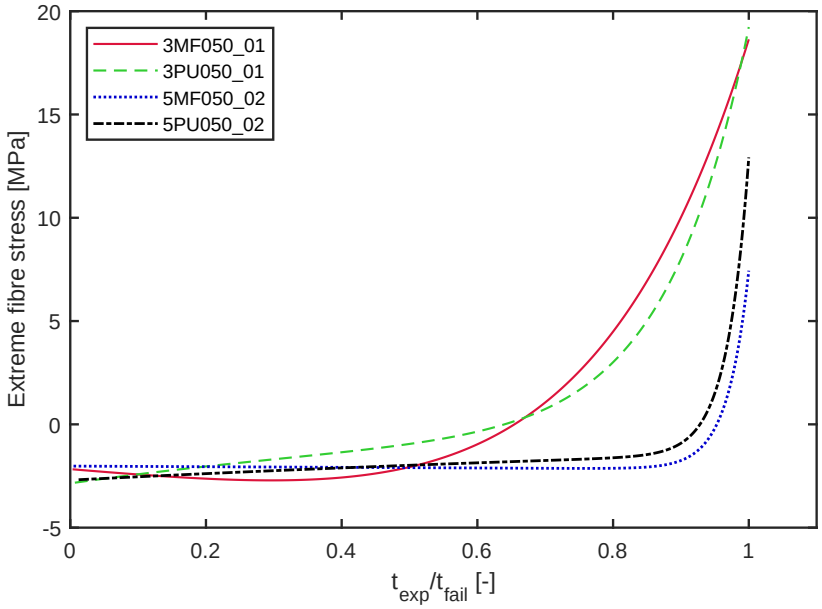

Figure 7.10. Tension stresses as exponential functions at the unexposed face plotted against normalised experimental duration.

7.3 Local heating allocation

As shown in Equation 7.1, analytical solutions are available to calculate the deflections of buckled columns and walls based on the underlying mechanics. However, these solutions are limited to cases where the mechanical properties are constant along the length of the assessed element.

In some (experimental or real) situations, a column or wall will not be exposed to fire uniformly and its mechanical properties will therefore vary along its length or across its surface. This was the case for the wall strip experiments presented in Chapter 6. To appropriately model these cases it is necessary to approximate the analytical solutions numerically; this can be achieved by dividing a column into multiple smaller elements and then assigning each element its respective mechanical properties, i.e. damaged by heating or assumed at ambient temperatures.

For the simulations in this thesis, the wall strips were represented by Euler-Bernoulli beam-column finite elements; this procedure is also often referred to as a direct stiffness approach. The initial lateral deflections are modelled as uniform bending moments equal to the product of the applied load and the eccentricity arising from the

heat induced loss of elastic modulus in the cross-section. The deflections arising from this bending moment are calculated from the global stiffness matrix and the resulting additional bending moments are applied to the system iteratively until the arising deflections (and resulting bending moments) are below a set tolerance (herein somewhat arbitrarily chosen as 0.001 mm of increase in deflection) and convergence is achieved.

The validity of this approach is assessed below for a simple case where a wall is exposed to a constant rate of charring across its whole cross-section. Since the analytical solution for this case is known, it can be compared to the numerical procedure of incremental moments described above. The deflection paths for a theoretical load application of 5 % of the ultimate buckling load of both a three and a five ply CLT wall heated from one side with a theoretical constant charring rate of 1 mm/min are shown in Figure 7.11. The load deflection paths show the close approximation of the numerical iterative approach to the analytical one and suggests that the eccentricity induced buckling can be approximated by the chosen numerical approach to enable the specification of multiple elements along the height of the simulated wall strips.

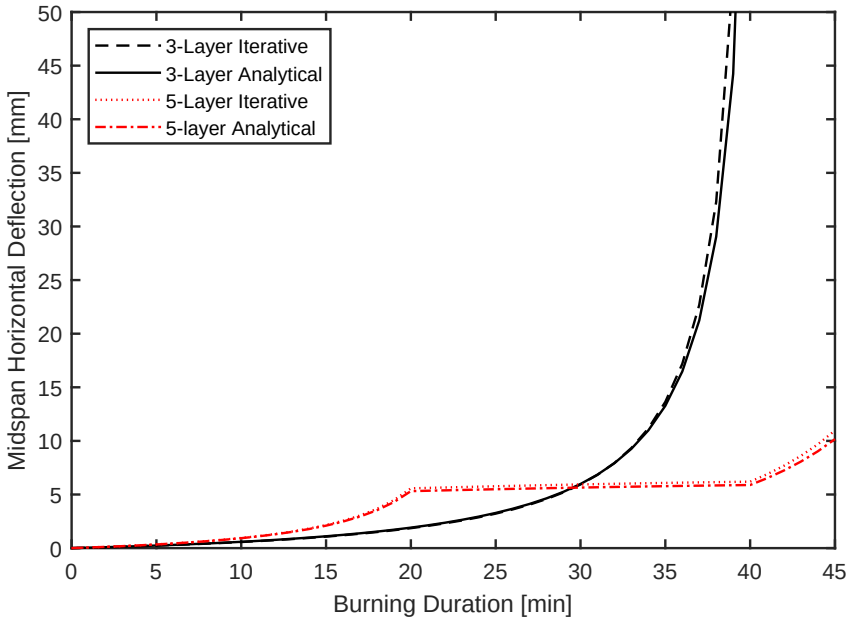

Figure 7.11. Comparison of analytically and iteratively calculated midspan lateral deflections for a CLT column loaded to 5 % of its ultimate buckling load.

7.4 Model approach

7.4.1 Input parameters

In order to simulate the observed experimental deflections, input parameters are required for the model in this chapter. The three main parameters that are required are the elastic modulus, the compressive yield strength, and the temperature profile through the cross-section.

A distribution of 1000 possible cases has been created for the two mechanical input parameters; it is based on the measured compressive yield strengths observed in Chapter 4, which suggested a mean strength of 36.7 and 43.1 MPa for three and five ply CLT, respectively. For the elastic modulus the recommended mean expected value [96] of 11,600 MPa is assumed for both ply configurations. Coefficients of variance (CoV) of 20 and 13 % are assumed for strength and elastic modulus, respectively, and for both parameters a lognormal distribution is assumed [201]. The correlation factor between these parameters is assumed as 0.6 [201]. The resulting mechanical input parameters are shown in Figure 7.12. Based on the observations in Subsection 7.2.3.2 it is assumed that the failure is caused by runaway deflections and the influence of tensile stresses on material failure is negligible, therefore no tensile stresses are assumed for the proposed model.

The temperature profile can be estimated from the thermocouple readings at each time step. Uncertainty in the temperature measurements is accounted for through the bootstrap approach that is explained in Appendix B Subsection B.1.1. The simulations herein are based on a bootstrap sample size of 1000, and for each simulation run a set of the correlated mechanical input parameters is paired with on temperature profile estimation, thereby accounting for uncertainty in all three major input parameters.

7.4.2 Elements

The wall strips were modelled using direct stiffness or Euler-Bernoulli beam column elements, which are described by the stiffness matrix shown in Equation 7.15, where E is the elastic modulus, A is the cross-sectional area, I is the second moment of area, and L is the length of the element considered.

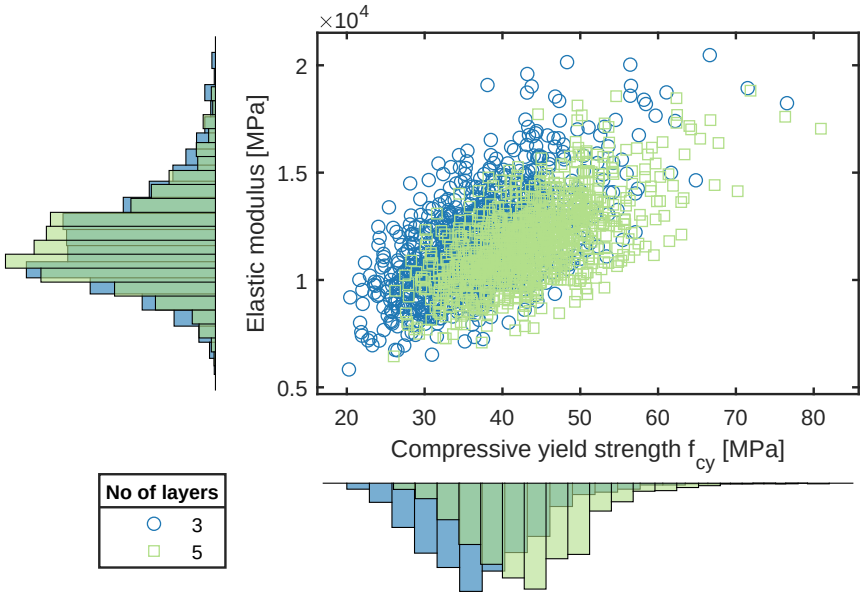

Figure 7.12. Distribution and correlation of compressive yield strength and elastic modulus as model input parameters.

$$K = \begin{bmatrix} \frac{EA}{L} & 0 & 0 & -\frac{EA}{L} & 0 & 0 \\ 0 & \frac{12EI}{L^3} & \frac{6EI}{L^2} & 0 & -\frac{12EI}{L^3} & \frac{6EI}{L^2} \\ 0 & \frac{6EI}{L^2} & \frac{4EI}{L} & 0 & -\frac{6EI}{L^2} & \frac{2EI}{L} \\ -\frac{EA}{L} & 0 & 0 & \frac{EA}{L} & 0 & 0 \\ 0 & -\frac{12EI}{L^3} & -\frac{6EI}{L^2} & 0 & \frac{12EI}{L^3} & -\frac{6EI}{L^2} \\ 0 & \frac{6EI}{L^2} & \frac{2EI}{L} & 0 & -\frac{6EI}{L^2} & \frac{4EI}{L} \end{bmatrix} \tag{7.15}$$

The elements themselves are subdivided into 100 slices and each slice is assigned an elastic modulus, strength, and second moment of area. The elastic modulus and strength of each slice at each time step are dependent on its temperature and orientation and the value of EI in Equation 7.15 is then obtained as the sum of $E_i I_i$ of all slices, and the same approach is taken for EA.

For each element a B-matrix is defined as shown in Equation 7.16, where $\mathbf{y}$ is a vector containing the vertical coordinates of the centroids of each slice, and x is the position along the longitudinal axis of the element. The B-matrix is then used to relate the nodal deflections $\mathbf{v}$ to the axial strains $\boldsymbol{\epsilon_x}$ in each slice of the element considered, as shown in Equation 7.17.

$$B = \left[-\frac{1}{L} \quad \frac{-\mathbf{y}\cdot(12x-6L)}{L^3} \quad \frac{-\mathbf{y}\cdot(6xL-4L^2)}{L^3} \quad \frac{1}{L} \quad \frac{-\mathbf{y}\cdot(-12x+6L)}{L^3} \quad \frac{-\mathbf{y}\cdot(6xL-2L^2)}{L^3} \right] \tag{7.16}$$

$$\boldsymbol{\epsilon_x} = B \cdot \mathbf{v} \tag{7.17}$$

7.4.3 Simulation procedure

The simplified direct stiffness approach is illustrated in Figure 7.13, which shows an approximated sketch of the original deflected shapes of the Euler Bernoulli elements. This is shown as an illustration and the actual simulation utilises more elements to reflect the heated region and its curvature more accurately. The initial bending moment, M_c, due to the eccentricity from charring, e_c at each time step is calculated according to Equation 7.18. This moment, will cause additional deflection e_s along the column height, from which further moments arise, as shown in Equation 7.19. The deflections e_s at each iteration step n are calculated from the direct stiffness matrix and the nodal loads (which contain the moments caused by the previous iteration's deflection $e_{s,n-1}$) are calculated according to Equation 7.20, where K is the global stiffness matrix.

$$M_c = P \cdot e_c \tag{7.18}$$

$$M_s = \lim_{n\to\infty} \sum_{i=1}^{n} P \cdot e_{s,n} \tag{7.19}$$

$$e_{s,n} = K^{-1} \cdot [P \cdot e_{s,n-1}] \tag{7.20}$$

After the iterations for each time step are finished and $e_{s,n}$ is found small enough to satisfy tolerance, the strain throughout the element at this time step is calculated in accordance with Equation 7.17 from the total nodal deflections of each element at this time step. The stress through the thickness of the element is then found from Equation 7.21, where E is the elastic modulus of each slice, and is scaled from the input value of E according to its temperature and orientation. It is assumed that crosswise plies have an elastic modulus that corresponds to an equivalent parallel elastic modulus divided by 30 [82, 208].

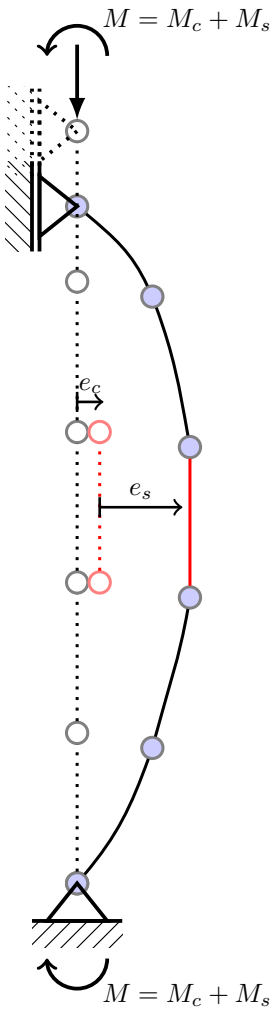

Figure 7.13. Direct stiffness approach schematic.

$$\sigma = E \cdot \boldsymbol{\epsilon_x} \tag{7.21}$$

The stress through the elements is assessed against the yield strength, which is also scaled with temperature of each slice; if any slice of any element is found to be yielding, the elastic modulus for this elements is updated to a tangent elastic modulus, to reflect a constant yield strength and the strain state and the deflection iterations are repeated with the updated tangent modulus values. In light of the findings in Chapter 5, where no deflection recovery was measured during the timber cooling phase, no recovery of the mechanical properties of heated timber is assumed for the model in this chapter.

Considering the symmetry of the measured deflected shapes in Figure 7.2 the wall strips are modelled until their mid-height as shown in Figure 7.14, with a zero rotation rolling support at its mid-height. For the simulations herein 17 elements of initial length of 50 mm each were used to model the wall strips. The number of elements was chosen as the smallest possible mesh size to capture the heated region. No mesh sensitivity was found.

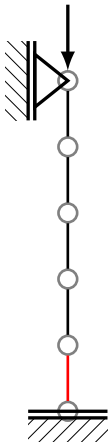

Figure 7.14. mid-height symmetry boundary conditions

7.5 Simulation/Model results

The median simulated mid-height deflections from the temperature bootstraps and the input parameters shown in Figure 7.12 are shown alongside 90 % confidence intervals, and the respective observed deflections in figures 7.15, 7.16, and 7.17 for the "high", "partial", and "low" heat flux exposure experiments described in Chapter 6, respectively.

7.5.1 "High" heat flux to failure

The simulation results for three ply CLT wall strips bonded with melamine formaldehyde in Figure 7.15 a) can be observed to fall within the specified confidence interval, and the trend of the measured deflections is approximated by the median model outputs. For the three ply specimens with polyurethane in Figure 7.15 b) the model does not represent the observed runaway deflections and does not predict buckling failure within the shown 90 % confidence interval.

For the five ply specimens bonded with melamine formaldehyde the model output initially follows the measured deflections but tends to overestimate deflections after approximately 20 minutes. While the measured deflection rates reduce in this time period those resulting from the model accelerate. The measured values fall within the 90 % confidence interval for the majority of the test duration, although given the extent of the confidence interval this might be more a reflection of the uncertainty in the input data rather than the performance of the model. For the five ply specimens bonded with polyurethane the model results initially approximate the experimental measurements closely. After approximately twelve minutes, the model fails to capture the accelerating deflections that were measured in the experiments. The experimental results deviate outside the 90 % confidence interval of the model.

7.5.2 "High" heat flux for a fixed time period

For the three ply specimens that were exposed to 15 minutes of the "high" heat flux in Figure 7.16 a) and b) the model captures the trend of the measured deflections within the estimated confidence interval. It does not reflect the continuing slow deflections that were observed. The increased deflection during the heating phase of the second repeat of the 3PU specimen can be seen to fall outwith the confidence interval, suggesting

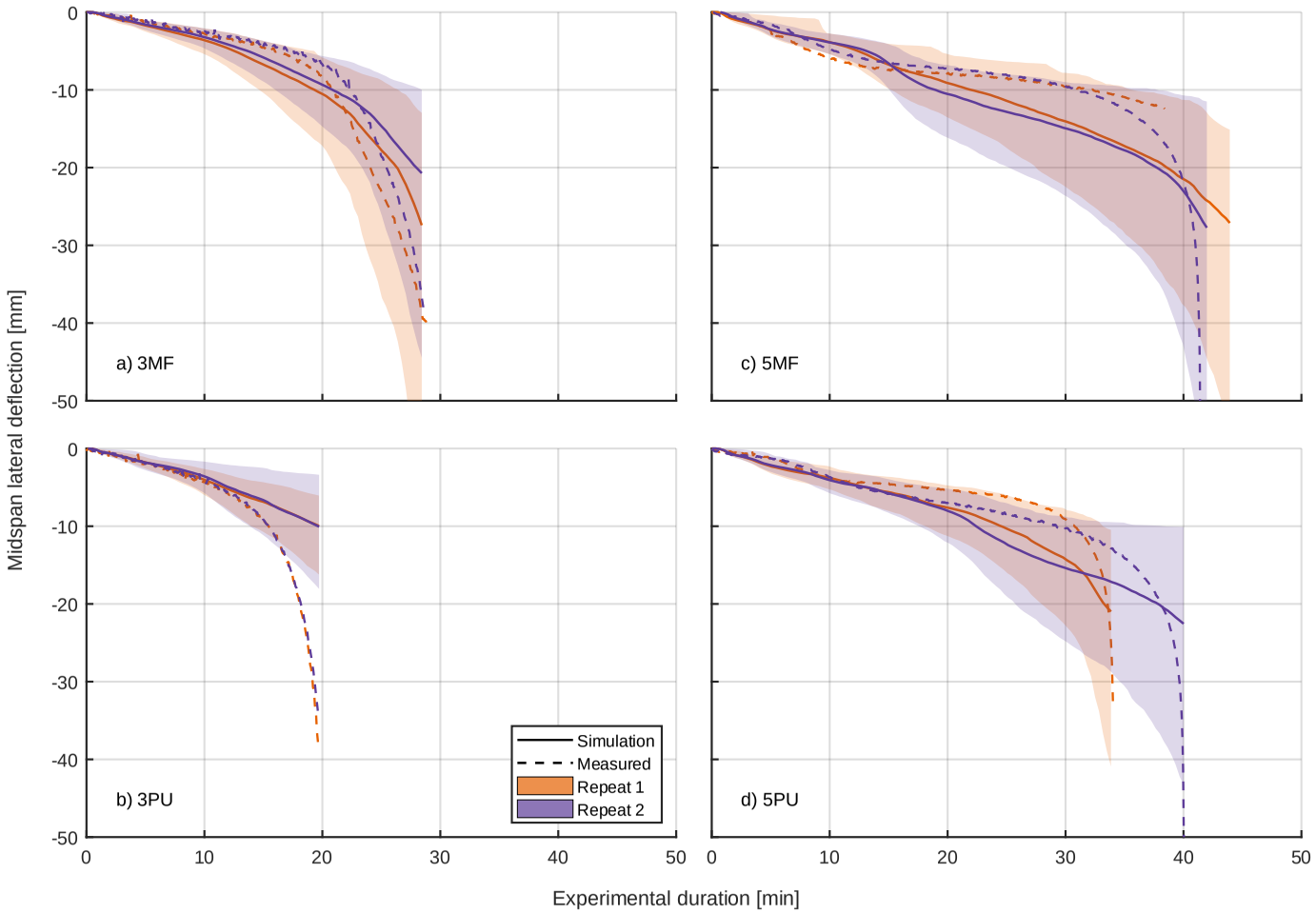

Figure 7.15. Simulated mid-height lateral deflections, their 90 % confidence interval, and observed results for exposure of wall strips to a "high" heat flux until structural failure.

that the specified uncertainty in the input parameters is not able to fully account for material variations that are apparent in the observed repeat experiments.

For the five ply specimens in Figure 7.16 c) and d) which were exposed to 25 minutes of the "high" heat flux the model captures the initial trend of the deflections but fails to predict the continuing deflections in the cooling phase.

7.5.3 "Low" heat flux to failure

The model output for the first repeat experiment of the three ply melamine formaldehyde in Figure 7.17 a) provides what can arguably be described as the best simulation performance in this chapter: both the trend and the magnitude of the observed data are reflected in the model output. On the contrary the first repeat experiment from this series deviates significantly from the predicted confidence range. It should be noted that this experiment was the first specimen in the "low" heat flux series and was run with a slightly higher heat flux (21 rather than 15 kW/m^2) than the other specimens for this set-up. This should, in theory be accounted for by the increased temperatures that are used as input parameters for the model, however, it can be seen that, while the model predicts higher deflections than for repeat 2, the increased input temperatures do not seem to sufficiently account for their effects on the deflections measured in the experiment.

As noted for the "high" heat flux results, the effect of weakening of the polyurethane adhesive is clearly visible in Figure 7.15 b), causing accelerating deflections that cannot be accounted for the by the model or the specified uncertainty in the input parameters.

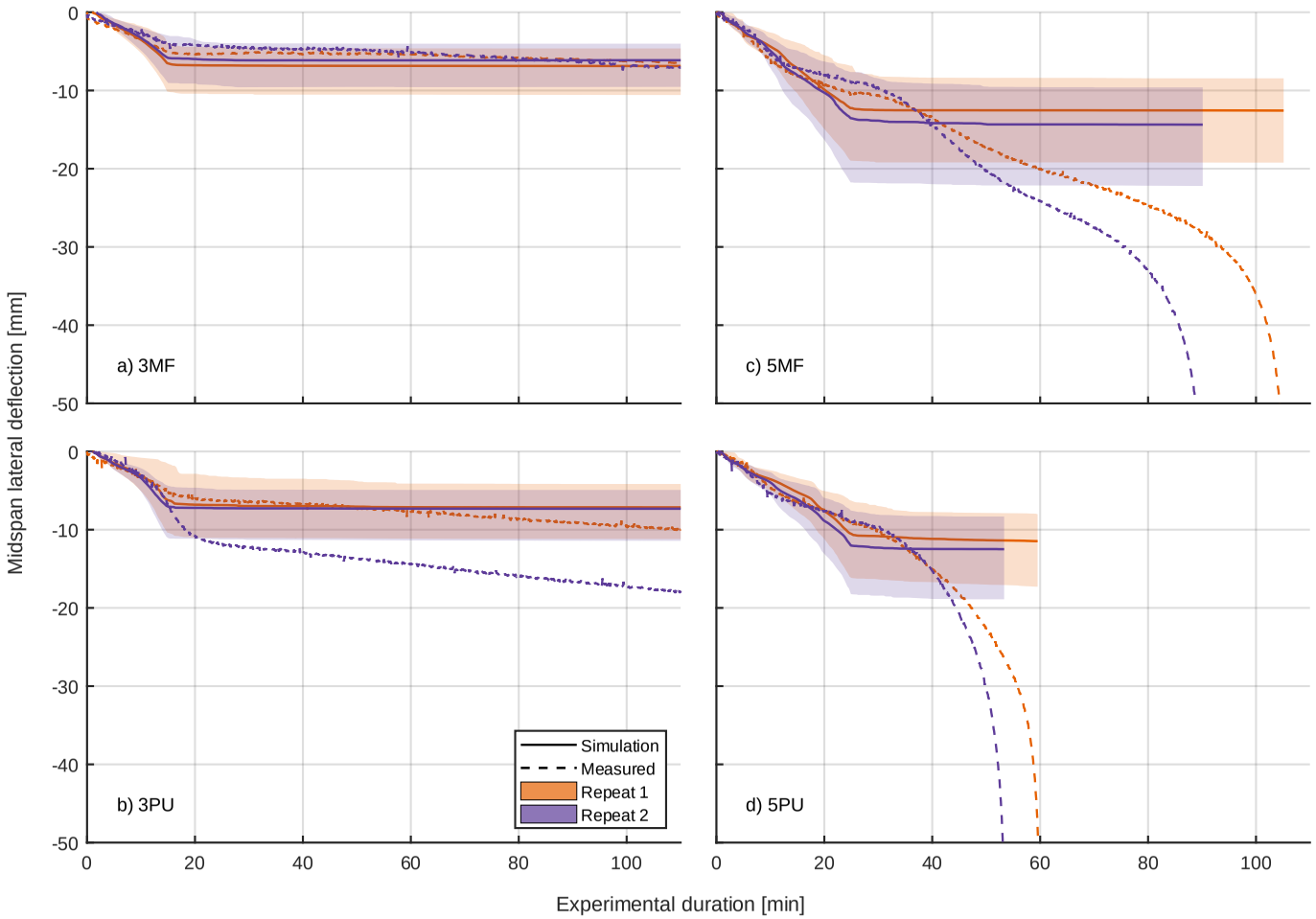

Figure 7.16. Simulated mid-height lateral deflections, their 90 % confidence interval, and observed results for exposure of wall strips to a "high" heat flux for predetermined times.

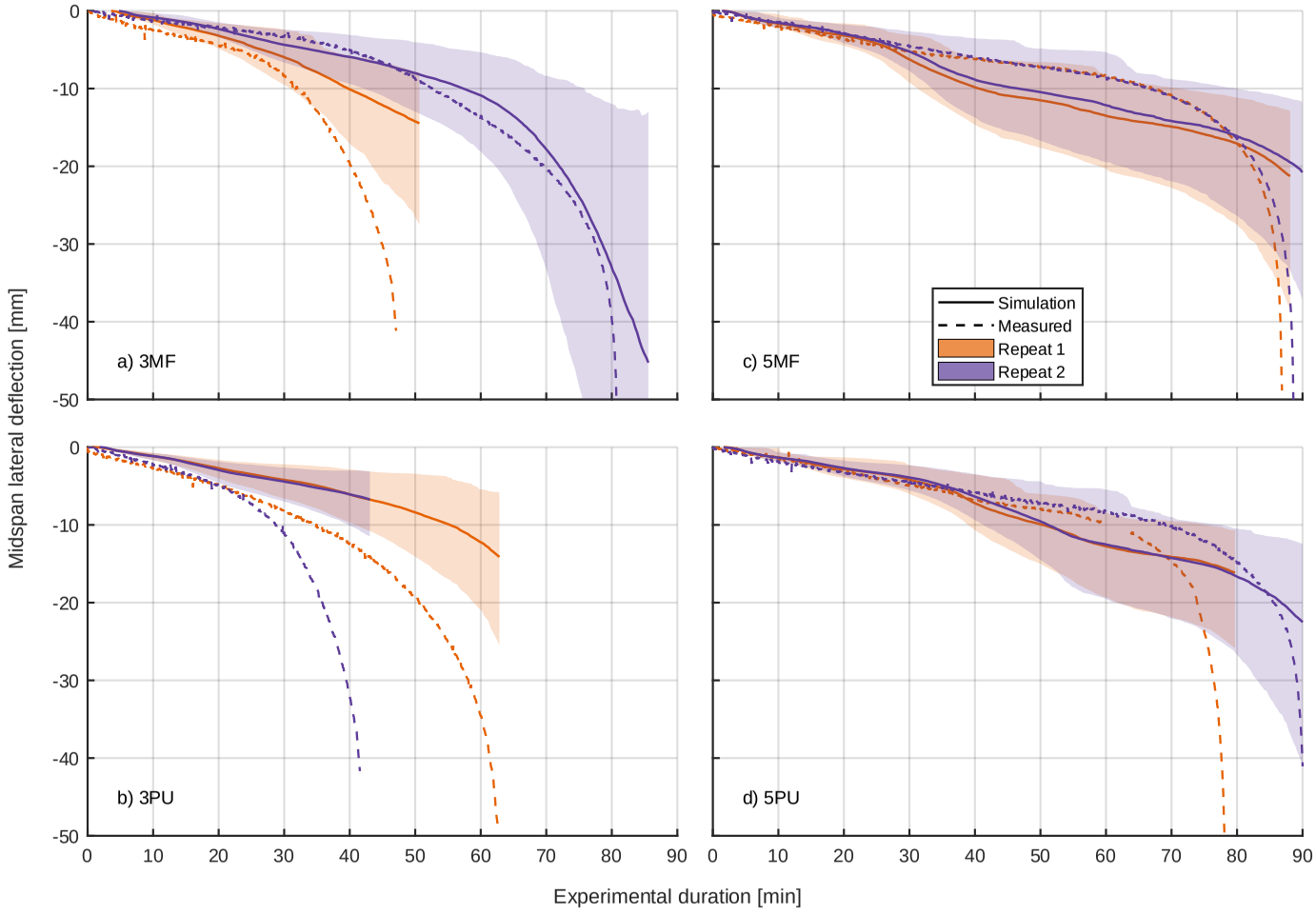

Figure 7.17. Simulated mid-height lateral deflections, their 90 % confidence interval, and observed results for exposure of wall strips to a "low" heat flux until structural failure.

7.6 Discussion of simulation results

> "All models are wrong, but some are useful."
> *George Edward Pelham Box* 1979 [228]

The utilised model presented in this chapter was deliberately kept to an accessible degree of simplicity and it was therefore unlikely that it would accurately model all of the different deflection curves that were observed in Chapter 6. This section discusses how the large deviations between model and reality can be interpreted in light of the underlying engineering principles.

The 3MF specimens exposed to full "high" heating provide the simplest model case, since the cross-lamination does not come into play and melamine formaldehyde adhesive types are generally not expected to induce adhesive failure at elevated temperatures [70, 73, 174]. The simulated output data confidence ranges capture both the trend and the magnitude of the measured deflections; this indicates that the basic underlying concepts of the model discussed in Subsection 7.4.3 provide a sufficient level of parsimony.

7.6.1 Confidence levels

For all the model outputs in this chapter the provided 90 % confidence intervals can be observed to grow larger with time and a sharp increase of the 5 %ile deflection (i.e. the lower confidence limit) can be observed as failure is approached. The increase in the range with time can be explained by increasing uncertainty in temperature readings deeper into the timber, as the instrumentation density of thermocouples reduced away from the exposed surface. Another reason for the widening confidence ranges with increasing defections is the occurrence of yielding for lower yield strengths, causing an increase in the deflection rate.

7.6.2 Influence of the adhesive

The comparison of modelled and measured results in figures 7.15 b), 7.16 d), 7.17 b) and d) provide further confirmation of the influence of the adhesive on the structural load bearing capacity in fire. Note that the model neither implicitly nor explicitly takes adhesive type into account, so these results are not unexpected. They show that the accelerating deflections in PU specimens were not caused by uncertainties in material

or temperature development but by structural effects that can be considered likely to originate from a loss of adhesion with increasing temperatures.

One major obstacle to taking adhesive behaviour in timber structures in fire into account is the fact that very little information on adhesive behaviour is available publicly. It is unsatisfactory that one of the largest sources of uncertainty for the assessment of timber structures in fire is not timber, a naturally grown material that is generally considered more variable than steel or concrete, but the adhesive, which is manufactured in well controlled conditions and to specific requirements. This uncertainty does not stem from a variability in specific adhesive behaviour itself, but the lack of information on the adhesives used. If engineered timber buildings are to continue to grow in numbers and heights, the adhesives that are used to manufacture the engineered timber elements should be subject to equal scrutiny as any other material in a building when it comes to fire safety. The recently introduced qualification requirements for adhesives in North America [208] show that steps towards improved fire safety with respect to adhesive performance are already being taken to minimise and prevent the occurrence of char fall-off. A correlation between adhesive char fall-off and their elevated temperature adhesion likely exists, and these steps are therefore also likely to implicitly improve the structural adhesive fire performance. However, more detailed understanding of adhesives, like the glass transition temperature or the reduction in shear strength at elevated temperature and moisture levels, are needed for proper structural fire safety assessment of engineered timber buildings.

7.6.3 Influence of latent heating

The simulated and observed deflection paths in figures 7.16 c) and d) show that the continued deflections of the five ply specimens, that were measured after the heat exposure was removed, are not captured by the model. This can have multiple causes: (1) the deflections in the cooling phase could be caused by heating due to smouldering in parts of the timber that were not instrumented with thermocouples, however, smouldering without an external heat source is a relatively slow process and could only partially explain the accelerating deflections that were observed in the specimens. (2) the reduction in strength and elasticity is not only affected by the increase in temperature but also by the loading duration, which would could be explained by creep, which has been shown in Chapter 5 to drive the deformations in timber subjected to heating under constant load. However, the experiments on beams in Chapter 5 also

halted any further deflections in the cooling phase, so no further deflections were observed as heat was removed, despite the continuous application of constant loading. (3) the reduction curves from the Eurocodes [145] that were used in this model originate from back calculations of timber studs in standard cellulosic time temperature curve furnace tests, with moisture movement considered implicitly [108]. Clearly the heating for the experiments considered here is very different from the conditions that arise in furnace tests that follow a standard time temperature curve, and CLT, due to the cross-wise orientation of some of its layers, is a more complex material than sawn lumber. Rehydration of previously dried timber could be a potential reason for continuous strength losses during cooling, and this is supported by findings by Armstrong [171, 172], which showed that both increases and decreases in moisture content can cause creep deflections in timber under constant load. In addition, moisture should perhaps be considered to move independently from heat during a fire decay phase as it can be moved by momentum and pressure differences. All of these possible causes require a better understanding of the structural properties of timber in non-standard heating conditions. Within the current knowledge framework it can be said that the measured temperatures are not sufficient in combination with the assumed reduction curves to predict failure in the timber cooling phase.

7.6.4 Influence of the cross plies

One interesting observation from comparing model and measured deflections is that, for five ply elements, the effect of the cross-plies is not accurately captured by the model. As the crosswise orientated plies have lower mechanical properties, they should, in theory, act as a sacrificial layer as the heat front passes through them and reduces their mechanical properties. An extreme case of this is shown for the theoretical considerations in Figure 7.11, where, for illustration purposes, a constant charring rate only is assumed and any timber beyond the char front retains 100 % of its mechanical properties. This results in a reduction in the rate of deflection as the cross-wise layers are charred, as these do not contribute significantly to the overall load bearing capacity to begin with. With the continuous temperature profiles that were used as model input parameters in this chapter the expected reduction in deflection rate does not appear to be captured at the correct time (when comparing to the measured deflections) and does not reflect the magnitude of the slowdown in deflections that is shown by the measured data, this is especially evident for five ply specimens exposed to a “high” heat flux in Figure 7.15 c) and d). This failure to properly represent the strength loss in the cross layers perhaps suggests that the influence of temperatures is not as continuous as

assumed herein, and that significant temperature reducing effects do not start at 20 °C but are linked to higher temperatures.

7.6.5 Yield and failure criteria

Barring the influence of the adhesive, the trend of the measured deflections in figures 7.15 and 7.17 is described well by the confidence ranges of the model output. One issue appears to be the correct forecasting of runaway deflections and the increase of the slope in the deflections paths. In Figure 7.15 a) it can be observed that the shape of the lower confidence range (i.e. the 0.05 quantile) is a reasonable representation of the shape of the measured deflection path, while the median model output does not accurately represent the runaway deflections. Assuming that yielding of timber in compression is a major contributor to the runaway deflections, this suggests that the input yield strengths were distributed around too high a yield input strength. The input yield strengths were taken from the pure compression results in Chapter 4 and the yield strengths in combined bending and compression should perhaps be drawn from lower distributions, considering that they occur in the extreme fibres of one ply and the lamination effect that was described in Chapter 4, and that was attributed to cause elevated peak strengths for five ply compared to three ply CLT, possibly does not apply in this case.

Overall it is clear that the presented model has a number of shortcomings, which are mainly rooted in its simplistic approach, that prevent it from accurately predicting the deflection paths of different CLT configurations exposed to changing heating regimes. The most concerning of the issues identified above are the effects of the adhesives, and the latent heat and moisture movements, because these represent fundamental knowledge gaps either in the required input data (for the heat performance of the adhesive), or a lack of understanding of the the drivers behind the observed effects, as in the case of the additional deflections caused by latent heating. While the other effects can be addressed through improved knowledge of the input parameters or more refined simulation procedures, the effect of adhesives and the problems raised with regards to the timber cooling phase will persist in alternative model approaches until the underlying causes are better understood.

7.7 Conclusions

This chapter provided a more in-depth investigation of the relevant factors that are necessary to analytically and numerically describe the failure (by global buckling) of the wall strip elements described in Chapter 6.

The basic principles of structural stability, and the lack thereof, were explained, and the role of inherent eccentricities on the load deflection path was discussed. The analytical solution for the lateral deflections of eccentrically loaded columns or walls was used to validate a numerical approach which simulates the occurrence of instability through the iteration of increasingly smaller moments arising from P-Delta effects.

The deflected shapes from the experiments in Chapter 6, which were found to be approximately sinusoidal, were used to determine the curvature of the wall strips through their experimental duration. From the curvature and the estimated temperature profiles, the stress distributions through the cross-sections were determined. For the purpose of determining the temperature induced reductions in mechanical properties, it was shown that, since the cross-section was mainly subjected to compression stresses, the errors arising from an assumption of compression only, compared to a combination of tension and compression, were small enough to be considered negligible for the overall structural performance for the cases considered in this thesis. This simplifies the required steps for structural analysis significantly, since it removes the need to iterate to find the location of the neutral axis in heated compression elements. The stress profile was also used to demonstrate that significant outer fibre tension stresses only become critical close to failure, when they rise exponentially.

A direct stiffness model was developed to simulate the midspan lateral deflections for the expected range of input temperature profiles. The model was compared to the measured deflections and while it was able to capture the trend and magnitude within its 90 % confidence range for simple cases, multiple shortcomings of the model were determined for more complex cases. The model was not equipped to deal with the effect of a loss of performance of the adhesives at elevated temperatures and this was reflected in the results, for which the deflections for PU bonded specimens were under predicted, thereby providing further confirmation that the lower structural fire performance of this adhesive compared to melamine formaldehyde is caused by the adhesive, rather than a difference in mechanical properties of the timber or different in-depth temperatures.

In addition to the adhesive performance, another critical error of the model was its failure to predict the continuing deflections in the timber cooling phase that were

observed for five ply specimens that were heated for 25 minutes. This suggested that the available knowledge on the reduction of mechanical timber properties in timber during a fire decay phase is insufficient to account for the observed deflections and failures. Multiple possible explanations for this behaviour were discussed, but none could be identified as the definite cause, and further research into the effects of creep and moisture movement in timber are recommended to address these knowledge gaps.

This chapter showed that engineered timber is a complex system of materials that presents multiple challenges to fire safety and that its design cannot be informed satisfactory by ignoring the effects of heat on individual components of this system.

This page is intentionally left blank.

CHAPTER 8

Conclusions

This page is intentionally left blank.

Previous chapters in this thesis described the state of the art, the nature and composition of the cross-laminated timber that was investigated for this thesis, the three experimental series that were completed, and the numerical analysis of the critical factors concerning instability of CLT walls in fires. This chapter summarises the main findings that arose from the experiments in chapters 4 to 6, and assesses their significance within the current state of the art. Some implications of the main findings for the design for timber buildings are communicated, and recommendations for further research are put forward to address knowledge gaps that currently hinder the safe design of mass timber buildings.

8.1 Main findings

8.1.1 Influence of adhesive type on structural capacity in fire

The adhesive type used to manufacture the CLT elements tested herein was shown to have a significant influence on the structural capacity of CLT exposed to fire or heat. This effect on the structural performance was independent of previously known effects of adhesive performance on the fire dynamics in CLT compartment fires, e.g. char fall-off. For all of the three scales, which all represented different loading conditions, no significant difference was found in structural performance indicators at ambient temperatures between adhesive types. At elevated temperatures a statistically significant reduction in structural stiffness and load bearing capacity was measured for specimens bonded with polyurethane adhesive when compared to those bonded with melamine formaldehyde.

- For small scale compression elements, the strength retention in samples subjected to the combined effects of heat and moisture was, on average, 9 percentage points lower for PU bonded specimens compared to those bonded with MF. This effect was not observed for samples heated uniformly to a steady state temperature above 100 °C, which implied that the transient effects of changes in moisture content have a significant influence on the load bearing capacity in compression.
- For constantly loaded large scale CLT beams that were heated to non-charring temperatures, the sustained deflections in heating were higher for those beams that were manufactured with the PU adhesive compared to those with the MF adhesive. The deflection paths were clearly distinguishable by adhesive type, and after three hours of heating the sustained mean deflections were 40 % higher for

CLT beams bonded with PU as compared with those bonded with MF.

- For wall strips exposed to radiant heating, as descried in Chapter 6, a significant reduction in failure time was measured for PU bonded samples compared those utilising MF as the adhesive. On average the failure time was 36 % lower for PU bonded specimens. Numerical simulations with a wide distribution of mechanical input parameters, in Chapter 7, further strengthened the assessment that heated PU bond lines are a significant contributing factor to shorter failure times.

8.1.2 Influence of ply configuration on structural capacity in fire

The CLT assessed in this thesis was 100 mm thick, and was formed of either three plies with 40 mm outer plies orientated in parallel to the main loading direction, or of five plies with a thickness of 20 mm for both parallel and crosswise layers. The ply configuration was determined to be influential to the load bearing capacity of CLT at elevated temperatures for both beams and wall strips, but not for the small scale compression elements.

- For small scale compression elements, a higher effective strength was observed for five ply specimens in ambient temperature reference experiments; this was attributed to a lamination effect wherein deficiencies in individual timber boards were compensated by other boards. This effect was maintained at elevated temperatures, i.e. no adverse effect in compression was found between ply configurations at elevated temperatures.

- For beams tested at ambient temperatures, a lower effective elastic modulus was determined in four point bending for three compared to five ply CLT; this suggests that, as would be expected from bending theory, shear deflections increase the overall deflections for three ply beams. At elevated temperatures under equivalent load levels, CLT made of three plies experienced 15 % larger mean deflections than those consisting of five plies after three hours of heating under sustained loading.

- Wall strips of three ply CLT exposed to one sided radiant heat flux exposure experienced larger deflections and, on average (median), 34 % earlier failure time than five ply CLT specimen under equivalent nominal load levels. This was attributed to the fact that, for a three ply configuration, the majority of load bearing timber is placed on the outside and the overall reduction in structural capacity therefore progresses faster than for five ply CLT.

8.1.3 Fire decay phase effects and creep

From beams under constant load and exposed to non-charring uniform heating it was observed that heat induced deflections did not recover upon cooling and that these deformations did not recover after all load and heat was removed. These measurements suggest that the deflections were not caused by a loss in elasticity but by creep, indicating that the mechano-thermal history of CLT is an influencing factor for its structural performance in fire, as are changes in moisture content and transport in the timber.

Five ply CLT wall strips that were heated for 25 minutes with a nominally "high" heat flux which was subsequently removed were observed to fail during their cooling phase. From structural modelling with the measured temperature profiles as input values, it was determined that this behaviour could not be attributed solely to the movement of the thermal wave into previously unheated timber, at least not within commonly applied assumptions of the reduction in mechanical properties with elevated temperatures. This suggests that there is a knowledge gap on how the strength and stiffness of timber under sustained load is affected by heating and subsequent cooling, and by associated moisture movement.

8.1.4 Failure modes

Failure of CLT wall strips exposed to one-sided radiant heat flux was observed to be deflection dominated, with large lateral mid-height deflections preceding tensile rupture. The manner of runaway deflections suggests yielding in compression; numerical assessments of the curvature from the deflected shapes showed that the tensile stresses on the unexposed face only became relevant when structural failure was already in progress through loss of stability. This indicates that the focus for structural fire safety assessment of CLT walls should be on the compressive stress and strength development, and that the yield strength in compression is an important factor to consider to assess structural failure of CLT walls in fire.

8.2 Implications

This section lists and assesses the implications that arise from the findings in this thesis for the design of timber buildings that use CLT (or other engineered timber products) as a major contributor to its load bearing capacity.

The experimental results clearly highlight that CLT slabs and panels bonded with a PU adhesive will maintain their load bearing capacity in fire for a shorter duration than those bonded with the MF adhesive. Within the fire resistance framework, this will be reflected in shorter/lower fire resistance ratings for CLT utilising PU; this highlights an opportunity for building designers to enhance the structural fire safety performance through selection of a targeted adhesive. At the same time, the significant differences in performance between adhesive types should be considered where codified numerical methods are used to obtain fire resistance times through calculations. Currently no known codified calculation methods provide means to account for adhesive performance and, unless these calculation procedures implicitly base their input parameters and assumptions on the adhesive with the worst possible thermal performance, the numerically determined fire resistance will be potentially non-conservative.

In addition to the adhesive, the number and configuration of plies was shown to exert significant influence on the time to failure, when nominally equivalent loads were applied. Thicker outer layers, orientated parallel to the main loading direction, increase the structural capacity at ambient temperatures and also reduce the risk of char-fall off. However, from a structural fire engineering perspective this configuration is problematic as it exposes a large proportion of load bearing timber to the fire early on and the ensuing eccentricities and deflections will bring the wall close to stability point of no return before the heating front reaches a 'sacrificial' crosswise ply. In combination with the adhesive this presents an optimisation problem, to find the best possible solution taking into account ambient temperature loading capacity, the prevention of char fall off, and the structural behaviour in fire. Obviously, this is a complex and challenging task for engineers, and highlights why fundamental and novel research, such as that presented in this thesis, is of critical importance to knowingly designing mass timber buildings.

The structural failures that were observed in the timber cooling phase should make all practitioners involved in the design of timber buildings consider whether their current provisions for structural fire safety adequately take reductions of mechanical properties in a fire decay phase and beyond into account. Some researchers and designers might argue that fire resistance ratings obtained from furnace tests implicitly account for further structural weakening after burn-out and associated temperature decay; however, this cannot capture the involved physics and mechanics, and its perceived level of safety can therefore not be quantified adequately.

While the focus of this thesis is on the structural capacity in fire, some of the findings also reinforce why timber should be considered distinctly compared to steel or concrete;

timber burns, and as a non-inert material it poses a multitude of challenges to fire safety design. The fall off of char was observed for PU bonded specimens only; in a compartment fire this can potentially extend the fire duration indefinitely. Small scale specimens were observed to self heat beyond the set temperature in the environmental chamber they were heated in; this emphasizes the possibility of heat generation from the timber itself, even in the absence of flaming combustion. This issue was also evident in experiments on wall strips; for heating with a subsequent cooling phase, localised smouldering was observed to last for at least three hours after the externally applied radiative heat flux was removed. The current dominance of testing elements of construction in furnaces according to standard temperature curves means that the contribution of timber itself to its own heating, and thereby reduction in its load bearing capacity, are not captured adequately within the fire resistance framework.

Overall the presented results and their implications highlight a multitude of knowledge gaps in the current state of the art with regards to fire safety of engineered timber products; this should be of great interest to engineers working on tall timber projects. The current practice of applying design parameters that can be traced back to a limited number of glulam beams in the 1980s should be critically reviewed, since the results in this thesis suggest that this approach is not applicable for more complex engineered timber products (e.g. CLT), for heating scenarios that do not follow a standard cellulosic temperature time curve, or for stress distributions that deviate from simple assumptions of equal measures of tension and compression stress through a cross-section.

Tall timber buildings have been, and are currently being built or planned all over the world. The results of this thesis, and the multitude of knowledge gaps highlighted, should be of considerable concern to the fire engineering community. To truly enable the use of timber as an alternative to steel and concrete for tall buildings the fire and the timber engineering community (and this explicitly includes the author of this thesis), as well as architects and developers, should take caution to realise that the current state of the art is only located at the edge of the knowledge required to safely design tall timber buildings; more research is required to ensure that the building stock that is currently created does not deliver a level of safety that will be considered insufficient in the coming decades.

8.3 Recommendations for further research

A number of knowledge gaps in the state of the art for fire safety of CLT are identified in this thesis. As engineered timber is utilised for taller buildings it is recommended that further experimental studies are carried out to address these knowledge gaps and to incorporate them into the fire safety design of timber structures.

- The use of different adhesives as bonding agent had a significant influence on the structural capacity in heat and fire. It was not possible to accurately model this adhesive influence, due to a lack of available knowledge on the heat performance of adhesives. The historical information on available adhesives is limited and this effect is compounded by the ongoing development of novel adhesives. It is recommended that adhesive manufacturers provide quantified, or at least qualified data on the elevated temperature performance of their products, if these are to be used in timber buildings.
- The detrimental effect of moisture on the structural capacity was evident in all experimental series in this thesis. It has long been known that elevated moisture content reduces the mechanical properties of timber. However, for fire safety considerations moisture is often only accounted for implicitly via temperature estimations, where it is tied to the evaporation point of water. The temperature development in large engineered timber sections is well documented through a multitude of studies, however, the movement of moisture is not investigated to the same degree. It is therefore recommended that (1) standardised methods to measure transient moisture contents in timber exposed to fire are developed, and (2), that these are used for detailed studies on the movement of moisture in engineered timber and its influencing factors (e.g. grain orientation).
- The role of temperature or moisture driven creep in deflections and deformations of timber and engineered timber in fire or elevated temperature situations should be further investigated. The proportions and therefore the relative importance of creep in deflections in fire should be quantified, so that designers can account for this.

BIBLIOGRAPHY

[1] UN Department of Economic and Social Affairs Population Division. *World Population Prospects: The 2015 Revision, Key Findings and Advance Tables*. Report. United Nations, 2015.

[2] UN Department of Economic and Social Affairs Population Division. *World Urbanization Prospects: The 2014 Revision*. Report. United Nations, 2014.

[3] H. Buhaug and H. Urdal. "An urbanization bomb? Population growth and social disorder in cities". In: *Global Environmental Change* 23.1 (2013), pp. 1–10. ISSN: 0959-3780. DOI: 10.1016/j.gloenvcha.2012.10.016.

[4] D. Johnson. *Oregon Company is First Certified U.S. Manufacturer of Cross-Laminated Timbers*. Sept. 2015. URL: https://oregonclt.com/oregon-company-first-us-manufacturer-of-cross-lamianted-timber-certified/.

[5] R. Brandner, G. Flatscher, A. Ringhofer, G. Schickhofer, and A. Thiel. "Cross laminated timber (CLT): overview and development". In: *European Journal of Wood and Wood Products* 74.3 (2016), pp. 331–351. ISSN: 1436-736X. DOI: 10.1007/s00107-015-0999-5.

[6] M. F. Laguarda Mallo and O. Espinoza. "Awareness, perceptions and willingness to adopt Cross-Laminated Timber by the architecture community in the United States". In: *Journal of Cleaner Production* 94 (2015), pp. 198–210. ISSN: 0959-6526. DOI: "10.1016/j.jclepro.2015.01.090".

[7] M. Kurihara and Y. Shimbun. "Japan embraces era of CLT timber". In: *Asianews* (2015). URL: http://annx.asianews.network/content/japan-embraces-era-clt-timber-5811.

[8] R. M. Foster and M. H. Ramage. "Briefing: Super tall timber – Oakwood Tower". In: *Proceedings of the Institution of Civil Engineers - Construction Materials* (2016), pp. 1–5. DOI: 10.1680/jcoma.16.00034.

[9] K. A. Malo, R. B. Abrahamsen, and M. A. Bjertnaes. "Some structural design issues of the 14-storey timber framed building "Treet" in Norway". In: *European Journal of Wood and Wood Products* 74.3 (2016), pp. 407–424. ISSN: 1436-736X. DOI: 10.1007/s00107-016-1022-5.

[10] H. Buri and Y. Weinand. "Origami - Folded Plate Structures, Architecture". In: *World Conference on Timber Engineering*. 2008. URL: http://infoscience.epfl.ch/record/118687.

[11] A. Falk, P. Von Buelow, and P. H. Kirkegaard. "Folded plate structures as building envelopes". In: *World Conference on Timber Engineering*. 2012, pp. 155–164.

[12] "The doomed city". In: *The New York Times* (Oct. 10, 1871). URL: https://www.nytimes.com/1871/10/10/archives/the-doomed-city-later-details-of-the-appalling-fire-in-chicago.html.

[13] M. Fuyuko. "Fires and Recoveries Witnessed by the Dutch in Edo and Nagasaki: The Great Fire of Meireki in 1657 and the Great Fire of Kanbun in 1663". In: *Itinerario* 37.3 (2014), pp. 172–187. ISSN: 0165-1153. DOI: 10.1017/S0165115313000892.

[14] L. E. Frost and E. Jones. "The fire gap and the greater durability of nineteenth century cities". In: *Planning Perspectives* 4.3 (1989), pp. 333–347. ISSN: 0266-5433. DOI: 10.1080/02665438908725687.

[15] T. Koshun. *Picture Scroll of Fires in Edo*. Artwork. 18/02/2019 1814.

[16] M. F. Laguarda Mallo and O. Espinoza. *Cross-laminated timber vs. concrete/steel: cost comparison using a case study*. Conference Paper. Aug. 2016.

[17] M. C. Green. *The Case For Tall Wood Buildings*. Report. mgb Architecture + Design, 2012.

[18] Skidmore Owings & Merrill LLP. *Timber Tower Research Project*. Report. 2013.

[19] P. Oldfield, D. Trabucco, and A. Wood, eds. *Roadmap on the Future Research Needs of Tall Buildings*. Chicago: Council on Tall Buildings and Urban Habitat, 2014.

[20] B. Östman and B. Källsner. "National building regulations in relation to multi-storey wooden buildings in Europe". In: *SP Trätek Växjö University: Kalmar, Sweden* (2011), pp. 1–26.

[21] J. Sanner, A. Fernandez, R. Foster, M. Ramage, T. Snapp, and D. Weihing. "River Beech Tower: A Tall Timber Experiment". In: *CTBUH Journal* 2 (2017). ISSN: 1946-1186.

[22] N. Werther, M. Gräfe, C. Fülle, N. Leopold, and M. Brunn. *Erarbeitung weiterführender Konstruktionsregeln/-details für mehrgeschossige Gebäude in Holzbauweise der Gebäudeklasse 4*. Report. Frauenhofer IRB Verlag, 2014.

[23] J. Heitz. *Fire Resistance in American Heavy Timber Construction*. 2016. ISBN: 3319321269.

[24] S. H. Ingberg, H. K. Griffin, W. C. Robinson, and R. E. Wilson. "Fire tests of building columns". In: *Journal of the Franklin Institute* 191.6 (1921), pp. 823–827. ISSN: 0016-0032. DOI: 10.1016/S0016-0032(21)90681-1.

[25] J. Braidwood, R. N. Jackson, C. May, I. Anson, J. Barrett, H. A. Hunt, J. M. Rendel, Penrose, Edington, and J. Simpson. "Discussion On The Construction Of Fireproof Buildings". In: *Minutes of the Proceedings of the Institution of Civil Engineers* 12.1853 (1853), pp. 266–272. DOI: doi:10.1680/imotp.1853.23988.

[26] H. O. Fleischer. *The performance of wood in fire*. Report. US Dept. of Agriculture, Forest Service, Forest Products Laboratory, 1960.

[27] C. Walford. "Fires and Fire Insurance Considered Under their Historical, Financial, Statistical, and National Aspects". In: *Journal of the Statistical Society of London* 40.3 (1877), pp. 347–432. ISSN: 09595341. DOI: 10.2307/2339074.

[28] ISO. *ISO 834-1-1999 Fire-resistance Test - Elements of Building Construction*. Standard. 2002. URL: https://books.google.co.uk/books?id=K0y1tgAACAAJ.

[29] S. H. Ingberg. "Tests of the severity of building fires". In: *NFPA Quarterly* 22.1 (1928), pp. 43–61.

[30] A. Pearson. "Dalston Lane: Tall Timber". In: *Building.co.uk* (2016). URL: https://www.building.co.uk/technical-case-studies/dalston-lane-tall-timber/5079749.article.

[31] A. Law and R. M. Hadden. "Burnout means Burnout". In: *SFPE Europe Q* 1 (2017).

[32] F. Wiesner and L. Bisby. "The structural capacity of laminated timber compression elements in fire: A meta-analysis". In: *Fire Safety Journal* 107 (2019), pp. 114–125. ISSN: 0379-7112. DOI: 10.1016/j.firesaf.2018.04.009.

[33] J. Schmid, M. Klippel, R. Fahrni, A. Frangi, M. Tiso, A. Just, and N. Werther. "An improved model for the fire design of Cross Laminated Timber in bending". In: *World Conference on Timber Engineering*. Seoul, Republic of Korea, 2018.

[34] R. Stürzenbecher, K. Hofstetter, and J. Eberhardsteiner. "Structural design of Cross Laminated Timber (CLT) by advanced plate theories". In: *Composites Science and Technology* 70.9 (2010), pp. 1368–1379. ISSN: 0266-3538. DOI: 10.1016/j.compscitech.2010.04.016.

[35] J.-K. Oh, J.-J. Lee, and J.-P. Hong. "Prediction of compressive strength of cross-laminated timber panel". In: *Journal of Wood Science* 61.1 (2015), pp. 28–34. ISSN: 1435-0211. DOI: 10.1007/s10086-014-1435-x.

[36] J. Bodig and B. A. Jayne. *Mechanics of wood and wood composites*. New York, USA: Van Nostrand Reinhold Company Inc., 1982. ISBN: 0442008228.

[37] M. H. Ramage et al. "The wood from the trees: The use of timber in construction". In: *Renewable and Sustainable Energy Reviews* 68, Part 1 (2017), pp. 333–359. ISSN: 1364-0321. DOI: 10.1016/j.rser.2016.09.107.

[38] F. F. P. Kollman and W. A. Côté. *Principles of wood science and technology: solid wood*. Berlin, Germany: Springer-Verlag, 1968.

[39] P. U. A. Grossman and M. B. Wold. "Compression fracture of wood parallel to the grain". In: *Wood Science and Technology* 5.2 (1971), pp. 147–156. ISSN: 1432-5225. DOI: 10.1007/bf01134225.

[40] H. D. Tiemann. *Effect of moisture upon the strength and stiffness of wood*. Vol. 63. US Dept. of Agriculture, Forest Service, 1906.

[41] J. Barrett, F. Lam, and W. Lau. "Size Effects in Visually Graded Softwood Structural Lumber". In: *Journal of Materials in Civil Engineering* 7.1 (1995), pp. 19–30. ISSN: 0899-1561. DOI: 10.1061/(ASCE)0899-1561(1995)7:1(19).

[42] C. Scheer, M. Peter, and T. Göckel. *Bemessung von Voll-und Brettschichtholz für den Brandfall: theoretische Grundlagen;[Forschungsbericht; DFfH, E-2000/08]*. Fraunhofer-IRB-Verlag, 2003. ISBN: 3816765246.

[43] J. M. Dinwoodie. *Timber, its nature and behaviour*. 2nd. New York, USA: Taylor & Francis, 2000. ISBN: 0419255508.

[44] J. Stanke. "Ein Beitrag zur theoretischen Ermittlung der Feuerwiderstandsdauer von einteiligen brettschichtverleimten Stutzen unter Druckbeanspruchung". In: *VFDB-Zeitschrift* 19 (1970), pp. 67–71.

[45] J. Hartley and J. Marchant. *Methods of determining the moisture content of wood*. Report. 1995.

[46] R. Jönsson and O. Pettersson. *Timber structures and fire: a review of the existing state of knowledge and research requirements*. Swedish Council for Building Research, 1985. ISBN: 9154043093.

[47] N. Bergen. "Case study of UBC Brock Commons - construction details and methods". In: *World Conference on Timber Engineering*. Ed. by J. Eberhardsteiner, W. Winter, A. Fadai, and M. Pöll. Vienna University of Technology.

[48] D. Barber and R. Gerard. "Summary of the fire protection foundation report - fire safety challenges of tall wood buildings". In: *Fire Science Reviews* 4.1 (2015), p. 5. ISSN: 2193-0414. DOI: 10.1186/s40038-015-0009-3.

[49] I. Smith and A. Frangi. "Technologies enabling advanced urban timber construction". In: *Proceedings of the Institution of Civil Engineers - Civil Engineering* 168.6 (2015), pp. 17–22. DOI: 10.1680/cien.14.00053.

[50] G. Kippenberg. *Timber comes first in Hackney*. Electronic Article. 2017. URL: https://www.ribaj.com/intelligence/innovation-timber.

[51] A.-L. Niemann. "Mit Holz geht's aufwärts". In: *F.A.Z.* (Aug. 14, 2017). URL: http://www.faz.net/-gz7-90oo1.

[52] J. W. G. Van De Kuilen, A. Ceccotti, Z. Xia, and M. He. "Very Tall Wooden Buildings with Cross Laminated Timber". In: *Procedia Engineering* 14 (2011), pp. 1621–1628. ISSN: 1877-7058. DOI: 10.1016/j.proeng.2011.07.204.

[53] I. Smith and A. Frangi. "Overview of design issues for tall timber buildings". In: *Structural Engineering International* 18.2 (2008), pp. 141–147. ISSN: 1016-8664.

[54] R. E. Smith, G. Griffin, T. Rice, and B. Hagehofer-Daniell. "Mass timber: evaluating construction performance". In: *Architectural Engineering and Design Management* (2017), pp. 1–12. ISSN: 1745-2007. DOI: 10.1080/17452007.2016.1273089.

[55] P. Zumbrunnen and J. Fovargue. "Mid-rise CLT buildings-the UK's experience and potential for AUS and NZ". In: *World Conference on Timber Engineering*. 2012.

[56] A. Frangi, M. Fontana, M. Knobloch, and G. Bochicchio. "Fire behaviour of cross-laminated solid timber panels". In: *Fire Safety Science* 9 (2008), pp. 1279–1290.

[57] R. A. Birdsey. *Carbon storage and accumulation in United States forest ecosystems*. Report. United States Department of Agriculture, 1992.

[58] S. Winter. "Wood is good!? - worldwide threats and consequent opportunities for building with wood". In: *World Conference on Timber Engineering*. Ed. by J. Eberhardsteiner, W. Winter, A. Fadai, and M. Pöll. Vienna University of Technology.

[59] R. H. Falk, D. Green, D. Rammer, and S. F. Lantz. "Engineering evaluation of 55-year-old timber columns recycled from an industrial military building". In: *Forest Products Journal* 50.4 (2000), pp. 71–76. ISSN: 00157473.

[60] Global Witness. *Two Worlds Collide*. Blog. 2014. URL: https://www.globalwitness.org/olympics/.

[61] D. Hindman and J. Bouldin. "Mechanical Properties of Southern Pine Cross-Laminated Timber". In: *Journal of Materials in Civil Engineering* 27.9 (2014), p. 04014251. ISSN: 0899-1561. DOI: 10.1061/(ASCE)MT.1943-5533.0001203.

[62] S. A. Young and P. Clancy. "Compression mechanical properties of wood at temperatures simulating fire conditions". In: *Fire and Materials* 25.3 (2001), pp. 83–93. ISSN: 1099-1018. DOI: 10.1002/fam.759.

[63] D. Ridley-Ellis, P. Stapel, and V. Baño. "Strength grading of sawn timber in Europe: an explanation for engineers and researchers". In: *European Journal of Wood and Wood Products* 74.3 (2016), pp. 291–306. ISSN: 1436-736X. DOI: 10.1007/s00107-016-1034-1.

[64] A. H. Buchanan. "Combined bending and axial loading in lumber". In: *Journal of Structural Engineering* 112.12 (1986), pp. 2592–2609. ISSN: 0733-9445.

[65] A. H. Buchanan. "Strength model and design methods for bending and axial load interaction in timber members". PhD Thesis. Department of Civil Engineering, University of British Columbia, 1984. DOI: 10.14288/1.0062943.

[66] M. Brunner. "On the plastic design of timber beams with a complex cross-section". In: *World Conference on Timber Engineering*. Ed. by J. Eberhardsteiner, W. Winter, A. Fadai, and M. Pöll.

[67] G. Fink, J. Kohler, and R. Brandner. "Application of European design principles to cross laminated timber". In: *Engineering Structures* (2018). ISSN: 0141-0296. DOI: 10.1016/j.engstruct.2018.02.081.

[68] J. J. Morrell. "Wood-based building components: what have we learned?" In: *International Biodeterioration & Biodegradation* 49.4 (2002), pp. 253–258. ISSN: 0964-8305. DOI: 10.1016/S0964-8305(02)00052-5.

[69] J. Konnerth, A. Jäger, J. Eberhardsteiner, U. Müller, and W. Gindl. "Elastic properties of adhesive polymers. II. Polymer films and bond lines by means of nanoindentation". In: *Journal of Applied Polymer Science* 102.2 (2006), pp. 1234–1239. ISSN: 1097-4628. DOI: 10.1002/app.24427.

[70] F. Stoeckel, J. Konnerth, and W. Gindl-Altmutter. "Mechanical properties of adhesives for bonding wood—A review". In: *International Journal of Adhesion and Adhesives* 45.Supplement C (2013), pp. 32–41. ISSN: 0143-7496. DOI: 10.1016/j.ijadhadh.2013.03.013.

[71] B. Burchardt. "3 - Advances in polyurethane structural adhesives". In: *Advances in Structural Adhesive Bonding*. Ed. by D. A. Dillard. Woodhead Publishing, 2010, pp. 35–65. ISBN: 978-1-84569-435-7. DOI: 10.1533/9781845698058.1.35.

[72] A. Frangi, M. Fontana, and A. Mischler. "Shear behaviour of bond lines in glued laminated timber beams at high temperatures". In: *Wood science and technology* 38.2 (2004), pp. 119–126. ISSN: 0043-7719.

[73] K. Richter and R. Steiger. "Thermal Stability of Wood-Wood and Wood-FRP Bonding with Polyurethane and Epoxy Adhesives". In: *Advanced Engineering Materials* 7.5 (2005), pp. 419–426. ISSN: 1527-2648. DOI: 10.1002/adem.200500062.

[74] E. Serrano and B. Källander. "Building and construction - timber". In: *Adhesive Bonding*. Ed. by R. Adams. Woodhead Publishing, 2005. Chap. 15, pp. 328–356. ISBN: 978-1-85573-741-9. DOI: 10.1533/9781845690755.3.328.

[75] L. Hasburgh, K. Bourne, P. Peralta, P. Mitchell, S. Schiff, and W. Pang. "Effect Of Adhesives And Ply Configuration On The Fire Performance Of Southern Pine Cross-Laminated Timber". In: *World Conference on Timber Engineering*. Ed. by J. Eberhardsteiner, W. Winter, A. Fadai, and M. Pöll. Vienna University of Technology, 2016.

[76] O. Kläusler, S. Clauß, L. Lübke, J. Trachsel, and P. Niemz. "Influence of moisture on stress–strain behaviour of adhesives used for structural bonding of wood". In: *International Journal of Adhesion and Adhesives* 44 (2013), pp. 57–65. ISSN: 0143-7496. DOI: 10.1016/j.ijadhadh.2013.01.015.

[77] A. Vilguts, D. Serdjuks, and L. Pakrastins. "Design Methods of Elements from Cross-laminated Timber Subjected to Flexure". In: *Procedia Engineering* 117 (2015), pp. 10–19. ISSN: 1877-7058. DOI: 10.1016/j.proeng.2015.08.117.

[78] S. T. Smith and J. Teng. "Interfacial stresses in plated beams". In: *Engineering Structures* 23.7 (2001), pp. 857–871. ISSN: 0141-0296.

[79] M. Okabe, M. Yasumura, K. Kobayashi, and K. Fujita. "Prediction of bending stiffness and moment carrying capacity of sugi cross-laminated timber". In: *Journal of Wood Science* 60.1 (2014), pp. 49–58. ISSN: 1435-0211. DOI: 10.1007/s10086-013-1377-8.

[80] M. S. Williams and J. D. Todd. *Structures - theory and analysis*. Basingstoke: Palgrave Macmillan, 2000. ISBN: 9780333677605.

[81] APA. *PRG 320 Standard for Performance-Rated Cross-Laminated Timber*. Standard. 2012.

[82] N. Doyle, R. Emberley, and J. L. Torero. "Fire Behavior of Cross-Laminated Timber (CLT Slabs: Two-Way Action". In: *Fire Science and Technology 2015*. Ed. by K. Harada, K. Matsuyama, K. Himoto, Y. Nakamura, and K. Wakatsuki. Springer, pp. 281–288.

[83] M. Wallner-Novak, J. Koppelhuber, and K. Pock. *Brettsperrholz Bemessung-Grundlagen für Statik und Konstruktion nach Eurocode ("Cross Laminated Timber Design-Construction and Design according to Eurocode")*. Report. 2013.

[84] H. J. Blass and P. Fellmoser. "Design of solid wood panels with cross layers". In: *World Conference on Timber Engineering*. 2004.

[85] S. Gagnon and M. Popovski. "Structural design of cross-laminated timber elements". In: *CLT handbook : cross-laminated timber*. Ed. by S. Gagnon and C. Pirvu. Québec: FPInnovations, 2011. Chap. 3.

[86] P. Fellmoser and H. Blaß. "Influence of rolling shear modulus on strength and stiffness of structural bonded timber elements". In: *CIB-W18 Meeting*. Vol. 37.

[87] CEN. *EN 1995-1-1 Eurocode 5. Design of timber structures. Part 1-1: General. Common rules and rules for buildings*. Standard. 2014.

[88] Mayr-Meinhof Holz Holding AG. *MM crosslam Technical Data*. Brochure. 2016. URL: http://www.mm-holz.com/fileadmin/user_upload/Downloads/Folder/Englisch/MM_crosslam_E_web_Eeinzelseiten.pdf.

[89] T. Technology. *WIS 2/3-62: Cross -laminated timber: structural principles*. Pamphlet. High Wycombe, 2011.

[90] H. Kreuzinger. "Platten, Scheiben und Schalen: Ein Berechnungsmodell für gängige Statikprogramme". In: *bauen mit holz* 1 (1999), pp. 34–39.

[91] C. O'Ceallaigh, K. Sikora, and A. Harte. "The Influence of Panel Lay-Up on the Characteristic Bending and Rolling Shear Strength of CLT". In: *Buildings* 8.9 (2018), p. 114.

[92] E. I. S. Flores, K. Saavedra, J. Hinojosa, Y. Chandra, and R. Das. "Multi-scale modelling of rolling shear failure in cross-laminated timber structures by homogenisation and cohesive zone models". In: *International Journal of Solids and Structures* 81 (2016), pp. 219–232. ISSN: 0020-7683. DOI: 10.1016/j.ijsolstr.2015.11.027.

[93] R. Emberley, A. Nicolaidis, D. Fernando, and J. L. Torero. *Changing Failure Modes of Cross-Laminated Timber*. Conference Paper. 2016.

[94] S. Aicher and G. Dill-Langer. "Basic considerations to rolling shear modulus in wooden boards". In: *Otto-Graf-Journal* 11 (2000), pp. 157–165.

[95] T. Ehrhart, R. Brandner, G. Schickhofer, and A. Frangi. *Rolling shear properties of some European timber species with focus on cross laminated timber (CLT): test configuration and parameter study*. Conference Paper. 2015.

[96] CEN. *EN 338 Structural timber - Strength classes*. Standard. 2009.

[97] TRADA Technology. *Guidance Document 10 (GD10) Cross-laminated Timber (Eurocode 5) Design Guide for Project Feasibility*. Report. 2009.

[98] H. Y. Rassam and J. Goodman. "Buckling behavior of layered wood columns". In: *Wood science* 2.4 (1970), pp. 238–46.

[99] EU Regulation. *305/2011 of the European Parliament and of the Council of 9 March 2011 laying down harmonised conditions for the marketing of construction products and repealing Council Directive 89/106*. 2011.

[100] *The Building Regulations*. Government Document. 2010.

[101] D. Drysdale. *An Introduction to Fire Dynamics*. Chichester: John Wiley & Sons, Ltd, 2011.

[102] B. Fredlund. *The ignition and combustion mechanism of wood (In Swedish)*. Report. Department of Structural Mechanics and Concrete Construction, Lund Institute of Technology, 1979.

[103] R. Emberley, A. Inghelbrecht, Z. Yu, and J. L. Torero. "Self-extinction of timber". In: *Proceedings of the Combustion Institute* (2016). ISSN: 1540-7489. DOI: 10.1016/j.proci.2016.07.077.

[104] E. Mikkola. "Charring of wood based materials". In: *Fire Safety Science* 3 (1991), pp. 547–556.

[105] F. L. Browne. *Theories of the combustion of wood and its control*. Report. US Dept. of Agriculture, Forest Service, Forest Products Laboratory, 1958.

[106] A. Frangi and M. Fontana. "Charring rates and temperature profiles of wood sections". In: *Fire and Materials* 27.2 (2003), pp. 91–102. ISSN: 1099-1018.

[107] J. König. "Structural fire design according to Eurocode 5—design rules and their background". In: *Fire and materials* 29.3 (2005), pp. 147–163. ISSN: 1099-1018.

[108] J. König and L. Walleij. "Timber frame assemblies exposed to standard and parametric fires: part 2: a design model for standard fire exposure". In: *Institutet för Träteknisk Forskning* 0001001 (2000), pp. 1–76. ISSN: 1102-1071.

[109] R. H. White and M. Dietenberger. "Wood products: thermal degradation and fire". In: *Encyclopedia of materials: science and technology* (2001), pp. 9712–9716.

[110] R. H. White and E. Schaffer. "Transient Moisture Gradient in Fire-Exposed Wood Slab". In: *Wood and Fiber* 13.1 (1981), pp. 17–38.

[111] American Wood Council. *National Design Specification for Wood Construction*. Standard. 2016.

[112] American Wood Council. *Technical Report 10 - Calculating the Fire Resistance of Exposed Wood member*. Standard. 2016.

[113] J.-i. Suzuki, T. Mizukami, T. Naruse, and Y. Araki. "Fire Resistance of Timber Panel Structures Under Standard Fire Exposure". In: *Fire Technology* 52.4 (2016), pp. 1015–1034. ISSN: 1572-8099. DOI: 10.1007/s10694-016-0578-2.

[114] M. Peter and T. Göckel. *Bemessung von Voll- und Brettschichtholzbauteilen aus maschinell sortiertem Schnittholz für den Brandfall. Teil 2: Brandversuche zur Bestätigung der theoretischen Ergebnisse*. Report. Institut des Zimmerer- und Holzbaugewerbes e. V., 2006.

[115] J. Stiller. *Berechnungsmethode für brandbeanspruchte Holzstützen und Holzbalken aus brettschichtverleimtem Nadelholz*. Report. Technische Universitat Braunschweig, 1983.

[116] R. Fahrni, M. Klippel, A. Just, A. Ollino, and A. Frangi. "Fire tests on glued-laminated timber beams with specific local material properties". In: *Fire Safety Journal* 107 (2019), pp. 161–169. ISSN: 0379-7112. DOI: 10.1016/j.firesaf.2017.11.003.

[117] A. Bartlett, R. Hadden, L. Bisby, and A. Law. "Analysis of Cross-Laminated Timber Charring Rates upon Exposure to Non-standard Heating Condition". In: *14th International Conference on Fire and Materials*. Intersciences Communications, pp. 667–681.

[118] A. Bartlett, F. Wiesner, R. Hadden, L. Bisby, B. Lane, A. Lawrence, P. Pedro, and F. Andrea. "State-Of-The-Art And Research Needs For Total Fire Engineering Of Mass Timber Buildings". In: *World Conference on Timber Engineering*. Ed. by J. Eberhardsteiner, W. Winter, A. Fadai, and M. Pöll.

[119] T. T. Lie. "A method for assessing the fire resistance of laminated timber beams and columns". In: *Canadian Journal of Civil Engineering* 4.2 (1977), pp. 161–169. ISSN: 0315-1468.

[120] J. Stanke, E. Klement, and R. Rudolphi. *Das Brandverhalten von Holzstützen unter Druckbeanspruchung*. Report. Bundesanstalt fuer Materialpruefung (BAM), 1973.

[121] A. Haksever. "Brandverhalten von brettschichtverleimten Holzstutzen und Holzbalken". In: *Der Bauingenieur* 57 (1982), pp. 19–26.

[122] Standards Australia. *AS 1720.4 - Timber structures Part 4: Fire resistance for structural adequacy of timber members*. Standard. 2006.

[123] M. Goina. "Resistenza al fuoco di pareti compresse in legno lamellare incrociato (Fire resistance of cross-laminated timber wall panels)". Tesi di Laurea. Facolta di Ingegneria, Universita degli Studi di Trieste, 2010.

[124] X. Li, X. Zhang, G. Hadjisophocleous, and C. McGregor. "Experimental Study of Combustible and Non-combustible Construction in a Natural Fire". In: *Fire Technology* 51.6 (2014), pp. 1447–1474. ISSN: 1572-8099. DOI: 10.1007/s10694-014-0407-4.

[125] E. Johansson and A. Svenningsson. "Delamination of Cross-laminated timber and its impact on fire development — Focusing on different types of adhesives". Masters Thesis. Division of Fire Safety Engineering, Faculty of Engineering, Lund University, 2018.

[126] R. Crielaard, J.-W. van de Kuilen, K. Terwel, G. Ravenshorst, and P. Steenbakkers. "Self-extinguishment of cross-laminated timber". In: *Fire Safety Journal* 105 (2019), pp. 244–260. ISSN: 0379-7112. DOI: 10.1016/j.firesaf.2019.01.008.

[127] H. Quiquero, B. Chorlton, and J. Gales. "Performance of Adhesives in Glulam After Short Term Fire Exposure". In: *International Journal of High Rise Buildings* 7.4 (2018).

[128] A. Frangi and M. Fontana. "Fire performance of timber structures under natural fire conditions". In: *Fire Safety Science* 8 (2005), pp. 279–290.

[129] R. M. Hadden, A. I. Bartlett, J. P. Hidalgo, S. Santamaria, F. Wiesner, L. A. Bisby, S. Deeny, and B. Lane. "Effects of exposed cross laminated timber on compartment fire dynamics". In: *Fire Safety Journal* 91 (2017), pp. 480–489. ISSN: 0379-7112. DOI: 10.1016/j.firesaf.2017.03.074.

[130] R. Emberley et al. "Description of small and large-scale cross laminated timber fire tests". In: *Fire Safety Journal* 91 (2017), pp. 327–335. ISSN: 0379-7112. DOI: 10.1016/j.firesaf.2017.03.024.

[131] J. Su, P. S. Lafrance, M. S. Hoehler, and M. F. Bundy. *Fire Safety Challenges of Tall Wood Buildings–Phase 2: Task 3-Cross Laminated Timber Compartment Fire Tests*. Report. NIST, 2018.

[132] S. L. Zelinka, L. E. Hasburgh, K. J. Bourne, D. R. Tucholski, J. P. Ouellette, V. Kochkin, E. Hudson, R. J. Ross, K. L. Martinson, and S. T. Lebow. *Compartment fire testing of a two-story mass timber building*. Report. United States Department of Agriculture, 2018.

[133] C. J. Bateman, A. I. Bartlett, L. Rutkauskas, and R. Hadden. "Effects of Fuel Load and Exposed CLT Surface Configuration in Reduced-Scale Experiments". In: *World Conference on Timber Engineering*. Seoul, Republik of Korea, 2018.

[134] C. Gorska, J. P. Hidalgo, and J. L. Torero. "An Experimental Study Of Medium-Scale Compartment Fire Tests With Exposed Cross Laminated Timber". In: *International Fire Safety Symposium*. Ed. by E. Nigro and A. Bilotta. Vol. 2nd. Doppiavoce.

[135] M. Klippel and J. Schmid. "Design of cross-laminated timber in fire". In: *Structural Engineering International* 27.2 (2017), pp. 224–230. ISSN: 1016-8664.

[136] L. Osborne, C. Dagenais, and N. Benichou. "Preliminary CLT fire resistance testing report". In: *FPInnovations, Pointe-Claire* (2012).

[137] B. Östman, E. Mikkola, R. Stein, A. Frangi, J. König, D. Dhima, T. Hakkarainen, and J. Bregulla. *Fire safety in timber buildings - Technical guideline for Europe*. Generic. 2010.

[138] R. Emberley, T. Do, J. Yim, and J. L. Torero. "Critical heat flux and mass loss rate for extinction of flaming combustion of timber". In: *Fire Safety Journal* 91 (2017), pp. 252–258. ISSN: 0379-7112. DOI: 10.1016/j.firesaf.2017.03.008.

[139] A. Frangi, M. Fontana, E. Hugi, and R. Jübstl. "Experimental analysis of cross-laminated timber panels in fire". In: *Fire Safety Journal* 44.8 (2009), pp. 1078–1087. ISSN: 0379-7112. DOI: 10.1016/j.firesaf.2009.07.007.

[140] J. P. Fackler. *Essais de resistance auf feu*. Report. CSTB, 1961.

[141] S. A. Lineham, D. Thomson, A. I. Bartlett, L. A. Bisby, and R. M. Hadden. "Structural response of fire-exposed cross-laminated timber beams under sustained loads". In: *Fire Safety Journal* 85 (2016), pp. 23–34. ISSN: 0379-7112. DOI: 10.1016/j.firesaf.2016.08.002.

[142] J. Schmid, J. König, and J. Köhler. "Fire-exposed cross-laminated timber–Modelling and tests". In: *World Conference on Timber Engineering*. Riva del Garda, Italy, 2010.

[143] S. Poncsák, D. Kocaefe, M. Bouazara, and A. Pichette. "Effect of high temperature treatment on the mechanical properties of birch (Betula papyrifera)". In: *Wood Science and Technology* 40.8 (2006), pp. 647–663. ISSN: 1432-5225. DOI: 10.1007/s00226-006-0082-9.

[144] P. Reszka and J. L. Torero. "In-depth temperature measurements in wood exposed to intense radiant energy". In: *Experimental Thermal and Fluid Science* 32.7 (2008), pp. 1405–1411. ISSN: 0894-1777. DOI: 10.1016/j.expthermflusci.2007.11.014.

[145] CEN. *EN 1995-1-2 Eurocode 5. Design of timber structures. Part 1-2: General. Structural fire design*. Standard. 2009.

[146] C. Scheer, T. Knauf, and C. Meyer-Ottens. "Rechnerische Brandschutzbemessung unbekleideter Holzbauteile". In: *Bautechnik* 69.4 (1992), pp. 179–189.

[147] R. H. White and F. E. Woeste. "Post-fire analysis of solid-sawn heavy timber beams". In: *STRUCTURE magazine* November (2013), pp. 38–40.

[148] D. Hopkin, J. Schmid, and K. L. Friquin. "Timber Structures Subject To Non-Standard Fire Exposure–Advances & Challenges". In: *World Conference on Timber Engineering*. Ed. by J. Eberhardsteiner, W. Winter, A. Fadai, and M. Pöll. Vienna University of Technology, 2016, pp. 22–25.

[149] H. L. Malhotra and B. F. Rogowski. "Fire resistance of laminated timber columns". In: *Fire Safety Science* 671 (1967).

[150] K. Odeen. "Fire resistance of glued laminated timber structures". In: *Symposium No 3 Fire and Structural Use of Timber in Buildings*, pp. 7–15.

[151] L. Metz. "Untersuchungen über den Feuerschutz von Holz. (7. Mitteilung.)" In: *Holz als Roh- und Werkstoff* 1.6 (1938), pp. 217–225. ISSN: 1436-736X. DOI: 10.1007/bf02612244.

[152] "Secret of fire proof construction". In: *The New York Times* (26th November 1871). URL: https://www.nytimes.com/1871/11/26/archives/the-secret-of-fireproof-construction.html.

[153] L. Hasburgh, K. Bourne, C. Dagenais, and L. Ranger. "Fire Performance of Mass-Timber Encapsulation Methods and the Effect of Encapsulation on Char Rate of Cross-Laminated Timber". In: *World Conference on Timber Engineering*. Ed. by J. Eberhardsteiner, W. Winter, A. Fadai, and M. Pöll. Vienna University of Technology, 2016.

[154] V. Babrauskas and R. B. Williamson. "The historical basis of fire resistance testing — Part I". In: *Fire Technology* 14.3 (1978), pp. 184–194. ISSN: 1572-8099. DOI: 10.1007/bf01983053.

[155] V. Babrauskas and R. B. Williamson. "The historical basis of fire resistance testing — Part II". In: *Fire Technology* 14.4 (1978), pp. 304–316. ISSN: 1572-8099. DOI: 10.1007/bf01998390.

[156] ASTM International. *E119 Standard Test Methods for Fire Tests of Building Construction and Materials*. Standard. 2016.

[157] M. L. Janssens and R. H. White. "Short communication: Temperature profiles in wood members exposed to fire". In: *Fire and Materials* 18.4 (1994), pp. 263–265. ISSN: 1099-1018. DOI: 10.1002/fam.810180410.

[158] P. H. Thomas. "The Fire Resistance Required to Survive a Burn Out". In: *Fire Research Note 901* (1970).

[159] T. Harmathy and J. Mehaffey. "Design of Buildings for Prescribed Levels of Structural Fire Safety". In: *Fire Safety: Science and Engineering* ASTM STP 882 (1985), pp. 160–175.

[160] D. Hopkin, J. El-Rimawi, V. Silberschmidt, and T. Lennon. "Advanced Fire Design of Timber Structures Using Computational Techniques - Simple Indeterminate Structures". In: *Journal of Structural Fire Engineering* 3.3 (2012), pp. 215–234. DOI: doi:10.1260/2040-2317.3.3.215.

[161] M. Klippel, J. Schmid, and A. Frangi. "Fire design of CLT". In: *COST Actions FP1402 & FP1404 KTH Building Materials, Cross Laminated Timber - A competitive wood product for visionary and fire safe buildings*. 2016, pp. 101–22.

[162] E. L. Schaffer. "Effect of pyrolytic temperatures on the longitudinal strength of dry Douglas-fir". In: *Journal of Testing and Evaluation* 1.4 (1973), pp. 319–329. ISSN: 0090-3973.

[163] I. Van Zeeland, J. Salinas, and J. Mehaffey. "Compressive strength of lumber at high temperatures". In: *Fire and materials* 29.2 (2005), pp. 71–90. ISSN: 1099-1018.

[164] P. Glos and D. Henrici. "Festigkeit von Bauholz bei hohen Temperaturen, Abschlussbericht 87505". In: *Institut für Holzforschung der Universität München* unpublished (1990).

[165] M. J. Manriquez Figueroa and P. Dias de Moraes. "Temperature reduction factor for compressive strength parallel to the grain". In: *Fire Safety Journal* 83 (2016), pp. 99–104. ISSN: 0379-7112. DOI: 10.1016/j.firesaf.2016.05.005.

[166] R. M. Knudson and A. Schniewind. "Performance of structural wood members exposed to fire". In: *Forest Products Journal (USA)* (1975). ISSN: 0015-7473.

[167] E. Sano. "Effects of temperature on the mechanical properties of wood. I. Compression parallel-to-grain". In: *Journal of the Japanese Wood Research Society* 7 (1961), pp. 147–50.

[168] F. Jong and P. Clancy. "Compression properties of wood as functions of moisture, stress and temperature". In: *Fire and materials* 28.2-4 (2004), pp. 209–225. ISSN: 1099-1018.

[169] C. Kaku, Y. Hasemi, N. Yasui, M. Yasukawa, D. Kamikawa, N. Kameyama, T. Ono, M. Koshihara, and H. Nagao. "Influence of fire exposure on the mechanical properties of wood". In: *Journal of Structural and Construction Engineering* 79.701 (2014), pp. 1065–1072. ISSN: 1340-4202.

[170] C. C. Gerhards. "Effect of moisture content and temperature on the mechanical properties of wood: an analysis of immediate effects". In: *Wood and Fiber Science* 14.1 (1982), pp. 4–36. ISSN: 0735-6161.

[171] L. D. Armstrong and R. S. T. Kingston. "Effect of Moisture Changes on Creep in Wood". In: *Nature* 185.4716 (1960), pp. 862–863. ISSN: 1476-4687. DOI: 10.1038/185862c0.

[172] L. D. Armstrong and G. N. Christensen. "Influence of Moisture Changes on Deformation of Wood Under Stress". In: *Nature* 191.4791 (1961), pp. 869–870. ISSN: 1476-4687. DOI: 10.1038/191869a0.

[173] F. Wiesner, L. A. Bisby, A. I. Bartlett, J. P. Hidalgo, S. Santamaria, S. Deeny, and R. M. Hadden. "Structural capacity in fire of laminated timber elements in compartments with exposed timber surfaces". In: *Engineering Structures* 179 (2019), pp. 284–295. ISSN: 0141-0296. DOI: 10.1016/j.engstruct.2018.10.084.

[174] S. Clauß, M. Joscak, and P. Niemz. "Thermal stability of glued wood joints measured by shear tests". In: *European Journal of Wood and Wood Products* 69.1 (2011), pp. 101–111. ISSN: 0018-3768.

[175] R. H. White. "Analytical Methods for Determining Fire Resistance of Timber Members". In: *SFPE Handbook of Fire Protection Engineering*. Ed. by M. J. Hurley, D. T. Gottuk, J. R. Hall Jr, K. Harada, E. D. Kuligowski, M. Puchovsky, J. Torero, J. M. Watts Jr, and C. J. Wieczorek. 5th. London: Springer, 2015.

[176] E. L. Schaffer. *Structural Fire Design: Wood*. Report. Madison, WI, USA: Forest Products Lab, 1984.

[177] R. Emberley and J. L. Torero. "Cross-laminated timber failure modes for fire conditions". In: *International Conference on Performance-based and Life-cycle Structural Engineering*. School of Civil Engineering, The University of Queensland, pp. 1023–1030. ISBN: 1742721478.

[178] A. Nicolaidis, R. Emberley, D. Fernando, and J. L. Torero. "Thermally Driven Failure Mode Changes In Bonded Timber". In: *World Conference on Timber Engineering*. Ed. by J. Eberhardsteiner, W. Winter, A. Fadai, and M. Pöll. Vienna University of Technology, 2016, Poster.

[179] P. Niemz and K. Allenspach. "Untersuchungen zum Einfluss von Temperatur und Holzfeuchte auf das Versagensverhalten von ausgewählten Klebstoffen bei Zugscherbeanspruchung". In: *Bauphysik* 31.5 (2009), pp. 296–304. DOI: doi:10.1002/bapi.200910039.

[180] M. Verdet, A. Salenikovich, A. Cointe, J.-L. Coureau, P. Galimard, W. M. Toro, P. Blanchet, and C. Delisée. "Mechanical performance of polyurethane and epoxy adhesives in connections with glued-in rods at elevated temperatures". In: *BioResources* 11.4 (2016), pp. 8200–8214. ISSN: 1930-2126.

[181] CEN. *EN 301 Adhesives, phenolic and aminoplastic, for loadbearing timber structures - Classification and performance requirements*. Standard. 2013.

[182] O. F. Kläusler. "Improvement of one-component polyurethane bonded wooden joints under wet conditions". PhD Thesis. ETH Zurich, 2014.

[183] J. Konnerth, M. Kluge, G. Schweizer, M. Miljković, and W. Gindl-Altmutter. "Survey of selected adhesive bonding properties of nine European softwood and hardwood species". In: *European Journal of Wood and Wood Products* 74.6 (2016), pp. 809–819. ISSN: 1436-736X. DOI: 10.1007/s00107-016-1087-1.

[184] M. Klippel. "Fire safety of bonded structural timber elements". PhD Thesis. Diss., Eidgenössische Technische Hochschule ETH Zürich, Nr. 21843, 2014.

[185] M. Klippel and A. Frangi. "Einfluss des Klebstoffes auf das Brandverhalten von Brettschichtholz". In: *Bauphysik* 34.4 (2012), pp. 142–152. ISSN: 1437-0980.

[186] J. Schmid, A. Menis, M. Fragiacomo, I. Clemente, and G. Bochicchio. "Behaviour of Loaded Cross-Laminated Timber Wall Elements in Fire Conditions". In: *Fire Technology* 51.6 (2015), pp. 1341–1370. ISSN: 0015-2684. DOI: 10.1007/s10694-015-0516-8.

[187] M. Kippel, C. Leyder, A. Frangi, and M. Fontana. "Fire tests on loaded cross-laminated timber wall and floor elements". In: *Fire Safety Science* 11 (2014), pp. 626–639.

[188] Canadian Wood Council. *Report of testing cross-laminated timber panels fo compliance with the applicable requirements of the following criteria ASTM E119-14*. Report. Intertek, 2014.

[189] American Wood Council. *Test Report Cross Laminated Timber and Gypsum Board Wall Assembly. Fire Tests of Building Construction and Materials.* Report. Intertek, 2012.

[190] F. Wiesner, F. Randmael, W. Wan, L. Bisby, and R. M. Hadden. "Structural response of cross-laminated timber compression elements exposed to fire". In: *Fire Safety Journal* 91.Supplement C (2017), pp. 56–67. ISSN: 0379-7112. DOI: 10.1016/j.firesaf.2017.05.010.

[191] E. L. Schaffer, C. Marx, D. Bender, and F. Woeste. "Strength validation and fire endurance of glued-laminated timber beams". In: *United States Department of Agriculture Research Paper* (1986).

[192] F. Wiesner, M. Klippel, C. Dagenais, A. Dunn, B. Östman, M. L. Janssens, and K. Kagiya. "Requirements For Engineered Wood Products And Their Influence On The Structural Fire Performance". In: *World Conference on Timber Engineering*. 2018.

[193] Canadian Standards Association. *O86-14 Engineering design in wood*. Design guidance. 2014.

[194] J. Schmid, A. Just, M. Klippel, and M. Fragiacomo. "The Reduced Cross-Section Method for Evaluation of the Fire Resistance of Timber Members: Discussion and Determination of the Zero-Strength Layer". In: *Fire Technology* 51.6 (2015), pp. 1285–1309. ISSN: 0015-2684. DOI: 10.1007/s10694-014-0421-6.

[195] J. Schmid, M. Klippel, A. Just, and A. Frangi. "Review and analysis of fire resistance tests of timber members in bending, tension and compression with respect to the reduced cross-section method". In: *Fire Safety Journal* 68 (2014), pp. 81–99. ISSN: 0379-7112.

[196] D. Hopkin, J. El-Rimawi, T. Lennon, and V. Silberschmidt. "Effect of fire-induced damage on the uniaxial strength characteristics of solid timber: A numerical study". In: *Journal of Physics: Conference Series*. Vol. 305. IOP Publishing, p. 012039. ISBN: 1742-6596.

[197] A. Ylinen. "A method of determining the buckling stress and the required cross-sectional area for centrally loaded straight columns in elastic and inelastic range". In: *Zurich, Switzerland: Publication of the IABSA (International Association for Bridge and Structural Engineering)* 16 (1956).

[198] M. Tavakkol-Khah and W. Klingsch. "Calculation model for predicting fire resistance time of timber members". In: *Fire Safety Science* 5 (1997), pp. 1201–1211.

[199] L. M. P. Simpson. "Predicting the Failure Times of Glulam Members Exposed to Fire". Masters Thesis. University of Ottawa, 2006.

[200] J. A. Neale. *Fire Exposure Tests of Loaded Timber Columns*. Report. Underwriters Laboratory, 1939.

[201] Joint Committee on Structural Safety (JCSS). *Probabilistic Model Code*. Standard. 2001. URL: `http://www.jcss.byg.dtu.dk/Publications/Probabilistic_Model_Code.aspx`.

[202] CEN. *EN 1912 Structural Timber - Strength Classes - Assignment of visual grades and species*. Standard. 2012.

[203] R. J. Hyndman and A. B. Koehler. "Another look at measures of forecast accuracy". In: *International journal of forecasting* 22.4 (2006), pp. 679–688. ISSN: 0169-2070.

[204] J. Wang, M. Mohammad, B. Di Lenardo, and M. Sultan. "CLT panels subjected to combined out-of-plane bending and compressive axial loads". In: *World Conference on Timber Engineering*. Ed. by J. Eberhardsteiner, W. Winter, A. Fadai, and M. Pöll. Vienna University of Technology, 2016.

[205] J. J. Zahn and D. R. Rammer. "Design of glued laminated timber columns". In: *Journal of Structural Engineering* 121.12 (1995), pp. 1789–1794. ISSN: 0733-9445.

[206] CEN. *EN 14080 Timber structures - Glued laminated timber and glued solid timber - Requirements*. Standard. 2013.

[207] CEN. *EN 322 Wood-based panels - Determination of moisture content*. Standard. 1993.

[208] APA. *PRG 320 Standard for Performance-Rated Cross-Laminated Timber*. Standard. 2018.

[209] D. White, W. Take, and M. Bolton. "Soil deformation measurement using particle image velocimetry (PIV) and photogrammetry". In: *Geotechnique* 53.7 (2003), pp. 619–631. ISSN: 1751-7656.

[210] Student. "The probable error of a mean". In: *Biometrika* (1908), pp. 1–25. ISSN: 0006-3444.

[211] S. L. Zabell. "On Student's 1908 Article "The Probable Error of a Mean"". In: *Journal of the American Statistical Association* 103.481 (2008), pp. 1–7.

[212] R. Nuzzo. "Scientific method: statistical errors". In: *Nature News* 506.7487 (2014), p. 150.

[213] T. Technology. *Worked Example 12-storey building of cross-laminated timber (Eurocode 5)*. Report. 2009.

[214] B. Cuzzillo. "Pyrophoria". PhD Thesis. Mechanical Engineering, University of Berkeley, 1997.

[215] V. Babrauskas. "'Pyrophoric Carbon'and Long-term, Low-temperature Ignition of Wood". In: *Fire and Arson Investigator* 51.2 (2001).

[216] V. M. Muggeo. "Estimating regression models with unknown break-points." In: *Statistics in Medicine* 22 (2003), pp. 3055–3071.

[217] J. D'Errico. *SLM - Shape Language Modeling*. `https://www.mathworks.com/matlabcentral/fileexchange/24443-slm-shape-language-modeling`. Computer Program. 2017.

[218] Instron. *3690 Series Servohydraulic Actuators Reference Manual*. 2008.

[219] D. J. Othman. "Influence of adhesive curing temperature upon the performance of FRP strengthened steel structures at ambient and elevated temperatures". PhD Thesis. The School of Engineering, The University of Edinburgh, 2017.

[220] S. A. Stanier, J. Blaber, W. A. Take, and D. J. White. "Improved image-based deformation measurement for geotechnical applications". In: *Canadian Geotechnical Journal* 53.5 (2015), pp. 727–739. ISSN: 0008-3674. DOI: `10.1139/cgj-2015-0253`.

[221] V. Babrauskas. "Ignition of wood: a review of the state of the art". In: *Journal of Fire Protection Engineering* 12.3 (2002), pp. 163–189. ISSN: 1042-3915.

[222] R. L. Graham, B. D. Lubachevsky, K. J. Nurmela, and P. R. Östergård. "Dense packings of congruent circles in a circle". In: *Discrete Mathematics* 181.1-3 (1998), pp. 139–154. ISSN: 0012-365X.

[223] MathWorks. *MATLAB*. Computer Program. 2016.

[224] R. O. Duda and P. E. Hart. "Use of the Hough transformation to detect lines and curves in pictures". In: *Communications of the ACM* 15.1 (1972), pp. 11–15. ISSN: 0001-0782.

[225] P. Reszka. "In-depth temperature profiles in pyrolyzing wood". PhD Thesis. The University of Edinburgh, 2008.

[226] T. Gernay. "Fire resistance and burnout resistance of reinforced concrete columns". In: *Fire Safety Journal* 104 (2019), pp. 67–78. ISSN: 0379-7112. DOI: 10.1016/j.firesaf.2019.01.007.

[227] T. Gernay. "Defining a burnout resistance rating to compare structural components under real fires". In: *3rd International Fire Safety Symposium (IFireSS)*. 2019.

[228] G. E. P. Box. "Robustness in the Strategy of Scientific Model Building". In: *Robustness in Statistics*. Ed. by R. L. Launer and G. N. Wilkinson. Academic Press, 1979, pp. 201–236. ISBN: 978-0-12-438150-6. DOI: 10.1016/B978-0-12-438150-6.50018-2.

[229] B. Delaunay. "Sur la sphere vide". In: *Izv. Akad. Nauk SSSR, Otdelenie Matematicheskii i Estestvennyka Nauk* 7.793-800 (1934), pp. 1–2.

[230] P. J. Green and B. W. Silverman. *Nonparametric regression and generalized linear models: a roughness penalty approach*. CRC Press, 1993. ISBN: 0412300400.

[231] M. A. Babyak. "What you see may not be what you get: a brief, nontechnical introduction to overfitting in regression-type models". In: *Psychosomatic medicine* 66.3 (2004), pp. 411–421. ISSN: 0033-3174.

[232] R Core Team. *R: A Language and Environment for Statistical Computing*. R Foundation for Statistical Computing. Vienna, Austria, 2013. URL: http://www.R-project.org/.

[233] J. V. Beck. "Thermocouple Temperature Disturbances in Low Conductivity Materials". In: *Journal of Heat Transfer* 84.2 (1962), pp. 124–131. ISSN: 0022-1481. DOI: 10.1115/1.3684310.

[234] R. Fahrni, J. Schmid, M. Klippel, and A. Frangi. "Correct Temperature Measurements in Fire Exposed Wood". In: *World Conference on Timber Engineering*. Seoul, Republic of Korea, 2018.

This page is intentionally left blank.

APPENDIX A

Supplementary information to Chapter 4

This page is intentionally left blank.

A.1 Supplementary information

A.1.1 Load crosshead stroke response

The load responses to the imposed crosshead stroke for samples tested at ambient temperature are shown in Figure A.1. A significant difference in peak load can be observed between three and five ply CLT configurations. This is due to two reasons; (1) the three ply CLT has more timber orientated parallel to the loading direction compared to 5 ply. In addition the depth of the samples was reduced from 150 mm to 100 mm for the five ply samples in order to reduce the peak loads required to fail the samples after damage to the threads of the load platens was detected in early testing. This also explains why two of the 5MF samples reach distinctively higher loads than the remaining specimen in that sample, as these two were still tested with a depth of 150 mm before the decision to resize the samples was taken.

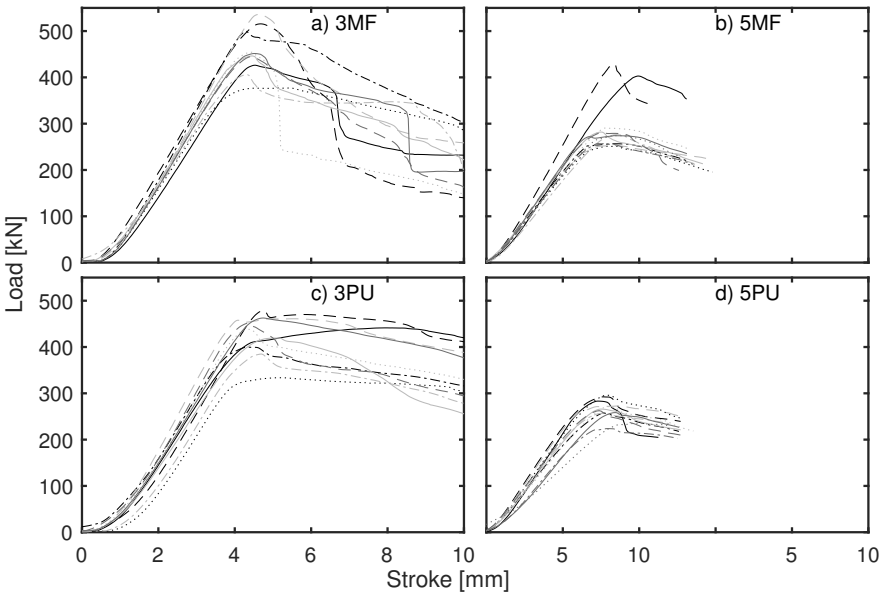

Figure A.1. Load response against imposed deflections for small scale CLT samples at ambient temperatures for the four configurations assessed.

A.2 Strain calculation from DIC

Digital image correlation (DIC) [209] provides the coordinates of a predetermined grid of points with progressing experimental duration from photographs of a specimen's

surface. The movement of these points can be used to compute the strain across the investigated grid. The use of linear strain triangles for the computation of strain is outlined below. The gridded points are turned into triangles using a Delaunay triangulation algorithm. This method computes triangles with the requirement that each triangles circumcircle only contains points of its respective triangle [229]. The result is demonstrated in Figure A.2, showing the DIC points amd corresponding triangles over a CLT surface.

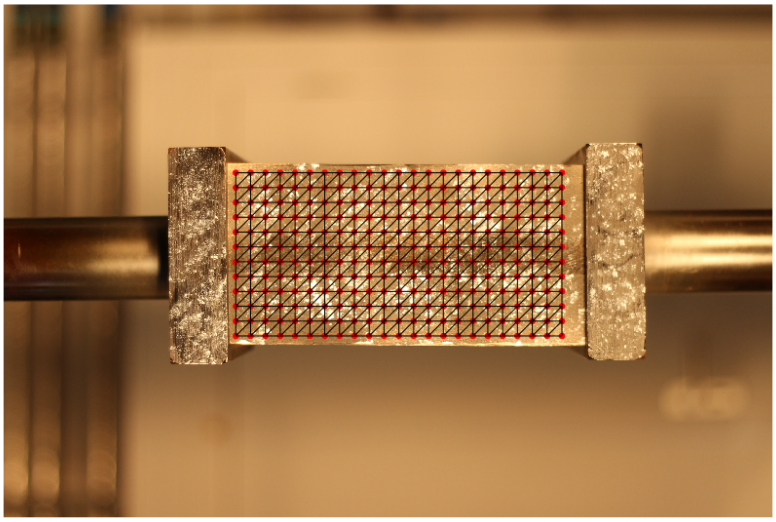

Figure A.2. Delauney triangulation over grid points for a CLT compression sample.

The schematic movements of a triangle based on the movement of its coordinates are shown in Figure A.3 and it can be seen that in this example a mix of rigid body movement and compression acts on the element. The corresponding B matrix is shown in Equation A.1, and this can be used in conjunction with the coordinate displacement, which is known from the application of DIC between subsequent images, to calculate the normal and shear strains as shown in Equation A.2. The obtained strain can the be utilised in conjunction with the stress, which is derived from the measured applied load, to calculate the elastic modulus for each fitted triangle at different load stages. The elastic modulus for the example herein is shown in Figure A.4 alongside the histogram of the computed elastic modulus values. In this case it can be seen that the distribution is relatively uniform over the assessed surface area. Empty grid points show negative values, which arise primarily near the edges where the pixel tracking can be difficult. The histogram for this example follows a log normal distribution, as would be expected for the elastic modulus of timber. One major difficulty for the use

of DIC for the determination of the elastic modulus were out of plane movements of the push rods (and therefore the specimens), which were observed visually for some of the specimens as the load increased. In some cases image anomalies or out of plane movement could induce unrealistically large or, as mentioned above, negative values for the elastic modulus. For these cases the values are limited to realistic expected values. This is done by assuming an expected mean elastic modulus of 11000 MPa [96] and a coefficient of variance (CoV) of 13 % [201]. It is then assumed that any values that fall outwith the 99.995 % confidence interval are caused by DIC measurement errors rather than the actual underlying population data. The lower limit is set to 0 for heated samples since the expected reduction and arising distribution is unknown for these cases.

While this approach works well for most of the specimens that were tested at ambient temperatures, it becomes increasingly unstable and unreliable once the heating chamber is involved. The chamber narrows the view of the camera and also shades part of the sample. In addition, the chamber's view port is triple glazed, which increases the probability of reflections on the view port that can then be interpreted as movement of the sample by the DIC analysis. In addition the elevated temperatures of the timber lead to discolouration over time which changes the point of reference for the tracked DIC clusters, and flow of sap and water from the surface will also cause the DIC to register strains that are not reflective of the actual deformation of the timber surface. An example where the DIC analysis did not yield satisfactory results is shown in Figure A.5, where it can clearly be seen that the majority of the strain triangles result in values outwith the expected range and the bounding of the value that is described above would only return a small proportion of the available data; this means that the bounding would return values that are expected but that are not necessarily true and is therefore not reliable.

$$B = \begin{bmatrix} y_2 - y_3 & 0 & y_3 - y_1 & 0 & y_1 - y_2 & 0 \\ 0 & x_3 - y_2 & 0 & x_1 - x_3 & 0 & x_2 - x_1 \\ x_3 - x_2 & y_2 - y_3 & x_1 - x_3 & y_3 - y_1 & x_2 - x_1 & y_1 - y_2 \end{bmatrix} \tag{A.1}$$

$$\begin{bmatrix} \epsilon_x \\ \epsilon_y \\ \gamma_{xy} \end{bmatrix} = \frac{1}{2A} B \cdot \begin{bmatrix} x'_1 - x'_1 \\ y'_1 - y'_1 \\ x'_2 - x'_2 \\ y'_2 - y'_2 \\ x'_3 - x'_3 \\ y'_3 - y'_3 \end{bmatrix} \tag{A.2}$$

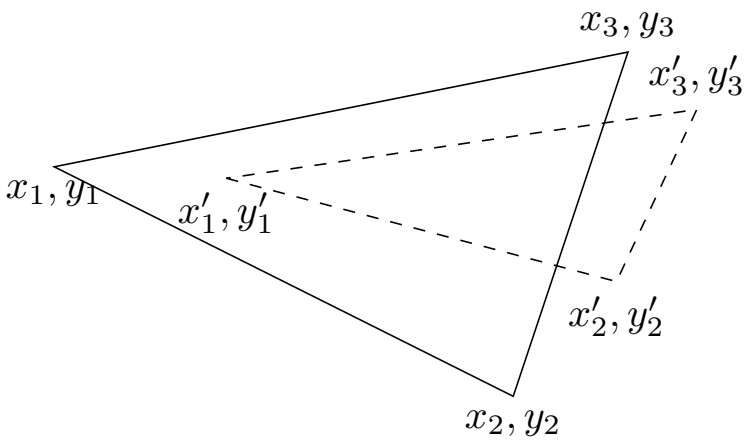

Figure A.3. Single schematic linear strain triangle element movement.

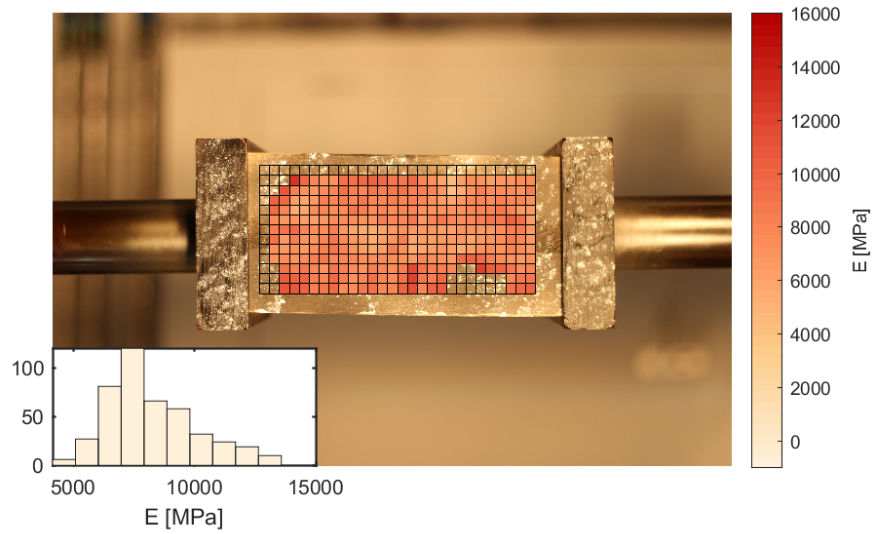

Figure A.4. Elastic modulus distribution over CLT ambient temperature specimen surface at 50 % of the ultimate load with histogram of values.

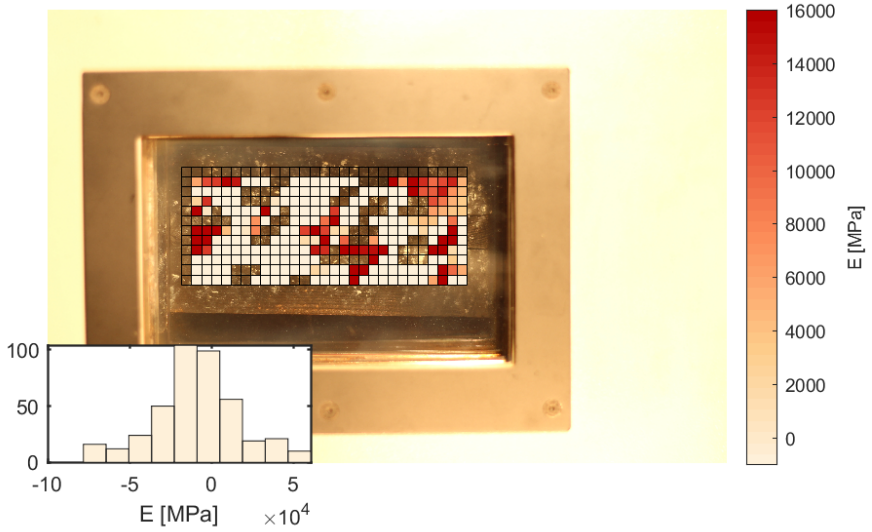

Figure A.5. Elastic modulus distribution over CLT 200 °C temperature specimen surface at 50 % of the ultimate load with histogram of values.

APPENDIX B

Thermocouple correction

This page is intentionally left blank.

B.1 Temperature profiles in timber

Thermocouples are point sensors, measuring the temperature at their tip through a voltage generation that arises from two dissimilar metals being fused together. As a consequence any temperatures measured will only represent point measurements. For an assessment of the structural capacity in fire it is beneficial to know the distribution of temperatures through the timber cross-section. To obtain a continuous temperature profile a fit can be created from the available temperature measurements at known depths. There are no detailed studies into best practice for this procedure, so a short comparison and explanations of two fitting methods will be provided below. Previous studies [141, 190] have utilised 3rd order (cubic) polynomial curves to locate the 300 °C isotherm and thereby the char timber boundary. Other recent research publications [173] have relied on a smoothing spline curve fit instead. A smooting spline curve, named after the splines tradespeople used to use to approximate curved lines, essentially fits a series of curves to the datapoint and *smoothness* is controlled via the smoothing parameter λ, which scales a roughness penalty based on the second derivative of the fitted functions [230]. A λ value close to 0 will reduce this roughness penalty and thereby cause the fitted curve to be less smooth, approximating a perfect interpolation of the individual data points as λ approaches 0. For λ values close to 1 more smoothing will be applied and the resulting fit will resemble a linear least square. Obviously this results in a trade-off between closely matching the profile of the fitted data and the potential for over fitting.

B.1.1 Uncertainty quantification

Since thermocouples provide spot measurements the resulting measured values at each time step can be seen as samples from a population of possible temperature measurements over the assessed area. Hence, any fit of the temperature profile will provide an estimated mean value for the expected temperatures at all fitted depths and of course there will be uncertainty associated with this mean fit. For polynomial fits an uncertainty can be associated with the associated polynomial coefficients, although these will not capture issues of over fitting [231]. Most curve fitting algorithms in commonly used programs for data analysis (e.g. R [232] or MATLAB [223]) will not provide confidence intervals for smoothing spline fits, due to the complexity of the underlying stored values. For this study the uncertainty of the fits is therefore quantified via bootstrapping. Bootstrapping is a statistical technique involving repeated sampling *with replacement*.

For each of the obtained samples a fit can be provided to the drawn data and for a sufficiently high number of fits the distribution of the fitted values can be approximated and confidence intervals can be obtained for the distribution of the underlying population data. This approach is taken for both the smoothing spline fit and polynomial fit in the comparison presented below, to ensure a consistent approach is taken for both methods.

A comparison of fitted values and their 95 % confidence intervals for both a smoothing spline and a cubic polynomial fit at different times through the test is shown in Figure B.1 for a column heated by a high heat flux throughout and for a column subjected to a high heat flux with a subsequent cooling phase in Figure B.2. Refer to Chapter 6 for details on the heat exposure in these experiments.

From Figure B.1 it can be seen that both fits give a good approximation of the steep temperature gradient in hot timber above 100 °C. For the polynomial fit it can be seen that issues exists in the colder regions of the timber and that temperatures below the last thermocouple at 80 mm from the surface are approximated as negative and temperatures between 100 and 20 °C are prone to overestimation. This issue is exasperated for the cooling phase shown in Figure B.2 with a wide confidence interval in the region between 300 and 100 °C for the polynomial fit. It can be seen that the smoothspline fit also has a region of large uncertainty in the cooling phase, however this is for depths that were previously heated to 300 °C and are therefore charred and of little interest in a structural assessment since their strength and stiffness will be zero. From the provided comparison it can be concluded that both methods seem to be equally suitable for the determination of charring depths in standard fire or (temporal) uniform heat flux exposure but the smoothing spline is more suitable to accurately define the temperatures at deeper positions in the timber and in the cooling phase. Hence the smoothing spline is used for all required temperature fits for burning timber in this work.

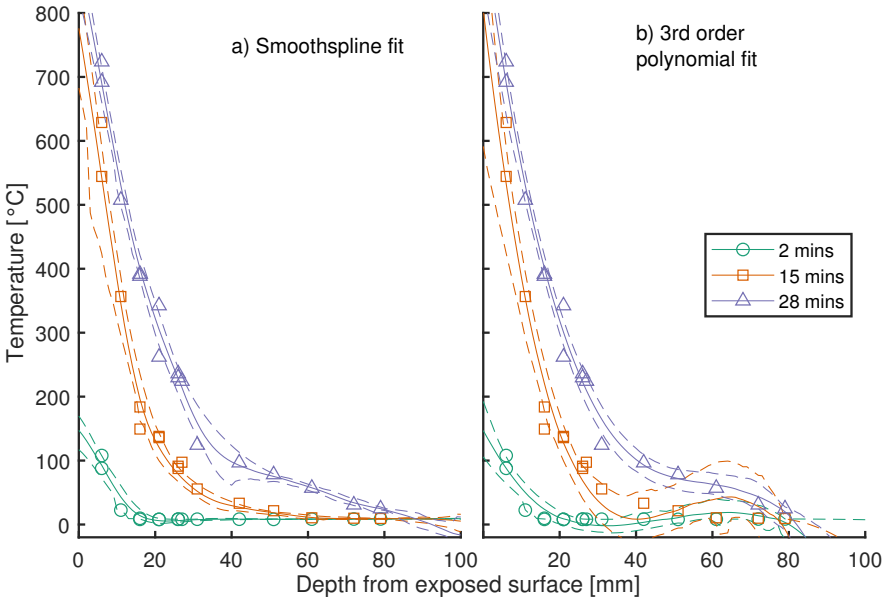

Figure B.1. Fitted temperature profiles with 95 % confidence intervals at selected time steps for a five ply polyurethane column subjected to a high heat flux.

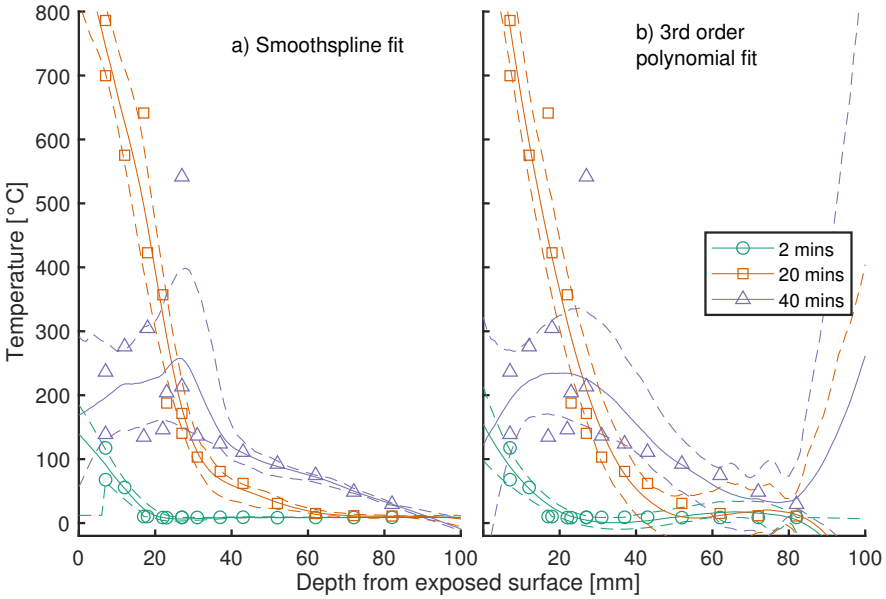

Figure B.2. Fitted temperature profiles with 95 % confidence intervals at selected timesteps for a five ply polyurethane column subjected to a high heat flux with subsequent cooling phase.

B.2 Thermocouple correction

Due to the large difference between the thermal conductivity of the inconel sheathed thermocouples and both timber and char, the temperature readings from the thermocouples are influenced by a temperature field distortion which is caused by the thermocouples as they conduct heat away from the hot zone at the tip and move it further down into colder depth of the timber [225, 233, 234] . Essentially the temperatures readings obtained with thermocouples inserted from the back are therefore lower than what the actual temperature in the timber would be without any thermocouples present. One potential solution to this problem is the insertion of thermocouples parallel to the isotherms, which in an experimental setting, means that the thermocouples are inserted from the side rather than the back of an exposed specimen. This, however, has other negative consequences for the reliability of the temperature measurements. If thermocouples are inserted through drilled holes from the sides, any small deviation of the insertion angle will change the depth of the thermocouple tip relative to the exposed surface [225]. In addition it is often not possible to drill small holes to a depth of more than 150 mm and therefore this option can prevent placement of thermocouples in large samples. As a solution to this it has been suggested to inlay thermocouples between lamellae during the production of CLT [234]. This option, however, is not readily available to many researchers as it requires either significant equipment investment or specified agreements with manufacturers. In addition, the placement of thermocouples along the glue line has been shown to potentially favour delamination of char along those glue lines [234] and if thermocouples are only placed on glue lines, it will reduce the in-depth resolution of temperature readings.

The experiments described in Chapter 6 were performed with thermocouples inserted from the back, and it can therefore be assumed that the measured temperatures are underestimations of the real temperatures. Therefore a correction procedure was applied which is described below. It is based on work by Beck [233] who has given a detailed description of the problem and a potential solution to apply a correction factor. The procedure involves the determination of a dimensionless undisturbed temperature in Equation B.1 in a heat conducting material at a distance z behind a heated surface, where τ is dimensionless time and R is the radius of the thermocouple considered. The resulting dimensionless temperature dimension is subsequently used in Equation B.2 to determine the absolute temperature disturbance from the heat flux q_e (at a distance z above the point where disturbance is to be calculated) and the conductivity of the thermocouple k_{TC}. The resulting $\Delta\ T$ is then added to the disturbed temperature

readings to obtain the corrected undisturbed temperature.

$$\theta_\infty = \tau^{\frac{1}{2}} \cdot 2ierfc[\tau^{-\frac{1}{2}} \cdot (\frac{z}{2R})] \tag{B.1}$$

$$\Delta T = \frac{\theta_\infty \cdot q_e \cdot R}{k_{TC}} \tag{B.2}$$

The heat flux at the surface at the beginning of the experiments is known from the radiation heat flux mapping that was obtained before the experiments were started (refer to Figure 6.4.1.3). However, the procedure described above assumes one uniform material in which the thermocouples are placed. In reality, as the heating progresses, the outer parts of the timber will turn to char, which has different material properties, and this will cause the corrected temperatures to overestimate the actual temperatures with progressing heating duration. This problem has also been discussed by Reszka [225], whose solutions for thermocouple corrections treated char and timber independently. This can be corrected by scaling the heat flux q_e in Equation B.2 by a factor that accounts for the change in material. For this the char depth, c_d is calculated from the corrected temperatures at each time step and subsequently used in Equation B.3 to calculate a scaling factor for q_e, where d is the overall thickness of the timber section.

$$f_s = 1 - \frac{c_d}{2d} \tag{B.3}$$

Assuming that temperature variation at similar or equal depths are caused by random variation, the temperature profile can be estimated through a fit through the available temperature data. For a smooth fit, bootstrapping can be utilised to estimate the standard error (amongst other model parameters) of the fits and hence the confidence interval of the sampled data [231] (see Subsection B.1.1).

The outcome of the applied thermocouple corrections is shown comparatively in figures B.3 and B.4, which show the char depth calculated from a 300 °C isotherm for non corrected and corrected temperature readings respectively. From these figures it can be seen that the corrections provide a significant improvement on estimating the final measured charring depths compared to the the uncorrected thermocouple readings. The mean absolute percentage error (MAPE) between final observed and char depths inferred from temperature readings reduces from 14.4 % to 4.2 %. Of course this does not give an indicator on the reliability of the thermocouple corrections *during* the experiments, as there is no ground truth to compare the TC readings to. Given that

the chosen correction method is relatively simple, there are no reasons to believe that the corrections will not induce serious thermocouple deviations in this phase.

The chosen correction model is perhaps overly simplistic and a more sophisticated approach would be to calculate q_e from the measured temperature profiles at each time step to avoid the need to scale the heat flux q_e based on the char progression. However, this would also require a more sophisticated understanding of the changes in thermal conductivity of timber and char through the cross-section. In addition an estimation of the conductive heat flux based on thermocouple readings will depend on temperature readings close to the exposed surface but will always be subject to uncertainty as the actual surface temperature of char or timber can never truly be distinguished from the gas phase temperature. For the temperatures in this study, the applied corrections are deemed sufficient, although with the increasing global interest in tall timber structures and the accompanying need for better understanding of their fire safety, it can be anticipated that further studies will aim to provide further and more sophisticated illumination to the topic of temperature corrections for thermocouples.

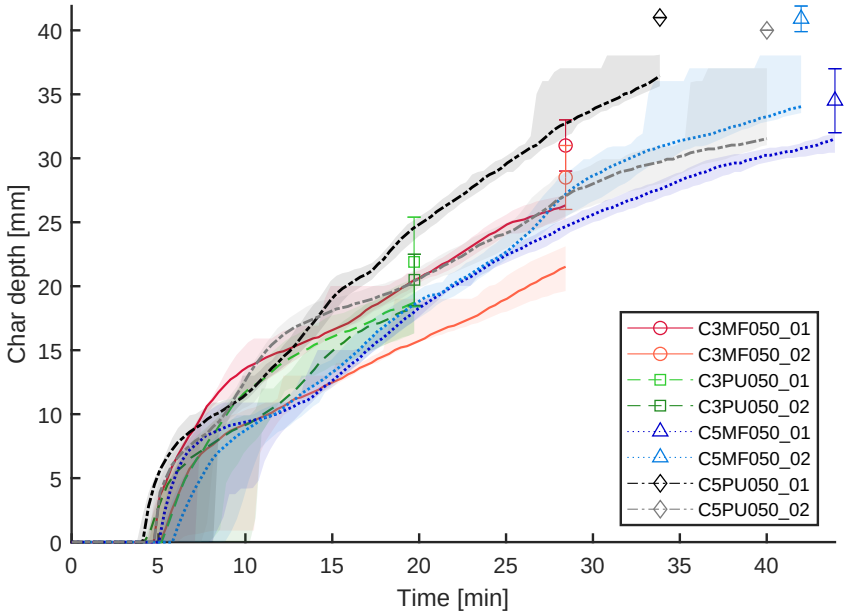

Figure B.3. Progression of the char front for CLT specimens exposed to a surface heat flux of 51 kW/m^2 from uncorrected thermocouple readings.

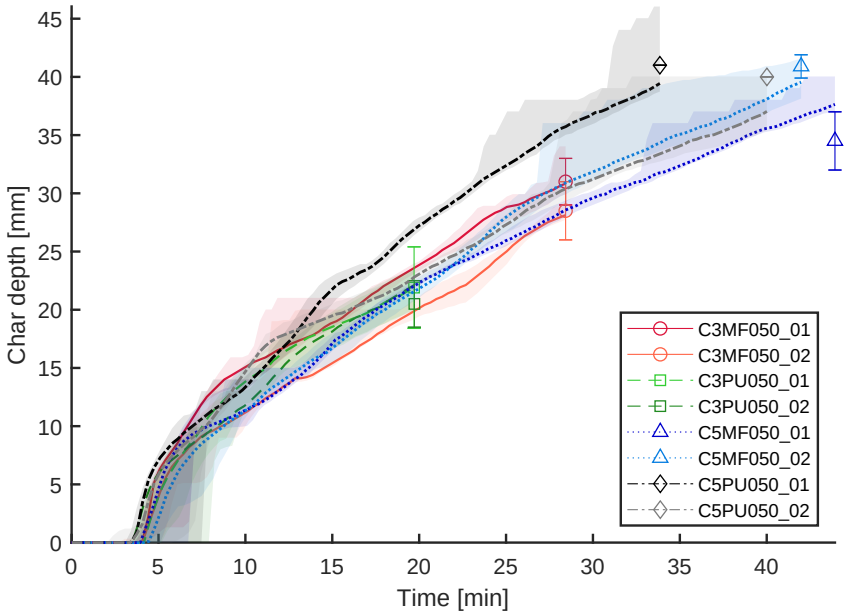

Figure B.4. Progression of the char front for CLT specimens exposed to a surface heat flux of 51 kW/m^2 from corrected thermocouple readings.